NEURAL REPRESENTATION OF MOVEMENT TAU (τ)

by

HENG-RU MAY TAN

A thesis submitted in partial fulfilment of the requirements for the degree of

DOCTOR OF PHILOSOPHY

THE UNIVERSITY OF EDINBURGH

2007

THE UNIVERSITY OF EDINBURGH

DECLARATION

This thesis has been composed by the candidate
HENG-RU MAY TAN.
The presented work is the candidate's own,
and has not been submitted for any other degree or professional qualification.

SIGNED: _____

ON THE _____ OF THE YEAR _____

The presented work has been critically examined and appraised by

COLWYN TREVARTHEN, PhD.
Professor (Emeritus) of Child Psychology and Psychobiology
in the Department of Psychology, The University of Edinburgh, UK

GIUSEPPE PELLIZZER, PhD.
Associate Professor in the Department of Neuroscience,
The University of Minnesota, USA

THE UNIVERSITY OF EDINBURGH

ABSTRACT

Neural representation of movement *tau* (τ)

Heng-Ru May Tan

Supervisors: Prof. David N. Lee[1] and Prof. Apostolos P. Georgopoulos[2]

[1] School of Philosophy, Psychology, and Language Sciences, Perception-Movement-Action Research Centre, Perception-in-Action Laboratories, The University of Edinburgh.

[2] Brain Sciences Center, Departments of Neuroscience, Neurology, and Psychiatry, The University of Minnesota Medical School, The University of Minnesota.

A fundamental aspect of goal-directed behaviour concerns the closure of motion-gaps in a timely fashion. An influential theory about how this can be achieved is provided by the *tau*-theory (Lee, 1998). *Tau* (τ) is defined as the ratio of the current distance-to-goal gap over the current instantaneous speed towards the goal. In this work we investigated the neural representation of *tau* in two sets of experiments. In one study we recorded neuromagnetic fluxes (using magnetoencephalography, MEG) from the whole brain of human subjects performing discrete hand movements aimed to targets in space, whereas the other study involved recordings of single cell activity from prefrontal and posterior parietal areas of a behaving monkey during geometrical shape-copying tasks. These two studies provided complementary information, for the former covered the whole brain (at the cost of weak localization), whereas the latter used the finest neural grain (at the expense of limited brain regions). However, the two studies together yielded valuable information concerning the dynamic, time-varying neural representation of *tau*, with respect to both integrated synaptic events in neuronal ensembles (recorded by MEG) and neural spike outputs (recorded by microelectrodes). The relations between neural signals and *tau* were analyzed using a linear regression model where the time-varying neural signal (magnetic field strength in fT or spike density function) was the dependent variable and the corresponding value of movement *tau* and speed were the independent variables. In addition, the model included an autoregressive term to account for the expected correlated errors, given the time series nature of the data. The neurophysiological study revealed a statistically significant ($p < 0.05$) relation of spike density function to *tau* (in the presence or absence of a significant speed effect) in 17% of cells in the posterior parietal cortex (N = 399) and 8% of cells in the prefrontal cortex (N = 163). These results are in accord with previous findings in an interception task. The MEG study revealed that a mean of 21.98 (± 6.08) % of sensor signals had a statistically significant ($p < 0.05$) relation to *tau* across all subjects. These effects were distributed predominantly over the left parietal-temporo-occipital sensor space, with additional foci over the frontal sensorimotor regions. Altogether, these findings demonstrate a specific involvement of neurons and neuronal ensembles with the *tau* variable and pave the way for further studies on predictive *tau* control.

CONTENTS:

CONTENTS: *– continued*

LIST OF FIGURES:

Chapter *Page*

LIST OF FIGURES: *– continued*

Chapter *Page*

LIST OF FIGURES: *– continued*

Chapter *Page*

LIST OF TABLES:

Chapter *Page*

Acknowledgements

This research is unique in bridging techniques of inquiry as well as people and minds from various institutes and nationalities. I thank Profs David N. Lee and Apostolos P. Georgopoulos for this collaborative opportunity, the intellectual challenge, and supervision.

I am indebted to the funding generously provided by The Carnegie Trust for The Universities of Scotland, The Overseas Research Students Awards Scheme of The United Kingdom, The American Legion Brain Sciences Chair, and The Tan Kah Kee Foundation of Singapore that have made this research and scientific collaboration possible.

I owe thanks to Katie Keltie, Postgraduate Administrative Assistant of the School of Philosophy, Psychology, and Language Sciences at The University of Edinburgh, who has been very patient and helpful with the necessary administrative bureaucracies. Likewise, I could not have managed without the administrative support of Penny Becker and Gail Hollstadt at the Brain Sciences Center who dealt with the relevant paper work for my presence in the United States of America.

Colleagues and friends from The University of Edinburgh and from the Brain Sciences Center at The University of Minnesota have rendered help during the course of the research and transition between the countries. In particular, I am grateful to Bruno Averbeck, previous member of the Brain Sciences Center who is presently at the University College of London, for access to the neurophysiology data that is used as part of the investigation, Scott Lewis for all the IRB consents he had to administer, Nancy Tabaka, for help in recruiting additional participants, Art Leuthold, for assisting in the MEG acquisitions and pre-processing of data, Roger Dumas, for constructing the spiffy joystick support and for the gentle reminders of the 'Elements of Style' pertaining to the English language, Joshua Lynch and Alex Merkle, who are both amazing programming advisers and code simplifiers, Emad Al-Ramahi, who has been most patient and helpful with my computing needs, Dale Boeff, who introduced me to Visual Basic, and whose family have been most generous and welcoming. I am also tremendously grateful to Lucy MacGregor for her kindness, generosity, and help during my hops across the Atlantic pond.

This research journey has enjoyed the constant cheer-leading and encouragements from family and friends, near and far, who are all gratefully thanked.

I am also grateful to Profs Colwyn Trevarthen and Giuseppe Pellizzer, who critically appraised the presented work, guided me in the process of fine-tuning the thesis, shared their scientific insights, and in so doing, helped me arrive at the end of this seemingly never-ending journey.

For Mum and Dad,
who have always been there for me
despite being so far away.

CHAPTER 1:

Overview

In trying to understand how the motor system achieves the coordination of movements despite the numerous degrees of freedom (Bernstein 1967), theorists have commonly conceptualized its role in generating behaviours as an optimization problem. That is, movements are controlled through the minimization of certain cost-function e.g. jerk (Flash, Hogan 1985, Todorov, Jordan 1998), or muscle-torque (Nakano, Imamizu et al. 1999, Uno, Kawato et al. 1989), etc. While these optimizations can provide detailed and accurate predictions of average (ideal) behaviours, they are not able to explain the trial-to-trial variability inherent in movements, nor do they intuitively acknowledge that movements need to be perceptually guided. Alongside these theories on movement that view the motor system as solving an engineering problem is a theory that seeks to place the actor within the context of her behaviours through the role of perceptual information in guiding actions. In the realm of the General *Tau* Theory (Lee 1998), movements are conceived as the closure of motion gaps, while the coordination and regulation of the rate of closure of motion gaps are the essence of movement guidance. A simple means of controlling movement could evolve through sensing (or learning to

sense) the time-to-closure of a motion-gap (termed *tau*) directly and using it to steer movement prospectively. *Tau* is the time before the animal (or its effectors) would reach its desired destination, at its current speed of approach. An organism's ability to exploit sensory information in its behavioural repertoire to attain its goals within environmental constraints is not only important with regards to arriving at intended destinations but to avoid collision with other objects, as well.

Evidence that the nervous system can represent an ecological affordance like *tau* has been provided by neurophysiological studies. A certain population of thalamic neurons (within nucleus rotundus) in pigeons responded to looming stimuli; their activities signalled (optical) *tau* and correlated with the creatures' startle response level (Sun, Frost 1998, Wang, Frost 1992). Neural activities in monkeys' motor and posterior parietal cortices were also found to be related to the *tau*-variable, and a varying percentage of neurons in these areas are significantly related to *tau* depending on the type of visual information about the interception target (Merchant, Battaglia-Mayer et al. 2004, Merchant, Georgopoulos 2006). In addition, a recent functional magnetic resonance imaging (fMRI) study also implicated the role of a fronto-parietal system in the perceptual judgements of time-to-contact in humans (Field, Wann 2005).

If the theory can be applied generally, prospective information like *tau* that has been shown to be useful in completing interceptions should also afford practical information for guiding non-interceptive movements. We were interested in whether the *tau* of simple, visually-directed, self-paced movements would also have a neural correlate in brain areas previously observed in studies that addressed the neural correlates of *tau* in avoidance/collision-perception and interceptive movements. We studied the neural representation of the *tau* of movement gaps (referred to as movement *tau* in this thesis) during non-interceptive movements in two parallel investigations. One study involved the multiple single-cell neurophysiological data recorded from the prefrontal and

parietal cortices of a behaving non-human primate during shape-copying performance. The other involved the time-varying neuromagnetic signals recorded during simple target-to-target movement performances in twenty healthy human volunteers. Both tasks can be regarded as involving the closure of motion gaps between targets (MEG Study) or between shape-corners of each copied shape (Shape Copying Study), and were therefore similar in nature.

These investigations are detailed in the following chapters. Chapter Two provides an outline of the General Tau Theory, which ends with the research motivation for the two separate but related inquiries to the neural representation of movement *tau*. Chapter Three details the investigation of the neural representation of movement *tau* involving the multiple single-cell activities recorded from the prefrontal and parietal (area 5) cortices of a behaving non-human primate engaged in a shape-copying task. The introduction in Chapter Three provides an overview of the anatomical, physiological, behavioural, and imaging studies pertaining to the parietal cortex and its implicated interaction with the frontal areas of the brain, alluding to the current appreciation that the dynamical parieto-frontal network is involved in the sensorimotor integration for purposeful behaviour.

An overview of neuroimaging, discussed in Chapter Four, focuses on magnetoencephalography (MEG), relevant issues of analyses related to the neuroimaging method, and analyses adopted in the research. This is followed in Chapter Five by the methodology of the studies conducted using the MEG technique. The second inquiry into the neural correlate of movement *tau*, described in Chapter Six, involves the time-varying neuromagnetic signals (simultaneously recorded at 248 sensor sites covering the whole brain using the MEG technique) during simple target-to-target movement performances by twenty healthy human volunteers. The study of the neural correlate of movement *tau* in humans offers a physiological explanation of

the reported involvement of the *tau-guide* in self-regulated behaviours. An additional part of the research, presented in Chapter Seven, investigates the synchronicity of neural ensembles by studying the relations of neuromagnetic signals between MEG sensors during the rest and performance sections of the target-to-target movement task. The stability and configuration of the dynamic interactions across the two task conditions are explored in our population of normal human volunteers. Finally, a summary of the findings, how the different parts of the investigation are related in general, and the potential applications of the findings and/or analyses are discussed in Chapter Eight.

These different techniques and approaches are complementary in the study of the processes that lead to the evolution of movements. The findings indicate that the variable *tau*, which is implicated in the active and dynamic sensorimotor dialogue during the guidance of self-regulated movement performance, is represented neurally.

Bibliography for this section

BERNSTEIN, N.A., 1967. The co-ordination and regulation of movements, Oxford; New York: Pergamon Press.

FIELD, D.T. and WANN, J.P., 2005. Perceiving time to collision activates the sensorimotor cortex. *Current Biology,* **15**(5), pp. 453-458.

FLASH, T. and HOGAN, N., 1985. The coordination of arm movements: an experimentally confirmed mathematical model. *The Journal of Neuroscience,* **5**(7), pp. 1688-1703.

LEE, D.N., 1998. Guiding Movement by Coupling Taus. *Ecological Psychology,* **10**(3&4), pp. 221-250.

MERCHANT, H., BATTAGLIA-MAYER, A. and GEORGOPOULOS, A.P., 2004. Neural responses during interception of real and apparent circularly moving stimuli in motor cortex and area 7a. *Cerebral Cortex,* **14**(3), pp. 314-331.

MERCHANT, H. and GEORGOPOULOS, A.P., 2006. Neurophysiology of perceptual and motor aspects of interception. *Journal of Neurophysiology,* **95**(1), pp. 1-13.

NAKANO, E., IMAMIZU, H., OSU, R., UNO, Y., GOMI, H., YOSHIOKA, T. and KAWATO, M., 1999. Quantitative examinations of internal representations for arm trajectory planning: minimum commanded torque change model. *Journal of Neurophysiology,* **81**(5), pp. 2140-2155.

SUN, H. and FROST, B.J., 1998. Computation of different optical variables of looming objects in pigeon nucleus rotundus neurons. *Nature Neuroscience,* **1**(4), pp. 296-303.

TODOROV, E. and JORDAN, M.I., 1998. Smoothness maximization along a predefined path accurately predicts the speed profiles of complex arm movements. *Journal of Neurophysiology,* **80**(2), pp. 696-714.

UNO, Y., KAWATO, M. and SUZUKI, R., 1989. Formation and control of optimal trajectory in human multijoint arm movement. Minimum torque-change model. *Biological cybernetics,* **61**(2), pp. 89-101.

WANG, Y. and FROST, B.J., 1992. Time to collision is signalled by neurons in the nucleus rotundus of pigeons. *Nature,* **356**(6366), pp. 236-238.

CHAPTER 2:

The General *Tau* Theory

Within the framework of the General *Tau* Theory, all behaviours are thought of as goal-directed actions that involve the closure of gaps between the current (or initial) point of action to the final intended goal. Where such gaps need to be closed within a certain time-frame, the temporal aspect of these gap-closures becomes pertinent information in guiding behaviour. For example, knowing when an object that is approaching at a head-on collision might hit you can help you avoid its impending impact appropriately. The precise timing of such avoidance responses was hypothesized to critically involve the variable *tau* (τ), which provides the temporal measure of the closure of motion gaps (e.g. the changing retinal image-size of the looming object or the changing distance between you and the approaching object) at their respective speed of closure (Lee 1976, Lee 1998). This is formally given as:

$$\tau_{(t)} = \frac{x_{(t)}}{\dot{x}_{(t)}} \qquad \text{EQ 2.1}$$

where x is the motion gap and $\dot{x}$ is the speed of the motion gap.

The optical variant of the *tau* variable is equivalent to the inverse of the relative rate of retinal expansion (Hoyle 1957, Lee 1976, Lee 1980), or the ratio between a small optical angle subtended by a looming object towards the observer and its rate of change. This has been shown to aptly describe, for example, the initiation of wing-folding manoeuvres of gannets plummeting into water (Lee, Reddish 1981), and landing behaviours in flies (Wagner 1982) predictably at a given 'threshold' value deemed salient for the specie. However, *tau* is not restricted to threshold responses nor is any information on motion gaps limited to that provided by changing optical input arrays (Lee 1998). Any given motion's frame of reference encompasses both body and environmental information, i.e. it is *expropriospecific* (Lee 1978, Lee 1980), and therefore, changes in sensory gaps of different modalities can, *in principle*, provide (or in Gibsonian (Gibson 1966) terms, '*afford'*) information about changes in motion gaps, or motion-gap *taus*. As such, inherent in this theory is that *tau* is a measure applicable to any motion-gap (be it described in terms of distance, angle, force, pitch frequency etc.) and that it can be directly perceived through any modality (e.g. vision, acoustics, haptics, force, echo-location etc.); if a sensory gap in a sensory array can be described as a power function of a motion-gap, the *tau* of the sensory gap can be informative of the tau of the motion-gap (Lee 1998).

This idea is in line with Bernstein's perspective of the '*movement-formulae*' (Bernstein 1967), which correspond to the "*intended form of the movement*". However, as Bernstein emphasised, such formulae should not be misunderstood as being in one-to-one correspondence with efferent commands for movements, because the influence from environmental forces is not always predictable, and different movements can be achieved through innervating the same muscles. Instead, the movement intention is more akin to an internal schema that is amenable to modulation and feedback from predictive sensory information like the *tau* variable.

Extending the ideas further, the theory proposed that the coordination of multiple processes can also be described in terms of gap closure. This is achieved by *tau-coupling*, wherein two (or more) *taus* remain at a constant ratio over some time. Thus, *tau-coupling* can ensure that both motion gaps (e.g. the changing gap between the moving object to a goal point and that between your hand and the moving object, or a sensory gap and a motion gap) close at the same time, if so desired. When *tau*-coupled, the relationship between the *taus* of the two motion gaps can be described as:

$$\tau_{x(t)} = k\,\tau_{y(t)} \qquad \text{EQ 2.2}$$

where k is the coupling (or gain) constant. Support for *tau*-coupling has been demonstrated behaviourally in echo-locating bats (Lee, Simmons et al. 1995, Lee, van der Weel et al. 1992), which appeared to *tau*-couple the acoustically sensed distance-to-perch gap and the angular action-gap (i.e. the angle between the bat's path of approach and the direct line between the bat and the perch), and the hand-to-mouth and associated angular action-gap (in this case, the angle between the hand's path and the direct line between the hand and mouth) movements in feeding studies (Lee, Craig et al. 1999). Similarly, *tau*-coupling was demonstrated in interceptive tasks (Lee, Georgopoulos et al. 2001) where human participants appeared to *tau*-couple the hand-to-target and target-to-goal gaps.

In addition to externally cued behaviour, it has also been proposed that many skilled and self-regulated movements are governed by or follow the form of a "generalized" process that is internally generated (*intrinsic*), denoted the *tau-guide* (τ_g) onto which *taus* of motion-gaps are coupled (Lee 1998):

$$\tau_{x(t)} = k\tau_{g(t)} \qquad \text{EQ 2.3}$$

In general, motion gaps can be closed in different ways. Two basic forms of gap closure can be described: a *deceleration-only* way as, for example, when a driver brakes to stop before an automobile in front, and another, an *accelerating-then-decelerating* manner, as when one reaches out from rest to an object of interest. These two types of gap closures can both be *tau*-guided although their respective *intrinsic tau*-guides (which are based on Newton's Laws of motion) take different forms mathematically.

In the *decelerating-only* manner, the *tau* of an intrinsic gap $(\tau_{g_D(t)})^I$ is formally given as:

$$\tau_{g_D(t)} = t/2 \qquad \text{EQ 2.4}$$

where t is zero when the goal is reached. When the *tau* of motion gap $(\tau_{d(t)})$ is coupled to $\tau_{g_D(t)}$ (EQ2.5) it is as though the rate of change of the *tau* of this gap is kept at a constant value (EQ2.6):

$$\tau_{d(t)} = k\tau_{g_D(t)} = k\ t/2 \qquad \text{EQ 2.5}$$

$$\frac{\tau_{d(t)}}{t} = \dot{\tau}_d = \frac{k}{2} \qquad \text{EQ 2.6}$$

Lee (1976) termed this as *tau-dot* $(\dot{\tau}_d)$ and its involvement in controlling braking has since been tested in real (Bardy, Warren 1997, Rock, Harris et al. 2006) and simulated driving tasks (Yilmaz, Warren 1995). These braking studies showed that rather than keeping *tau-dot* strictly constant, it fluctuates about a margin depending on task conditions and current velocity.

In the *accelerating-then-decelerating* scenario, as is in most action gaps which start from rest, the *tau* of an intrinsic gap ($\tau_{g_{A-D}(t)}$)[II] is formally given as:

$$\tau_{g_{A-D}(t)} = \frac{1}{2}\left(t - \frac{T^2}{t}\right) \qquad \text{EQ 2.7}$$

where t is the instantaneous time from the action onset and is zero when the goal is reached, while T is the duration of the whole movement.

Therefore, to reiterate, $\tau_{g_D(t)}$ and $\tau_{g_{A-D}(t)}$ are two forms of intrinsic *tau*-guidance (τ_g). When motion gaps are τ_g-coupled, the constant k is related to the kinematics (speed profile) of gap closure for $k > 0$. When $0 < k \leq 0.5$ the speed profile peaks at the start of the movement and gap closure is gentle, with speed reaching zero at the goal. When $0.5 < k < 1$ the speed profile peaks towards the end of the movement and while the final approach is decelerative, it is progressively harsher with increase in the value of k. In this scenario, the final speed does not reach zero at the goal. When $k \geq 1$, the final approach is accelerative and the closure of gaps is achieved with great impact, i.e. collision occurs; the impact is progressively harsher with increase in k (FIG 2.1). In other words, one could also describe the varied characteristics of motion closure that follows a *tau*-guide.

Investigations into whether skilled movements are *tau*-coupled onto the *tau*-guide have been performed in a few behavioural studies. *Tau*-guidance was demonstrated in the control of intra-oral pressure during infants' nutritive sucking (and relaxing) of the teat to draw milk from the bottle (Craig, Grealy et al. 2000, Craig, Lee 1999, Lee 2005, Lee, Craig et al. 1999). It was also observed in the control of golfers' putting swing (Craig, Delay et al. 2000), wherein, as a means of spatial scaling, the forward swing time may

be kept constant while the *tau*-coupling constant is varied proportionally to the required putting distance. Higher *tau*-coupling constants (*k*) were linearly associated with longer putting distances as well as larger mean amplitudes of the forward swings. This indirectly alters the putting velocity, acceleration and required force between the golf-club and ball at impact (Craig, Delay et al. 2000).

In these cases, the measured strength of *tau-coupling* as indicated by the percentage of the *tau* of the movement gap being coupled onto the *tau-guide* was reportedly close to 100%. The percentage of *tau-coupling* is determined by the proportion of movement data relative to the whole length of movement segment, which accounted for the derived linear regression between *tau* of the movement gap and the *tau-guide* satisfying a regression R^2 – the proportion of variance explained – of no less than 0.95, without which the regression is recursively repeated with the exclusion of a pair of *tau-guide* and movement *tau* variables from movement onset, until the R^2 criteria is met (this is further elaborated in the Shape Copying Study in Chapter 3 and the methods section for the MEG Study in Chapter 5).

The observed high percentages of *tau-coupling* have been interpreted as evidence for the existence of such an intrinsic guide. In addition, the strength of *tau-coupling* was much lower for preterm babies having difficulties in controlling their intra-oral sucking pressure, as demonstrated by Craig & Lee (2000). Therefore, these studies also showed the potential of the *tau*-guide model being applied in clinical diagnostics and sportsmanship training, to measure the poor guidance of unskilled movements and how experience may improve them.

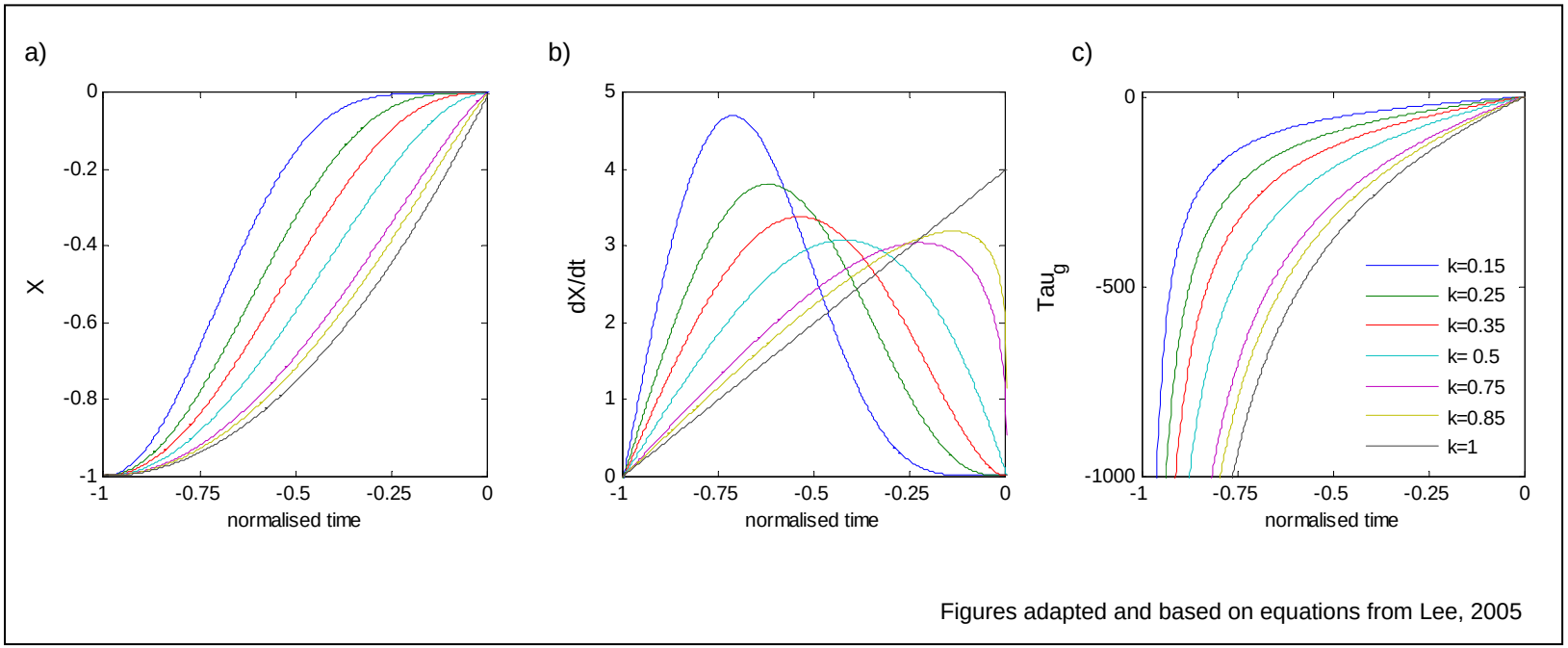

FIG 2.1: Kinematics of τ_g-guided gap closure. (a) Motion gaps (X) which are τ_g-coupled manifest differing dynamics, which can be described by the parameter *k*. These dynamics are better illustrated by the motion gaps' respective speed profiles (dX/dt) in (b). Plots of motion gaps' τ_x with different *k* values are illustrated in (c). The tau (τ) of each of the motion gaps is defined as $\tau = \frac{x}{\dot{x}}$; where x is the varying motion gap, and $\dot{x}$ is the rate of closure of the motion gap x.

– Putative Forms of Tau

Given that all behaviours are, in part, the consequence of neural processes, working with the body, there can, in general, be various putative forms of neural information which provide changing values of *tau* information in guiding goal-directed behaviours. As many skilled behaviours that are biologically finite (involving a definite start and end point) have been shown to be related to the *tau*-guide, it has since been supposed that the neural correlate of such an intrinsic guide ought to be of the same dynamical form; specifically:

"the neural information directing movement resides in the *taus* of neural action-gaps (the gap between the present level of neural current and a goal level), and not in the amplitude of neural current (often measured as spike-rate), as is frequently assumed.",

Lee (2007, *personal communication*)

This idea is formally described by the relation:

$$\tau_{x(t)} = k\,\tau_{N(t)} \qquad \text{EQ 2.8}$$

where τ_N denotes the *tau* of a putative neural gap and as before, k is the coupling constant.

The feasibility of this hypothesis is currently being explored by Lee, Georgopoulos et al. (2007) in single-cell electrophysiological recordings in the motor and parietal cortices associated with highly-trained reaching movements in monkeys. In the time-lagged linear regression analyses of the averaged activities of neural ensembles, the *tau* of a putative neural gap (i.e. the gap between the present level of neural current and a

goal level) was found to correlate highly to the movement-*tau* and the theoretical *tau-guide* at approximately 25ms prior to movement onset in the motor cortex (M1) and about 135ms after movement onset in area 5 of the parietal cortex. However, there were other temporal shifts that yielded equally high R^2 values in the regression analyses apart from these that occurred closest to the movement onset. An account of the different time indices for the onset of the putative neural-*tau* coming into play especially with reference to known and /or possible neurophysiological processes would be useful, particularly since temporal profile of neural activities are known to be modulated by context and expectancy (Asaad, Rainer et al. 1998). Conceptually, it is conceivable that these different highly correlated temporal sections could hypothetically be a reflection of the different portions of the '*movement-formulae*' (Bernstein 1967, Lashley 1951) being fine-tuned and integrated into the global intention, or 'task'. It is nonetheless difficult to determine, at present and experimentally, what a neural representation of an intended gap-closure in the form of a neural gap would be.

Another putative neural representation of *tau* could also be in the form of a composite neural representation that combines the information from the neural representations of motion gaps (N_{gap}) and that of the rate of change of such gaps (e.g. speed; N_{gap_speed}) to provide *tau* information (N_{τ}), was proposed by Georgopoulos (2007):

$$N_{\tau(t)} \approx \frac{N_{gap(t)}}{N_{gap\_speed(t)}} \qquad \text{EQ 2.9}$$

While our current understanding of the neural correlates of control for amplitudes and speeds of movements is still inadequate, available neurophysiological studies have shown that areas of the brain e.g. neural activities in the middle temporal area (MT) are tuned to direction-specific motions at different speeds (Maunsell, Van Essen 1983),

and activities in motor and parietal cortices have also been demonstrated to represent movement kinematics, including direction and speed (Averbeck, Chafee et al. 2005, Georgopoulos, Kalaska et al. 1982, Moran, Schwartz 1999). It remains to be elucidated whether a composite neural correlate of *tau* exists.

A different and more general concept of the putative neural correlate is adopted here. The dynamics of neural activities are presumed to be in some way related to the integrated temporo-spatial unfolding of movements; either as a correlate of the time-varying sensory *tau* information picked up to guide ongoing action in time, and /or as part of the anticipatory neural information that is integrated into the 'movement-formulae' directing the muscles to modify the *taus* of motion gaps as intended. Therefore, it is <u>not</u> assumed in this work that the neural correlate takes a specific form, for example, as that of the *tau* of a putative neural gap as specified by Lee (2007; *personal communication cited above*), or as a composite of neural correlates of movement speed and amplitudes (Georgopoulos, 2007).

– *Neurophysiological Studies*

Behavioural studies in both animals and humans have demonstrated that *tau* information is used in guiding actions, and a number of neurophysiological studies (see review by Merchant, Georgopoulos 2006) have investigated whether brain activities underlying visuo-motor task performance might also be shown to involve the variable *tau*. The earliest of these investigations was by Frost and colleagues who first classified a certain population of neurons in the pigeon's thalamic nucleus rotundus that responded to looming stimuli and such responses correlated with physiological effects of increased heart-rate and muscle contractions related to avoidance response (Wang, Frost 1992). Subsequently, Sun & Frost (1998) delineated three subgroups

within these neurons whose activities were found to relate to three different optical variables. In one subgroup, neurons fired consistently at a 'threshold' period before collision regardless of velocity or size of the stimuli; their activities are related to the relative expansion rates; the inverse of which is equivalent to the variable *tau* (τ). The activities of another subgroup of neurons are modulated by the absolute expansion rate (ϱ) and the responses of the third subgroup of neurons peaked earlier to larger and faster approaching stimuli. These latter neurons appeared to respond to the complex optical variable (η), which has been used to model the collision avoidance response of locusts' lobular giant-movement detector (LGMD) neurons (Hatsopoulos, Gabbiani et al. 1995, Rind, Simmons 1999). The computation of τ and η depends on the absolute rate of expansion (ϱ), and their ecological functions may be to provide '*time-to-contact*' or early warning signals for approaching objects (Sun, Frost 1998).

The nucleus rotundus of the pigeon is homologous to the mammalian lateral posterior and pulvinar thalamic nuclei (LP-PUL), which have reciprocal connections to posterior parietal areas 5 and 7 (Baldauf, Chomsung et al. 2005, Jones, Coulter et al. 1978, Jones, Wise et al. 1979, Petras 1971). Apart from cortico-thalamic connections, these parietal regions are reciprocally connected to multiple sensorimotor areas in the frontal brain (e.g. areas 4, 6; refer to the review by Hyvärinen 1982, and Battaglia-Mayer, Archambault et al. 2006). Parietal-frontal areas (e.g. Areas 5 and 7a of the parietal cortex, motor, and premotor cortices) are known to be involved in the kinaesthetic and kinematic representations of spatial information relevant for planning and guiding movement (Duffy, Burchfiel 1971, Kalaska 1988, Kalaska, Caminiti et al. 1983), and in the processing of optic flow (Battaglia-Mayer, Caminiti et al. 2003, Duffy, Wurtz 1991, Marconi, Genovesio et al. 2001, Merchant, Battaglia-Mayer et al. 2001, Merchant, Battaglia-Mayer et al. 2003a, Siegel, Read 1997). These findings prompted studies to investigate whether neural processes within these regions might also involve similar collision-detection or *tau* signalling mechanisms in non-human primates.

To that end, studies (Lee, Port et al. 1997, Lee, Port et al. 2001, Merchant, Battaglia-Mayer et al. 2003b, Merchant, Battaglia-Mayer et al. 2004a, Merchant, Battaglia-Mayer et al. 2004b, Port, Kruse et al. 2001, Port, Lee et al. 1997) have explored the plausible neural correlates using interception tasks. Intercepting moving objects, like avoiding impending collision, is an ecologically relevant adaptive behaviour in which prospective control is crucial for success. As the variable *tau* can provide prospective gap-closure information, it can potentially play an important role in interceptive tasks. Although psychometric performance of humans and monkeys (Lee, Port et al. 1997, Port, Lee et al. 1997, van Donkelaar, Lee et al. 1992) during target interception highlighted that task requirements, for example, accuracy demands, duration of movement allowed, target's kinematics (e.g. fast vs. slow targets), and subjective strategic preferences (e.g. reactive–threshold-distance model vs. predictive–threshold-*tau* model) are important in initiating and achieving the interception, *tau*-coupling of motion gaps can also adequately describe how subjects achieve interception: by keeping the *taus* of the hand-to-target and the target-to-goal gaps in a constant ratio (Lee, Georgopoulos et al. 2001). Therefore, as has been explained, by constantly sensing the *taus* of gaps (e.g. those between effectors and goals) a subject can guide movements with the appropriate kinematics to keep the *taus* coupled for gap closure, and achieve interception.

Early neurophysiological studies by Port et al. (2001) and Lee et al. (2001b) using a Go/NoGo paradigm demonstrated that activities of subgroups of motor cortical (M1) cells are modulated by the kinematics (e.g. target direction, acceleration, total movement time, initial target velocity) of the moving target. In addition, the time-varying activities of M1 neurons also varied with the estimate of movement *tau* (Port et al., 2001). These findings highlighted that the M1 has access to relevant sensorimotor transformations for interceptive behaviour and the *tau* of the gap

between hand and interception destination could be dynamically represented in M1 and used in controlling interception. Subsequent studies in both motor (M1) and parietal (7a) cortical areas by Merchant et al. (2004a, b) demonstrated that neurons sensitive to sensory and/or motor aspects of the (Go/NoGo) interception task can be found in both parietal and frontal areas. Nonetheless a predominance of M1 activity was triggered by hand-related interceptive movements, while parietal activity was largely linked to the sensory features of the moving stimulus, for example, stimulus angular position.

Importantly, neural activities in both areas are modulated by task features; where task-targets could move at different angular velocities and manifest either real (continuously present visual angular position), or apparent (intermittently present visual angular position) motion. Neuron activity in the motor cortex was highly correlated to movement hand force during real-motion-target interception, while parietal activities were highly associated with stimulus angular position in the same condition. During apparent-motion interceptions, the largest proportion of motor cortical activity was best explained by their association to *tau*. As for parietal neurons, *tau* was the second best explanatory parameter following stimulus angular position. Furthermore, the activities of those neurons, best characterised by the *tau* variable, increased in an inversely proportional way to the decreasing time-to-contact between target and interception-zone. Such *tau*-ramps, observed in parietal and (especially in) motor areas, are neural correlates of 'time-to-contact' of motion gaps and are useful signals for initiating interception. Interestingly, similar ramping activities have also been observed in the lateral-inferior parietal (LIP) neurons of the posterior parietal cortex (Leon, Shadlen 2003), which varied systematically with the monkey's perception of elapsed time.

These neurophysiological findings are complemented by those from a recent

functional magnetic resonance imaging (fMRI) study that showed the activation of sensorimotor areas and motion-sensitve area MT during perceptual judgements of 'time-to-collision' in humans (Field, Wann 2005). Specifically, the study consisted of three conditions, each with a different type of stimulus involving two objects approaching or expanding at different velocities: 1) looming (L), 2) horizontal gap-closure of objects approaching a vertical mid-line (GC), and 3) lateral image-expansion (IE). Participants of the study had to indicate which of the two moving or expanding objects would arrive first. The investigators found that after accounting for the visual responses (i.e. using IE-task as the control condition in the contrast analyses), the looming stimulus-activated brain areas consisted primarily of supplementary motor area (SMA), M1, somatosensory association, and premotor areas that are thought to be the targets of the dorsal visual stream implicated in action (as opposed to the ventral visual stream implicated in perception; Goodale, Milner 1992). Moreover, activations in these areas have also been documented in reaching (Binkofski, Dohle et al. 1998, Simon, Mangin et al. 2002) and grasping (Culham, Danckert et al. 2003, Culham, Valyear 2006, Grafton, Fagg et al. 1996).

Interestingly, in addition to the weaker activations within the sensorimotor regions observed during the gap-closure task, the task elicited the unique involvement of the ventral portion of the premotor cortex, the bilateral superior parietal sulci, and the marginal ramus; areas implicated in cognitive processing to solve visuo-spatial tasks (Buneo, Andersen 2006, Graziano, Cooke 2006, Kakei, Hoffman et al. 2001). It should be noted that the gap-closure task of this fMRI study is similar to the interceptive tasks used in the above-mentioned neurophysiological studies apart from the required interception. Therefore, in both the perception of gap-closures and in the participation of closing gaps during interception, the parietal and motor areas are actively involved.

Research Motivation

These studies have demonstrated that sensorimotor systems are also involved in the perception of 'time-to-gap-closure' and they suggest that the association areas of the brain are involved in similar temporal representation of actions. Given that the tasks used in these studies involved explicit, temporally salient stimuli (e.g. looming and moving targets, which needed to be intercepted within a temporal constraint), the question remains as to whether the neural underpinnings for the perception of 'time-to-gap-closure' documented in the sensorimotor areas are specific to these stimuli remains. Would the neural mechanisms underlying movements that are not temporally constrained by external cues also involve the *tau* variable? If *tau* is a variable that is useful for guiding self-regulated actions, they should do so.

In addition, are there other neural areas, apart from those identified in the above neurophysiological studies, involved in the processing or representation of *tau*? Furthermore, while the behaviour and movements of human agents in many tasks have been shown to be *tau*-guided, a neural correlate of *tau* during self-regulated movement performance has not been demonstrated in humans. These questions are important. Neurophysiological evidence, either in support for or against the numerous behavioural studies that have implicated the hypothesis that the *tau* function governs self-regulated actions, would further our understanding of the theory, and clarify its potential and limitations.

The Present Research

In this research, the neural representation of the *tau* variable was investigated in two sets of experiments. In one study, the neuromagnetic fluxes (using magnetoencephalography, MEG) from the whole brain of human participants were recorded while they performed self-paced discrete hand movements aimed to stationary targets in space. In the other study, the recordings of single-cell activity from prefrontal and posterior parietal areas of a behaving monkey were performed during geometrical shape-copying tasks. The tasks involved self-regulated movements that can be described as closing motion gaps between targets (MEG Study) or between shape-corners for each shape segment (Shape Copying Study) and are therefore similar.

In both studies, the questions asked were:

Q: Are the movements *tau*-guided?

Q: Is there a neural correlate of the variable *tau* (henceforth denoted as movement *tau*) during the self-paced movements?

Q: If so, to what extent does the neural signal associated with movement *tau* vary in relation to movement speed, a prominent motor variable encoded by neural activities?

These two studies provided complementary information. The MEG study with humans covered the whole brain with (coarse) general localization in large areas, whereas the neurophysiological study of a monkey tapped the finest neural grain in limited brain regions. Together, the two studies yielded valuable insights concerning the dynamic, time-varying neural representation of *tau*, with respect to both integrated synaptic events in large neuronal ensembles (recorded by MEG) and neural spike outputs of single cells recorded by microelectrodes.

Bibliography for this section:

ASAAD, W.F., RAINER, G. and MILLER, E.K., 1998. Neural activity in the primate prefrontal cortex during associative learning. *Neuron,* **21**(6), pp. 1399-1407.

AVERBECK, B.B., CHAFEE, M.V., CROWE, D.A. and GEORGOPOULOS, A.P., 2005. Parietal representation of hand velocity in a copy task. *Journal of Neurophysiology,* **93**(1), pp. 508-518.

BALDAUF, Z.B., CHOMSUNG, R.D., CARDEN, W.B., MAY, P.J. and BICKFORD, M.E., 2005. Ultrastructural analysis of projections to the pulvinar nucleus of the cat. I: Middle suprasylvian gyrus (areas 5 and 7). *Journal of Comparative Neurology,* **485**(2), pp. 87-107.

BARDY, B.G. and WARREN, W.H.,JR, 1997. Visual control of braking in goal-directed action and sport. *Journal of Sports Sciences,* **15**(6), pp. 607-620.

BATTAGLIA-MAYER, A., ARCHAMBAULT, P.S. and CAMINITI, R., 2006. The cortical network for eye-hand coordination and its relevance to understanding motor disorders of parietal patients. *Neuropsychologia,* **44**(13), pp. 2607-2620.

BATTAGLIA-MAYER, A., CAMINITI, R., LACQUANITI, F. and ZAGO, M., 2003. Multiple Levels of Representation of Reaching in the Parieto-frontal Network. *Cerebral Cortex,* **13**(10), pp. 1009-1022.

BERNSTEIN, N.A., 1967. The co-ordination and regulation of movements, Oxford; New York: Pergamon Press.

BINKOFSKI, F., DOHLE, C., POSSE, S., STEPHAN, K.M., HEFTER, H., SEITZ, R.J. and FREUND, H.J., 1998. Human anterior intraparietal area subserves prehension: a combined lesion and functional MRI activation study. *Neurology,* **50**(5), pp. 1253-1259.

BUNEO, C.A. and ANDERSEN, R.A., 2006. The posterior parietal cortex: sensorimotor interface for the planning and online control of visually guided movements. *Neuropsychologia,* **44**(13), pp. 2594-2606.

CRAIG, C.M., DELAY, D., GREALY, M.A. and LEE, D.N., 2000. Guiding the swing in golf putting. *Nature,* **405**(6784), pp. 295-296.

CRAIG, C.M., GREALY, M.A. and LEE, D.N., 2000. Detecting motor abnormalities in preterm infants. *Experimental Brain Research,* **131**(3), pp. 359-365.

CRAIG, C.M. and LEE, D.N., 1999. Neonatal control of nutritive sucking pressure: evidence for an intrinsic tau-guide. *Experimental Brain Research,* **124**(3), pp. 371-382.

CULHAM, J.C., DANCKERT, S.L., DESOUZA, J.F., GATI, J.S., MENON, R.S. and GOODALE, M.A., 2003. Visually guided grasping produces fMRI activation in dorsal but not ventral stream brain areas. *Experimental Brain Research,* **153**(2), pp. 180-189.

CULHAM, J.C. and VALYEAR, K.F., 2006. Human parietal cortex in action. *Current Opinion in Neurobiology,* **16**(2), pp. 205-212.

DUFFY, C.J. and WURTZ, R.H., 1991. Sensitivity of MST neurons to optic flow stimuli. I. A continuum of response selectivity to large-field stimuli. *Journal of Neurophysiology,* **65**(6), pp. 1329-1345.

DUFFY, F.H. and BURCHFIEL, J.L., 1971. Somatosensory system: organizational hierarchy from single units in monkey area 5. *Science,* **172**(980), pp. 273-275.

FIELD, D.T. and WANN, J.P., 2005. Perceiving time to collision activates the sensorimotor cortex. *Current Biology,* **15**(5), pp. 453-458.

GEORGOPOULOS, A.P., 2007. A tribute to tau. In: G.-. PEPPING and M.A. GREALY, eds, *Closing the Gap The Scientific Writings of David N. Lee.* Lawrence Erlbaum Assoc Inc., pp. 157-161.

GEORGOPOULOS, A.P., KALASKA, J.F., CAMINITI, R. and MASSEY, J.T., 1982. On the relations between the direction of two-dimensional arm movements and cell discharge in primate motor cortex. *Journal of Neuroscience,* **2**(11), pp. 1527-1537.

GIBSON, J.J., 1966. The senses considered as perceptual systems. Boston: Houghton Mifflin.

GOODALE, M.A. and MILNER, A.D., 1992. Separate visual pathways for perception and action. *Trends in Neurosciences,* **15**(1), pp. 20-25.

GRAFTON, S.T., FAGG, A.H., WOODS, R.P. and ARBIB, M.A., 1996. Functional anatomy of pointing and grasping in humans. *Cerebral Cortex,* **6**(2), pp. 226-237.

GRAZIANO, M.S. and COOKE, D.F., 2006. Parieto-frontal interactions, personal space, and defensive behavior. *Neuropsychologia,* **44**(13), pp. 2621-2635.

HATSOPOULOS, N., GABBIANI, F. and LAURENT, G., 1995. Elementary computation of object approach by wide-field visual neuron. *Science,* **270**(5238), pp. 1000-1003.

HOYLE, F., 1957. The black cloud. New York: Harper.

HYVÄRINEN, J., 1982. Posterior Parietal Lobe of the Primate Brain. *Physiological Reviews,* **62**(3), pp. 1060-1129.

JONES, E.G., COULTER, J.D. and HENDRY, S.H., 1978. Intracortical connectivity of architectonic fields in the somatic sensory, motor and parietal cortex of monkeys. *Journal of Comparative Neurology,* **181**(2), pp. 291-347.

JONES, E.G., WISE, S.P. and COULTER, J.D., 1979. Differential thalamic relationships of sensory-motor and parietal cortical fields in monkeys. *Journal of Comparative Neurology,* **183**(4), pp. 833-881.

KAKEI, S., HOFFMAN, D.S. and STRICK, P.L., 2001. Direction of action is represented in the ventral premotor cortex. *Nature Neuroscience,* **4**(10), pp. 1020-1025.

KALASKA, J.F., 1988. The representation of arm movements in postcentral and parietal cortex. *Canadian Journal of Physiology and Pharmacology,* **66**(4), pp. 455-463.

KALASKA, J.F., CAMINITI, R. and GEORGOPOULOS, A.P., 1983. Cortical mechanisms related to the direction of two-dimensional arm movements: relations in parietal area 5 and comparison with motor cortex. *Experimental Brain Research,* **51**(2), pp. 247-260.

LASHLEY, K., 1951. The problem of seiral order in behaviour. In: L.A. JEFFRESS, ed, *Cerebral mechanisms in behavior : the Hixon Symposium.* New York: Wiley, pp. pp 112-136.

LEE, D., PORT, N.L. and GEORGOPOULOS, A.P., 1997. Manual interception of moving targets. II. On-line control of overlapping submovements. *Experimental Brain Research,* **116**(3), pp. 421-433.

LEE, D., PORT, N.L., KRUSE, W. and GEORGOPOULOS, A.P., 2001. Neuronal clusters in the primate motor cortex during interception of moving targets. *Journal of Cognitive Neuroscience,* **13**(3), pp. 319-331.

LEE, D.N., 2005. Tau in Action in Development. In: J.J. RIESER, J.J. LOCKMAN and C.A. AND NELSON, eds, *Action as an Organiser of Learning.* Hillsdale, N.J.: Erlbaum., .

LEE, D.N., 1998. Guiding Movement by Coupling Taus. *Ecological Psychology,* **10**(3&4), pp. 221-250.

LEE, D.N., 1980. The optic flow field: the foundation of vision. *Philosophical Transactions of the Royal Society of London.Series B, Biological sciences,* **290**(1038), pp. 169-179.

LEE, D.N., 1978. The functions of vision. In: H.L. PICK and E. SALTZMAN, eds, *Modes of Perceiving and Processing Information.* Hillsdale, N.J.: Erlbaum Assoc., pp. 159-170.

LEE, D.N., 1976. A theory of visual control of braking based on information about time-to-collision. *Perception,* **5**(4), pp. 437-459.

LEE, D.N., CRAIG, C.M. and GREALY, M.A., 1999. Sensory and intrinsic coordination of movement. *Proceedings of the Royal Society B: Biological Sciences,* **266**(1432), pp. 2029-2035.

LEE, D.N., GEORGOPOULOS, A.P., LEE, T.M. and PEPPING, G.-., 2007. A theory of neural guidance of movement based on *tau*..

LEE, D.N., GEORGOPOULOS, A.P., CLARK, M.J., CRAIG, C.M. and PORT, N.L., 2001. Guiding contact by coupling the taus of gaps. *Experimental Brain Research,* **139**(2), pp. 151-159.

LEE, D.N. and REDDISH, P.E., 1981. Plummeting gannets: a paradigm of ecological optics. *Nature,* **293**, pp. 293-294.

LEE, D.N., SIMMONS, J.A., SAILLANT, P.A. and BOUFFARD, F., 1995. Steering by echolocation: a paradigm of ecological acoustics. *Journal of Comparative Physiology. A: Sensory, Neural, and Behavioral Physiology,* **176**(3), pp. 347-354.

LEE, D.N., VAN DER WEEL, F.R., HITCHCOCK, T., MATEJOWSKY, E. and PETTIGREW, J.D., 1992. Common principle of guidance by echolocation and vision. *Journal of Comparative Physiology. A: Sensory, Neural, and Behavioral Physiology,* **171**(5), pp. 563-571.

LEON, M.I. and SHADLEN, M.N., 2003. Representation of time by neurons in the posterior parietal cortex of the macaque. *Neuron,* **38**(2), pp. 317-327.

MARCONI, B., GENOVESIO, A., BATTAGLIA-MAYER, A., FERRAINA, S., SQUATRITO, S., MOLINARI, M., LACQUANITI, F. and CAMINITI, R., 2001. Eye-Hand Coordination during Reaching. I. Anatomical Relationships between Parietal and Frontal Cortex. *Cerebral Cortex,* **11**(6), pp. 513-527.

MAUNSELL, J.H. and VAN ESSEN, D.C., 1983. Functional properties of neurons in middle temporal visual area of the macaque monkey. I. Selectivity for stimulus direction, speed, and orientation. *Journal of Neurophysiology,* **49**(5), pp. 1127-1147.

MERCHANT, H., BATTAGLIA-MAYER, A. and GEORGOPOULOS, A.P., 2004a. Neural responses during interception of real and apparent circularly moving stimuli in motor cortex and area 7a. *Cerebral Cortex,* **14**(3), pp. 314-331.

MERCHANT, H., BATTAGLIA-MAYER, A. and GEORGOPOULOS, A.P., 2004b. Neurophysiology of the parieto-frontal system during target interception. *Neurology & Clinical Neurophysiology,* **2004**, pp. 1.

MERCHANT, H., BATTAGLIA-MAYER, A. and GEORGOPOULOS, A.P., 2003a. Functional organization of parietal neuronal responses to optic-flow stimuli. *Journal of Neurophysiology,* **90**(2), pp. 675-682.

MERCHANT, H., BATTAGLIA-MAYER, A. and GEORGOPOULOS, A.P., 2003b. Interception of real and apparent motion targets: psychophysics in humans and monkeys. *Experimental Brain Research,* **152**(1), pp. 106-112.

MERCHANT, H., BATTAGLIA-MAYER, A. and GEORGOPOULOS, A.P., 2001. Effects of optic flow in motor cortex and area 7a. *Journal of Neurophysiology,* **86**(4), pp. 1937-1954.

MERCHANT, H. and GEORGOPOULOS, A.P., 2006. Neurophysiology of perceptual and motor aspects of interception. *Journal of Neurophysiology,* **95**(1), pp. 1-13.

MORAN, D.W. and SCHWARTZ, A.B., 1999. Motor cortical representation of speed and direction during reaching. *Journal of Neurophysiology,* **82**(5), pp. 2676-2692.

PETRAS, J.M., 1971. Connections of the parietal lobe. *Journal of Psychiatric Research,* **8**(3), pp. 189-201.

PORT, N.L., KRUSE, W., LEE, D. and GEORGOPOULOS, A.P., 2001. Motor cortical activity during interception of moving targets. *Journal of Cognitive Neuroscience,* **13**(3), pp. 306-318.

PORT, N.L., LEE, D., DASSONVILLE, P. and GEORGOPOULOS, A.P., 1997. Manual interception of moving targets. I. Performance and movement initiation. *Experimental Brain Research,* **116**(3), pp. 406-420.

RIND, F.C. and SIMMONS, P.J., 1999. Seeing what is coming: building collision-sensitive neurones. *Trends in Neurosciences,* **22**(5), pp. 215-220.

ROCK, P.B., HARRIS, M.G. and YATES, T., 2006. A test of the tau-dot hypothesis of braking control in the real world. *Journal of Experimental Psychology: Human Perception and Performance.,* **32**(6), pp. 1479-1484.

SIEGEL, R.M. and READ, H.L., 1997. Analysis of optic flow in the monkey parietal area 7a. *Cerebral Cortex,* **7**(4), pp. 327-346.

SIMON, O., MANGIN, J.F., COHEN, L., LE BIHAN, D. and DEHAENE, S., 2002. Topographical layout of hand, eye, calculation, and language-related areas in the human parietal lobe. *Neuron,* **33**(3), pp. 475-487.

SUN, H. and FROST, B.J., 1998. Computation of different optical variables of looming objects in pigeon nucleus rotundus neurons. *Nature Neuroscience,* **1**(4), pp. 296-303.

VAN DONKELAAR, P., LEE, R.G. and GELLMAN, R.S., 1992. Control strategies in directing the hand to moving targets. *Experimental Brain Research,* **91**(1), pp. 151-161.

WAGNER, H., 1982. Flow-field variables trigger landing in flies. *Nature,* **297**, pp. 147-148.

WANG, Y. and FROST, B.J., 1992. Time to collision is signalled by neurons in the nucleus rotundus of pigeons. *Nature,* **356**(6366), pp. 236-238.

YILMAZ, E.H. and WARREN, W.H.,JR, 1995. Visual control of braking: a test of the tau hypothesis. *Journal of Experimental Psychology: Human Perception and Performance,* **21**(5), pp. 996-1014.

N*ote:* _____

[1] The derivation of *decelerating* intrinsic *tau*-guide ($\tau_{g_D(t)}$) is based on the following equations of motion:

$$d = \mu t - \tfrac{1}{2} a t^2 \quad (2.i)$$

$$s = \mu - at \quad (2.ii)$$

where d is the distance to goal, μ is the initial rate of change (speed), a is the second order of rate of change (i.e. acceleration, is a negative value) is assumed constant in this case, and t is the instantaneous time and s is the instantaneous speed. Given that μ is zero, the equations are thus simplified as:

$$d = -\tfrac{1}{2} a t^2 \quad (2.iii)$$

$$s = -at \quad (2.iv)$$

And therefore:

$$\tau_{g_D(t)} = d/s = t/2 \quad (2.v)$$

where t is zero at the goal as time is referenced relative to the goal; it starts from negative total movement time and moves positively towards zero when the goal is reached.

[II] The derivation of *accelerating-then-decelerating tau*-guide ($\tau_{g_{A-D}(t)}$) is based also on the equations of motion (2.i) to (2.iv) in footnote [I].

In the scenario of an *accelerating-then-decelerating* motion gap, one can think of the initial distance to goal as the 'total' distance to cover ($d_{T_{(t=0)}}$), assuming that the trajectory of motion towards a goal is relatively straight. After time t the distance travelled would be ($d_{(t)}$). The actual distance left to be covered (D) or '*gap-to-goal*', can therefore be expressed as:

$$D = \tfrac{1}{2} a T^2 - \tfrac{1}{2} a t^2 \quad (2.vi)$$

In other words, the *gap-to-goal* gets progressively smaller as the distance travelled increases with time. The rate of change of this gap D is given by equation (iv) above, and hence:

$$\tau_{g_{A-D}(t)} = \left(\frac{\tfrac{1}{2} a T^2 - \tfrac{1}{2} a t^2}{-at} \right) = -\tfrac{1}{2} \left(-\frac{t^2}{t} + \frac{T^2}{t} \right) = \tfrac{1}{2} \left(t - \frac{T^2}{t} \right) \quad (2.vii)$$

In the formula, t is zero at the start and *T* at the end. Hence τ_g is infinite at the start and zero at the end.

CHAPTER 3:

Parietal and Prefrontal Neural Representations of Movement *Tau*

Introduction

The coordination of a visually guided movement, such as reaching out to a cup of tea, typically involves the assimilation of visual information, which is retino-topically coded in the receptor-array (i.e. in the extrinsic eye-centred reference frame), into the space of a sequence of body postures (i.e. in the intrinsic motor coordinates) necessary for directing one's hand to arrive at the cup. A combination of retinal, extra-retinal eye signals, together with proprioception and efference copy signals (in intrinsic coordinates) are involved in sensing such a dynamic process, and the final position of the reach may be recoded from retinotopic frame of reference to other body (egocentric) or object (allocentric) frames of reference (Gordon, Ghilardi et al. 1994, Lacquaniti, Guigon et al. 1995). Psychophysical studies have shown that the frame of reference used to specify the reach is dependent on the available sensory cues (e.g. the visibility of ones hand), task requirements (e.g. reaching in the dark vs. light), the contextual cues (e.g. environmental settings, landmarks), as well as any prior cognitive

information (Battaglia-Mayer, Caminiti et al. 2003, Carrozzo, Stratta et al. 2002, McIntyre, Stratta et al. 1998). Together with the observation that movements of the eye and hand are functionally coupled (Neggers, Bekkering 2000, Neggers, Bekkering 2001, Snyder, Calton et al. 2002, van Donkelaar, Lee et al. 1994), these findings have elucidated components of the action-perception cycle that are essential to visually guided reaching.

Clinical cases show that damage to the posterior parietal cortex (PPC) commonly affects patients' visual spatial representation (e.g. such as a hemi-visual field is neglected) and /or lead to impairments in their planning as well as coordination of goal-directed movements (e.g. as observed in ideomotor limb apraxic patients who are impaired in making purposeful voluntary movements and optic ataxic patients who are unable to guide their movements visually). As such, the PPC is implicated in playing an important role in the representation of body and extra-personal space, as well as the associated sensorimotor transformations for movement planning and coordination (Fogassi, Luppino 2005, Jackson, Husain 2006). The role of the PPC in visually guided behaviour has been studied quite considerably since the early investigations of Mountcastle, Lynch et al. (1975) and Hyvärinen (1982) who documented that apart from the classically attributed higher-level sensory processes, the PPC is also involved in the animal's motivational state, the initiation, and the control of voluntary eye and limb movements.

Anatomically, the PPC comprises of the superior parietal and the inferior parietal lobules (designated as SPL and IPL respectively), as well as the intermediate intra-parietal sulcus (IPS). The SPL in the macaque monkey is classically known as Brodmann's (1909) area 5, while the monkey IPL is known as area 7. Human SPL consists of both areas 5 and 7, while the human IPL comprises areas 39 and 40. Within the different divisions of the PPC smaller subsections have been further parcelled

resulting in a mosaic of areas thought to process specific sensorimotor transformations for action (Fogassi, Luppino 2005, Rizzolatti, Fogassi et al. 1997). To keep terminology simple, I will refer mainly to the divisions SPL or IPL in general, which are characteristic of the PPC in both monkeys and humans.

Like other goal-directed behaviours, reaching to targets is not mediated by only a single cortical area, such as the PPC. Distributed networks of brain regions are recruited and are linked by reciprocal connections with the PPC. The main areas involved in these connections are the (somato- and visual) sensory cortices, the frontal lobe (particularly the agranular motor and premotor areas), the posterior temporal lobe, the limbic cingular cortex, the basal ganglia, the thalamus (e.g. the lateral posterior nucleus), the brain stem, and the cerebellum (Hyvärinen 1982). Thus, the PPC plays an important intermediary role in the processing of sensory information for intended movements.

Various studies controlling for both movement and sensory related activities have observed that the PPC is involved in both sensory and motor processing (Andersen, Essick et al. 1987, Snyder, Batista et al. 1998). For example, the activities of the dorsal-medial portion of the IPL (area 7a) and the lateral intra-parietal area (LIP) have been found to be strongly related to saccadic eye movements, yet the state of sensory attention and eye movement activations within the LIP have been shown to coexist (Corbetta, Akbudak et al. 1998). Likewise, although sensory and motor related activities are recorded in both SPL and IPL, the IPL (particularly area 7a) has been observed to be strongly influenced by visual related activities, e.g. passive visual awareness, fixation of attention, and eye movements (Caminiti, Ferraina et al. 1996, Hyvärinen 1982). Visually stimulated neurons of the IPL have directional tuning (Sakata, Shibutani et al. 1980) and in some cases where bi-lateral representations exist, such directional preferences are opposite in the hemi-fields (inward cf. outward

directional preference, i.e. opponent vector organization with reference to the bi-lateral symmetry of the body; Motter, Mountcastle 1981), and in others, the eye- and hand-related signals for one side of the body are more strongly represented in the contralateral hemisphere (Battaglia-Mayer, Mascaro et al. 2005). IPL neurons are particularly excited by stimuli on the visual periphery which appears to trigger attention-related activities, likely to bring the object of interest within the receptive field of the fovea (Motter, Mountcastle 1981). Recent studies demonstrated that IPL (7a) neurons respond to optic-flow stimuli; clusters of neurons are responsive to rotational optic-flow stimuli in both clockwise and counter clockwise directions (c.f the specific selectivity of neurons to preferred directional optic-flow cues within the medial superior temporal (MST) area), with particular sensitivity to expansion cues (Merchant, Battaglia-Mayer et al. 2001, Siegel, Read 1997). Apart from visual signals, auditory and vestibular information also arrive at the IPL; the former complements the observation of head-orienting responses to directionally salient sounds, while the latter implicates the role of IPL in vestibular-visual transformation, e.g. in optokinetic responses (Hyvärinen 1982).

The activities related to arm movements have been demonstrated in both the IPL (area 7a) and the many subdivisions of the SPL (Marconi, Genovesio et al. 2001), which include the dorsal area 5 (also termed PE), its lateral and medial neighbouring areas (PEa and PEc), and the medial intra-parietal areas (MIP and V6a) that form the parietal reach region (PRR). Distributed preferred directions of area 5 neurons tend to cluster in the cardinal axes (Lacquaniti, Guigon et al. 1995), which reflect the body-centred coordinates. With the uniform distribution of positive and negative coefficients for these axes, summed individual contributions of the neural population could, *in principle*, provide the limb position information (Battaglia-Mayer, Caminiti et al. 2003, Lacquaniti, Guigon et al. 1995). In additon, multi-parametric (i.e. position, velocity, direction, and /or amplitude) control of movement has also been observed in (M1 and)

area 5 of the parietal cortex (Ashe, Georgopoulos 1994, Fu, Flament et al. 1995, Fu, Suarez et al. 1993, Johnson, Mason et al. 2001).

In a recent study using an instructed delay reaching task in which the initial eye and hand positions were varied, Buneo, Jarvis et al. (2002) observed that neurons in the dorsal area 5 of the PPC were best characterised as coding the target locations directly in both hand and eye coordinates even though there were neurons whose activities coded the target locations in either eye or hand coordinates. The investigators also found that PRR neural activities that were strongly related to the target locations were coded in eye coordinates (Batista, Buneo et al. 1999), and some cells were also 'gain-modulated' by the initial hand location; neural activities still signalled, for example, hand location tuning (e.g. in the upper or lower visual field) but the activities varied in magnitude relative to the actual hand position (e.g. left, centre, right of the upper or lower visual field). They inferred that direct eye-to-hand transformation may be achieved by integrating both target and initial hand location information in eye-centred coordinates. On the other hand, indirect transformations could also occur in the PPC, through computation of the difference between initial hand and target locations information (vector-subtraction) via the PRR in eye-coordinates and then translating this difference into the body frame of reference based on the gain-fields in PRR neurons. Additional findings that eye-centred cells were generally found deeper in the sulcus (PRR) compared to the hand-centred cells, which were generally located more superficially on the cortex (area 5), led Buneo & Andersen (2006) to propose the process of a gradual transformation of a vector-subtraction from eye-centred to hand-centred reference frame along the caudal-rostral axis of the SPL (from PRR to area 5). They also speculated that the coexistence of eye- and hand-centred representations of parietal area 5 might be a consequence of converging eye-centred signals with concomitant efference-copy information derived from frontal areas, known to have

reciprocal connections with the SPL (Johnson, Ferraina et al. 1996, Marconi, Genovesio et al. 2001).

Indeed, the parietal-frontal network has been characterised by gradients of visual, eye, and hand-related signals along the caudal-rostral and tangential axis of the PPC and frontal motor areas (Battaglia-Mayer, Archambault et al. 2006, Battaglia-Mayer, Ferraina et al. 2001, Johnson, Ferraina et al. 1996). Eye signals dominate over concomitantly present hand information in the intra-parietal (e.g. V6a, LIP) areas, the IPL (7a), and in the dorso-rostral premotor cortex. On the contrary, hand signals dominate over coexisting eye information in the rostral SPL (area 5a / PE) and caudal areas of the premotor and motor (M1) frontal cortex. Intermediary to these two streams of connections, are areas in both IPS (MIP, PEc, and PEa) and frontal areas bordering the caudal premotor and M1, which manifest both eye and hand signals with varying strengths depending on the cortical area (Pesaran, Nelson et al. 2006). In general, within the PPC, there is a gradual transition of strong-to-weak eye signals caudal-rostrally along the tangential axis, and an opposite weak-to-strong gradient in the same direction is observed for hand signals. Within the frontal motor regions, the transition is reversed; the gradient of strong-to-weak eye signals transit rostro-caudally and this is in parallel with the gradient of weak-to-strong hand signals in the same direction.

Apart from the network of functional gradients, similar activations within the parietal-frontal areas are linked by reciprocal connections (Johnson, Ferraina et al. 1996, Marconi, Genovesio et al. 2001), which could bring about the similar properties manifested in (pre-)frontal and parietal neurons (Chafee, Goldman-Rakic 1998, Chafee, Goldman-Rakic 2000). Additionally, parietal and frontal neurons that share similar properties can manifest different temporal activity profiles, relative to sensory and task stimuli depending on what these cues signify (Johnson, Ferraina et al. 1996); stimuli

relating to target location in an instructed-delay task recruited parietal and frontal neurons in a similar time-frame, while stimuli triggering movement recruited frontal cortical neurons earlier, followed by the parietal cells. Moreover, within the different regions of the SPL and IPL, partially overlapping preferred directions within a restricted spatial location (i.e. *global tuning field*, GTF) have been observed in different task conditions (e.g. instruction stimulus, memory delay, reaction time, movement time, target holding time, or No-go) involving arm and /or eye movements (e.g. reaching to foveal or extra-foveal targets, saccadic eye movements, delayed reaching, reaching or saccadic movements to visual targets, and peripheral memorized targets with or without central fixation; Battaglia-Mayer, Ferraina et al. 2000, Battaglia-Mayer, Ferraina et al. 2001). Therefore, not only is the combination of information integrated in the PPC related to different effectors in different coordinates, the invariance in the neural activities associated with eye- and /or hand-related direction tuning implies an object-centred (allocentric) frame of reference.

Evidently, the view that visually-guided reaching is a consequence of a succession of coordinate transformations either by a cortical area with its unique (eye-centred) reference frame, or by linking areas with different frames of reference (Batista, Buneo et al. 1999, Buneo, Andersen 2006) may not be adequate. The preference for initial and target positions coded in eye-centred (over body- or object-centred) coordinates (Batista, Buneo et al. 1999, Buneo, Andersen 2006) has been attributed to practical reasons; simpler computations are involved when intrinsic transformation can be avoided (cf. Sabes, Jordan 1997), and therefore render the possibility of realistic online modifications (Georgopoulos, Kalaska et al. 1983). In addition, strong visual influence on executed movement trajectories have been demonstrated in behavioural studies that introduced perturbed illusory feedback of movement path (Flanagan, Rao 1995, Wolpert, Ghahramani et al. 1995), while the update of reaching plans have been shown to occur in eye-centred coordinates (Henriques, Klier et al. 1998). However, such a

view that the vector of intended hand movement between the current hand position and the target (motor error) is derived in eye-centred (retinotopic) coordinates may not be realistically practical. Crucial retinal and extra-retinal information is derived through proprioception and efference copy of gaze movements. Simultaneously, profound changes in the retinotopic map of the motor error occur when intermittent gaze is oriented to the target before and during the reach. Moreover, even if hand positions can be visually coded, proprioception and efference copy of the intended movements are relayed to arm muscles in intrinsic (body) coordinates, particularly when the hand is out of view. In addition, the existence of GTFs in the SPL (and more recently observed in the IPL; Battaglia-Mayer, Mascaro et al. 2005) that points to the other coordinate information necessary for reaching, as well as recent findings that activities of neurons within the PRR encode movement (velocity) in hand coordinates during shape-copying (Averbeck, Chafee et al. 2005), imply that reach plans in SPL are unlikely to be encoded only in eye-centred coordinates (Battaglia-Mayer, Archambault et al. 2006).

An alternative view is that eye-hand coordination in reaching is achieved through the recursive refinement of ipsilateral and intra-cortical (excitatory and inhibitory) signalling, relative to salient context-dependent cues, which modify the strengths of eye and /or hand signals within the dynamic parietal-frontal network (Battaglia-Mayer, Archambault et al. 2006, Battaglia-Mayer, Caminiti et al. 2003). Equally important is the signalling from the frontal to the parietal regions within the system. The fronto-parietal network, rending the sensory consequences of motor plans with feedback, could be involved in current estimation of the limb state (velocity or position etc.), i.e. forward mechanisms (Battaglia-Mayer, Archambault et al. 2006).

Indeed, transient disruption of PPC function by transcranial magnetic stimulation (TMS) impairs normal subjects' movement correction to a sudden change in target

location (Desmurget, Epstein et al. 1999, Desmurget, Grea et al. 2001). This is also observed in patients with bilateral lesion of the PPC when reaching to targets within foveal vision (Grea, Pisella et al. 2002, Pisella, Grea et al. 2000). Electrophysiological studies have demonstrated that parietal neurons show characteristic anticipatory activities when intended movements need to be redirected in instructed delay tasks (Eskandar, Assad 1999, Kalaska, Crammond 1995, Snyder, Calton et al. 2002). Predictive signals in the form of an early change in neural activity relating to a sudden target jump in reaching (Archambault, Battaglia-Mayer et al. 2005 in Battaglia-Mayer, Archambault et al. 2006), as well as hand velocity signals related to the future movement trajectory (Averbeck, Chafee et al. 2005) have recently been shown in the parietal cortex. Therefore, when intentional plans are suddenly altered, as in a change of target location, such anticipatory activity are likely to exert on the system and the effects of TMS (or chronic ablation) can disrupt the process of updating sensorimotor representations (Rushworth, Ellison et al. 2001, Rushworth, Taylor 2006). Thus, the dense interplay of parietal and frontal areas through their cortico-cortical connections and the coordinated eye and hand movement representations within SPL and IPL are involved in visually guided movements. From this perspective, the impairments of eye-hand coordination manifested in patients with damage to the PPC, optic ataxia and /or neglect may therefore emerge as a consequence of the breakdown of these networks (Battaglia-Mayer, Archambault et al. 2006, Battaglia-Mayer, Mascaro et al. 2005).

Beyond the parietal-frontal network, other areas involved in processing or integrating sensory and /or motor signals are likely to participate in the evolution of visually-guided movements. Interestingly, accumulating findings are beginning to show that an extended association from the dorsolateral prefrontal cortex (DLPFC) is intricately linked to the sub-areas that contribute to the functional gradients within the parietal-frontal network (Barbas, Pandya 1987, Hoshi 2006, Petrides, Pandya 1984, Petrides,

Pandya 1999, Petrides, Pandya 2002). Anatomically, the DLPFC lies in and around the principal sulcus of the macaque monkey (Brodman's (1909) areas 9 and 10, Walker's (1940) area 46), while it is found in the middle frontal gyrus of the human (Brodman's areas 9/46). DLPFC can be subdivided as the dorsal (DLPFCd) and ventral (DLPFCv) portions of the principal sulcus (Petrides, Pandya 1999). In general, it has been observed that the rostral portion of the DLPFC is linked to the auditory temporal cortex and the caudal portion of DLPFC is connected to the PPC (Barbas, Mesulam 1985).

Within the PPC, DLPFCd is connected to the SPL via the superior longitudinal fasciculus (Petrides, Pandya 2006), the dorso-caudal regions, including areas 7a (also known as PG) and PGm (in the medial surface) of the IPL (Pandya, Seltzer 1982) as well as the posterior cingulate areas (Morecraft, Cipolloni et al. 2004, Petrides, Pandya 1999), while DLPFCv is linked to the ventro-caudal regions of the PPC in the areas 7b (also known as PF) and PFG of the IPL (Pandya, Seltzer 1982), and to the parietal operculum (Petrides, Pandya 2002, Preuss, Goldman-Rakic 1989). In addition, DLPFCd is connected to the dorsal premotor area, while DLPFCv is connected to the ventral premotor area (Barbas, Pandya 1987, Luppino, Rozzi et al. 2003, Petrides, Pandya 1999, Petrides, Pandya 2002); the respective premotor areas also receive similar afferents from the PPC as those of the DLPFC subdivisions (Cavada, Goldman-Rakic 1989, Morecraft, Cipolloni et al. 2004, Petrides, Pandya 1984). While both areas are reciprocally linked to the cerebellum via the pontine nuclei and receive its output via the thalamus, stronger connections between the DLPFCd and the cerebellum than that between DLPFCv and the cerebellum have been described (Middleton, Strick 2001).

With both the cortical and subcortical connections, the DLPFC is therefore considered to be centrally involved in the integration of sensory (and motor) information with ensuing action in goal-directed behaviour (Curtis, D'Esposito 2004, Goldman-Rakic

1996, Quintana, Fuster 1999, Tanji, Hoshi 2001). In particular, the activities of DLPFC neurons are related to spatial aspects of visual cues and movements plans among the range of task-related kinds of information, defining for example: object characteristics (Asaad, Rainer et al. 1998, Fuster, Bodner et al. 2000, Rao, Rainer et al. 1997), spatial information (Fukushima, Hasegawa et al. 2004a, Funahashi, Bruce et al. 1989, Quintana, Fuster 1992), reward predictability (Leon, Shadlen 1999, Tsujimoto, Sawaguchi 2004), movement sequences (Averbeck, Chafee et al. 2002, Averbeck, Chafee et al. 2003, Averbeck, Crowe et al. 2003, Fujii, Graybiel 2003, Funahashi, Inoue et al. 1997), as well as behavioural decisions and strategies (Barraclough, Conroy et al. 2004, Gold, Shadlen 2000), and uncertainty (Averbeck, Sohn et al. 2006).

However, the neural representations of these varying types of task-related information may be preferentially segregated within the DLPFC as suggested by Hoshi (2006). Neurons in the DLPFCv are mostly excited by visuospatial location (Lebedev, Messinger et al. 2004, di Pellegrino, Wise 1993b) and the characteristics (Hoshi, Tanji 2002, Saito, Mushiake et al. 2005) of attended cues, rather than what these cues might be associated with behaviourally. DLPFCd neurons, on the other hand, are more inclined to signal features of motor plans or ensuing actions (Hasegawa, Blitz et al. 2004, Hoshi, Tanji 2004a, Ninokura, Mushiake et al. 2004), relative to memorized locations or intentions (Fukushima, Hasegawa et al. 2004a, Lebedev, Messinger et al. 2004, Saito, Mushiake et al. 2005). Moreover similar segregated firing preferences to visuo-motor and visuo-spatial cues have also been observed in the associated dorsal and ventral premotor areas, which are connected to the DLPFC (Hoshi, Tanji 2002, Hoshi, Tanji 2004c, di Pellegrino, Wise 1993a, di Pellegrino, Wise 1993b). In addition, the pre-SMA, to which the prefrontal areas in discussion are connected (Luppino, Matelli et al. 1993), also exhibit similar neural activities to the dorsal and ventral areas of both DLPFC and premotor cortex (Hoshi, Shima et al. 2000, Hoshi, Tanji 2004b, Hoshi, Tanji 2004c). Thus, these two streams of perceptual and action information

could be integrated in pre-SMA before the relevant behaviour is executed via the motor system.

In sum, a dense and recursive network of connections and processing between the parietal, motor, and prefrontal areas are involved in initiating, planning, and remembering visual with mechano-receptive as well as auditory guidance of movements. The electrophysiological studies (Merchant, Battaglia-Mayer et al. 2004a, Merchant, Battaglia-Mayer et al. 2004b, Port, Kruse et al. 2001, Sun, Frost 1998) discussed in Chapter 2 demonstrated the involvement of PPC (e.g. area 7a of the IPL) and M1 (and also the pulvinar) in representing the variable *tau* (the time-to-closure of a motion gap at the current closing-rate) in both perception and action (i.e. interception) tasks. We extended the investigation here to other cortical areas, not yet known to be involved in representing *tau* in a non-interceptive task. The neural regions considered here are area 5 of the SPL and the area peri-principalis, which defines the dorsolateral prefrontal cortex (DLPFC) of the macaque monkey.

Shape Copying Study

Data were derived from studies in which two monkeys were trained to copy shapes as sequences of movement segments (Averbeck, Chafee et al. 2002, Averbeck, Chafee et al. 2003, Averbeck, Chafee et al. 2005, Averbeck, Crowe et al. 2003). Although the copy task has been designed to study the neural mechanisms in copying shapes and the neural correlates of serial order in movement sequences, the copy task itself can be appreciated as involving the closure of movement gaps in the completion of copying each shape segment. The self-paced movements and corresponding neural activities can be used to study the neural correlates of movement *tau* in the prefrontal and parietal cortices in non-human primate.

— *Subjects*

Two male rhesus macaques, Macaca mulatta (M157 and M555, body weight = 8-10 kg) were trained to perform in the experiments conducted by Averbeck et al. (2002, 2003, 2005). The care and experimental treatment of the monkeys adhered to the Principles of Laboratory Animal Care (NIH publication no. 86-23, revised 1995) and all experimental protocols were approved by the relevant Institutional Review Boards.

— *Self-paced copy task in Monkeys*

The monkeys were trained to copy geometric shapes (triangles, squares, rhombuses, and inverted triangles) displayed on a liquid-crystal display (LCD; NEC Model MT-820, 640x480 resolution, 1 cm = 1.2° visual angle, 9.5 pixels = 1°) projected 47 cm away, using a freely moving XY-joystick-controlled cursor (model 541 FP, Measurement

Systems, Norwalk, CT; sampled at 200 Hz) with their left hands. A 26 mm joystick-excursion (i.e. the length of a square) was manifested on the screen as a cursor-displacement of 113 mm (visual angle = 13.4°; 150 pixels; ref. FIG 3.1).

The task began with a solid white circle presented on the left side of the screen, which prompted the monkey to move the joystick-controlled cursor to it and hold the cursor there. They were required to hold the cursor in the white start circle for a waiting time (WT) of 1 – 2 s (WT for M157 = 1 s, WT for M555 = 2 s) before a shape template was presented on the right side of the screen. If they deviated from the holding circle, the task-trial was aborted and a new trial appeared. The monkeys had to copy the displayed shape on the left side with the cursor while keeping the cursor trajectory within a tolerance window and return to the hold circle before being rewarded with juice (FIG 3.2). For each of the 5 pseudo-randomised blocks, each shape had to be drawn correctly 6 times before a new shape was presented; a total of 30 drawings per shape were made in each session.

— Neurophysiological recordings

While the monkeys engaged in the copy task, the electrical activity of single neurons (in the peri-principalis area of the pre-frontal or in area 5 of the superior posterior lobule of the right hemisphere) was simultaneously recorded extracellularly at 200 Hz using 16 independently driven microelectrodes (Uwe Thomas Recording, Marburg, Germany). All present cells were recorded (ALPHA-OMEGA system, Multi-Spike Detector) without pre-selection in order to approximate random sampling of all possible layers of cortex. These multiple units were identified by means of waveform-template spike sorting discrimination (BAK Electronics Inc., model DDIS-1). More in-depth experimental details are described in Averbeck et al. (2002, 2003, and 2005).

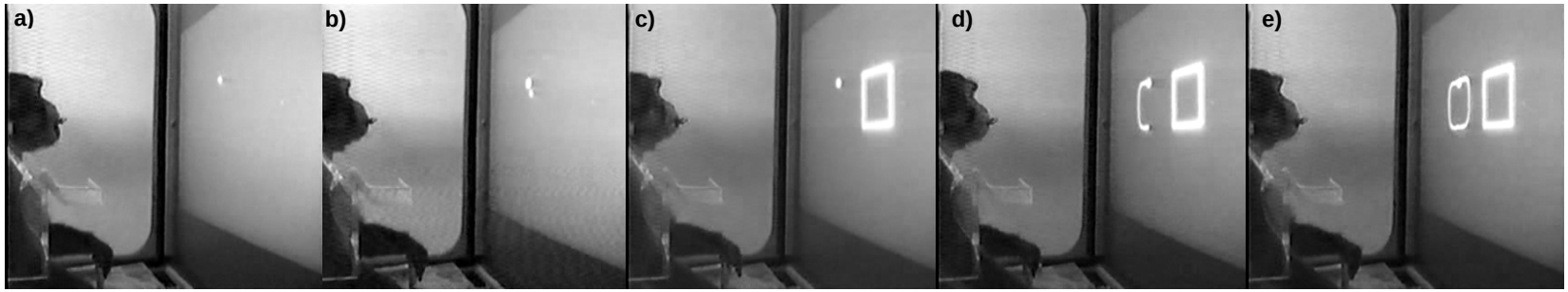

FIG 3.1: Experimental set-up of the Shape Copying Task. The animal was seated in a quiet room enclosure 47 cm away from a LCD screen display, with a screen resolution of 1 cm = 1.2° visual angle; 9.5 pixels = 1°. A 26 mm joystick-excursion (i.e. the length of a square) was manifested on the screen as a cursor-displacement of 113 mm (visual angle = 13.4°; 150 pixels). The freely-moving joystick was placed just comfortably in resting arm's reach of the left-hand as shown. The series of photographs show Monkey 157 before the initiation of the task with the display of a holding position (white circle) on the left side of the screen (a), and during initiation of the task when the monkey brought the cursor to the holding position using his left hand to control the freely-moving joystick (b). After holding the cursor at the holding position for a wait-time (WT) of 1 s, a shape template was presented to the right of the screen (c), which was itself the stimulus for copy response on the left side of the screen (d), and the trial is completed when the cursor is brought back to the holding position (e). Juice reward was provided by a feeding tube upon trial completion. Refer to text and Averbeck et al. (2002, and 2003) for further details. Photographs derived from video recording, courtesy of A. P. Georgopoulos.

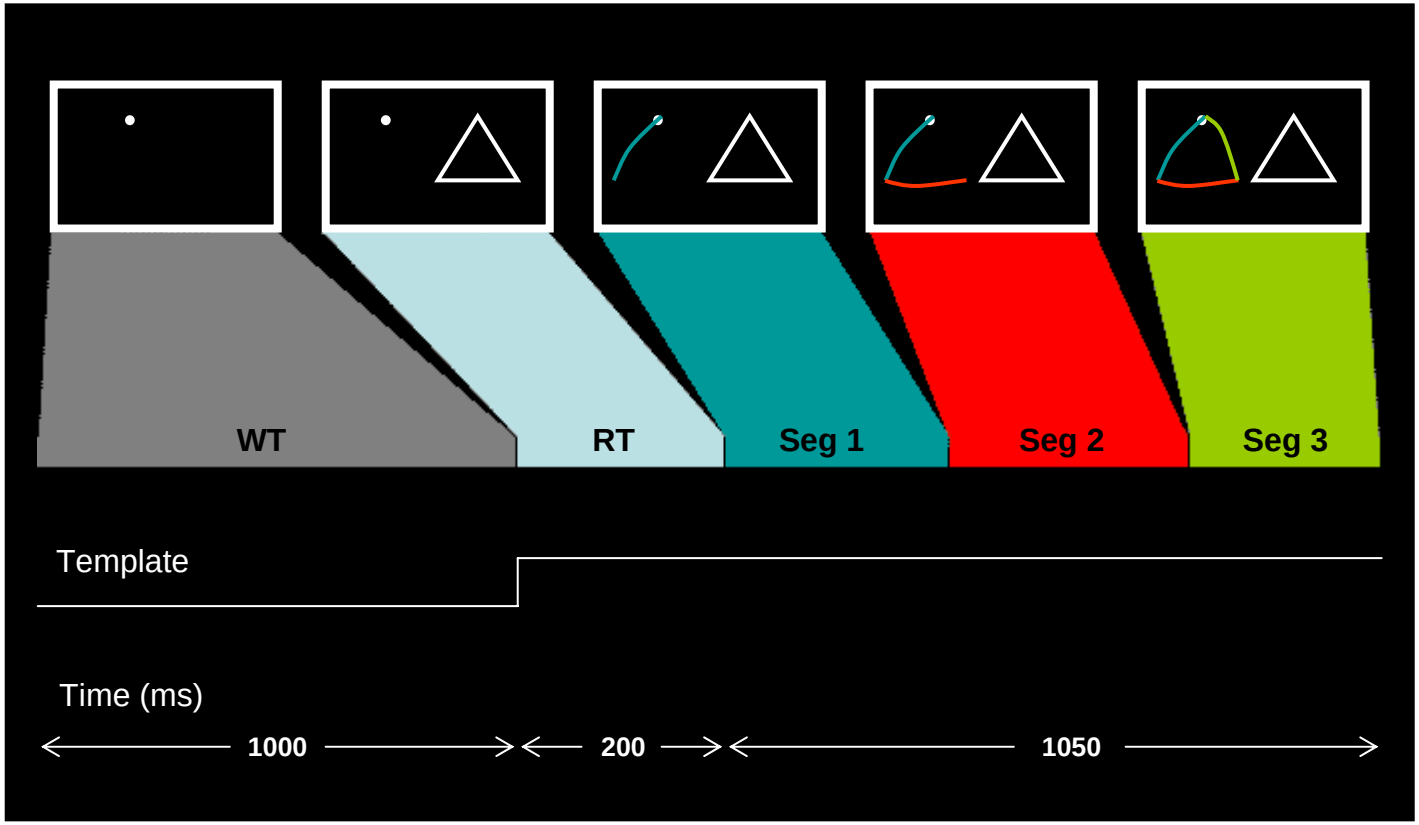

FIG 3.2: Shape Copying Task. A trial was initiated when the monkey moved the cursor to the start-hold circle on the left side of the screen. After a wait-time (WT) of 1000ms, a shape template (e.g. triangle, square, trapezoid, or an inverted triangle) was presented on the right-side of the screen. The monkey then copied the presented shape on the left starting from the start-hold position and returned to the start-hold position to complete the copy trial and to receive its juice reward. The duration of each segment is colour-coded for illustration purposes; the actual cursor displacement display was in white. Figure modified from Averbeck et al. (2002, and 2003).

— Data Analysis for the Present Investigation

The raw copy data from one monkey (M157) was available for use in an analysis, of the neural activity associated with the arm movements of the left arm and hand of the monkey made during the copying of the two copy shapes, triangles and squares. A total of 1220 neurons from both prefrontal (N = 349) and parietal (N = 871) cortices were recorded over 103 sessions from the monkey while he copied a total of 2689 trials of triangles and 2747 trials of squares. Neurons that on average fired less than 3 spikes per shape trial were excluded from the analyses. As a result of this criterion, a total of 562 neurons, of which 163 were from the prefrontal cortex (PFC) and 399 were from parietal area 5, were deemed task-related and their activities were thus further analysed.

— Movement data processing

Movement position XY-joystick data was converted from millivolts to the extent-of-joystick excursion in the positive quadrant of the 2D-axis and low-pass filtered using a Parks-MacClellan Finite-Impulse-Response with equi-ripple filter (FIR filter; of length 51, with a pass band edge of 0 to 1 Hz, a stop band edge of 20 Hz to Nyquist frequency). The designed filter has a frequency 'cut-off' of approximately 7.69 Hz (determined by the -3 dB threshold of the log-magnitude of the impulse response). It was noted that most of the movements were devoid of high-frequency components and so they were little changed after filtering.

The filtered movement XY time series for each trial were then segmented. Previous documentation of segmentation (Averbeck, Chafee et al. 2002, Averbeck, Chafee et al. 2003) using minima of tangential velocity was based on the principle of the 2/3 power-law (Lacquaniti, Terzuolo et al. 1983, Viviani, Terzuolo 1982), which relates to an inverse non-linear relationship between speed and the curvature of trajectory during curved motion. The principle predicts that movement speed along regions of high curvature, i.e. shape corners, would be much lower compared to the speed along regions of low curvature. This method was employed in the current shape-segmentation, which was achieved by a series of steps. First, the maxima and minima of both x and y velocities were determined. These indices were then used to find shape-segment borders by using the criteria of 10% maximum of the x and /or y velocities, depending on the shape segment. Subsequently, the maximum tangential velocity (speed) within each segment border was determined. Movement speed was calculated as:

$$s_{(t)} = \frac{\sqrt{(x_{(t)} - x_{(t-1)})^2 + (y_{(t)} - y_{(t-1)})^2}}{1/F} \qquad \text{EQ 3.1}$$

where sampling frequency (F) was 200 Hz and thus sample time-interval (1/F) at each instantaneous time-point, t, was 0.005 s. Finally, the start and end indices of each segment corresponded to the points during which the speed was the minimum between the speed maxima of each shape segment, with the exception that the first segment's start index was determined by the 5% of maximum speed threshold criteria and the end index of the last segment was determined by the 10% of maximum x or y velocity threshold, depending on the shape. The segmentation based on the x and y velocities and the tangential velocity are illustrated in FIG 3.3. A total of 8067 segments (2689 trials x 3) for triangles and 13735 segments (2747 trials x 5) for squares were segmented.

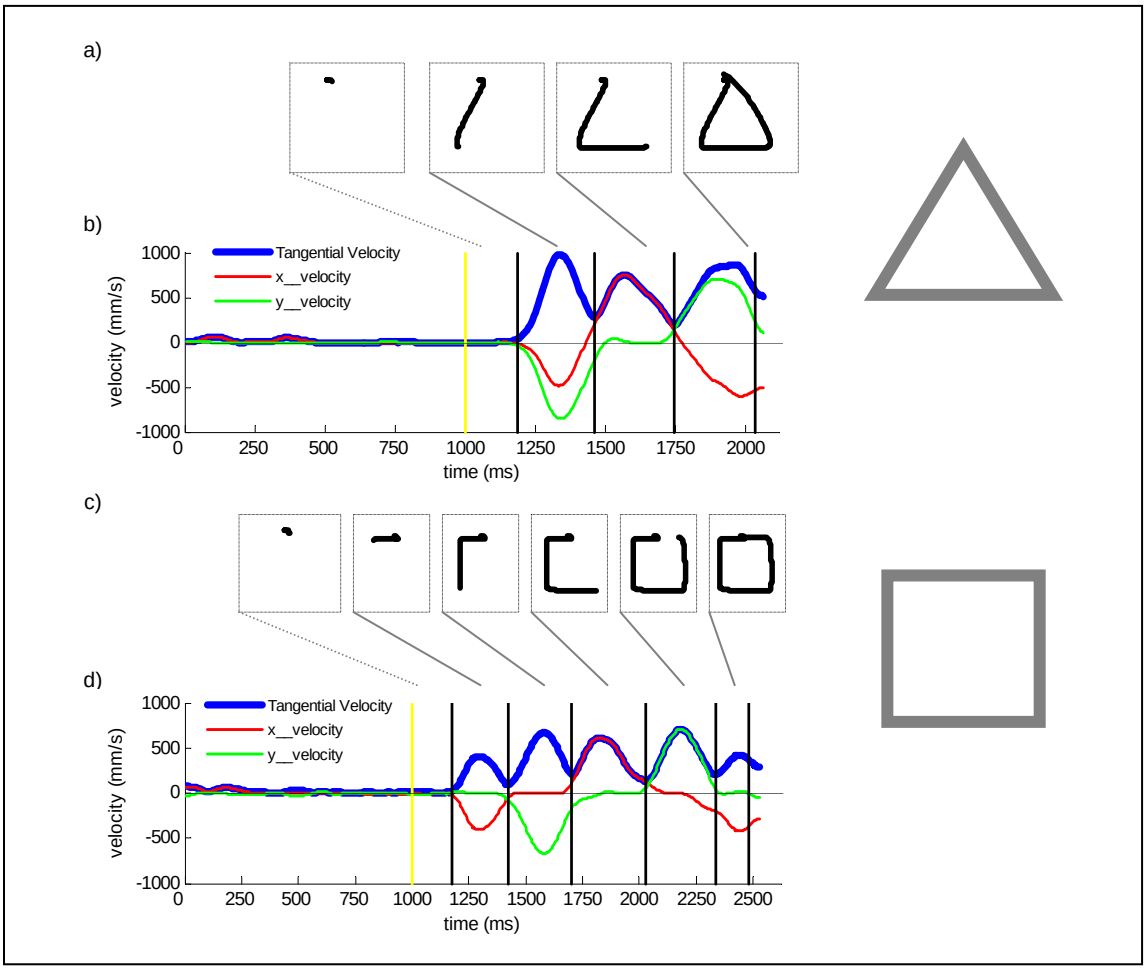

FIG 3.3: Copied shapes and shape segmentation. An example of the 2 copied shapes of interest from session 30 during the neural recordings from the prefrontal cortex of monkey M157: (a) & (b) trial no.7 for a triangle and (c) & (d) trial no.24 for a square. The segment borders are denoted as vertical black lines in (b) & (d) and are located at the minima of the tangential velocity (speed) profiles. The stimulus presentation is denoted by the yellow vertical lines. It was always after the initiation of the trial and a waiting-time of 1s during which the monkey had to hold the cursor within the white circle. The sequence of segments drawn are illustrated in (a) and (c) relative to the velocity profiles for the triangle and square respectively.

—Neural data processing

The recorded neural spike trains (Averbeck et al. 2002, 2003, 2005) were converted to spike density functions by convolving with a Gaussian kernel (s.d. = 5 ms). The corresponding neural spike density function time series of each shape segment was similarly segmented using the start and end indices of the movement segments, described earlier. Although there were a total of 562 neurons from both prefrontal cortex and area 5, which were recorded during the monkey's drawing of each shape trial, there was on average of 8 neurons being simultaneously recorded as an ensemble in one session. The spike density functions of each segment per trial are illustrated in FIGs 3.4 to 3.7 (d, e, f) for triangles and FIGs 3.4 to 3.7 (f, g, h, i, j) for squares.

— Movement Variables and Analyses

Given that the behavioural aspects of the copy task have been extensively characterized in Averbeck et al.'s (2003a) study with respect to copying attributes, including the internal angles of the shapes drawn (i.e. ~ 60° for triangles and ~ 90° for squares), the movement variables considered here will include only a few of relevant interest. It had been noted that the eye movements associated with the task were mainly saccades to the shape template and back to the drawing area; saccadic eye movements were accounted for by only 3.2% in the prefrontal and 2.7% in the parietal area 5 neural activities, based on Averbeck, Chafee et al.'s (2003a) analyses. Moreover, adding eye position information into the algorithm which modelled parietal neuron's representation of velocity did little to improve the fit of the model, which implied that the eye signals were not a strong contributing factor, and /or the neural signals were not tuned in eye-centred coordinates (Averbeck, Chafee et al. 2005). We did not, therefore, deem the eye movements as a potential confound.

Thus, apart from movement speed described above, the behavioural variables considered were the maximum movement speed, the time to maximum speed (from segment movement onset), the proportion of movement time to maximum speed, the movement time, and length of movement for each segment. In addition, variables related to the conventional *tau*-analysis were also considered. These were the % τ_g-coupling, which accounted for the strength of linear association between the theoretical *tau-guide* and the movement *tau*, and the regression slope (*k*). The derivations of these are further described below. General descriptive statistics were performed to assess the characteristics of movement within each shape's segment and a bivariate Pearson's correlation analysis on the mean movement variables was performed to assess how they might be associated in general.

— *Derivation of movement tau* (τ_{mv})

The time-varying movement *tau* (τ_{mv}) of each shape segment is calculated as the ratio of the changing instantaneous motion gap ($\lambda_{(t)}$) over the instantaneous rate of change of this motion gap ($\dot{\lambda}_{(t)}$). The instantaneous motion gap ($\lambda_{(t)}$) is derived based on the Euclidian distances between each instantaneous time-point (*t*) to the end (*T*) of the shape segment:

$$\lambda_{(t)} = \sqrt{(x_{(t)} - x_{(T)})^2 + (y_{(t)} - y_{(T)})^2} \qquad \text{EQ 3.2}$$

where x and y are values of the movement trajectory for each shape segment. The motion gaps described by $\lambda_{(t)}$, decrease in size as they approach the end of the shape segment. Subsequently, the rate of change of the closing gap is determined:

$$\dot{\lambda}_{(t)} = \frac{\lambda_{(t+1)} - \lambda_{(t)}}{1/\mathrm{F}} \qquad \text{EQ 3.3}$$

where sampling frequency (F) is 200 Hz and thus sample time-interval (1/F) at each instantaneous time-point, *t*, is 0.005 s. Finally, the instantaneous movement *taus* are derived as:

$$\tau_{mv\,(t)} = \frac{\lambda_{(t)}}{\delta\lambda_{(t)}/\delta t} = \frac{\lambda_{(t)}}{\dot{\lambda}_{(t)}} \qquad \text{EQ 3.4}$$

FIGs 3.4 to 3.7 illustrate the derived profiles of movement speed and movement *tau* from movement trajectory for three segments (FIGs 3.4 & 3.5 a, b, c) of the copied triangle and five segments (FIGs 3.6 & 3.7 a, b, c, d, e) of the copied square.

— *Recursive regression of movement tau* (τ_{mv}) against theoretical *tau-guide* (τ_g)

To determine how closely related the derived movement *taus* (τ_{Mv}) are to the theoretical *tau-guide* (τ_g), the percentage *tau*-coupling ($\%\tau_g$-coupling) is calculated by linearly regressing the two *taus* in a recursive manner to test the relation:

$$\tau_{mv} = k\tau_g \qquad \text{EQ 3.5}$$

where *k* (the slope) is a variable constant that describes the kinematics of the gap-closure for k > 0. The theoretical *tau-guide* (τ_g) is defined as:

$$\tau_g = \frac{1}{2}\left(t_{(i)} - \frac{T^2}{t_{(i)}}\right) \qquad \text{EQ 3.6}$$

where $t_{(i)}$ is the instantaneous time, and T is the total movement time.

The recursive regression criteria stipulates that the regression R^2 should exceed 0.95 and where it fails to achieve the threshold, a pair of variables from the time-series is excluded from the beginning of the movement time (i.e. $t = i\ldots\ i{+}1\ldots\ i{+}2\ldots T$) with each successive regression until the criteria is met. A means of quantifying the strength of the relationship whereby the theoretical *tau-guide* (τ_g) is closely associated with the movement is through the percentage coupling (% τ_g-coupling) between the two time variables. This is determined by the fraction of the data points, which accounts for the derived linear regression that has satisfied the criteria of achieving an R^2 value of no less than 0.95. % τ_g-coupling is considered a measure of the strength of the linear relation between the two *tau* time series, and an indication of how strongly the closure of a motion gap followed the temporal dynamics of the theoretical τ_g (Lee, 1998, 1999). The regression algorithm used is a MATLAB® function *lsqfitma.m* written by Edward T Peltzer (http://www.mbari.org/staff/etp3/regressindex.htm) and modified for the recursive procedure and the calculation of percentage couplings. The % τ_g-coupling was calculated for all shape segments.

In addition to the % τ_g-coupling, the *slope (k)* of the *tau*-analysis recursive regression (k, in EQ 3.5), was also considered. To reiterate, the slope (for which $k > 0$) describes the speed profile of the gap closure (refer to FIG 2.1 in chapter 2); low slope values indicate that the maximum speed during gap closure occurred early in a τ_g-coupled movement, while high slope values indicate that the maximum speed occurred late in a τ_g-coupled movement. The regression slope was derived for all segments of the two copied shapes.

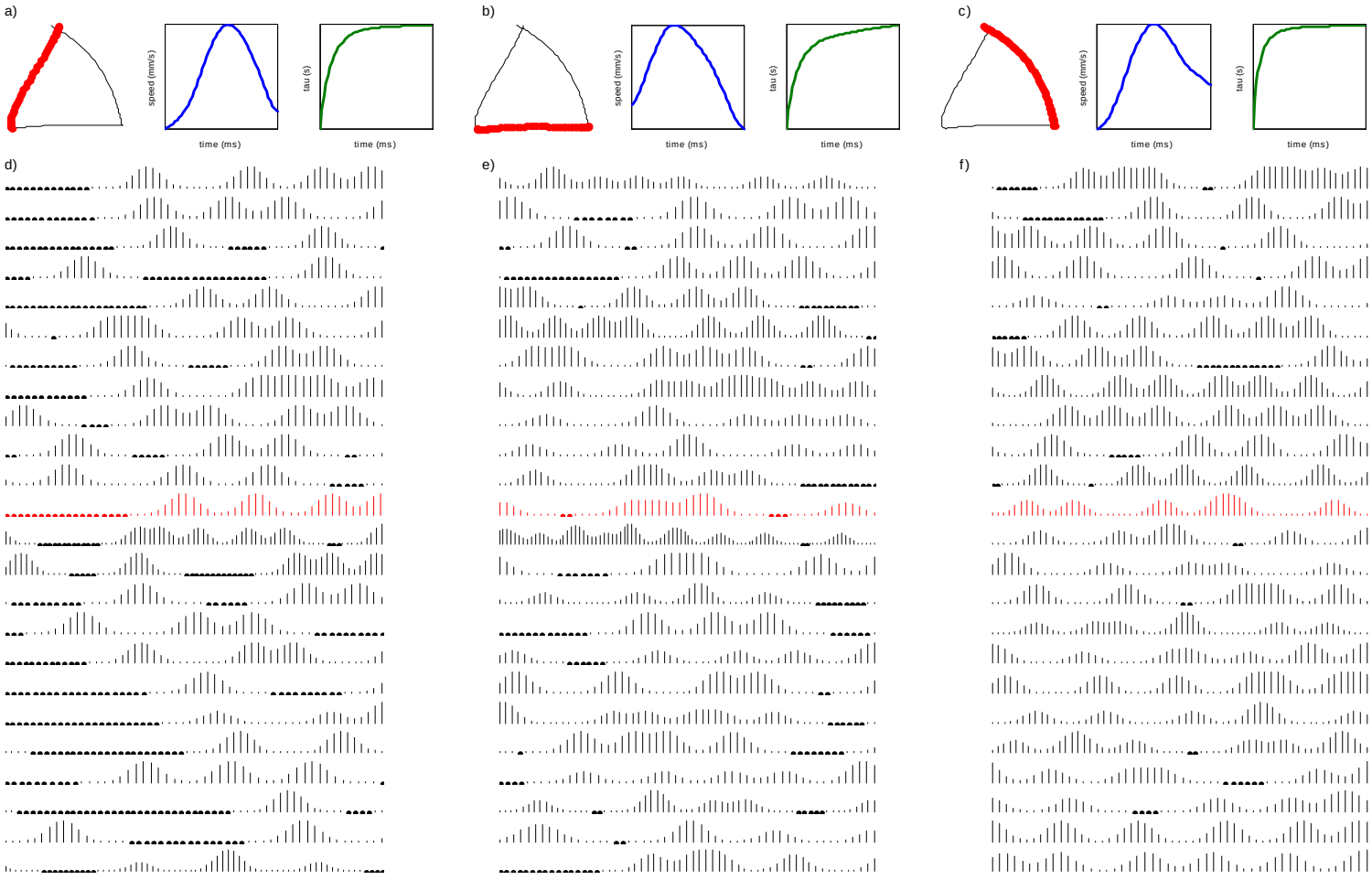

FIG 3.4: Spike density functions of a prefrontal cortical cell #8 during the performance of triangle copying. The corresponding trajectory, speed and movement *tau* are shown for each segment (a, b, c). The neural activities associated during each segment are shown (d, e, f), and trial #12 for which the movement parameters shown is highlighted in red. Cell #8 was recorded within an ensemble in session 30.

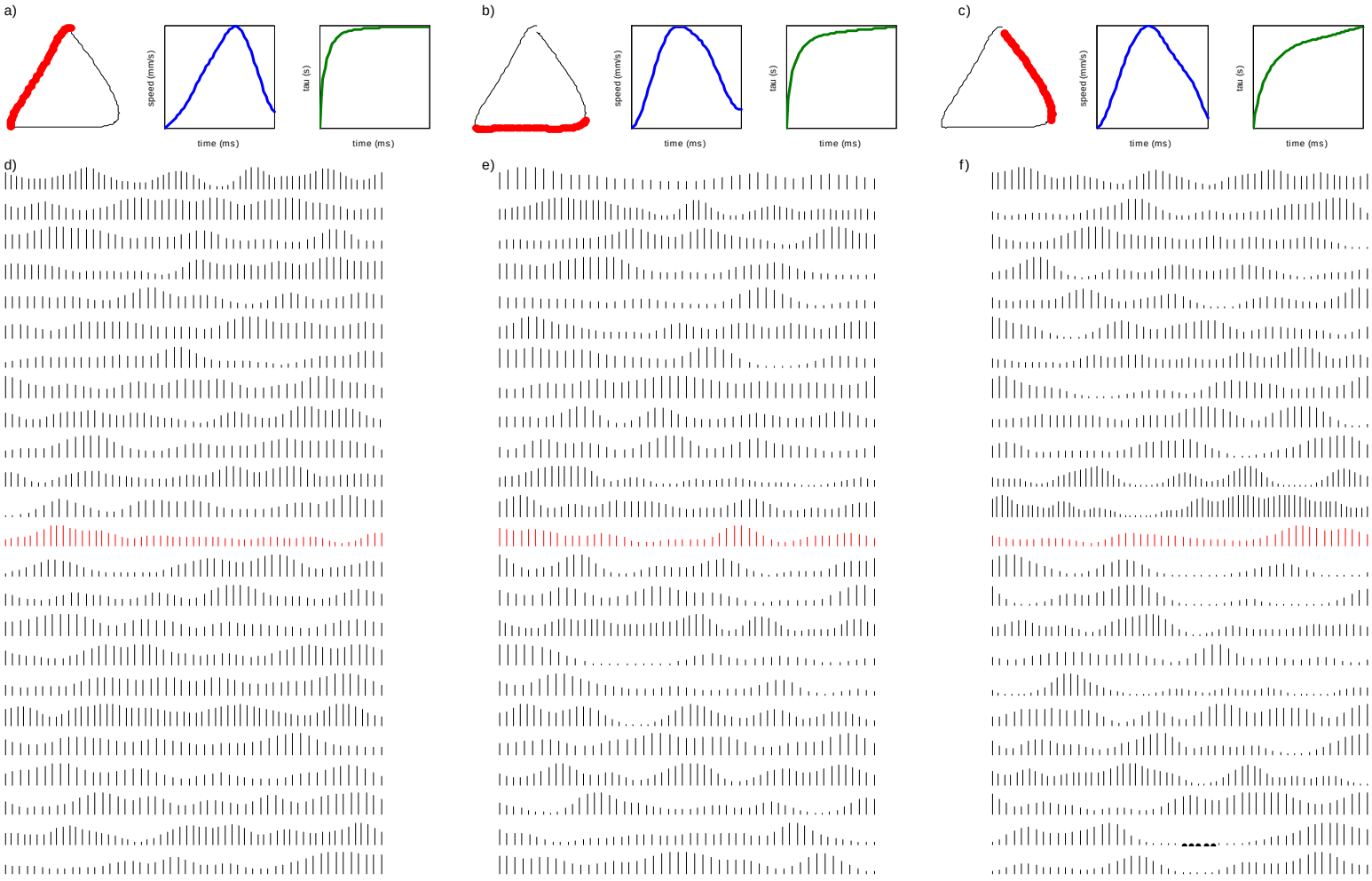

FIG 3.5: Spike density functions of a parietal area 5 cell #5 during the performance of triangle copying. The corresponding trajectory, speed and movement *tau* are shown for each segment (a, b, c). The neural activities associated during each segment are shown (d, e, f), and trial #13 for which the movement parameters shown is highlighted in red. Cell #5 was recorded within an ensemble in session 90.

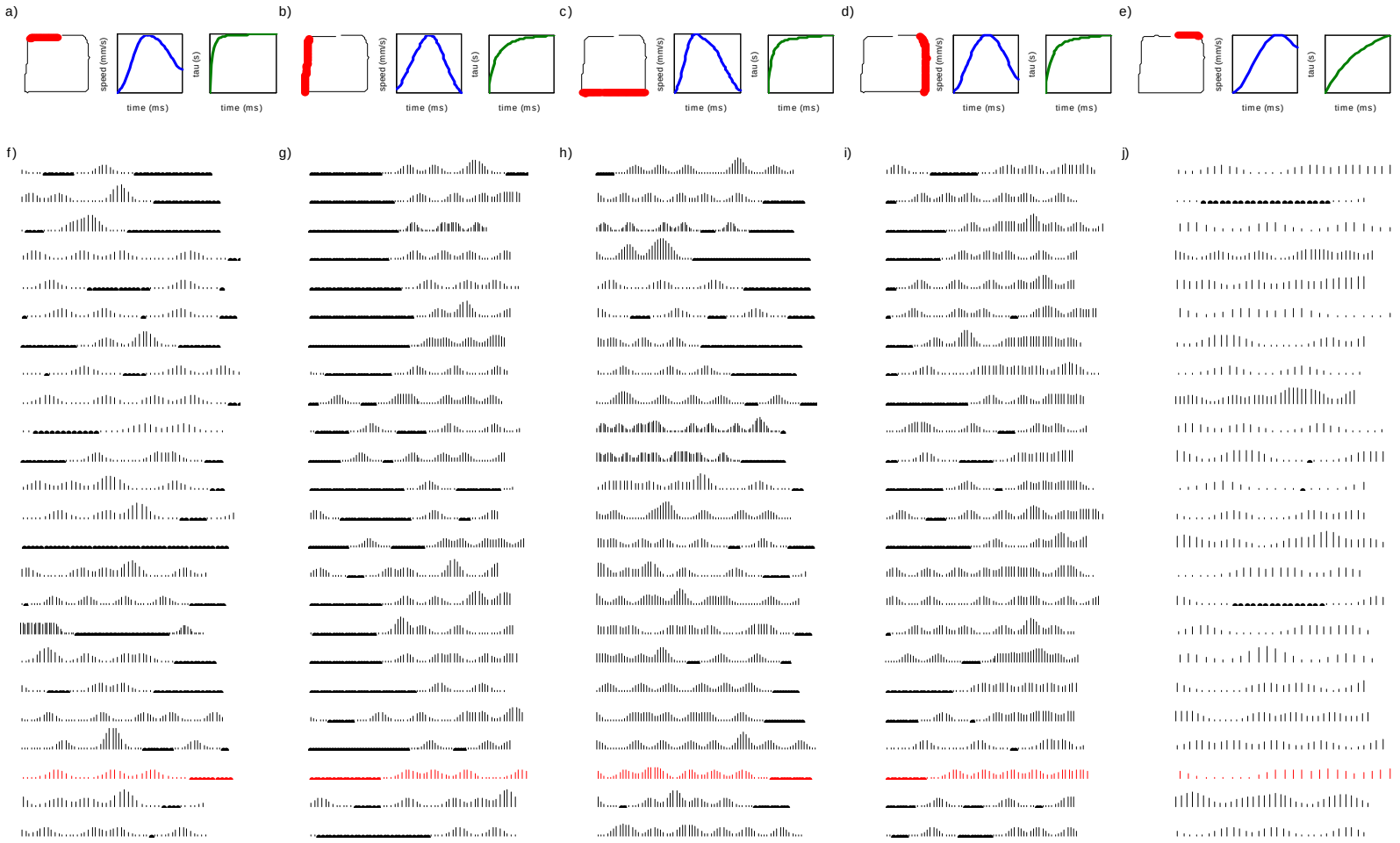

FIG 3.6: Spike density functions of a prefrontal cortical cell #8 during the performance of square copying. The corresponding trajectory, speed and movement *tau* are shown for each segment (a, b, c, d, e). The neural activities associated during each segment are shown (f, g, h, i, j), and trial #22 for which the movement parameters shown is highlighted in red. Cell #8 was recorded within an ensemble in session 30.

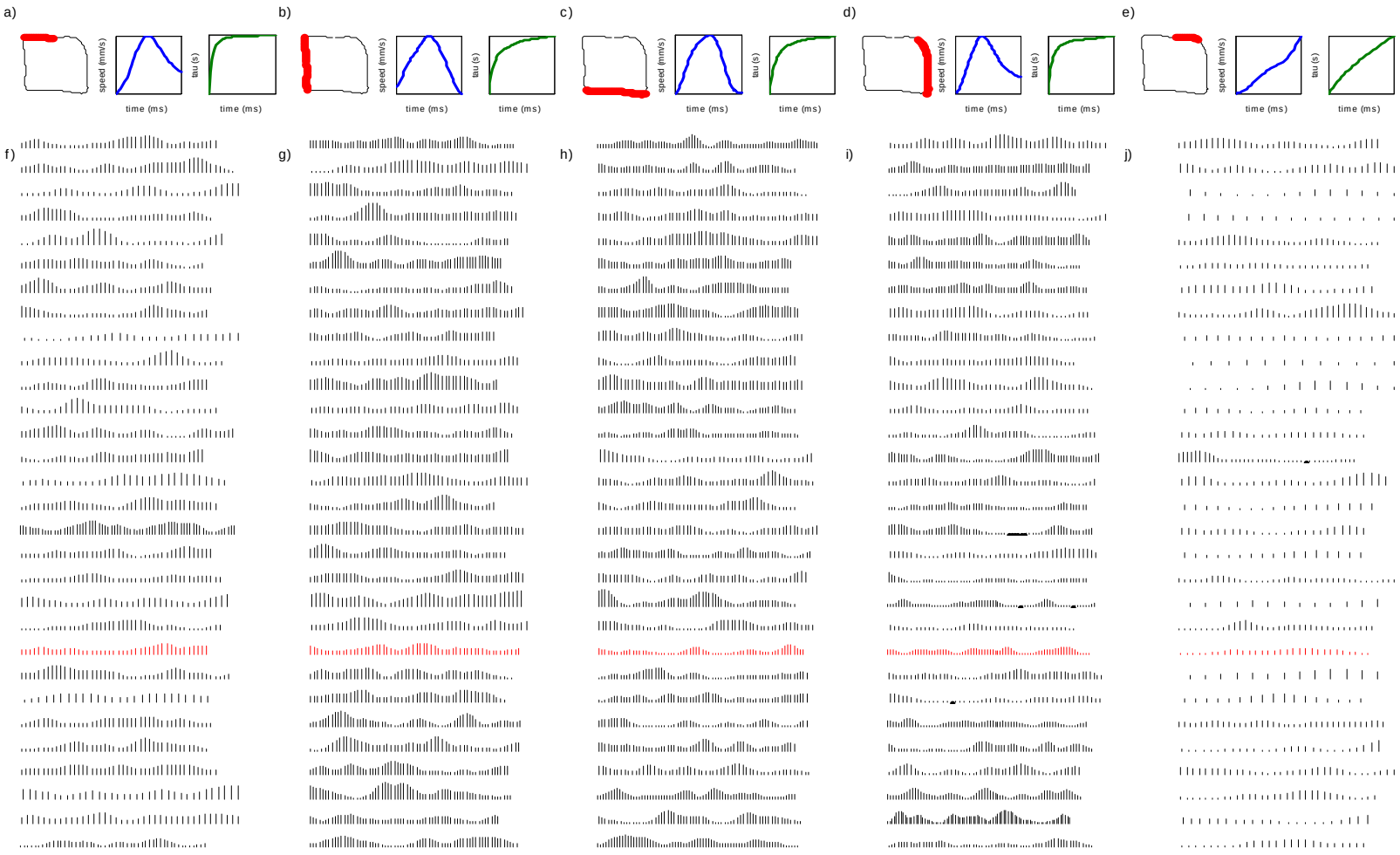

FIG 3.7: Spike density functions of a parietal area 5 cell #5 during the performance of square copying. The corresponding trajectory, speed and movement *tau* are shown for each segment (a, b, c, d, e). The neural activities associated during each segment are shown (f, g, h, i, j), and trial #22 for which the movement parameters shown is highlighted in red. Cell #5 was recorded within an ensemble in session 90.

Analysis of the relation between neural spike density functions and movement parameters: tau and speed

— Linear Regression with an Autoregressive Error Component (AREG)

The relations between the neural signals ($N_{(t,\ i=1to562)}$), corresponding speed ($s_{(t)}$) and movement *tau* ($\tau_{mv(t)}$) were assessed separately for each neuron for the two brain regions. For that purpose a linear regression analysis was performed in which the time-varying neural signal was the dependent variable, and the time-varying movement *tau* and / or the instantaneous speed were the independent variables.

Although the linear regression assumes uncorrelated errors, the regression errors involving time series are expected to be auto-correlated. Given that all of these variables are time series, the regression errors are likely to be non-independent. This could lead to spurious estimation of the significance of the regression coefficients by the linear regression that inherently assumes independent errors. Therefore, an autoregressive component ($\mu_{(t)}$) was included in the regression model to improve the estimation.

For each neuron, the associated movement and corresponding neural time-series of all shape-segments copied were considered but they were separated by an insertion of a 'NotANumber' (NaN) between segments to generate the full movement and neural time series for the AREG analyses. The regression coefficients and their statistical significance were estimated using the Exact Maximum-Likelihood method of the

AREG procedure and included a Kalman Filter to address the 'missing' data due to the incorporation of NaNs (SPSS statistical package for Windows, SPSS Inc., Chicago, IL).

The regression equations used are as follows:

$$N_{(t,i=1\rightarrow 562)} = b_0 + b_1\tau_{mv(t)} + \mu_{(t)} \qquad \text{EQ 3.7}$$

$$N_{(t,i=1\rightarrow 562)} = b_0 + b_1 s_{(t)} + \mu_{(t)} \qquad \text{EQ 3.8}$$

$$N_{(t,i=1\rightarrow 562)} = b_0 + b_1 s_{(t)} + b_2\tau_{mv(t)} + \mu_{(t)} \qquad \text{EQ 3.9}$$

$$\mu_{(t)} = \rho * \mu_{(t)-1} + \xi_{(t)} \qquad \text{EQ 3.10}$$

Where $b_{0,\,1,\,2}$ are the regression coefficients to be estimated, i is the cell number, t the sample time point, μ is the residual error, ρ is the 1st-order autoregressive coefficient, and $\xi_{(t)}$ is a normally distributed, uncorrelated random error with variance σ^2 and mean = 0.

Relations between the neural and movement variables were assessed for the significance of the regression coefficients. The percentage of neurons whose time-varying spike density function was significantly ($p < 0.05$) linearly related to movement speed, movement *tau*, both, or neither were determined for the prefrontal cortex and parietal area 5.

— Behavioural Movement Parameters:

The shapes drawn by the monkey (M 157) were very close to the attributes of the template (Averbeck et al., 2003a). Tables 3.1 to 3.3 show the means and standard deviations of the variables of interest. The three copied segments of the triangle were very similar in mean length, with the second segment being slightly shorter than the first and third segments. The mean movement times for these segments ranged from 288 ms to 308 ms, although in general, the monkey took a little longer to copy the last segment compared to the first two segments. Likewise, the segment lengths of the copied squares matched the proportions of the template and where segments were longer (i.e. segments 2 to 4), the movement times took longer too. It is worth noting here that the biomechanical constraints resulting from the monkey's choice to perform the copying task with his left arm in a counter-clockwise direction might have influenced the ease and durations of movements in different directions.

The mean maximum speed in each shape segment was higher in copying triangles compared to squares, although the monkey's vertical movements generally exhibited higher speeds relative to his horizontal trajectories. The mean time to maximum speed seemed to vary positively in proportional to mean movement length, as was the case for the mean proportion of movement time to maximum speed. However, the latter variable indicated that for the horizontal movements across the middle segment of the shapes, the peak movement speed generally occurred before half the segment had been copied, while speed peaked within the second half of the copying for the segments leading to and following the horizontal segment.

The mean percentage of τ_g-coupling for each segment of the triangle was greater than 95% (mean ± std. range: 95.95 ± 7.15% to 97.36 ± 7.13%), while it was greater than 82% (mean ± std. range: 83 ± 9.32% to 96.93 ± 9.03%) for the copying of squares; it was lowest for the final segment of the squares (83.39 ± 9.32%), which was more than one standard deviation away from the grand mean of mean % τ_g-couplings (93.25 ± 5.7%). Despite the apparent lower value for the last segment in the copied squares, the generally high percentages of τ_g-couplings indicated that there was high linear association between the movement *tau* and the theoretical *tau-guide* for all shape-segments. In addition, the τ_g-coupling slopes yielded an interesting trend: the slope was highest in the first segment of a shape (triangles and squares), but it decreased in the intermediate segments, and gradually increased again towards the end segment(s).

Given the large number of segments drawn, it would not be meaningful to include individual cases in the correlation analysis. The means of the derived variables for both shapes (i.e. the mean values reported in Tables 3.1, 3.2, and 3.3) were used instead. The correlation analysis revealed some interesting associations, particularly between movement speed attributes and % τ_g-coupling (Table 3.4). It was observed that movement time was positively related to movement length (r = 0.748, p = 0.033) and maximum movement speed (r = 0.799, p = 0.017), while it was negatively related to proportion of movement time to maximum speed (r = -0.861, p =0.006). This is not surprising as it is expected that longer segments would require a longer time to copy and higher movement speed to keep the trajectories within the tolerance window. In the copy performance, the monkey's % τ_g-coupling was positively associated with movement time (r = 0.769, p = 0.029), such that longer movement durations generally resulted in higher associations between movement *tau* and the theoretical *tau-guide*.

In addition, when the maximum speed occurred earlier in the movement, weaker % τ_g-coupling was found, as indicated by the negative association between % τ_g-coupling and the proportion of movement time to maximum speed (r = -0.815, p = 0.014). It was interesting to note that the regression slope (k) was positively related, albeit insignificantly, to the proportion of movement time lapsed to maximum speed that had been characterised in the *tau*-theory. The insignificance may be because the slope is derived based on the percentage of τ_g-coupled movement sections, while proportion of movement time to maximum speed is based on the whole segment duration.

Overall, it could be said that the monkey was able to couple his segment movements onto the theoretical *tau-guide* and manifested high τ_g-coupling slopes in the first segments but lower τ_g-coupling slopes in the middle segments of his shape-copying performance. When a longer duration was taken to copy segments, the τ_g-coupling was relatively stronger.

	N	Segment	Length (mm)	MV time (ms)
Triangle	2689	1	29.00 ± 2.44	288.87 ± 54.84
		2	27.30 ± 3.49	292.02 ± 60.29
		3	29.36 ± 2.81	307.94 ± 81.86

	N	Segment	Length (mm)	MV time (ms)
Square	2747	1	12.51 ± 2.28	256.40 ± 51.02
		2	24.81 ± 2.47	333.88 ± 73.89
		3	25.17 ± 3.55	354.22 ± 80.12
		4	25.40 ± 3.05	308.33 ± 48.64
		5	11.96 ± 4.33	164.24 ± 50.03

TABLE 3.1: Dimensions and movement duration of copied shape segments. Means and standard deviations of movement parameters: movement length (Length) as measured by extent of joystick excursion, and movement time (MV time), for both triangle and square.

	N	Segment	Max. Speed (mm/s)	Time-to-Max. Speed (ms)	Proportion of MV time to Max. Speed
Triangle	2689	1	181.88 ± 25.09	168.59 ± 36.09	0.58 ± 0.04
		2	150.41 ± 25.35	118.82 ± 28.59	0.41 ± 0.07
		3	143.38 ± 22.35	163.61 ± 46.10	0.54 ± 0.11

	N	Segment	Max. Speed (mm/s)	Time-to-Max. Speed (ms)	Proportion of MV time to Max. Speed
Square	2747	1	83.45 ± 17.33	144.51 ± 41.20	0.56 ± 0.10
		2	123.29 ± 21.48	169.25 ± 37.56	0.51 ± 0.07
		3	111.68 ± 20.25	163.22 ± 47.96	0.46 ± 0.08
		4	134.54 ± 22.11	159.38 ± 31.76	0.52 ± 0.06
		5	108.11 ± 34.56	136.29 ± 56.64	0.81 ± 0.26

TABLE 3.2: Speed-related parameters of copied shape segments. Means and standard deviations of movement parameters: maximum speed (Max. Speed), the time to maximum speed (Time-to-Max. Speed), and the proportion of movement time lapsed before maximum speed (Proportion of MV time to Max. Speed), for both triangle and square.

	N	Segment	R^2	% τ_g-coupling	Slope *(k)*
Triangle	2689	1	0.97 ± 0.01	97.36 ± 7.13	0.80 ± 0.34
		2	0.97 ± 0.01	95.95 ± 7.15	0.26 ± 0.12
		3	0.97 ± 0.01	96.55 ± 8.65	0.45 ± 0.24

	N	Segment	R^2	% τ_g-coupling	Slope *(k)*
Square	2747	1	0.97 ± 0.01	96.93 ± 9.03	0.80 ± 0.45
		2	0.96 ± 0.01	93.26 ± 6.69	0.35 ± 0.14
		3	0.97 ± 0.01	96.17 ± 4.39	0.32 ± 0.13
		4	0.97 ± 0.01	96.5 ± 4.73	0.47 ± 0.24
		5	0.96 ± 0.01	83.39 ± 9.32	0.57 ± 0.10

TABLE 3.3: Results of *tau*-analysis on copied shape segments. Means and standard deviations of movement parameters: recursive regression R^2 cut-off (R^2), Percentage of τ_g-*coupling* between movement *tau* and theoretical *tau-guide* (% τ_g-coupling), recursive regression slope (Slope *(k)*), for both triangle and square.

Correlations

		Length (mm)	MV time (ms)	Max. Speed (mm/s)	Time to Max. Speed (ms)	Proportion of MV time to Max. Speed	% τ_g-coupling	Slope *(k)*
Length (mm)	Pearson Correlation	1	.748(*)	.799(*)	.402	-.655	.614	-.415
	Sig. (2-tailed)	.	.033	.017	.323	.078	.105	.307
	N	8	8	8	8	8	8	8
MV time (ms)	Pearson Correlation	.748(*)	1	.257	.541	-.861(**)	.760(*)	-.465
	Sig. (2-tailed)	.033	.	.539	.166	.006	.029	.246
	N	8	8	8	8	8	8	8
Max. Speed (mm/s)	Pearson Correlation	.799(*)	.257	1	.196	-.232	.328	-.029
	Sig. (2-tailed)	.017	.539	.	.641	.580	.427	.945
	N	8	8	8	8	8	8	8
Time to Max. Speed (ms)	Pearson Correlation	.402	.541	.196	1	-.069	.325	.168
	Sig. (2-tailed)	.323	.166	.641	.	.870	.432	.690
	N	8	8	8	8	8	8	8
Proportion of MV time-to-Max. Speed	Pearson Correlation	-.655	-.861(**)	-.232	-.069	1	-.815(*)	.513
	Sig. (2-tailed)	.078	.006	.580	.870	.	.014	.194
	N	8	8	8	8	8	8	8
% τ_g-coupling	Pearson Correlation	.614	.760(*)	.328	.325	-.815(*)	1	.022
	Sig. (2-tailed)	.105	.029	.427	.432	.014	.	.959
	N	8	8	8	8	8	8	8
Slope *(k)*	Pearson Correlation	-.415	-.465	-.029	.168	.513	.022	1
	Sig. (2-tailed)	.307	.246	.945	.690	.194	.959	.
	N	8	8	8	8	8	8	8

TABLE 3.4: Correlation between mean movement variables for all segments copied in each shape. *: Correlation is significant at the 0.05 level (2-tailed). **: Correlation is significant at the 0.01 level (2-tailed).

—AREG Analysis:

The relations between individual neural activities, movement speed and movement *tau* were assessed for each of the neurons (parietal area 5 N = 399, prefrontal N = 163). The number of neurons which showed significant ($p < 0.05$) relation to movement *tau* and /or speed was calculated for the two brain regions.

—AREG analysis with movement tau and / or movement speed as the independent variable

To assess the percentage of neurons whose activities were significantly ($p < 0.05$) related to movement *tau*, the regression (AREG) analysis performed included only movement *tau* as the independent variable. It was found that the activities of 12.88% (21/163) of prefrontal cortical (PFC) neurons and 24.06% (96/399) of the parietal area 5 cells were significantly linearly related to the movement *tau* variable (FIG 3.8 a, b). A similar assessment of the association of movement speed and neural activities were performed to include only speed as the independent variable. To that end, it was found that 77.91% (259/399) of the prefrontal cortical neurons and 64.91% (127/163) of the parietal area 5 neurons were significantly linearly related to the movement speed (FIG 3.8 c, d).

Given that movement speed (in addition to other movement parameters e.g. position, direction etc.) has been reportedly found to be processed in the motor areas, e.g. M1, and area 5 of the parietal cortex (e.g. Ashe & Georgopoulos, 1994, Averbeck et al., 2005), it is therefore unlikely that neural activities are related solely to a specific parameter. Hence the percentages of neurons associated to either movement *tau* or speed were assessed taking into account of the possibility that the two parameters may

be processed by the same neurons. Therefore these two parameters were added as independent variables in the regression (EQ 3.9). It was observed that in both prefrontal cortex and area 5, the percentages of neurons significantly related only to movement speed were very high, accounting for at least half of the neurons in each region: PFC = 70.55% (115/163); Area 5 = 50.13% (200/399). These percentages were much greater than the percentages of neurons significantly related only to movement *tau*, which were markedly fewer: PFC = 1.84% (3/163); Area 5 = 6.14% (24/399); (FIG 3.9).

In considering those neurons whose activities were significantly related to movement *tau*, with or without the significant association to speed, we found the activities of 7.98% (13/163) prefrontal cortical neurons and 17.03% (68/399) of area 5 neurons to be associated with movement *tau*. The activities of the majority of cells in both cortical regions were significantly related to speed, whether or not the activities were also significantly related to movement *tau* (PFC = 76.69% (125/163); Area 5 = 61.15% (244/399)). A larger percentage of neurons were significantly related to both speed and movement *tau* in parietal area 5 (11.03%) compared to that observed for the prefrontal cortex (6.14%). The percentage of neurons unrelated to the two variables of interest were 21.47% (35/163) in the prefrontal cortex and 32.83% (131/299) in area 5, which highlighted the fact that other movement parameters, e.g. the kinematics and / or cognitive processes relevant to the task were also likely to be represented in both areas.

In general, there was a small subset of neurons in both prefrontal cortex and parietal area 5 whose activities were related to the time-varying aspect of movement *tau*, which was presumably sensed visually and via proprioception. A larger proportion of movement *tau*-related neurons were found in the parietal area 5 than in the prefrontal cortex.

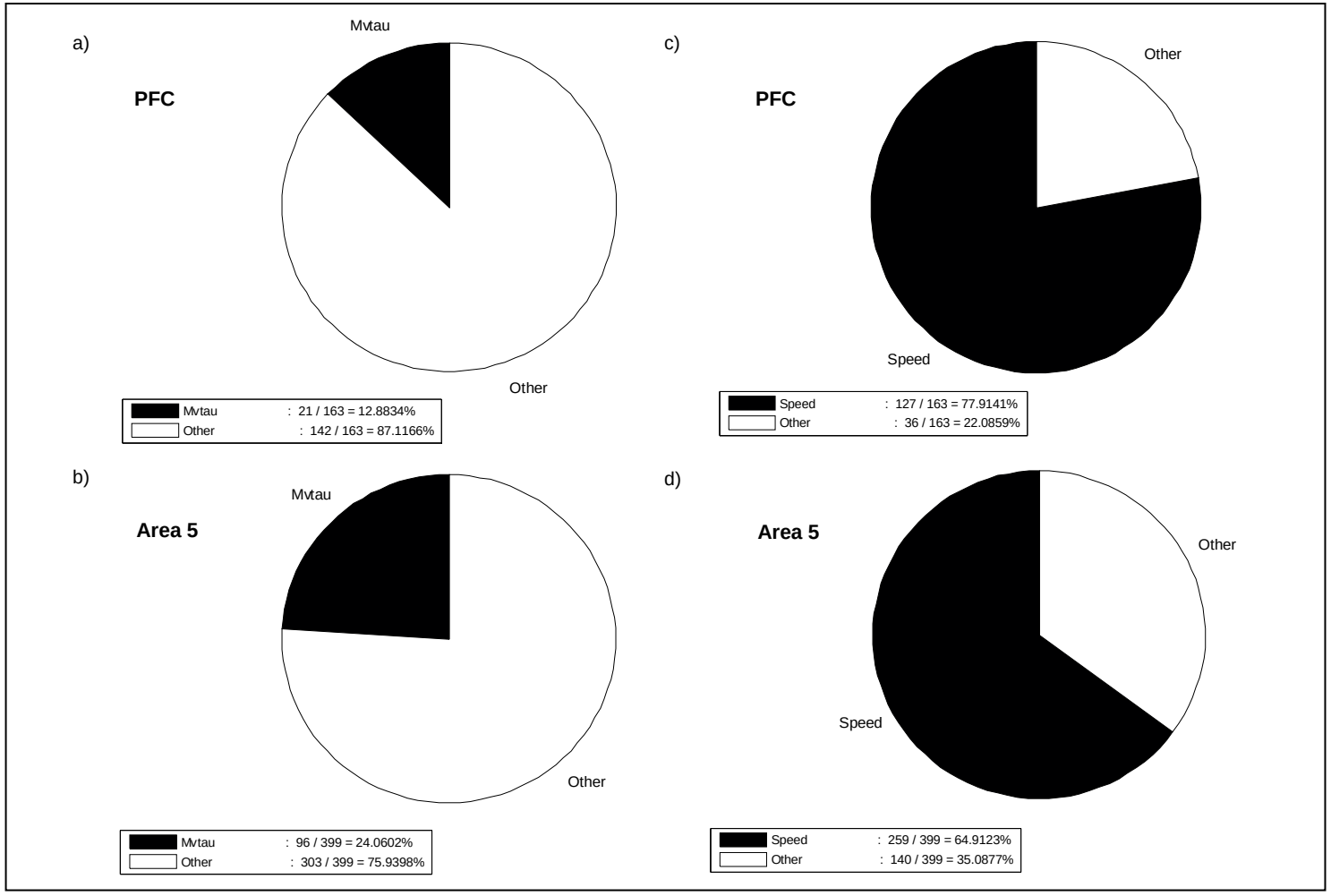

FIG 3.8: Prefrontal and parietal neural correlates of movement *tau* and speed. Percentage of neurons significantly related to movement *tau* (*Mvtau*) in prefrontal cortex (a) and parietal area 5 (b) and the percentage of neurons significantly related to speed in prefrontal cortex (c) and parietal area 5 (d).

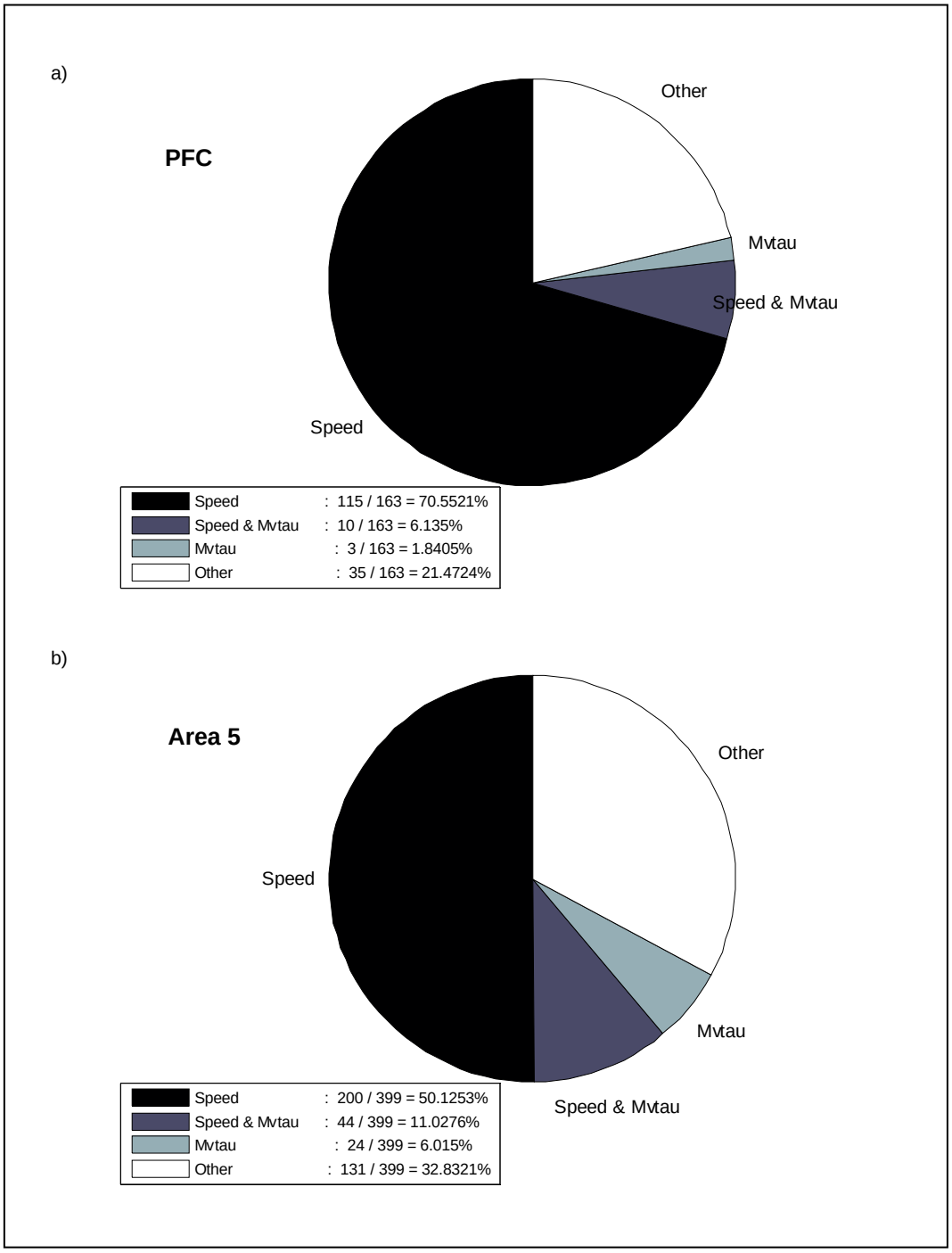

FIG 3.9: Prefrontal and parietal neural correlates of movement *tau* and /or speed. Percentage of neurons significantly related to movement *tau* (*Mvtau*) and/or speed in prefrontal cortex (a) and parietal area 5 (b).

Discussion

In this study, we conceived the copy-task as a sequence of segment gaps that the monkey had to close behaviourally, and we sought to ask two questions. First, we tested if the derived movement *taus* during gap closure would have high linear associations with the theoretical *tau-guide*, as measured by the % τ_g-coupling from the recursive regression. Second, we tested if the time-varying neural activities recorded from the monkey's prefrontal and parietal cortices during the copying performance were linearly related to the time-varying movement *tau* as well as time-varying movement speed.

While the monkey had been trained in the copy task, there were segments, which in the combination of their serial position, and the required movement direction, appeared to be relatively more challenging than others. For squares, the standard deviation for mean % τ_g-coupling was higher in the first and last segments, while for triangles, it was higher in the last segment compared to the others. Although mean % τ_g-coupling fluctuated across all shape segments copied by the monkey, it was generally very high, and generally above 90% (excluding the 83% observed in the last segment of copied squares). We observed that the τ_g-coupling tended to be stronger when movement durations were longer. It might be that in such instances, the animal took more time to control its movement speed (which in these cases, maximum speed was generally skewed towards the first half of the movement) and the approach to the end of the segments.

According to the general *tau*-theory, the τ_g-coupling slopes describe the dynamics of the portion of gap-closure that is τ_g-guided. A general trend in the mean slopes was manifested in both copied shapes. The monkey reached the first corner of the shape

with an abrupt contact (as indicated by the mean slopes; $k \approx 0.8$) but slowed down remarkably to approach the intermediate corners very gently and often under-reaching ($k < 0.5$), and finished off the last segment with a more tightly controlled contact ($0.5 < k < 0.7$). Therefore, the movements along each shape segment seemed to follow the general form described by the theoretical *tau-guide*, but with different gap-closure dynamics.

We found that there were generally more neurons in area 5 of the PPC whose activities (spike density functions) were significantly ($p < 0.05$) linearly related to movement *tau*, compared to the PFC neurons. This was the case when the regression considered movement *tau* as the single independent variable (24% in area 5; 13% in PFC) or when it also included speed as an additional parameter (17% in area 5; 8% in PFC). The majority of neural activities from both area 5 and the PFC were significantly linearly related to speed, with a higher percentage in the PFC (78%; cf. 65% in area 5) when it was the only independent variable in the regression, and also when movement *tau* was the additional parameter (71% in PFC; 50% in area 5). Our observation of parietal-prefrontal correlates of both speed and movement *tau* parallels those of other studies that have also demonstrated similar activities in parietal and prefrontal neurons, which are linked by reciprocal connections (Chafee, Goldman-Rakic 1998, Quintana, Fuster 1999)

It was interesting to find that there were more movement *tau*-related neurons in area 5 of the SPL compared to the PFC, while the latter had more speed-related neurons. Representation of movement speed in area 5 of the PPC was previously reported by Averbeck, Chafee, et al. (2005) and Ashe & Georgopoulos (1994). The finding that the majority of PFC activities was related to movement speed is perhaps surprising since it is commonly associated with more abstract, or 'intention-related' aspects of visuomotor representations (Hoshi 2006). However, the existence of reciprocal connections between

areas 5 and 7 of the PPC, projections from areas 7a and 7b to area 5, and the dorsal and ventral DLPFC (Hyvärinen 1982, Pandya, Seltzer 1982), as well as the recently described direct connections between SPL and DLPFCd (Petrides, Pandya 2006) make this observation less startling.

Using a similar regression analysis, Merchant et al. (2004a, b) demonstrated that activities of neurons in the area 7a of the IPL were correlated with movement *tau* in an interceptive task and the strength of this representation (i.e. the percentage of cells related to the variable *tau*) was modulated by the moving target's visuospatial attributes; whether it appeared as a real or an apparent target. In the condition where the target manifested real motion, 8% of the motor cortical neurons and 14% of the area 7a neurons were significantly linearly related to movement *tau*. When the target manifested 'apparent motion', a higher percentage of *tau*-related neurons was found in both areas (M1 = 31%, area 7a = 28%). Our findings were similar in range to Merchant et al. (2004)'s observation for targets in real motion (PFC = 8%; area 5 = 17%) and one might hypothesize that had the cursor's visual feedback been modified to appear more intermittently, or less continuously, more neurons might respond in relation to the variable *tau*. We also noted the similarity observed for movement speed in both tasks in that frontal areas (M1 or PFC) encompassed more speed-related neurons, compared to the parietal areas (areas 5 or 7a of the PPC).

The predominance of speed-related neurons relative to *tau*-related neurons in these neural areas seems to suggest that while movement *tau* provides useful timing information, the nervous system still requires relevant information regarding the status of the limb(s) in motion, i.e. velocity or direction, for implementing necessary forward control mechanisms. The current limb status can *in principle* be derived from movement speed (tangential velocity), through some form of integration (or differentiation; e.g. sensing acceleration within the vestibular system). In addition, a speculation that

warrants investigation is that the high speed-related coupling might be an inherent neurophysiological trait of the nervous system; from a measure of speed, position and acceleration can be derived.

What was perhaps remarkable was that the copy task, which did not require the monkey to intercept a moving object and therefore the saliency of the temporal aspect of gap-closure was not as prominent, also involved the neural representation of the movement *tau* in both parietal and prefrontal cortical neurons. This indicates that movement *tau* is processed in both interceptive and non-interceptive tasks. In addition, our findings are also in accord with Field and Wann (2005)'s fMRI imaging of human perception of time-to-contact and time-to-gap-closure; the latter condition indicated the involvement of bilateral superior parietal sulci (PPC), the left cingulate gyral, and left ventral premotor activations. Therefore, in perception and in action, there are correlates of movement *tau* within the neural system that are involved in visually guided behaviour.

The *tau* variable, which is the current time-to-closure of a motion-gap, is a form of prospective information and is potentially useful for updating sensorimotor representations. Its neural correlate within the parieto-frontal system renders the network an ideal role for the predictive forward motivating mechanism involved in visually-guided movements (Desmurget, Grafton 2000). Movement *tau*, which is temporal information, can *in principle* provide prediction of future estimation of limb state relative to the current movement speed, and such information can be used to regulate behaviour through the feedback loops. Therefore, not only could the estimation of current limb state be made, future movement status can be predicted and compared.

The PPC has been shown to exhibit anticipatory response to movement intentions (Eskandar, Assad 1999, Kalaska, Crammond 1995, Snyder, Batista et al. 1998), sudden changes in the movement plan (Archambault, Battaglia-Mayer et al. 2005), as well as being implicated in the update and adjustments of movement intentions (Desmurget, Epstein et al. 1999, Desmurget, Grea et al. 2001, Grea, Pisella et al. 2002, Rushworth, Taylor 2006). Moreover, the relevance of movement *tau* for the PFC, an area implicated in the assimilation of sensory cues for intended goals, is not only apt but important. It tells the system that within a certain time-frame, whether e.g. the limb will make it to the goal (or target) based on its current state of motion, and if it has to be at the goal within a time-constraint, it had better engage the motor system to accelerate the movement, or alternatively, if it seems as though the limb will arrive beyond the target location with the current motion status, the motor system would need to slow the movement down before resulting in the limb colliding (too strongly) with the goal. Therefore, the suggested role of PPC in online movement update could in part be that predictive information like the variable *tau*, which provides an efficient way for action intention to be integrated with exproprioceptive feedback in the ensuing motor commands, is represented within the dynamic parietal-frontal system.

With respect to the ongoing debate on the likely coordinate frame of reference in which visuospatial and /or visuomotor cues might be coded, the presence of aforementioned GTFs (i.e. the partially overlapping preferred directions within a restricted spatial location for different task conditions involving arm and/or eye movements) demonstrated in the PPC (Battaglia-Mayer, Archambault et al. 2006, Battaglia-Mayer, Caminiti et al. 2003, Battaglia-Mayer, Ferraina et al. 2001, Battaglia-Mayer, Mascaro et al. 2005) implied that movement *tau* and speed were probably encoded in both ego- and allocentric coordinates. However, given that the inclusion of eye position did not improve the modelling of neural representation of movement speed in the analyses performed by Averbeck, Chafee et al. (2005), it is likely that, at least for area 5 of the

PPC in this analysis, the neural representations of *tau* and speed were mainly coded in hand /body reference frame.

A recent conception of the possible segregation of PFC functional representation that reflected the preferential excitation of the ventral DLPFC neurons to visuospatial cues, and the preferential excitation of neurons within the dorsal DLPFC to visuomotor cues (Fukushima, Hasegawa et al. 2004b, Hasegawa, Blitz et al. 2004, Hoshi, Tanji 2004a, Lebedev, Messinger et al. 2004, Ninokura, Mushiake et al. 2004, Saito, Mushiake et al. 2005, di Pellegrino, Wise 1993b), was suggested by Hoshi (2006). The neurophysiological recordings from the PFC in monkey 157 included both dorsal and ventral portions surrounding the area peri-principalis, but were not classified with respect to their anatomical position. Hence, we could not determine if a difference in the percentage of *tau*- or speed-related neurons in the DLPFCd or DLPFCv exists. What we could speculate is that neurons whose activities are significantly related to *tau* (and /or speed) are likely to comprise both the dorsal and ventral DLPFC as it is a variable that is informative on both the spatial and temporal domains, and hence, it is both visuospatial and visuomotor.

The current analyses of neural activities recorded from the monkey PFC and SPL area 5 demonstrated that the time-varying aspects of movements were encoded in these brain regions. While the majority of neurons in both cortical regions were related to movement speed, significant relations between neural activities and movement *tau* were also found. These observations complemented previous findings that neural activities of area 7a in the IPL and the primary motor cortex were also related to movement speed and the variable *tau* (Averbeck, Chafee et al. 2005, Merchant, Battaglia-Mayer et al. 2004a, Merchant, Battaglia-Mayer et al. 2004b, Moran, Schwartz 1999, Port, Kruse et al. 2001, Schwartz 1993, Schwartz, Moran 2000). Together, these findings suggest that within the parieto-frontal network, chosen as the anatomical field

for study here, movement parameters which are pertinent for the intended goal, e.g. *tau* and /or speed, are likely to be represented. It remains to be tested if the neural activities recorded from humans engaging in a similar task would also be related to movement *tau* and /or speed, and whether the substrates underlying such related activities are homologous with those implicated from this and previous neurophysiological studies with animals.

Bibliography for this section:

ANDERSEN, R.A., ESSICK, G.K. and SIEGEL, R.M., 1987. Neurons of area 7 activated by both visual stimuli and oculomotor behavior. *Experimental Brain Research,* 67(2), pp. 316-322.

ARCHAMBAULT, P.S., BATTAGLIA-MAYER, A. and CAMINITI, R., 2005. Modulation of parietal cell activity associated with a target jump during hand reaching. *Society for Neuroscience Abstracts,* 2005, 363.10.

ASAAD, W.F., RAINER, G. and MILLER, E.K., 1998. Neural activity in the primate prefrontal cortex during associative learning. *Neuron,* **21**(6), pp. 1399-1407.

ASHE, J. and GEORGOPOULOS, A.P., 1994. Movement parameters and neural activity in motor cortex and area 5. *Cerebral Cortex,* **4**(6), pp. 590-600.

AVERBECK, B.B., CHAFEE, M.V., CROWE, D.A. and GEORGOPOULOS, A.P., 2005. Parietal representation of hand velocity in a copy task. *Journal of Neurophysiology,* **93**(1), pp. 508-518.

AVERBECK, B.B., CHAFEE, M.V., CROWE, D.A. and GEORGOPOULOS, A.P., 2003. Neural activity in prefrontal cortex during copying geometrical shapes. I. Single cells encode shape, sequence, and metric parameters. *Experimental Brain Research,* **150**(2), pp. 127-141.

AVERBECK, B.B., CHAFEE, M.V., CROWE, D.A. and GEORGOPOULOS, A.P., 2002. Parallel processing of serial movements in prefrontal cortex. *Proceedings of the National Academy of Sciences of the United States of America,* **99**(20), pp. 13172-13177.

AVERBECK, B.B., CROWE, D.A., CHAFEE, M.V. and GEORGOPOULOS, A.P., 2003. Neural activity in prefrontal cortex during copying geometrical shapes. II. Decoding shape segments from neural ensembles. *Experimental Brain Research,* **150**(2), pp. 142-153.

AVERBECK, B.B., SOHN, J.W. and LEE, D., 2006. Activity in prefrontal cortex during dynamic selection of action sequences. *Nature Neuroscience,* **9**(2), pp. 276-282.

BARBAS, H. and MESULAM, M.M., 1985. Cortical afferent input to the principalis region of the rhesus monkey. *Neuroscience,* **15**(3), pp. 619-637.

BARBAS, H. and PANDYA, D.N., 1987. Architecture and frontal cortical connections of the premotor cortex (area 6) in the rhesus monkey. *Journal of Comparative Neurology,* **256**(2), pp. 211-228.

BARRACLOUGH, D.J., CONROY, M.L. and LEE, D., 2004. Prefrontal cortex and decision making in a mixed-strategy game. *Nature Neuroscience,* **7**(4), pp. 404-410.

BATISTA, A.P., BUNEO, C.A., SNYDER, L.H. and ANDERSEN, R.A., 1999. Reach Plans in Eye-Centered Coordinates. *Science,* **285**(5425), pp. 257-260.

BATTAGLIA-MAYER, A., ARCHAMBAULT, P.S. and CAMINITI, R., 2006. The cortical network for eye-hand coordination and its relevance to understanding motor disorders of parietal patients. *Neuropsychologia,* **44**(13), pp. 2607-2620.

BATTAGLIA-MAYER, A., FERRAINA, S., GENOVESIO, A., MARCONI, B., SQUATRITO, S., MOLINARI, M., LACQUANITI, F. and CAMINITI, R., 2001. Eye-Hand Coordination during Reaching. II. An Analysis of the Relationships between Visuomanual Signals in Parietal Cortex and Parieto-frontal Association Projections. *Cerebral Cortex,* **11**(6), pp. 528-544.

BATTAGLIA-MAYER, A., FERRAINA, S., MITSUDA, T., MARCONI, B., GENOVESIO, A., ONORATI, P., LACQUANITI, F. and CAMINITI, R., 2000. Early coding of reaching in the parietooccipital cortex. *Journal of Neurophysiology,* **83**(4), pp. 2374-2391.

BATTAGLIA-MAYER, A., CAMINITI, R., LACQUANITI, F. and ZAGO, M., 2003. Multiple Levels of Representation of Reaching in the Parieto-frontal Network. *Cerebral Cortex,* **13**(10), pp. 1009-1022.

BATTAGLIA-MAYER, A., MASCARO, M., BRUNAMONTI, E. and CAMINITI, R., 2005. The Over-representation of Contralateral Space in Parietal Cortex: A Positive Image of Directional Motor Components of Neglect? *Cerebral Cortex,* **15**(5), pp. 514-525.

BRODMANN, K., 1909. Vergleichende Lokalisationslehre der Grosshirnrinde in ihren Prinzipien dargestellt auf Grund des Zellenbaues. Leipzig: Barth.

BUNEO, C.A. and ANDERSEN, R.A., 2006. The posterior parietal cortex: sensorimotor interface for the planning and online control of visually guided movements. *Neuropsychologia,* **44**(13), pp. 2594-2606.

BUNEO, C.A., JARVIS, M.R., BATISTA, A.P. and ANDERSEN, R.A., 2002. Direct visuomotor transformations for reaching. *Nature,* **416**(6881), pp. 632-636.

CAMINITI, R., FERRAINA, S. and JOHNSON, P.B., 1996. The sources of visual information to the primate frontal lobe: a novel role for the superior parietal lobule. *Cerebral Cortex,* **6**(3), pp. 319-328.

CARROZZO, M., STRATTA, F., MCINTYRE, J. and LACQUANITI, F., 2002. Cognitive allocentric representations of visual space shape pointing errors. *Experimental Brain Research,* **147**(4), pp. 426-436.

CAVADA, C. and GOLDMAN-RAKIC, P.S., 1989. Posterior parietal cortex in rhesus monkey: I. Parcellation of areas based on distinctive limbic and sensory corticocortical connections. *Journal of Comparative Neurology,* **287**(4), pp. 393-421.

CHAFEE, M.V. and GOLDMAN-RAKIC, P.S., 2000. Inactivation of parietal and prefrontal cortex reveals interdependence of neural activity during memory-guided saccades. *Journal of Neurophysiology,* **83**(3), pp. 1550-1566.

CHAFEE, M.V. and GOLDMAN-RAKIC, P.S., 1998. Matching patterns of activity in primate prefrontal area 8a and parietal area 7ip neurons during a spatial working memory task. *Journal of Neurophysiology,* **79**(6), pp. 2919-2940.

CORBETTA, M., AKBUDAK, E., CONTURO, T.E., SNYDER, A.Z., OLLINGER, J.M., DRURY, H.A., LINENWEBER, M.R., PETERSEN, S.E., RAICHLE, M.E., VAN ESSEN, D.C. and SHULMAN, G.L., 1998. A common network of functional areas for attention and eye movements. *Neuron,* **21**(4), pp. 761-773.

CURTIS, C.E. and D'ESPOSITO, M., 2004. The effects of prefrontal lesions on working memory performance and theory. *Cognitive, Affective, & Behavioral Neuroscience,* **4**(4), pp. 528-539.

DESMURGET, M., EPSTEIN, C.M., TURNER, R.S., PRABLANC, C., ALEXANDER, G.E. and GRAFTON, S.T., 1999. Role of the posterior parietal cortex in updating reaching movements to a visual target. *Nature Neuroscience,* **2**(6), pp. 563-567.

DESMURGET, M. and GRAFTON, S., 2000. Forward modeling allows feedback control for fast reaching movements. *Trends in Cognitive Sciences,* **4**(11), pp. 423-431.

DESMURGET, M., GREA, H., GRETHE, J.S., PRABLANC, C., ALEXANDER, G.E. and GRAFTON, S.T., 2001. Functional anatomy of nonvisual feedback loops during reaching: a positron emission tomography study. *Journal of Neuroscience,* **21**(8), pp. 2919-2928.

DI PELLEGRINO, G. and WISE, S.P., 1993a. Effects of attention on visuomotor activity in the premotor and prefrontal cortex of a primate. *Somatosensory & Motor Research,* **10**(3), pp. 245-262.

DI PELLEGRINO, G. and WISE, S.P., 1993b. Visuospatial versus visuomotor activity in the premotor and prefrontal cortex of a primate. *Journal of Neuroscience,* **13**(3), pp. 1227-1243.

ESKANDAR, E.N. and ASSAD, J.A., 1999. Dissociation of visual, motor and predictive signals in parietal cortex during visual guidance. *Nature Neuroscience,* **2**(1), pp. 88-93.

FIELD, D.T. and WANN, J.P., 2005. Perceiving time to collision activates the sensorimotor cortex. *Current Biology,* **15**(5), pp. 453-458.

FLANAGAN, J.R. and RAO, A.K., 1995. Trajectory adaptation to a nonlinear visuomotor transformation: evidence of motion planning in visually perceived space. *Journal of Neurophysiology,* **74**(5), pp. 2174-2178.

FOGASSI, L. and LUPPINO, G., 2005. Motor functions of the parietal lobe. *Current Opinion in Neurobiology,* **15**(6), pp. 626-631.

FU, Q.G., FLAMENT, D., COLTZ, J.D. and EBNER, T.J., 1995. Temporal encoding of movement kinematics in the discharge of primate primary motor and premotor neurons. *Journal of Neurophysiology,* **73**(2), pp. 836-854.

FU, Q.G., SUAREZ, J.I. and EBNER, T.J., 1993. Neuronal specification of direction and distance during reaching movements in the superior precentral premotor area and primary motor cortex of monkeys. *Journal of Neurophysiology,* **70**(5), pp. 2097-2116.

FUJII, N. and GRAYBIEL, A.M., 2003. Representation of action sequence boundaries by macaque prefrontal cortical neurons. *Science,* **301**(5637), pp. 1246-1249.

FUKUSHIMA, T., HASEGAWA, I. and MIYASHITA, Y., 2004a. Prefrontal neuronal activity encodes spatial target representations sequentially updated after nonspatial target-shift cues. *Journal of Neurophysiology,* **91**(3), pp. 1367-1380.

FUKUSHIMA, T., HASEGAWA, I. and MIYASHITA, Y., 2004b. Prefrontal neuronal activity encodes spatial target representations sequentially updated after nonspatial target-shift cues. *Journal of Neurophysiology,* **91**(3), pp. 1367-1380.

FUNAHASHI, S., BRUCE, C.J. and GOLDMAN-RAKIC, P.S., 1989. Mnemonic coding of visual space in the monkey's dorsolateral prefrontal cortex. *Journal of Neurophysiology,* **61**(2), pp. 331-349.

FUNAHASHI, S., INOUE, M. and KUBOTA, K., 1997. Delay-period activity in the primate prefrontal cortex encoding multiple spatial positions and their order of presentation. *Behavioural Brain Research,* **84**(1-2), pp. 203-223.

FUSTER, J.M., BODNER, M. and KROGER, J.K., 2000. Cross-modal and cross-temporal association in neurons of frontal cortex. *Nature,* **405**(6784), pp. 347-351.

GEORGOPOULOS, A.P., KALASKA, J.F., CAMINITI, R. and MASSEY, J.T., 1983. Interruption of motor cortical discharge subserving aimed arm movements. *Experimental Brain Research,* **49**(3), pp. 327-340.

GOLD, J.I. and SHADLEN, M.N., 2000. Representation of a perceptual decision in developing oculomotor commands. *Nature,* **404**(6776), pp. 390-394.

GOLDMAN-RAKIC, P.S., 1996. Regional and cellular fractionation of working memory. *Proceedings of the National Academy of Sciences of the United States of America,* **93**(24), pp. 13473-13480.

GORDON, J., GHILARDI, M.F. and GHEZ, C., 1994. Accuracy of planar reaching movements. I. Independence of direction and extent variability. *Experimental Brain Research,* **99**(1), pp. 97-111.

GREA, H., PISELLA, L., ROSSETTI, Y., DESMURGET, M., TILIKETE, C., GRAFTON, S., PRABLANC, C. and VIGHETTO, A., 2002. A lesion of the posterior parietal cortex disrupts on-line adjustments during aiming movements. *Neuropsychologia,* **40**(13), pp. 2471-2480.

HASEGAWA, R.P., BLITZ, A.M. and GOLDBERG, M.E., 2004. Neurons in monkey prefrontal cortex whose activity tracks the progress of a three-step self-ordered task. *Journal of Neurophysiology,* **92**(3), pp. 1524-1535.

HENRIQUES, D.Y., KLIER, E.M., SMITH, M.A., LOWY, D. and CRAWFORD, J.D., 1998. Gaze-centered remapping of remembered visual space in an open-loop pointing task. *Journal of Neuroscience,* **18**(4), pp. 1583-1594.

HOSHI, E., 2006. Functional specialization within the dorsolateral prefrontal cortex: A review of anatomical and physiological studies of non-human primates. *Neuroscience Research,* **54**(2), pp. 73-84.

HOSHI, E., SHIMA, K. and TANJI, J., 2000. Neuronal activity in the primate prefrontal cortex in the process of motor selection based on two behavioral rules. *Journal of Neurophysiology,* **83**(4), pp. 2355-2373.

HOSHI, E. and TANJI, J., 2004a. Area-selective neuronal activity in the dorsolateral prefrontal cortex for information retrieval and action planning. *Journal of Neurophysiology,* **91**(6), pp. 2707-2722.

HOSHI, E. and TANJI, J., 2004b. Differential roles of neuronal activity in the supplementary and presupplementary motor areas: from information retrieval to motor planning and execution. *Journal of Neurophysiology,* **92**(6), pp. 3482-3499.

HOSHI, E. and TANJI, J., 2004c. Functional specialization in dorsal and ventral premotor areas. *Progress in Brain Research,* **143**, pp. 507-511.

HOSHI, E. and TANJI, J., 2002. Contrasting neuronal activity in the dorsal and ventral premotor areas during preparation to reach. *Journal of Neurophysiology,* **87**(2), pp. 1123-1128.

HYVÄRINEN, J., 1982. Posterior Parietal Lobe of the Primate Brain. *Physiological Reviews,* **62**(3), pp. 1060-1129.

JACKSON, S.R. and HUSAIN, M., 2006. Visuomotor functions of the posterior parietal cortex. *Neuropsychologia,* **44**(13), pp. 2589-2593.

JOHNSON, M.T., MASON, C.R. and EBNER, T.J., 2001. Central processes for the multiparametric control of arm movements in primates. *Current Opinion in Neurobiology,* **11**(6), pp. 684-688.

JOHNSON, P.B., FERRAINA, S., BIANCHI, L. and CAMINITI, R., 1996. Cortical networks for visual reaching: physiological and anatomical organization of frontal and parietal lobe arm regions. *Cerebral Cortex,* **6**(2), pp. 102-119.

KALASKA, J.F. and CRAMMOND, D.J., 1995. Deciding not to GO: neuronal correlates of response selection in a GO/NOGO task in primate premotor and parietal cortex. *Cerebral Cortex,* **5**(5), pp. 410-428.

LACQUANITI, F., GUIGON, E., BIANCHI, L., FERRAINA, S. and CAMINITI, R., 1995. Representing spatial information for limb movement: role of area 5 in the monkey. *Cerebral Cortex,* **5**(5), pp. 391-409.

LACQUANITI, F., TERZUOLO, C. and VIVIANI, P., 1983. The law relating the kinematic and figural aspects of drawing movements. *Acta Psychologica,* **54**(1-3), pp. 115-130.

LEBEDEV, M.A., MESSINGER, A., KRALIK, J.D. and WISE, S.P., 2004. Representation of attended versus remembered locations in prefrontal cortex. *PLoS Biology,* **2**(11), pp. e365.

LEON, M.I. and SHADLEN, M.N., 1999. Effect of expected reward magnitude on the response of neurons in the dorsolateral prefrontal cortex of the macaque. *Neuron,* **24**(2), pp. 415-425.

LUPPINO, G., MATELLI, M., CAMARDA, R. and RIZZOLATTI, G., 1993. Corticocortical connections of area F3 (SMA-proper) and area F6 (pre-SMA) in the macaque monkey. *Journal of Comparative Neurology,* **338**(1), pp. 114-140.

LUPPINO, G., ROZZI, S., CALZAVARA, R. and MATELLI, M., 2003. Prefrontal and agranular cingulate projections to the dorsal premotor areas F2 and F7 in the macaque monkey. *European Journal of Neuroscience,* **17**(3), pp. 559-578.

MARCONI, B., GENOVESIO, A., BATTAGLIA-MAYER, A., FERRAINA, S., SQUATRITO, S., MOLINARI, M., LACQUANITI, F. and CAMINITI, R., 2001. Eye-Hand Coordination during Reaching. I. Anatomical Relationships between Parietal and Frontal Cortex. *Cerebral Cortex,* **11**(6), pp. 513-527.

MCINTYRE, J., STRATTA, F. and LACQUANITI, F., 1998. Short-term memory for reaching to visual targets: psychophysical evidence for body-centered reference frames. *Journal of Neuroscience,* **18**(20), pp. 8423-8435.

MERCHANT, H., BATTAGLIA-MAYER, A. and GEORGOPOULOS, A.P., 2004a. Neural responses during interception of real and apparent circularly moving stimuli in motor cortex and area 7a. *Cerebral Cortex,* **14**(3), pp. 314-331.

MERCHANT, H., BATTAGLIA-MAYER, A. and GEORGOPOULOS, A.P., 2004b. Neurophysiology of the parieto-frontal system during target interception. *Neurology & Clinical Neurophysiology,* **2004**, pp. 1.

MERCHANT, H., BATTAGLIA-MAYER, A. and GEORGOPOULOS, A.P., 2001. Effects of optic flow in motor cortex and area 7a. *Journal of Neurophysiology,* **86**(4), pp. 1937-1954.

MIDDLETON, F.A. and STRICK, P.L., 2001. Cerebellar projections to the prefrontal cortex of the primate. *Journal of Neuroscience,* **21**(2), pp. 700-712.

MORAN, D.W. and SCHWARTZ, A.B., 1999. Motor cortical activity during drawing movements: population representation during spiral tracing. *Journal of Neurophysiology,* **82**(5), pp. 2693-2704.

MORECRAFT, R.J., CIPOLLONI, P.B., STILWELL-MORECRAFT, K.S., GEDNEY, M.T. and PANDYA, D.N., 2004. Cytoarchitecture and cortical connections of the posterior cingulate and adjacent somatosensory fields in the rhesus monkey. *Journal of Comparative Neurology,* **469**(1), pp. 37-69.

MOTTER, B.C. and MOUNTCASTLE, V.B., 1981. The functional properties of the light-sensitive neurons of the posterior parietal cortex studied in waking monkeys: foveal sparing and opponent vector organization. *Journal of Neuroscience,* **1**(1), pp. 3-26.

MOUNTCASTLE, V.B., LYNCH, J.C., GEORGOPOULOS, A., SAKATA, H. and ACUNA, C., 1975. Posterior parietal association cortex of the monkey: command functions for operations within extrapersonal space. *Journal of Neurophysiology,* **38**(4), pp. 871-908.

NEGGERS, S.F. and BEKKERING, H., 2001. Gaze anchoring to a pointing target is present during the entire pointing movement and is driven by a non-visual signal. *Journal of Neurophysiology,* **86**(2), pp. 961-970.

NEGGERS, S.F. and BEKKERING, H., 2000. Ocular gaze is anchored to the target of an ongoing pointing movement. *Journal of Neurophysiology,* **83**(2), pp. 639-651.

NINOKURA, Y., MUSHIAKE, H. and TANJI, J., 2004. Integration of temporal order and object information in the monkey lateral prefrontal cortex. *Journal of Neurophysiology,* **91**(1), pp. 555-560.

PANDYA, D.N. and SELTZER, B., 1982. Intrinsic connections and architectonics of posterior parietal cortex in the rhesus monkey. *Journal of Comparative Neurology,* **204**(2), pp. 196-210.

PESARAN, B., NELSON, M.J. and ANDERSEN, R.A., 2006. Dorsal premotor neurons encode the relative position of the hand, eye, and goal during reach planning. *Neuron,* **51**(1), pp. 125-134.

PETRIDES, M. and PANDYA, D.N., 2006. Efferent association pathways originating in the caudal prefrontal cortex in the macaque monkey. *Journal of Comparative Neurology,* **498**(2), pp. 227-251.

PETRIDES, M. and PANDYA, D.N., 2002. Comparative cytoarchitectonic analysis of the human and the macaque ventrolateral prefrontal cortex and corticocortical connection patterns in the monkey. *European Journal of Neuroscience,* **16**(2), pp. 291-310.

PETRIDES, M. and PANDYA, D.N., 1999. Dorsolateral prefrontal cortex: comparative cytoarchitectonic analysis in the human and the macaque brain and corticocortical connection patterns. *European Journal of Neuroscience,* **11**(3), pp. 1011-1036.

PETRIDES, M. and PANDYA, D.N., 1984. Projections to the frontal cortex from the posterior parietal region in the rhesus monkey. *Journal of Comparative Neurology,* **228**(1), pp. 105-116.

PISELLA, L., GREA, H., TILIKETE, C., VIGHETTO, A., DESMURGET, M., RODE, G., BOISSON, D. and ROSSETTI, Y., 2000. An 'automatic pilot' for the hand in human

posterior parietal cortex: toward reinterpreting optic ataxia. *Nature Neuroscience,* **3**(7), pp. 729-736.

PORT, N.L., KRUSE, W., LEE, D. and GEORGOPOULOS, A.P., 2001. Motor cortical activity during interception of moving targets. *Journal of Cognitive Neuroscience*, **13**(3), pp. 306-318.

PREUSS, T.M. and GOLDMAN-RAKIC, P.S., 1989. Connections of the ventral granular frontal cortex of macaques with perisylvian premotor and somatosensory areas: anatomical evidence for somatic representation in primate frontal association cortex. *Journal of Comparative Neurology*, **282**(2), pp. 293-316.

QUINTANA, J. and FUSTER, J.M., 1999. From perception to action: temporal integrative functions of prefrontal and parietal neurons. *Cerebral Cortex*, **9**(3), pp. 213-221.

QUINTANA, J. and FUSTER, J.M., 1992. Mnemonic and predictive functions of cortical neurons in a memory task. *Neuroreport,* **3**(8), pp. 721-724.

RAO, S.C., RAINER, G. and MILLER, E.K., 1997. Integration of what and where in the primate prefrontal cortex. *Science,* **276**(5313), pp. 821-824.

RIZZOLATTI, G., FOGASSI, L. and GALLESE, V., 1997. Parietal cortex: from sight to action. *Current Opinion in Neurobiology,* **7**(4), pp. 562-567.

RUSHWORTH, M.F., ELLISON, A. and WALSH, V., 2001. Complementary localization and lateralization of orienting and motor attention. *Nature Neuroscience,* **4**(6), pp. 656-661.

RUSHWORTH, M.F. and TAYLOR, P.C., 2006. TMS in the parietal cortex: updating representations for attention and action. *Neuropsychologia,* **44**(13), pp. 2700-2716.

SABES, P.N. and JORDAN, M.I., 1997. Obstacle avoidance and a perturbation sensitivity model for motor planning. *Journal of Neuroscience,* **17**(18), pp. 7119-7128.

SAITO, N., MUSHIAKE, H., SAKAMOTO, K., ITOYAMA, Y. and TANJI, J., 2005. Representation of immediate and final behavioral goals in the monkey prefrontal cortex during an instructed delay period. *Cerebral Cortex*, **15**(10), pp. 1535-1546.

SAKATA, H., SHIBUTANI, H. and KAWANO, K., 1980. Spatial properties of visual fixation neurons in posterior parietal association cortex of the monkey. *Journal of Neurophysiology,* **43**(6), pp. 1654-1672.

SCHWARTZ, A.B., 1993. Motor cortical activity during drawing movements: population representation during sinusoid tracing. *Journal of Neurophysiology,* **70**(1), pp. 28-36.

SCHWARTZ, A.B. and MORAN, D.W., 2000. Arm trajectory and representation of movement processing in motor cortical activity. *European Journal of Neuroscience,* **12**(6), pp. 1851-1856.

SIEGEL, R.M. and READ, H.L., 1997. Analysis of optic flow in the monkey parietal area 7a. *Cerebral Cortex,* **7**(4), pp. 327-346.

SNYDER, L.H., BATISTA, A.P. and ANDERSEN, R.A., 1998. Change in motor plan, without a change in the spatial locus of attention, modulates activity in posterior parietal cortex. *Journal of Neurophysiology,* **79**(5), pp. 2814-2819.

SNYDER, L.H., CALTON, J.L., DICKINSON, A.R. and LAWRENCE, B.M., 2002. Eye-hand coordination: saccades are faster when accompanied by a coordinated arm movement. *Journal of Neurophysiology,* **87**(5), pp. 2279-2286.

SUN, H. and FROST, B.J., 1998. Computation of different optical variables of looming objects in pigeon nucleus rotundus neurons. *Nature Neuroscience,* **1**(4), pp. 296-303.

TANJI, J. and HOSHI, E., 2001. Behavioral planning in the prefrontal cortex. *Current Opinion in Neurobiology,* **11**(2), pp. 164-170.

TSUJIMOTO, S. and SAWAGUCHI, T., 2004. Neuronal representation of response-outcome in the primate prefrontal cortex. *Cerebral Cortex,* **14**(1), pp. 47-55.

VAN DONKELAAR, P., LEE, R.G. and GELLMAN, R.S., 1994. The contribution of retinal and extraretinal signals to manual tracking movements. *Experimental Brain Research,* **99**(1), pp. 155-163.

VIVIANI, P. and TERZUOLO, C., 1982. Trajectory determines movement dynamics. *Neuroscience,* **7**(2), pp. 431-437.

WALKER, A.E., 1940. A cytoarchitectural study of the prefrontal area of the macaque monkey. *Journal of Comparative Neurology,* **73**, pp. 59-86.

WOLPERT, D.M., GHAHRAMANI, Z. and JORDAN, M.I., 1995. Are arm trajectories planned in kinematic or dynamic coordinates? An adaptation study. *Experimental Brain Research,* **103**(3), pp. 460-470.

CHAPTER 4:

Neuroimaging:

Studying the Neural Correlates of Behaviour

Functional brain mapping has been the object of investigations by scientists and physicians over the last two centuries. While phrenology lacked scientific rigour in correlating cortical volume behind the cranial bumps and presumed cognitive attributes, it did spark the pursuit of functional localization that is still en vogue today. Through neuro-pathological (Broca 1861), and electro-stimulation (Fritsch, Hitzig 1870, Penfield 1954) studies, scientists have gleaned evidence that various functions e.g. speech, or movement, can be ascribed to different cortical areas of the brain. Some of the greatest insights gained in the field's history, which are still as important today, came from the astute inferences of Hughlings Jackson's observations on epileptic patients (Jackson 1875). Erratic as they may appear, epileptic seizures often manifest an orderly progression of the clonic and tonic muscular jerks from one body part to another. This phenomenon led Jackson to conceive the cortical brain as topographically organized and he concluded that a representation of the whole body exists within certain cortical areas, as for example, in the homunculi of the somatosensory cortices that we know today.

Yet, unlike most colleagues in his time who viewed the brain as divided in focal areas, each with a specific putative function, Jackson was aware that following brain damage, a person never loses a function such as speech or movement completely even if the voluntary ability to control them is lost. By the same logic, symptoms that manifest as a consequence of a cortical lesion do not necessarily imply that the damaged region is solely responsible for those abnormal functions. Jackson was ahead of his times in his view that many brain regions and their inter-connectivity contribute to any single behaviour. This wisdom is one that we have only really begun to appreciate with the advent of neuroimaging. Together with gradually improving computational algorithms and technology, neuroimaging is demonstrating dynamical activations of multiple brain regions associated with a myriad of cognitive processes and forms of behaviour.

Today, we are able to detect brain activities using a number of minimally invasive or non-invasive imaging techniques, each offering a particular means for detecting the neurophysiological changes associated with different behaviours and experiences in both healthy and pathological conditions. Changes in neural activity are accompanied by variations in blood flow and metabolic activities, either or all of which can *in principle* be monitored by measuring devices sensitive enough to detect the parameter of interest either directly or indirectly. Although the one imaging technique employed in this research is magnetoencephalography (MEG), a brief overview of a few of the other popular methods is included for the appreciation of their relative limitations or advantages with respect to their resolution of temporal and spatial characteristics of localizable brain activity.

– Positron Emission Tomography

In a typical positron emission tomography (PET) imaging, radioactively labelled molecules (which emit positrons, e.g. ^{15}O, as they decay) are injected into the subject's blood stream, which pass through the blood-brain-barrier into the brain. Depending on the injected molecule, a change in regional distribution will occur. In the case of ^{15}O, which is used in blood-flow PET studies, active engagement in a cognitive task (relative to a baseline e.g. eyes-closed control task) leads to areas more engaged in the processing to experience an increase in blood flow. Thus the level of radioactive decaying isotopes and estranged positrons will be higher in these regions (i.e. positrons leave the unstable isotopes), resulting in a higher number of positron-electron collisions within the vicinity (~2 mm) and consequentially, a higher emission of paired bidirectional (~180°) gamma rays. It is the paired gamma rays that are detected by the PET detector, which allows the inference of the source of collision based on the simultaneously emitted gamma rays. Spatial resolution of PET imaging is approximately 5mm, but the temporal resolution is limited by radioactive half-lives (e.g. 123 s for ^{15}O) and the photon-counting noise, which can add up to a few minutes (Baillet, Mosher et al. 2001, Cherry, Phelps 2002). In addition, the exposure to radiation limits repeated measures of the same subjects, and makes it disadvantageous for e.g. longitudinal studies (Kimberley, Lewis 2007).

– Functional Magnetic Resonance Imaging

A more direct measure of neural activity is through haemodynamic changes, which are commonly measured by functional magnetic resonance imaging (fMRI). Localized blood flow and corresponding blood oxygenation levels are imaged as a correlate of the underlying neural activity. While oxygenated haemoglobin is non-magnetic,

deoxygenated haemoglobin has magnetic properties. Therefore changes in brain activity alter the ratio between these two forms of haemoglobins, e.g. higher oxygenated relative to deoxygenated blood flow during cognitive processing. The blood-oxygen level-dependent (BOLD) contrast is thus exploited in fMRI. Within the MRI scanner, a constant field is induced which aligns the normally randomly arranged proton that is part of the hydrogen atoms within our brain (and body) in the same direction. An additional magnetic field and its applied pulse sequence (e.g. radio-frequency or echo-planar) induces these hydrogen atoms to spin about their aligned axis and desynchronize when the applied pulse sequence ends. The time taken for the relaxation (T2-weighting) and realignment (T1-weighting) of the atoms and molecules is measured in the MRI. The different time-constants are influenced by non-excited molecules within the surrounding tissue, which allow for grey and white matter (or other) differentiation. By accounting for the non-homogeneity of the magnetic field when hydrogen atoms and haemoglobin molecules are considered during the relaxation time (T2*-weighting), BOLD-fMRI is thus achieved (DeYoe, Bandettini et al. 1994, Ugurbil, Ogawa et al. 1999). Specifically, the paramagnetic deoxygenated haemoglobin disturbs the local magnetic environment, resulting in surrounding protons to de-phase in their spins even faster than they would otherwise. The neuronal activity-related increase in blood flow, which decreases the amount of deoxygenated relative to oxygenated haemoglobin, leads to a less rapid spin de-phasing, and thus increases the MR signal (Berns 1999).

Although fMRI is an indirect measure of neural activity, recent studies have demonstrated significant correlations between the BOLD signal and local field potentials (Logothetis 2003, Logothetis, Pauls et al. 2001), as well as neural firing rate (Mukamel, Gelbard et al. 2005). Standard clinical fMRI scanners (that induce a constant 1.5 or 3 Tesla magnetic field) are capable of achieving a spatial resolution of 3 to 5 mm, and newer scanners with stronger magnets are expected to do better (Ugurbil, Toth et

al. 2003). Nonetheless, the temporal resolution of fMRI is limited by the relatively slow haemodynamic response which is around 3 to 5 seconds (Kim, Richter et al. 1997), and is therefore most suitable for studying the neural activity related to tasks that would span several seconds before completion (Kimberley, Lewis 2007).

– Magnetoencephalography (and Electroencephalography)

Unlike the indirect measures of neural activity via PET and fMRI, MEG and its electrical complement, electroencephalography (EEG), measure signals that directly reflect electromagnetic brain activity and they do so non-invasively. While EEG taps the electric potentials on the scalp resulting from volume currents associated with the flux of ionic currents in the underlying population of active neurons, MEG measures the biomagnetic fields, induced by the source currents, outside the head. Bio-electromagnetic fields are generated by the influx of ions during synaptic activities between neurons. Excitatory (or inhibitory) synapses from neighbouring neurons onto another's apical dendrite lead to the influx of positive (or negative) ions within the dendrite. The sudden depolarization results in a simultaneous positive-to-negative flow of ions within the cell (the primary current) and an extracellular negative-to-positive flow of ions (the secondary or volume current). The denser intracellular current is what induces the biomagnetic field that the MEG sensors pick up while EEG electrodes detect the extracellular currents that find their way to the scalp (through the path of least resistance).

However, the electromagnetic field generated by a single neuron is far too weak (~20fAm) to be detected. Approximately 100,000 synchronously active neurons aligned in parallel are required for the summation of currents (~10nAm) large enough to induce a detectable magnetic field from outside the head (Hämäläinen, Hari et al. 1993).

Fortunately, pyramidal cells with large apical dendrites are 1) tightly interconnected, 2) clustered in parallel, 3) aligned perpendicular to the cortical surface, and have therefore been thought to contribute to most of the measured electromagnetic field. A small patch of synchronously activated pyramidal cortical cells (~ 5x5 mm^2 and assuming that the cortex is approximately 4 mm thick) is believed to yield a biomagnetic field of about 10 nAm, which is in the order of measurements recorded in empirical and invasive studies (Baillet, Mosher et al. 2001, Hämäläinen, Hari et al. 1993, Okada, Wu et al. 1997).

While scalp voltages typically measure about tens of microvolts and are readily detected by relatively more affordable EEG electrode-systems (which consists of 32 – 256 electrodes covering the whole head), the extremely weak biomagnetic field (~50 to 1000 femtoTeslas; 10^{-15} T) induced by the same neural currents require highly sensitive sensor systems that are not only able to tap the transient field changes but also isolate them against the backdrop of stronger magnetic fields that act as noise, e.g. the magnetic field of the earth (~$5x10^{10}$ fT; approximately 1 billion times larger than the brain's magnetic field), and that of one's heartbeat (~$1x10^5$ fT) etc. As a consequence, highly sophisticated flux-to-voltage converters known as Superconducting QUantum Interference Devices (SQUIDs), which operate at the very low temperature maintained by liquid helium (-269°C), are necessarily incorporated into the design of MEG sensors. Newer MEG systems improve the quality of signal-detection through combining multiple rings of magnetometers to create gradiometers (e.g. 1st-order axial gradiometers) that respond to the spatial gradients of very small field changes induced within the immediate vicinity of the head relative to larger but stable distant sources, e.g. earth's magnetic field. For both EEG and MEG techniques, environmental noise is further attenuated by conducting the experimental acquisition within a magnetically shielded chamber.

Current whole-head MEG systems typically consist of 250 to 300 (or more) sensors spatially arranged to complement the curvature of the head and encased within a helmet-like vessel (dewar), which also contains the helium bath. Due to the cancellation of volume and source currents when sources of current aligned perpendicular to the surface of the head (i.e. on the cortical gyri; radial sources.), their corresponding magnetic fields are not detected; in a 'perfectly spherical' head (which is often assumed for the derivation of source currents) a radial current dipole generates a substantial homogeneous field and the volume currents exactly cancel this field everywhere. Consequently, the MEG signals measured primarily reflect the synchronous activity within the brain sulci (tangential sources) that induce biomagnetic fields which have a component perpendicular to the surface of the head (Lounasmaa, Hämäläinen et al. 1996). While EEG sensors are able to pick up both radial and tangential current sources, the measured scalp potentials are heavily distorted by the inhomogeneous conductivity of the intervening tissues (e.g. skull, meninges, cerebral fluid etc.), which on the other hand, have little effect on magnetic fields. Thus, the higher spatial precision of MEG imaging makes the detected signals at each sensor typically evident without having to rely on overly complicated analyses.

Due, in part, to the direct reflection of neural activities, MEG and EEG signals can benefit from sampling at very high temporal resolutions e.g. millisecond range or finer, and the only limiting factor is the analog-to-digital conversion rates (Baillet, Mosher et al. 2001). Thus, these non-invasive techniques are ideal for studying the temporal dynamics of cell assemblies and /or their networks, which commonly occur in the range of tens or hundreds of milliseconds. However, the spatial resolution achieved is not quite as impressive as that offered by fMRI unless restrictive modelling algorithms are used that are potentially capable of yielding a spatial resolution of 5 mm (Lounasmaa, Hämäläinen et al. 1996). The inferior spatial resolution is due to the smaller number of spatial measurements that are made by a few hundred sensors or electrodes in contrast

to the tens of thousands of voxels of finer spatial resolutions per volume of brain resolved in fMRI or PET, and the *non-unique* inverse solution(s) to equations used to pinpoint the source(s) underlying the recorded electromagnetic signals (Baillet, Mosher et al. 2001); a mathematical problem identified by von Helmholtz (1853).

– No single ideal method of inquiry

It is acknowledged that each imaging technique has its flaws and unique advantages. Therefore, the choice of any one method over another depends on the nature of inquiry. When temporal resolution is not of vital importance and /or when specific biochemical metabolic processes or structural morphology are of interest, PET and fMRI are suitable methods of inquiry and offer high spatial resolution. When the investigation of real-time neural dynamics is pursued, temporal resolution can be crucial to a technique in offering a measure of abnormality. For example, EEG has enjoyed a long history of clinical application in monitoring the abnormal electrical activities of neurons in epileptic patients. Typically, standard pattern analysis of prominent timing peaks or frequencies (alpha: 8 – 12 Hz, beta: 15 – 30 Hz, or theta: 4 – 8 Hz waves etc.) of neural dynamics associated with simple tasks or behavioural activities (e.g. wakefulness vs. sleep) are used to deduce characteristic differences between patient and control groups. However, when the localization of the focus of epileptic seizure is necessary, not only is the temporal aspect crucial, but the spatial resolution is critical, especially if surgical removal of the epileptic centre is essential for maintaining a patient's quality of life. In the latter case, the use of MEG technique coupled with anatomical MRI or fMRI currently provides a clinical standard for pre-surgical functional mapping and localisation of the central sulci (Castillo, Simos et al. 2004, Korvenoja, Kirveskari et al. 2006).

The MEG was chosen as the method of inquiry for the current study because we were primarily interested in the temporal aspects of neural activities and their relation to the time-varying movement *tau*, a parameter that provides prospective temporal information for guiding behaviour. The fact that biomagnetic signals pass undistorted through the brain tissues is an added advantage. However, each technique's disadvantages as well as 'established' methods of analysis often impose constraints on the type of experimentation, which may not always be appropriate for studying dynamic performance or behaviour that typically does not conform to fixed stimulus-response durations. This is further discussed below.

– MEG analyses

The main goal of most MEG (and many recent EEG) studies has been focused on localizing the generator(s) of the recorded signals. In order to determine the underlying generator(s) for the recorded field signals two problems need to be solved. Given a neural source of known location, strength and orientation, the determination of the resulting distribution of electrical (EEG) or magnetic (MEG) signals is referred to as the *forward* problem. On the other hand, the determination of the location, orientation and strength of the underlying source(s) which could explain the observed recorded signals is known as the *inverse* problem. With known or estimated conductivities and appropriate assumptions e.g. assuming the electrical conductivity of the head is homogeneous and isotropic, approximating the head as a spherically symmetric volume conductor, or that the source-space of continuous current density resides only within the grey matter etc. (Baillet, Mosher et al. 2001, Hämäläinen, Ilmoniemi 1994, Ioannides 1994, Ioannides 2006, Leahy, Mosher et al. 1998), the solution to the forward problem is unique. The measured field is therefore the sum of the individual fields of all instantaneously active current source(s), each with a uniquely defined contribution

to the total field (Ioannides 2006). However, the inverse problem of deducing the source(s) of activity within a confined volume based on the measures of surface electromagnetic signals outside a spherical body, does not lend itself to a unique solution (Hämäläinen, Ilmoniemi 1994, von Helmholtz 1853), unless suitable constraints are imposed to yield probabilistic estimates.

The classical constraint applied to the inverse problem is the *Current-dipole*. It models the distribution of the electromagnetic field measured at any time point as that produced by a single source, the *equivalent current dipole* (ECD) – described as the elementary flow of the primary current for MEG, or a pair of source and sink monopoles for EEG. A variation of this is the modelling of the measured field within a temporal duration by a set of current dipoles whose orientation and locations are fixed but whose strengths vary with time. This corresponds to the notion of simultaneous or sequential activations of multiple cortical areas (Hämäläinen 2004). The reality of the ECD model is that it is an oversimplification, which works well for a single shallow focal source or two distant focal sources. Moreover, it is unlikely that a single source is the only activation within the brain at any time point, nor is it possible to predict the number of sources active for any given behaviour. For multiple ECDs, non-linear least-squares minimization algorithms would have to be applied, which is computationally costly and becomes more unreliable with increasing number of ECDs (Ioannides 1994).

An alternative to the ECD is the *Current-distribution* (CD) model, which assumes the sources with constrained orientation (e.g. normal to the cortical layer) as distributed within a volume or source-space defined by the brain or cortical area (determined by MRI). The continuous current density can be conceived as a linear sum of each sensor's lead field, which decays rapidly away from the sensor. A weighting function is incorporated into the algorithm to compensate for the tendency toward estimating superficial sources. The solution is a current distribution which has either the minimum

magnitude (L2-norm) or that which has the minimum spread (L1-norm) that explains the overall signal variance. While these minimum norm solutions provide a convenient way of displaying time-varying intensities of sources, which can be overlaid onto MRI scans (Uutela, Hamalainen et al. 1999), these assumptions are difficult to justify physiologically. Often, further constraints are incorporated through similar experimental paradigm using fMRI even though time-scales involved differ and neural activations may not necessarily concur. In addition, simulation studies (Ioannides, Bolton et al. 1990) highlighted that electromagnetic laws allow only the direction of the primary current to be represented by a weighted linear sum of lead fields; not the primary current per se, which has been assumed in the minimum-norm methods (Ioannides 2006). A means of quantifying the non-linear relation between measured field and source distribution is through an iterative solution that incorporates posterior probability weightings, and is employed in the Magnetic Field Tomography (MFT) algorithm (Taylor, Ioannides et al. 1999). Nonetheless, running the MFT algorithm require immense computing power (Ioannides 1994), a resource that very few imaging centres enjoy. Even when the quest for a practical solution to the inverse problem is still being pursued, the 'ill-posed' problem has not deterred research from using currently available methods of analyses or exploring new ways to understand brain activity with the high temporal resolution offered by MEG (and EEG).

– Sensor-space vs source-space

The result of the different methods of MEG data analysis can be presented in a number of ways. The common forms of presentation include ECDs or activation intensity estimated via minimum-norms projected onto a source-space, e.g. the brain anatomy derived from MRI, or tessellated brain volume normalized to subjects' head-size. In addition, magnetic contour-fields and time-varying magnetic field-strengths can also be

superimposed onto 2D or 3D sensor-space. While the analysis of raw signals in sensor-space deals with the cleanest data without any distortion from the algorithms used (and associated assumptions) in estimating activations or current generators in a given source-space, the standardization of sensor-space is not as easily achieved in MEG as it is in EEG studies. Unlike the removable EEG cap, which is fitted onto each subject in the same way (e.g. 10-20 system) and standardized with regards to the reference electrodes in the conventionalized landmarks (nasion, inion, vertex, and mastoids), the MEG helmet is generally larger than most humans' heads and it is not possible to position all subjects in the same ideal helmet-to-head arrangement for subsequent group analyses. While reference electrodes and head-shape digitization are routinely performed in MEG experiments, which is used for co-registering subjects' head-size to their MRI scans, these references are primarily used to monitor motion and shifts in head location before and after each acquisition to aid in deciding acceptance or rejection (e.g. if shift in location is greater than 1 cm) of the recording. In fact, any attempt to extrapolate sensor-space onto a standardized sensor arrangement is, likewise, subjected to the same 'ill-posed' problem.

In an attempt to resolve this issue, a recent classical-conditioning study by Junghöfer, Peyk et al. (2006) comparing statistical significant auditory N1 dipole field with and without applied sensor-standardization demonstrated that the increased significance in N1 dipole field distribution due to sensor-standardization is most pronounced for small subject samples (e.g. N=12 vs. N=24), and when MEG systems have fewer sensor coverage. With a larger subject sample, the improvement in significance was minimal. Moreover, while the effective distribution of significance without standardization is limited to areas (and associated sensor detection) active in the majority of subjects, the topographical distributions of significant dipole fields projected onto non-standardized or standardized sensor-space are qualitatively similar. Hence, it is possible to

circumvent this issue, without resorting to complicated algorithms, by increasing subject sample-size.

– Averaging across trials vs. single-trial

Most analyses of evoked brain responses in EEG and MEG studies have relied on averaging numerous responses that are time-locked to a stimulus onset, such that any activity that is not relevant to the stimulus response (considered as 'noise') would be averaged out; thereby increasing the signal-to-noise ratio. The process of averaging relies on the heavy assumption that the brain is in a relatively steady state during the course of the experimental condition(s), with little habituation or adaptation to the stimuli or task. In reality, such steady-states do not generally exist; particularly when the number of trials is large (Baillet, Mosher et al. 2001). In addition, the variability of brain responses from trial to trial is a stark contrast to the regularity of the QRS component of the heartbeat; the averages of which are difficult to discern from traces of individual cycles (Ioannides 1994). Nonetheless, there are reasons why such reductionistic averaging has been necessary and important.

Given that electrical current travels through the path of least resistance, the high resistivity of the human skull prevents the volume current from reaching the scalp through a direct path. The indirect paths through the eye sockets, for example, contribute to the uncertainties in EEG localisation (in non-clinical research); the source(s) would be widely distributed. Thus, any evoked response(s) is akin to a needle being buried within a haystack of 'biological noise'. To improve signal-to-noise ratios and to account for the variations in skull conductivity, averaging is necessary across repeated trials of the same duration, and often across subjects performing the same task(s). This is true even when skull conductivity is estimated through MRI and when many

electrodes (i.e. over 124) are used (Ioannides 1994). As the development of EEG predates MEG, many of the existing practices have an enduring influence on the newer technology. Although early MEG systems, equipped with only one or a few sensors, required averaging of signals sampled at different probe locations surrounding a cortical area of interest, the need for averaging stemmed from reasons different to that due to the inhomogeneous conductivity of brain tissues.

Modern multi-channel whole-head MEG systems are capable of capturing magnetic flux gradients with reliable spatiotemporal coherence such that they offer the possibility to study single trial analyses or ensembles of neural signal in addition to signal averages (Ioannides 1994, Liu, Ioannides 1996). The MFT and related virtual channel analyses on the distribution of signal intensity using whole-head multi-channel MEG systems demonstrated that individual trial traces showed similar focal solutions to the average, despite the variations in latencies in the individual waveforms (Ioannides 2006, Liu, Ioannides 1996). It is worth noting that the variability in amplitudes and latencies of single trials has often been classified as physiological noise. Additional studies by Ioannides and colleagues (Ioannides 2001, Ioannides 2006) have shown that the averaging of signals across trials, experimental sessions, and subjects usually reveals stereotypical responses that capture real-time activities of early responses in primary sensory to strong sensory stimuli, but provides poor classification of late evolving and general underlying neural dynamics. The average signal can be viewed as a superimposition of subsets of histories, which does not necessarily reflect the temporal dynamics of neural processing (Liu, Ioannides 1996). The gradual appreciation that noise-elimination through averaging unwittingly undermines interpretation has motivated others (e.g. Jerbi, Lachaux et al. 2007, Karjalainen, Kaipio et al. 1999, Langheim, Leuthold et al. 2006) to analyze single-trial non-averaged data where possible.

– Time-series analyses

Analysis of non-averaged data often involves time-series analyses, which aim to describe, explain, predict, and /or offer control to discrete or continuous observations (Chatfield 2004). For example, the various observed waveforms recorded by EEG during sleep are *in essence* descriptions of neural time-series classified at different oscillating frequency bands. While time-series analyses of recorded electromagnetic signals do not render simple relations to the underlying topography of generators, they offer a direct investigation into whether two or more variables might be related. It might be possible to explain the variation of one time-series with another and thereby gain a better appreciation of possible mechanisms giving rise to a time-series. The various methods used in these analyses seek to minimise spurious correlations between two or more time-series by 'pre-whitening', or in other words, by removing possible trends, seasonal changes, and /or oscillatory behaviour in each time-series prior to relating one 'pre-whitened' series to the other(s) statistically. However, not many studies have incorporated the 'pre-whitening' procedure or accounted for potential auto-correlated errors in their analyses.

Studies investigating the relation between two time-varying observations have typically employed coherence as a measure of the linear dependence between two time-series (e.g. signals recorded from two sensors) in the frequency domain. Early studies have explored the functional coupling between signals recorded by sensors. Recent developments of spatial filter algorithms to localize the coherent sources within the brain, which also provide time courses of their intensity, have enabled the putative cortical regions involved in the functional interactions to be highlighted. Cortico-muscular coherence at the beta range (14-32 Hz) is commonly reported in healthy controls (Gerloff, Braun et al. 2006, Gross, Kujala et al. 2001, Gross, Timmermann et al. 2002), while cortico-muscular coherence is noted in the theta range (6-12 Hz) for patient

groups (Schnitzler, Timmermann et al. 2006, Timmermann, Gross et al. 2002, Timmermann, Gross et al. 2003). Cortico-cortical and cortico-subcortical coherences were also reported in these studies, which implicated the involvement and alterations of oscillatory dynamics in sensorimotor areas including the primary motor, premotor, somatosensory, supplementary motor, parietal, prefrontal areas, the cerebellum, and the thalamus. Interestingly, similar brain regions were also shown to be involved in their oscillatory coupling to instantaneous movement velocity at low frequencies of 2 to 5 Hz, although maximum significant coherence phase-locking was found between velocity and the contralateral primary motor cortex (Jerbi, Lachaux et al. 2007).

While neuromagnetic imaging methods have provided a form of source-analysis that is much desired, the functional relevance and strength of such coherence during movements are still uncertain (Salenius, Hari 2003). Moreover, the potential correlation artefacts introduced by the use of spatial filters have not been assessed nor addressed. An alternative approach using time-series analysis was performed by Langheim, Leuthold et al. (2006). Rather than associating the oscillations of muscle electromyogram and cortical signals at specific frequencies, for example, pre-whitened MEG signals (ranging from 0.1 to 400 Hz) were cross-correlated in sensor-space during an eyes-open fixation task. Consistent positive and negative correlations between subsets of sensors were observed across subjects, suggesting a plausible fundamental pattern of interactions between neural ensembles in healthy populations. In testing this idea, preliminary application of such an analysis in discriminating between patient groups and healthy controls has yielded promisingly accurate classifications (Georgopoulos, Karageorgiou et al. 2007).

It cannot be denied that the results of neuromagnetic imaging analyses are attractive, with putative activations superimposed onto subjects' brains. However, when theoretical assumptions and uncertainties are involved in deriving these images and

associated time-courses, analyses performed in sensor-space may provide a cleaner picture of the associations under inquiry. In the studies described within this thesis, the relation between recorded neural signals and behavioural performance was investigated using time-series analyses. Specifically, in this MEG section, the associations between the time-varying movement *tau* or speed and the recorded MEG signals were probed. In addition, we investigated the interactions between neural signals tapped by each sensor during performance and rest sections of the simple movement task in an attempt to understand the underlying interactions between neural ensembles in different task conditions.

BAILLET, S., MOSHER, J.C. and LEAHY, R.M., 2001. Electromagnetic brain mapping. *Signal Processing Magazine, IEEE,* **18**(6), pp. 14-30.

BERNS, G.S., 1999. Functional neuroimaging. *Life Sciences,* **65**(24), pp. 2531-2540.

BROCA, P., 1861. Sur siege de la faculte du langage articule avec deux observations d'aphemie (perte de la parole). Paris: Victor Masson et Fils.

CASTILLO, E., SIMOS, P., WHELESS, J., BAUMGARTNER, J., BREIER, J., BILLINGSLEY, R., SARKARI, S., FITZGERALD, M. and PAPANICOLAOU, A., 2004. Integrating sensory and motor mapping in a comprehensive MEG protocol: Clinical validity and replicability. *NeuroImage,* **21**(3), pp. 973-983.

CHATFIELD, C., 2004. The Analysis of Time Series : An Introduction. Boca Raton, FL: Chapman & Hall/CRC.

CHERRY, S.R. and PHELPS, M.E., 2002. Imaging brain function with positron emission tomography. In: A.W. TOGA and J.C. MAZZIOTTA, eds, *Brain Mapping: The Methods.* 2nd edn. San Diego, California: Academic Press, pp. 485-511.

DEYOE, E.A., BANDETTINI, P., NEITZ, J., MILLER, D. and WINANS, P., 1994. Functional magnetic resonance imaging (FMRI) of the human brain. *Journal of Neuroscience Methods,* **54**(2), pp. 171-187.

FRITSCH, G.T. and HITZIG, E., 1870. Über die elektrische Erregbarkeit des Grosshirns. *Archiv fur Anatomie, Physiologie und wissenschaftliche Medizin,* **37**, pp. 300-332.

GEORGOPOULOS, A.P., KARAGEORGIOU, E., LEUTHOLD, A.C., LEWIS, S.M., LYNCH, J.K., ALONSO, A.A., ASLAM, Z., CARPENTER, A.F., GEORGOPOULOS, A., HEMMY, L.S., KOUTLAS, I.G., LANGHEIM, F.J.P., MCCARTEN, J.R., MCPHERSON, S.E., PARDO, J.V., PARDO, P.J., PARRY, G.J., ROTTUNDA, S.J., SEGAL, B.M., SPONHEIM, S.R., STANWYCK, J.J., STEPHANE, M. and WESTERMEYER, J.J., 2007. Synchronous neural interactions assessed by magnetoencephalography: a functional biomarker for brain disorders. *Journal of Neural Engineering,* **4**, pp. 349-355.

GERLOFF, C., BRAUN, C., STAUDT, M., HEGNER, Y.L., DICHGANS, J. and KRAGELOH-MANN, I., 2006. Coherent corticomuscular oscillations originate from primary motor cortex: evidence from patients with early brain lesions. *Human Brain Mapping,* **27**(10), pp. 789-798.

GROSS, J., KUJALA, J., HAMALAINEN, M., TIMMERMANN, L., SCHNITZLER, A. and SALMELIN, R., 2001. Dynamic imaging of coherent sources: Studying neural interactions in the human brain. *Proceedings of the National Academy of Sciences of the United States of America,* **98**(2), pp. 694-699.

GROSS, J., TIMMERMANN, L., KUJALA, J., DIRKS, M., SCHMITZ, F., SALMELIN, R. and SCHNITZLER, A., 2002. The neural basis of intermittent motor control in humans. *Proceedings of the National Academy of Sciences of the United States of America,* **99**(4), pp. 2299-2302.

HÄMÄLÄINEN, M., 2004. Introduction to MEG as a tool for functional imaging: sources, measurements, and analysis. *International Course on Mind and Brain IV. Images of the working brain.* 2004, .

HÄMÄLÄINEN, M., HARI, R., ILMONIEMI, R.J., KNUUTILA, J. and LOUNASMAA, O.V., 1993. Magnetoencephalography-theory, instrumentation, and applications to noninvasive studies of the working human brain. *Reviews of Modern Physics,* **65**(2), pp. 413-497.

HÄMÄLÄINEN, M. and ILMONIEMI, R.J., 1994. Interpreting magnetic fields of the brain: minimum norm estimates. *Medical & Biological Engineering & Computing,* **32**(1), pp. 35-42.

IOANNIDES, A.A., 2006. Magnetoencephalography as a Research Tool in Neuroscience: State of the Art. *The Neuroscientist,* **12**(6), pp. 524-544.

IOANNIDES, A.A., BOLTON, J.P.R. and CLARKE, C.J.S., 1990. Continuous probabilistic solutions to the biomagnetic inverse problem. *Inverse Problems,* **6**, pp. 523-542.

IOANNIDES, A.A., 2001. Real time human brain function: observations and inferences from single trial analysis of magnetoencephalographic signals. *Clinical EEG (electroencephalography),* **32**(3), pp. 98-111.

IOANNIDES, A.A., 1994. Estimates of Brain Activity Using Magnetic Field Tomography and Large Scale Communication within the Brain. In: M. HO, F. POPP and U. WARNKE, eds, *Bioelectrodynamics and Biocommunication.* Singapore: World Scientific Publishing Co. Pte. Ltd., pp. 319-353.

JACKSON, J.H., 1875. Clinical and physiological researches on the nervous system. (Reprints). No. I. On the localisation of movements in the brain. London: J. and A. Churchill.

JERBI, K., LACHAUX, J.P., N'DIAYE, K., PANTAZIS, D., LEAHY, R.M., GARNERO, L. and BAILLET, S., 2007. Coherent neural representation of hand speed in humans revealed by MEG imaging. *Proceedings of the National Academy of Sciences of the United States of America,* **104**(18), pp. 7676-7681.

JUNGHÖFER, M., PEYK, P., FLAISCH, T. and SCHUPP, H.T., 2006. Neuroimaging methods in affective neurosciences: Selected methodological issues. In: S. ANDERS, G. ENDE, M. JUNGHÖFER, J. KISSLER and D. WILDGRUBER, eds, *Progress in Brain Research. Volume 156. Understanding Emotions.* Amsterdam: Elsevier, pp. 123-146.

KARJALAINEN, P.A., KAIPIO, J.P., KOISTINEN, A.S. and VAUHKONEN, M., 1999. Subspace regularization method for the single-trial estimation of evoked potentials. *IEEE transactions on bio-medical engineering,* **46**(7), pp. 849-860.

KIM, S.G., RICHTER, W. and UGURBIL, K., 1997. Limitations of temporal resolution in functional MRI. *Magnetic Resonance in Medicine,* **37**(4), pp. 631-636.

KIMBERLEY, T.J. and LEWIS, S.M., 2007. Understanding neuroimaging. *Physical Therapy,* **87**(6), pp. 670-683.

KORVENOJA, A., KIRVESKARI, E., ARONEN, H., AVIKAINEN, S., BRANDER, A., HUTTUNEN, J., ILMONIEMI, R., JAASKELAINEN, J., KOVALA, T., MAKELA, J., SALLI, E. and SEPPA, M., 2006. Sensorimotor Cortex Localization: Comparison of Magnetoencephalography, Functional MR Imaging, and Intraoperative Cortical Mapping. *Radiology,* **241**(1), pp. 213-222.

LANGHEIM, F.J., LEUTHOLD, A.C. and GEORGOPOULOS, A.P., 2006. Synchronous dynamic brain networks revealed by magnetoencephalography. *Proceedings of the National Academy of Sciences of the United States of America,* **103**(2), pp. 455-459.

LEAHY, R.M., MOSHER, J.C., SPENCER, M.E., HUANG, M.X. and LEWINE, J.D., 1998. A study of dipole localization accuracy for MEG and EEG using a human skull phantom. *Electroencephalography and Clinical Neurophysiology,* **107**(2), pp. 159-173.

LIU, L. and IOANNIDES, A.A., 1996. A correlation study of averaged and single trial MEG signals: the average describes multiple histories each in a different set of single trials. *Brain Topography,* **8**(4), pp. 385-396.

LOGOTHETIS, N.K., 2003. The underpinnings of the BOLD functional magnetic resonance imaging signal. *Journal of Neuroscience,* **23**(10), pp. 3963-3971.

LOGOTHETIS, N.K., PAULS, J., AUGATH, M., TRINATH, T. and OELTERMANN, A., 2001. Neurophysiological investigation of the basis of the fMRI signal. *Nature,* **412**(6843), pp. 150-157.

LOUNASMAA, O.V., HÄMÄLÄINEN, M., HARI, R. and SALMELIN, R., 1996. Information processing in the human brain: magnetoencephalographic approach. *Proceedings of the National Academy of Sciences of the United States of America,* **93**(17), pp. 8809-8815.

MUKAMEL, R., GELBARD, H., ARIELI, A., HASSON, U., FRIED, I. and MALACH, R., 2005. Coupling between neuronal firing, field potentials, and FMRI in human auditory cortex. *Science,* **309**(5736), pp. 951-954.

OKADA, Y.C., WU, J. and KYUHOU, S., 1997. Genesis of MEG signals in a mammalian CNS structure. *Electroencephalography and Clinical Neurophysiology,* **103**(4), pp. 474-485.

PENFIELD, W., 1954. Mechanisms of voluntary movement. *Brain,* **77**(1), pp. 1-17.

SALENIUS, S. and HARI, R., 2003. Synchronous cortical oscillatory activity during motor action. *Current Opinion in Neurobiology,* **13**(6), pp. 678-684.

SCHNITZLER, A., TIMMERMANN, L. and GROSS, J., 2006. Physiological and pathological oscillatory networks in the human motor system. *Journal of physiology, Paris,* **99**(1), pp. 3-7.

TAYLOR, J.G., IOANNIDES, A.A. and MULLER-GARTNER, H.W., 1999. Mathematical analysis of lead field expansions. *IEEE Transactions on Medical Imaging,* **18**(2), pp. 151-163.

TIMMERMANN, L., GROSS, J., DIRKS, M., VOLKMANN, J., FREUND, H.J. and SCHNITZLER, A., 2003. The cerebral oscillatory network of parkinsonian resting tremor. *Brain,* **126**(Pt 1), pp. 199-212.

TIMMERMANN, L., GROSS, J., KIRCHEIS, G., HAUSSINGER, D. and SCHNITZLER, A., 2002. Cortical origin of mini-asterixis in hepatic encephalopathy. *Neurology,* **58**(2), pp. 295-298.

UGURBIL, K., OGAWA, S., KIM, S.G., HU, X., CHEN, W. and ZHU, X.H., 1999. Imaging brain activity using nuclear spins. In: B. MARAVIGLIA, ed, *Magnetic Resonance and Brain Function: Approaches From Physics.* Amsterdam, the Netherlands: IOS Press, pp. 261-310.

UGURBIL, K., TOTH, L. and KIM, D.S., 2003. How accurate is magnetic resonance imaging of brain function? *Trends in Neurosciences,* **26**(2), pp. 108-114.

UUTELA, K., HAMALAINEN, M. and SOMERSALO, E., 1999. Visualization of magnetoencephalographic data using minimum current estimates. *NeuroImage,* **10**(2), pp. 173-180.

VON HELMHOLTZ, H., 1853. Über einige Gesetze der Vertheilung elektrischer Ströme in körperlichen Leitern, mit Anwendung auf die thierisch-elektrischen Versuche. *Annals of Physics and Chemistry,* **89**(211–33), pp. 353-377.

CHAPTER 5:

A MEG Study of Movement Performance:

METHODS

Subjects

Twenty healthy right-handed (Oldfield 1971) human subjects (10 females and 10 males; mean age ± SEM = 32.05 ± 1.86 years), with no known neurological or physical dysfunctions, participated in the MEG-imaging study. Their informed-consented participation adhered to the Declaration of Helsinki. All experimental protocols were approved by relevant institutional review boards.

Experimental task

The task involved simple wrist movements of the right hand. Subjects were requested to move a joystick-controlled cursor from one target to another. Each movement target was presented at one of the 6 vertices of a hexagon, with sides measuring 6.2 cm as displayed. The actual extent of joystick movement was approximately 0.4 times shorter;

a 5 cm joystick excursion was manifested as a cursor displacement of 13.5 cm on the screen, FIGs 5.1, 5.4). A series of 30 targets was presented in a manner such that the combination-pairs of current and future target positions only occurred once in the sequence. This meant that there was only one movement made between each vertex to every other vertex of the hexagon in the sequence (FIG 5.1).

The task began with the presentation of a (olive-green, diameter = 1.3 cm; 1.15° visual degrees) centre target which instructed the subject to move the (red, diameter = 0.75 cm; 0.66° visual degrees) joystick-controlled cursor into the target. When the cursor was held within the area of the centre target for 200 ms, a (white, diameter = 1.8 cm; 1.59° visual degrees) movement target appeared while the centre target disappeared. This movement target indicated the movement direction relative to the cursor at its current position which the subject should move the joystick. Subjects were instructed to move the cursor to the target in as straight a movement as possible, without pausing. Once the cursor reached the movement target and was held within it for approximately 200 ms, a new target appeared while the current target disappeared; there was only ever one target being presented at any one time. After the cursor was brought to the last target in the sequence, the centre target reappeared and the subject was instructed to bring the cursor back to the centre when the movement sequence was completed.

Six uniquely different sets of such movement sequences were presented to the subjects in 2 randomised blocks, with different start positions of the first movement target and involved 12 different movement directions (ranging between 30° – 360°, with 30° difference between each direction). A 5 s rest time was provided between the sets of movement sequences, during which the subject were required to bring the cursor back to the centre, and they could blink and/or rest their eyes. This was included to minimise the number of eye-blink artefacts during the actual movement tasks (FIG 5.1).

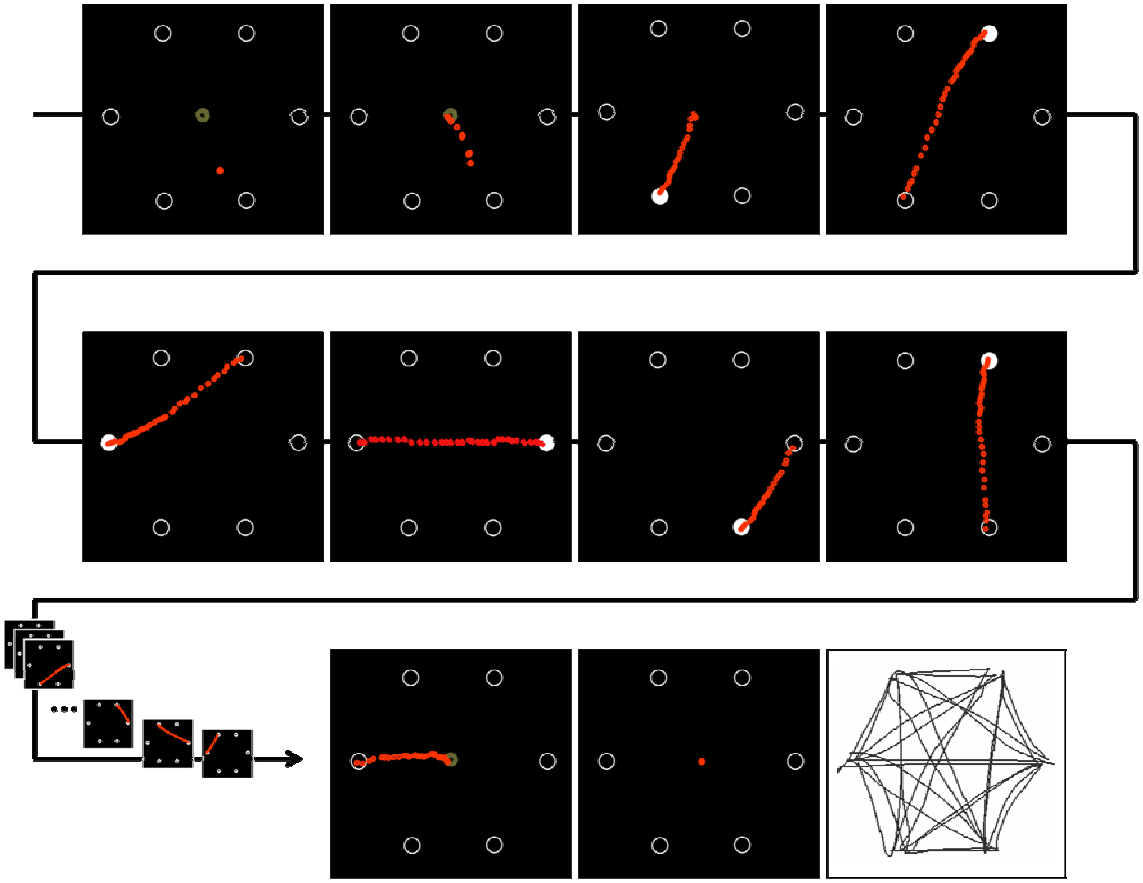

FIG 5.1: Target-to-target Movement Task. The task began with an olive green circle in the centre of the LCD display and the red joystick-controlled cursor was visible to the participant. When the cursor was brought within the olive green circle and held within it for approximately 200 ms, a white filled circle target appeared in one of the six vertices of the hexagon target-space while the olive green circle disappeared. When the cursor was brought into the white target and held within it for approximately 200 ms, a new target appeared in one of the other vertices while the previous target disappeared, and so forth. Movement trajectories were made in a pseudo-random sequence; there were no repeated target-to-target movements in each set of 30 target-to-target movements, which began from a different target. At the end of a sequence, the centre olive green circle reappeared as the red cursor was brought into the last white target. Participants were required to bring the red cursor back to the olive green target once again. When they do so, the olive green circle disappeared signalling a 5 s break. The olive green circle reappeared at the end of the 5 s break to indicate the start of a next set of 30 target-to-target movement sequence. The unfilled white circles merely denote the positions of the targets and were not visible to the participants. The insert in the bottom right is an illustration of the movement trajectories made in a sequence. Refer to text for further details.

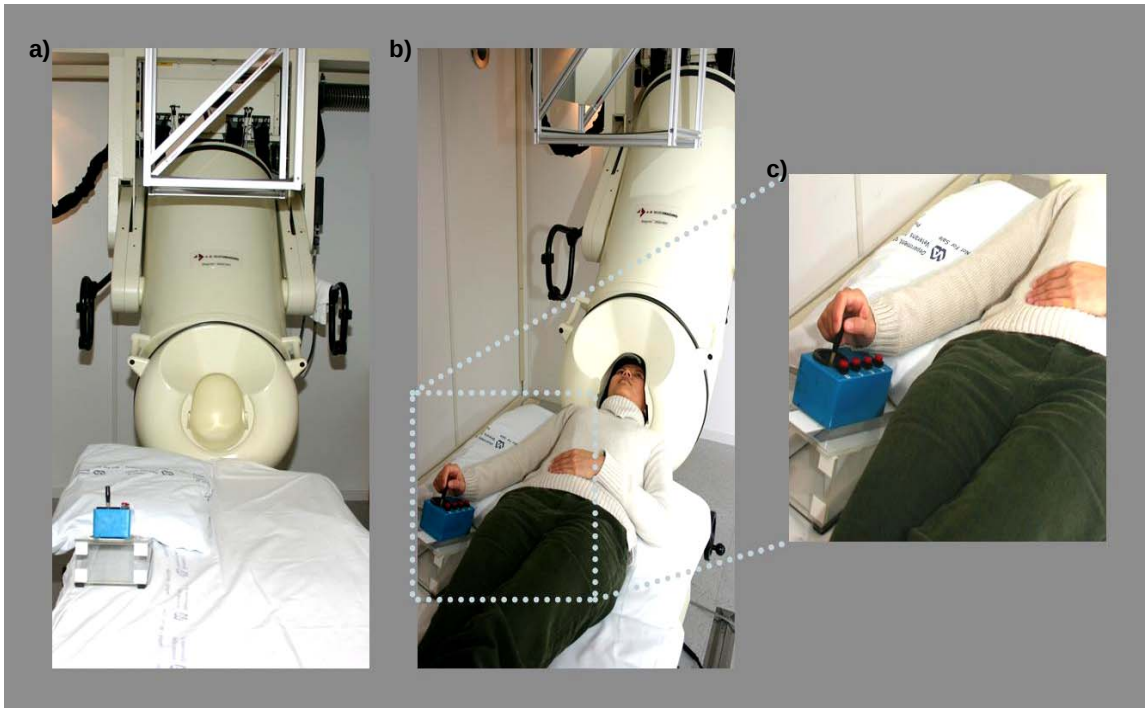

FIG 5.2: Experimental set-up, body, and hand posture during the Target-to-target Movement Task. The MEG system (a) was aligned to the supine resting position of the participant whose head was enclosed within the helmet (b). This resting position was chosen to prevent the gradual downward sliding movement of the sitting posture over time, which would increase head movements within the MEG helmet and lower the quality of the acquisition. The participant's right arm was placed on a cushion support and the freely moving joystick, propped at an angle (adjustable relative to each participant's comfort but was actually left unaltered across all subjects), was within comfortable reach. The participants held the joystick as shown in (c), and made simple but precise wrist movements to control the red cursor (see FIG 5.1) displayed on the LCD screen projected 65 cm above their eyes. In the actual acquisition, all subjects had a foam helmet to stabilize their head and electrodes were placed on their foreheads and peri-auricular points for head localisation and digitization procedures. For extra comfort, pillow support typically used for the lower legs was provided where necessary. Refer to text for further details.

Experimental setup

The task stimuli (FIG 5.1) were designed and implemented using Microsoft Visual Basic.NET 2003 (Microsoft Development Environment 2003 ver. 7.1.3088 ©1987-2002; Microsoft.NET Framework 1.1 ver. 1.1.4322 ©1998-2002, Microsoft Corporation), which integrated the display with the joystick to provide visual feedback of its position through the cursor. The stimuli were presented using a LCD projector and via periscope mirror reflections onto a display screen that was held approximately 65 cm in front of the subject's eyes. The 2-dimensional movement task-space subtended approximately 16.80° both horizontally and vertically, while the hexagonal target-space subtended 10.81° horizontally and 9.24° vertically of the visual field. All on- and offsets of a target presentation were accompanied by a trigger and photo-detector detection (of a light-bar from display screen, which was not visible to the subject) for subsequent alignment of target on- and offsets with the behavioural and neural data.

Prior to actual experimental acquisition, the subjects trained on the movement task for approximately half an hour under similar recording conditions so that the task and recording environment were familiar and the resultant movements from current cursor position to new targets were generally quick and non-hesitant. The required movement precision and the need to reduce large arm movement muscle artefacts also meant that the joystick had to be placed in a suitably comfortable position to compensate for the various arm-elbow-wrist-joints torques. To achieve this, the non-magnetic joystick (joystick model 541 FP, Measurement Systems, Norwalk, CT; remodeled with magnetic parts removed; a 5 cm joystick excursion is equivalent to a cursor displacement of 13.5 cm on the screen) was mounted on a rectangular plastic sheet (22.6 x 19.5 cm^2) that was raised 3.5cm above the resting bed and tilted at an angle of 30.6° and the whole setup was placed approximately 40cm away from the head-end edge of the resting bed, depending on the length of the subjects' arm. A soft cushion support was also placed

under each subject's right arm as they lay supine in the recording chamber with their head placed within the cryogenic helmet-shaped dewar (FIG 5.2).

Data acquisition

MEG data were acquired using a 248-channel axial gradiometer system (0-400Hz, Magnes 3600WH, 4-D Neuroimaging, San Diego, CA) within an electromagnetically shielded chamber. Head movements were minimised to within 5mm displacement using the individually made foam-helmet (using a 2-part foaming agent, Alpha Cradle®, commonly used for patient immobilization during radiotherapy, Smithers Medical Products Inc., Ohio, USA, www.alphacradle.com) that padded the space between the subject's head and the dewar helmet. Head localisation using 5 electrodes placed on the left and right peri-auricular fiducial points, and spaced out on the forehead, as well as the head-shape digitization employing a 3D digitizer (Fastrak 3SF0002, Polhemus Navigator Sciences, Colchester, VT, USA) were performed during the construction of the foam-helmet. The MEG data, joystick-output, trigger, and photo-detector signals were synchronously sampled at 1017.25Hz without any digital filtering during acquisition.

Data processing & analyses:

—Movement-data processing

Movement position data from the output of the XY-joystick coordinates were converted from milli-volts to the extent-of-joystick excursion (cm), and normalized by the extent of excursion. The XY time series were low-pass filtered using a Parks-MacClellan

Finite-Impulse-Response with equi-ripple filter (FIR filter; of length 127, with a pass band edge of 0 to 0.1 Hz, a stop band edge of 20 Hz to Nyquist frequency; FIG 5.3a). The designed filter has a frequency 'cut-off' of approximately 6 Hz (determined by the -3 dB threshold of the log-magnitude of the impulse response); which is within the 5—8 Hz range cited in movement research literature (e.g. Flanagan, Wing 1997). The resultant filtered XY position signals are plotted together with the raw signals (FIG 5.3b, c, e, g) to illustrate that while the high frequency components are dampened, the overall movement trajectory is preserved. The filtered trajectories are shown in FIG 5.4. Subsequently, the trajectories derived based on the normalized XY time series were shifted to the positive quadrant of the 2D-axis.

Using information of the on- and offsets of the trigger and photo-detector signals associated with each presentation of the target, the various trials of movements to peripheral targets can be indexed and easily segmented (FIG 5.5).

The onset and end of each movement were determined by the point in time the tangential velocity just exceeded 10% of its maximum value. Tangential velocity (speed) of the movement was calculated as:

$$s_{(t)} = \frac{\sqrt{(x_{(t)} - x_{(t-1)})^2 + (y_{(t)} - y_{(t-1)})^2}}{1/F} \qquad \text{EQ 5.1}$$

where sampling frequency (F) was 1017.25 Hz and thus sample time-interval (1/F) at each instantaneous time-point, t, was 0.000983 s. The corresponding XY position and movement speed time series were derived and used in calculating other movement parameters of interest.

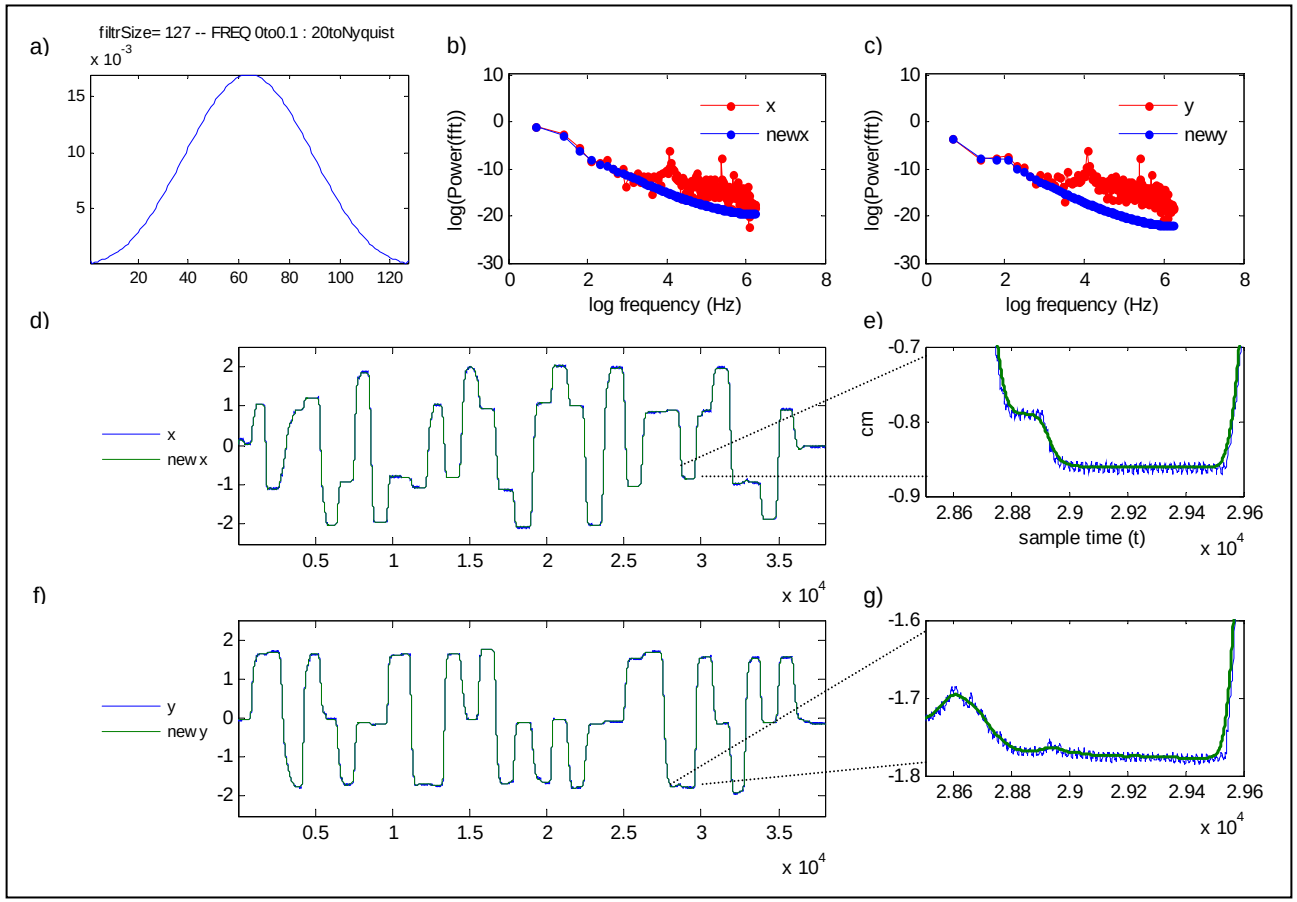

FIG 5.3: Filtering raw XY time series and outcome. a) The shape of the low-pass FIR-filter coefficient used for the low-pass filtering, (b, c) the natural logarithmic of power spectrum of the raw and filtered XY position signal. The power spectrums of the filtered signals have significantly reduced higher frequency components. (d, f) The filtered XY time series have mainly low-frequency components; (e, g) zoomed-in snapshots in sample time of the new XY filtered signals (green) compared to the raw signals (blue).; the high frequency components which contributed to the signal noise can be seen as the ripples of the blue time series (raw XY).

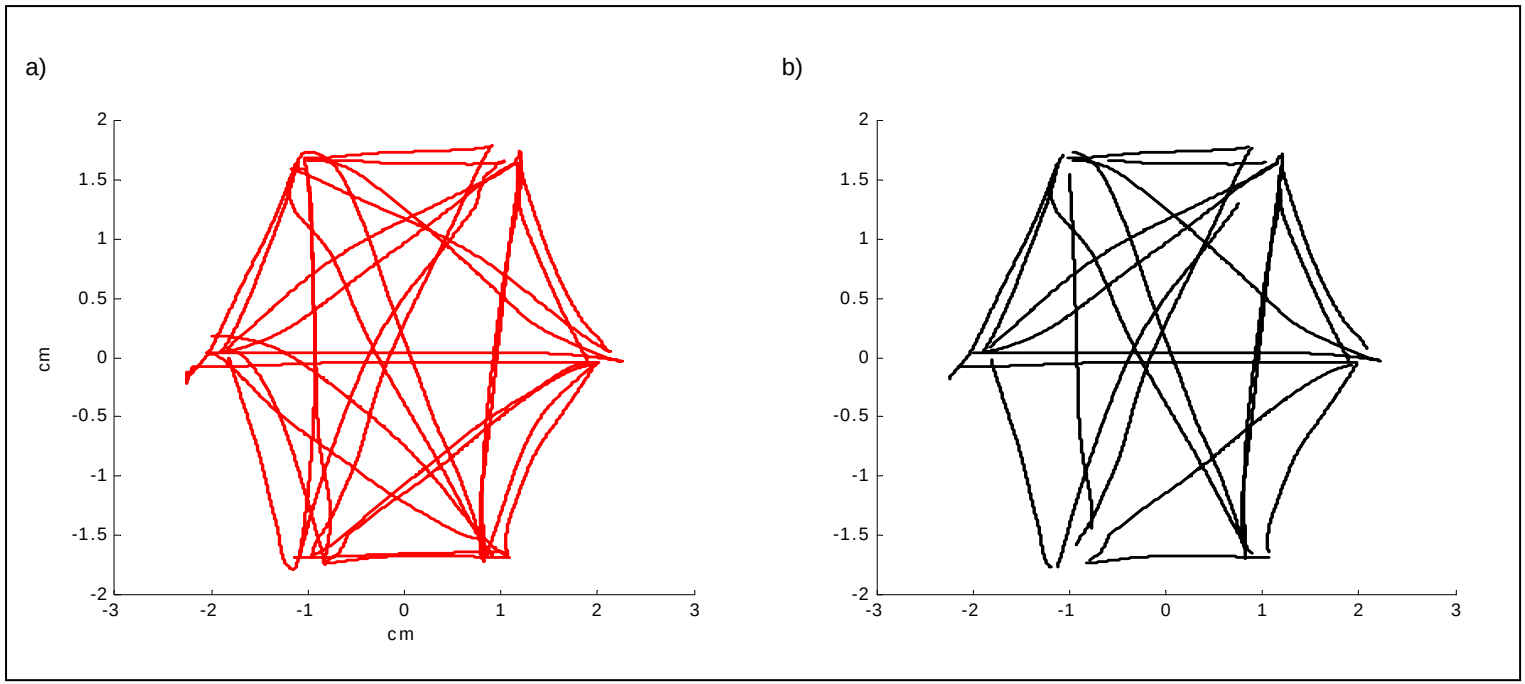

FIG 5.4: Illustration of filtered XY-joystick position signals. a) XY trajectories rendered within a set of 30 target-to-target movements, and b) segmented trajectories of movements uncontaminated by eye-blinks (see text for further details on MEG-data processing).

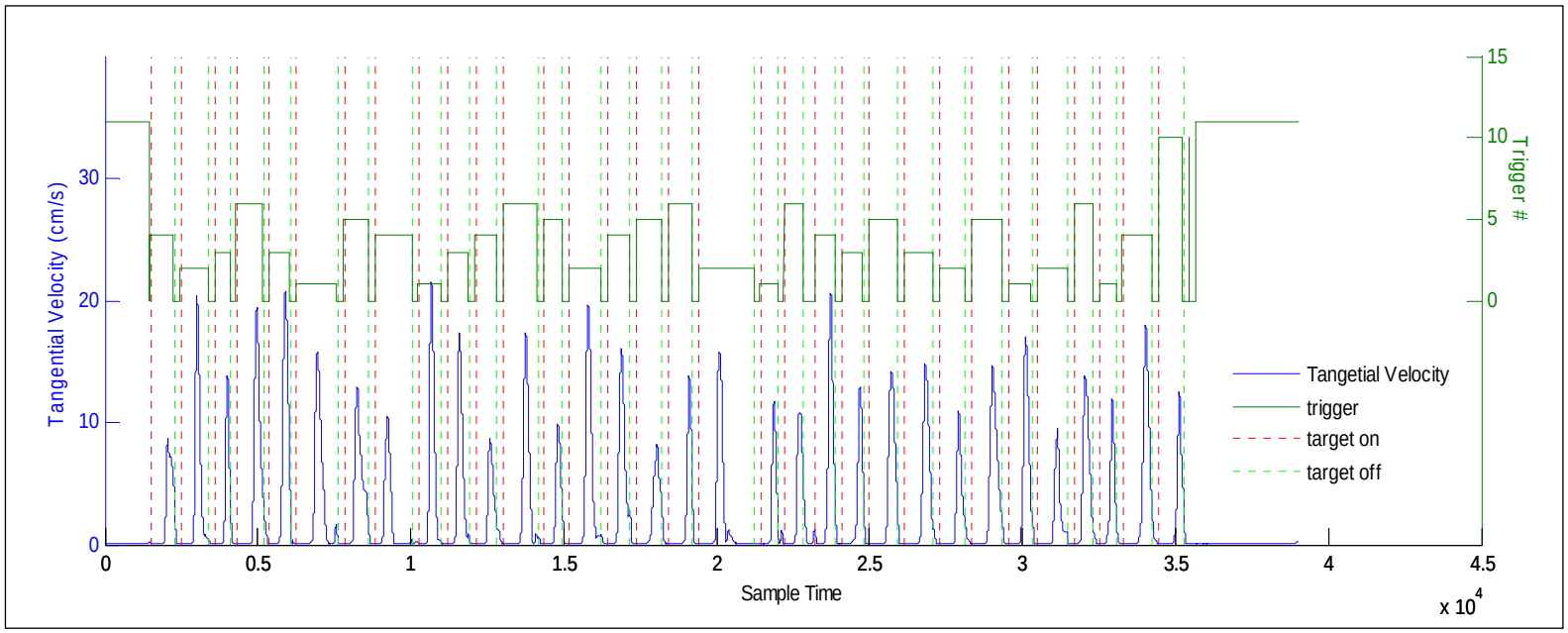

FIG 5.5: Illustration of the indexing of target-to-target movements. The on- and offsets of target display and the corresponding trigger signals indicated which target was displayed. Between the onset of two targets is a target-to-target movement and its corresponding speed (tangential velocity) profile.

Movement performance characteristics

The movement performance characteristics across all subjects were determined by the following parameters:

— *Index of Linearity*: a measure of the general straightness of the movement trajectory was calculated as the ratio between the maximum perpendicular distance from the distance described by the straight line connecting the start and end points of the movement and this movement distance (Atkeson, Hollerbach 1985). This was determined for all the movements considered to assess the general quality of movement trajectories.

— *Instantaneous Curvature (c)* of the movement for each segment, calculated based on the following equation for curvature:

$$c_{(t)} = \frac{\dot{x}_{(t)} * \ddot{y}_{(t)} - \dot{y}_{(t)} * \ddot{x}_{(t)}}{\left[\dot{x}^2_{(t)} + \dot{y}^2_{(t)}\right]^{3/2}} \qquad \text{EQ 5.2}$$

where $\dot{x}$ and $\dot{y}$ are the instantaneous velocity of x and y, respectively, $\ddot{x}$ and $\ddot{y}$ are the instantaneous acceleration of x and y, respectively, and t is the instantaneous time.

Instantaneous curvature was calculated from 50 sample time points from movement onset to 50 sample time points before the end of the movement ($t = t_{[n=50 \ldots n=N-50]}$, where t_N is the total movement time) for each movement segment. This is because at the starts and ends of movements when the subject was holding the cursor in place, velocity and acceleration are generally very small and negligible. Therefore, the estimation of movement curvature hovering about movement rests will not be meaningful; it is more

appropriate to measure the instantaneous curvature of the main portion of the movement trajectory, which will give an indication of the straightness of the performed movement. In order to obtain a single value of comparison across subjects, the mean instantaneous curvature for each movement segment was calculated for all movement segments considered for each subject.

— *Reaction time*, which was measured as the time between target onset and movement onset (determined by the time point that the tangential velocity first exceeded 10% of its maximum for a particular movement segment).

— *Movement time*, the total movement time taken for the subjects to initiate the cursor movement from the current target position to arrive at the new target position. This was determined by the time points that the movement speed first and subsequently exceeded 10% of its maximum for a particular movement segment (refer to movement data processing).

— *Maximum movement speed*, the maximum value of movement speed during each target-to-target movement.

— *Time to maximum movement speed*, the time taken for subjects' movement to reach maximum movement speed.

— *Proportion of movement time to maximum movement speed*, the time taken for subjects' movement to reach peak movement speed. This was calculated relative to the proportion of total movement time for each target-to-target movement; i.e. the *time to maximum movement speed* divided by *movement time*.

— *Difference between target-specified and actual movement directions (Directional Difference).* The (absolute) difference (measured in degrees) between the movement direction specified by the new target position (relative to current target) and the direction of actual movement made from current to new target.

— *Movement-tau (τ_{mv}).* The time-varying *tau* of each movement (τ_{mv}) was calculated as the ratio of the instantaneous distance-to-target ($\lambda_{(t)}$) over the instantaneous rate of change of distance-to-target ($\dot{\lambda}_{(t)}$). While it is conceivable that the distance-to-target may not necessarily be the direct distance between current position and target, the *tau* of a straight line distance is usually perceptible whereas the *tau* of a distance along a curved path is usually not; an exception is driving around a bend on a road, where the future path is perceptible. If one cannot perceive the *tau* of a gap, it is unlikely that one would guide their movement using movement *tau* information.

However, this does not mean that an organism cannot *tau*-guide their movement along a curved trajectory; the angle of approach of the curved trajectory can be determined by the angular action-gaps (e.g. the angle between the path of approach and the direct distance between e.g. the effectors and the goal), and its use in *tau*-guiding was demonstrate by Lee et al. (1999; 1995). It might be that the problem of moving around obstacles is solved in a similar way, but this is not the subject of study here.

In any case, the movements executed by the subjects of the current study were relatively straight, as the mean Index of Linearity for each subject demonstrated (TABLE 6.1). Thus, it was reasonable to assume that a straight line distance was the likely distance-to-target gap that one perceived in the current task.

The instantaneous distance-to-target ($\lambda_{(t)}$) was derived based on the Euclidean distances between each instantaneous time-point (*t*) to the end (*T*) of the movement segment:

$$\lambda_{(t)} = \sqrt{(x_{(t)} - x_{(T)})^2 + (y_{(t)} - y_{(T)})^2} \qquad \text{EQ 5.3}$$

where x and y were values of the movement trajectory for each segment. The motion gaps described by $\lambda_{(t)}$, decreased in size as they approach the target at the end of the movement segment. Subsequently, the speed of the closing gap was calculated as follows:

$$\dot{\lambda}_{(t)} = \frac{\lambda_{(t+1)} - \lambda_{(t)}}{1/\mathrm{F}} \qquad \text{EQ 5.4}$$

where sampling frequency (F) was 1017.25 Hz and thus sample time-interval (1/F) at each instantaneous time-point, *t*, was 0.000983 s. Finally, the instantaneous movement *taus* were derived as:

$$\tau_{mv\,(t)} = \frac{\lambda_{(t)}}{\delta\lambda_{(t)}/\delta t} = \frac{\lambda_{(t)}}{\dot{\lambda}_{(t)}} \qquad \text{EQ 5.5}$$

FIG 5.6 illustrates the derived movement speed and movement *tau* from movement trajectory for three movement segments.

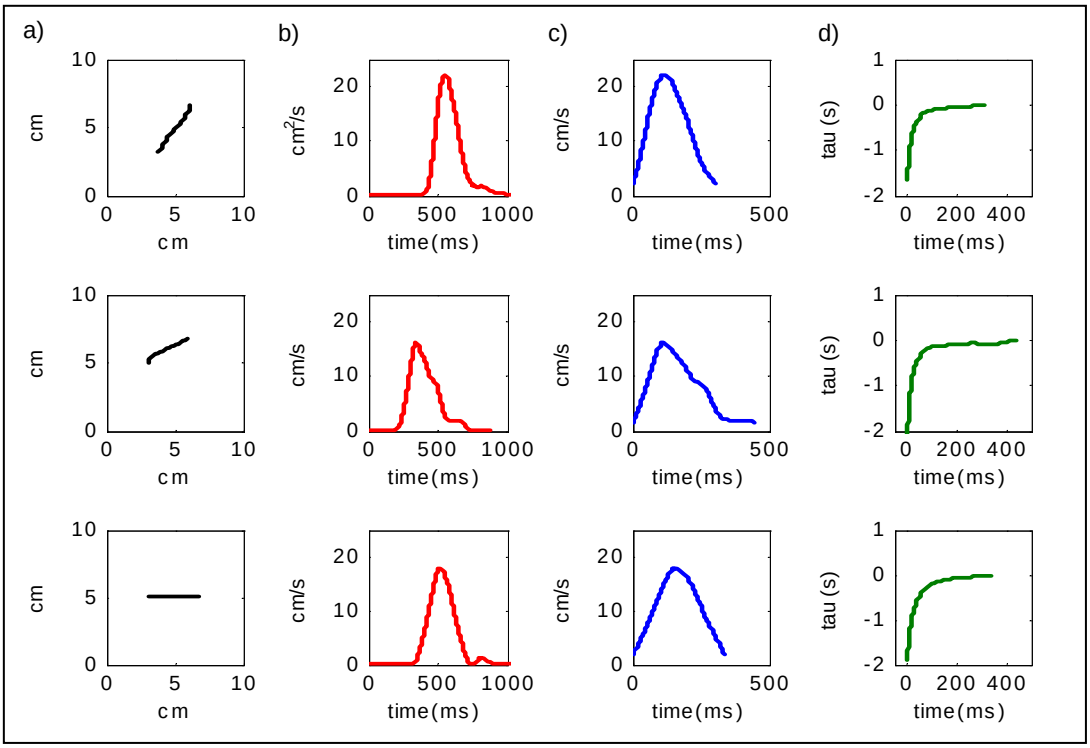

FIG 5.6: Movement variables. Examples of (a) movement trajectories, (b) corresponding speed profile within the segment, (c) the derived movement speed and (d) movement-*tau* of a subject's performance.

— *Percentage tau*-coupling (% τ_g-coupling) between movement *tau* (τ_{mv}) and theoretical *tau-guide* (τ_g). This coupling percentage measures how strong the linear relation between the two *taus* is. The theoretical *tau-guide* is defined as:

$$\tau_g = \frac{1}{2}\left(t_{(i)} - \frac{T^2}{t_{(i)}}\right) \qquad \text{EQ 5.6}$$

where $t_{(i)}$ is the instantaneous time, and T is the total movement time.

The two time series (τ_{Mv} and τ_g) were subsequently linearly regressed in a recursive manner to test the strength of the relation proposed by the theory:

$$\tau_g = k\tau_{mv} \qquad \text{EQ 5.7}$$

where k is a variable constant that describes the kinematics of the gap-closure for k > 0.

The recursive regression criteria was that the regression R^2 should exceed 0.95 and where it failed to achieve the threshold, a pair of variables from the time-series was excluded from the beginning of the movement time (i.e. $t = i\ldots\ i{+}1\ldots\ i{+}2\ldots T$) with each successive regression until the criteria was met. The method of quantifying the strength of the relationship between the theoretical *tau-guide* (τ_g) and movement *tau* is through the percentage coupling (% τ_g-coupling) between the two time variables. This is determined by the number of data points, relative to the size of the data, which accounted for the derived linear regression that satisfied the criteria of achieving an R^2 value of no less than 0.95. % τ_g-coupling is therefore a measure of the strength of the linear relation between the two *tau* time series, and an indication of how strongly the closure of a motion gap followed the temporal dynamics of the theoretical τ_g (Lee 1998,

Lee, Craig et al. 1999). Thus, a high percentage coupling is desirable. The regression algorithm used is a MATLAB® (v.7.3, The MathWorks, Inc., USA) function *lsqfitma.m* written by Edward T Peltzer (http://www.mbari.org/staff/etp3/regressindex.htm) and modified for the recursive procedure and the calculation of percentage couplings.

— *Slope* of the τ_g-coupling analysis recursive regression (*k*, in EQ 5.7), which describes the speed profile of the *tau-guided* gap closure (refer to FIG 2.1 in Chapter 2).

The mean movement performance characteristics (*Index of Linearity*; *Instantaneous Curvature*; *Reaction Time*; *Movement Time*; *Maximum movement speed*; *Time to maximum movement speed*; *Proportion of movement time to maximum movement speed*; *Directional difference*; % τ_g-coupling; τ_g-coupling *Slope*) were averaged across all movement segments for individual subjects. These means of movement parameters were entered in a bivariate Pearson's correlation analysis (SPSS correlation procedure, SPSS Inc., Chicago, IL) to investigate the extent in which the parameters were associated in the movement task performance.

MEG data processing

Given the sensitivity of the SQUID-detectors, the acquired MEG signals are often contaminated by various strong artefacts, e.g. eye-blinks, heartbeat, power-source, which require treatment prior to any data analyses. Noise-reduction of data was performed post acquisition on all the MEG sensor signals using 4D-Neuroimaging's algorithm (Magnes® Biomagnetometer System, 2500 WH, Software Reference Manual), which accounted for the environmental signals detected by reference channels during acquisition. Fixed fractions of reference channels' signals (i.e. summed 'weighted'

reference signals) were subtracted from the signals measured by MEG sensors in the noise-reduction procedure.

—Artefact removal

Cardiac-correction of the noise-reduced MEG signals was subsequently performed according to the method detailed by Leuthold (2003), which used the QRS component of a typical heartbeat waveform (FIG 5.7a) from the raw MEG signal (typically from one or more sensor(s), e.g. sensor 214, which is sensitive to cardiac artefacts) as a 'match-filter'. Segments of the MEG signal that correlated highly (or according to the set correlation threshold specific to each individual's cardiac idiosyncrasy) with the match-filter's form (i.e. the heart beats were identified by the peaks in correlation, FIG 5.7b, c) were used to create an averaged heartbeat waveform template (FIG 5.7d) for the individual subject for all sensors' signals. This subject-specific template was subsequently passed through the MEG signals a second time to improve the correlation and subsequent peak detection. This was done separately for each MEG channel.

Finally, for all channels, the channel-specific template was then passed through the acquired signals the corresponding channel to revisit the same time-indices (from FIG 5.7e) and the heartbeat waveform was subtracted from the sensor-signals (FIG 5.7f). In order to account for any remaining low-frequency artefacts due to environmental factors, the resultant cardiac-subtracted MEG data was high-pass filtered with a frequency cut-off at 0.1 Hz, using the MATLAB® (v.7.3, The MathWorks, Inc., USA) 4^{th} order (i.e. forward-backward high-pass of the 2^{nd} order) Butterworth function.

To account for artefacts due to eye-blinks and eye-movements during the task performance, the resultant filtered and cardiac-corrected MEG data was then subjected

to an Independent Component Analysis (ICA). The ICA is a process that detects and isolates independent sources of activity in signals consisting of mixed activity sources, e.g. MEG signals. The isolated components of the ICA are rank-ordered by magnitude, with the largest ordered first and gradually diminishing in order as with magnitude. Signal artefacts like eye-blinks are usually large in magnitude (e.g. vertical EOG can range around ± 100 micro-volts) and are typically ranked highly (and is usually the first or second component, if present) when their components are isolated using the ICA. The MATLAB function, *CubICA.m* (©Tobias Blaschke; Blaschke, Wiskott 2002) was used to isolate 6 main components (FIG 5.8) from all 248 MEG-sensor signals for the set of movements (without any segmentation into corresponding signals for separate target movements) and the first of the 6 components usually returned a waveform that contained peaks which closely resembled those of the typical eye-blink artefacts (highlighted in FIG 5.9).

It is common to use Electro-oculography (EOG) to monitor eye movements in EEG/MEG imaging and to detect eye-blinks for subsequent subtraction of eye-blink artefacts from the brain signals. In this study, eye-blinks and eye-movements were detected with similar ease using ICA and all neural data contaminated by eye-blink artefacts and corresponding behavioural data sections were excluded from subsequent analyses. In addition, the 2 highest-ranked ICA eye-related (horizontal and /or vertical) components (typically components 1, 5 and /or 6) were selected from the 6 isolated main ICA components (FIG 5.8) for all sets of movements for each subject. These ICA components were used as covariates in the subsequent regression analyses. This was done to account for any potential confound due to eye-related movements. A potential of using ICA components instead of EOG signals is that the signals are from the same brain source and measured in the same scale. The ICA component itself is a weighting of the MEG signals which best accounted for the eye-related component(s).

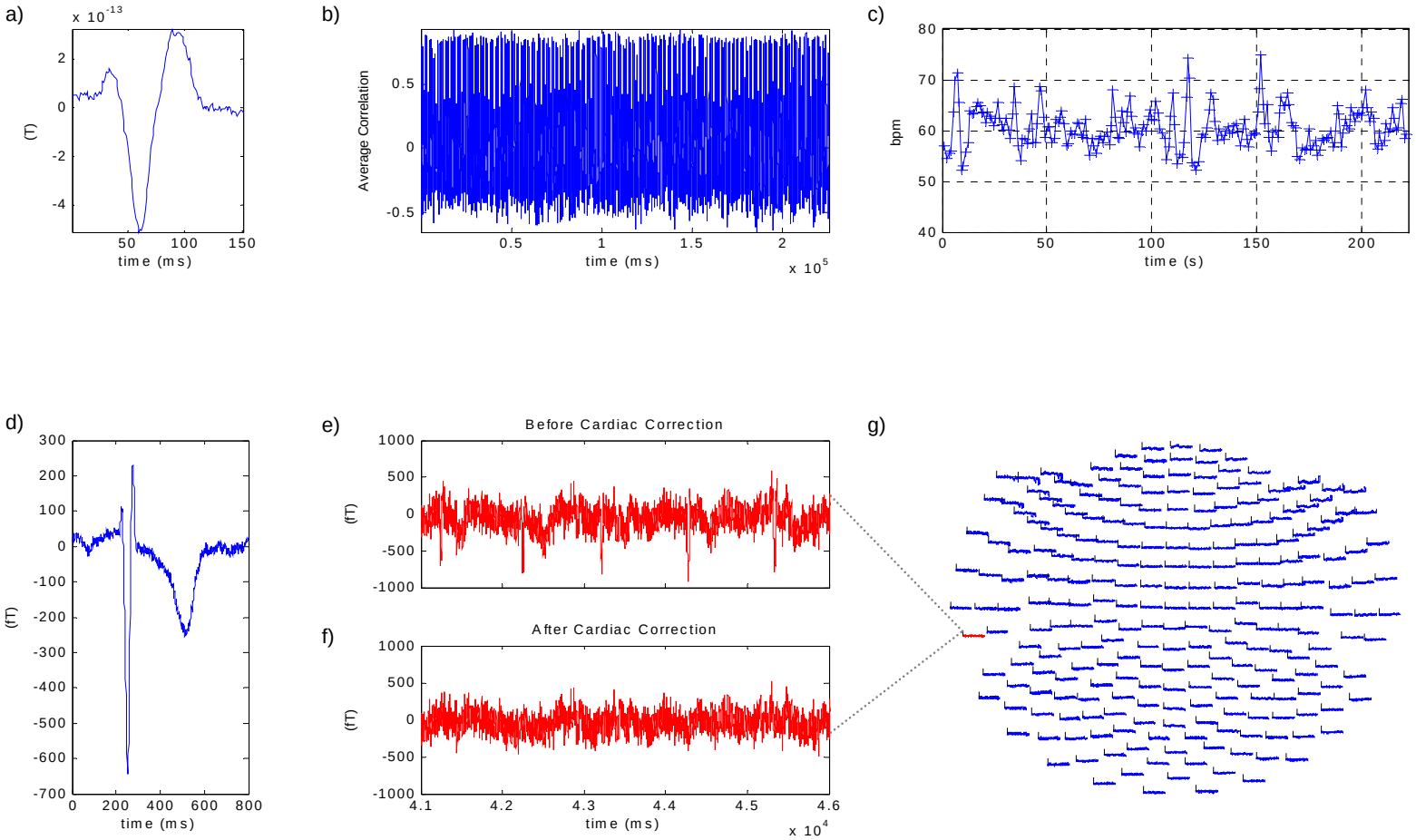

FIG 5.7: Steps involved in the cardiac-correction procedure. a) One typical QRS component of a heartbeat; b) correlations from the 2nd pass through data for QRS detection using correlation criteria set for individual subject (#11; detection threshold = ±0.5) on 1 (sensor 214) or more sensors; c) The average heart rate in beats per minute (bpm) corresponding to the time indices of each correlated QRS component d) An average of all detected heartbeats for subject's data; e) A segment of raw data from sensor 214 before correction illustrating the QRS components; f) and after cardiac correction; g) Likewise, the subtraction of QRS component was performed on all sensors' signals.

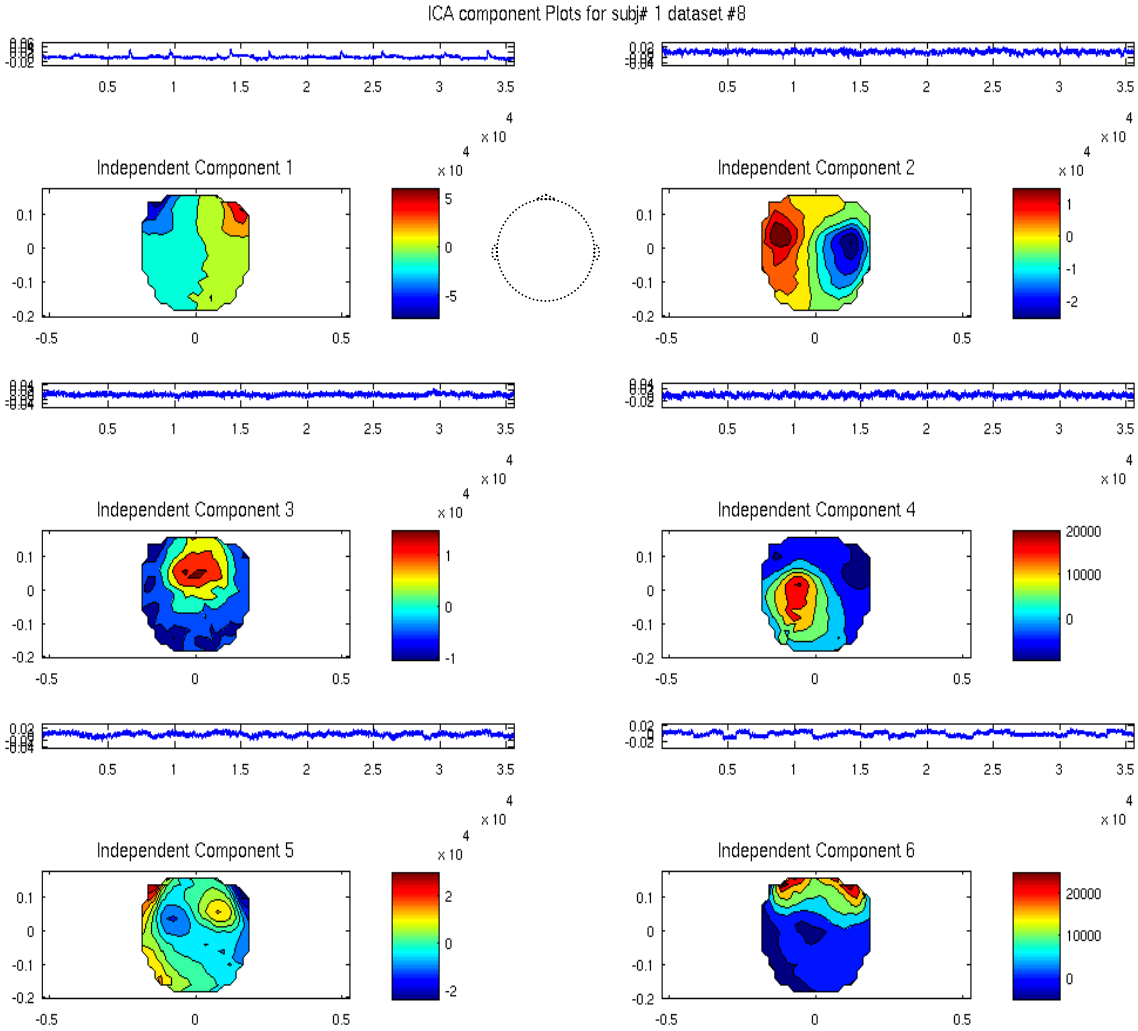

FIG 5.8: ICA components of MEG signals. The intensity distribution of the 6 main ICA components is portrayed spatially over the 2D sensor-space (top – anterior; bottom – posterior; front of the subjects' head is up) for a set of 30 target-to-target movements in one subject. Time series of each component's coefficients are displayed above each component's spatial map. Eye-related movement components exhibit strong component weights (coefficients) in the frontal areas near the eyes in the anterior. Component 1 illustrates a typical vertical component, dominated by eye blinks, as highlighted in FIG 5.8. The vertical component's intensity typically divides the spatial map symmetrically in the middle. Component 6 illustrates the horizontal saccadic movements typically manifested.

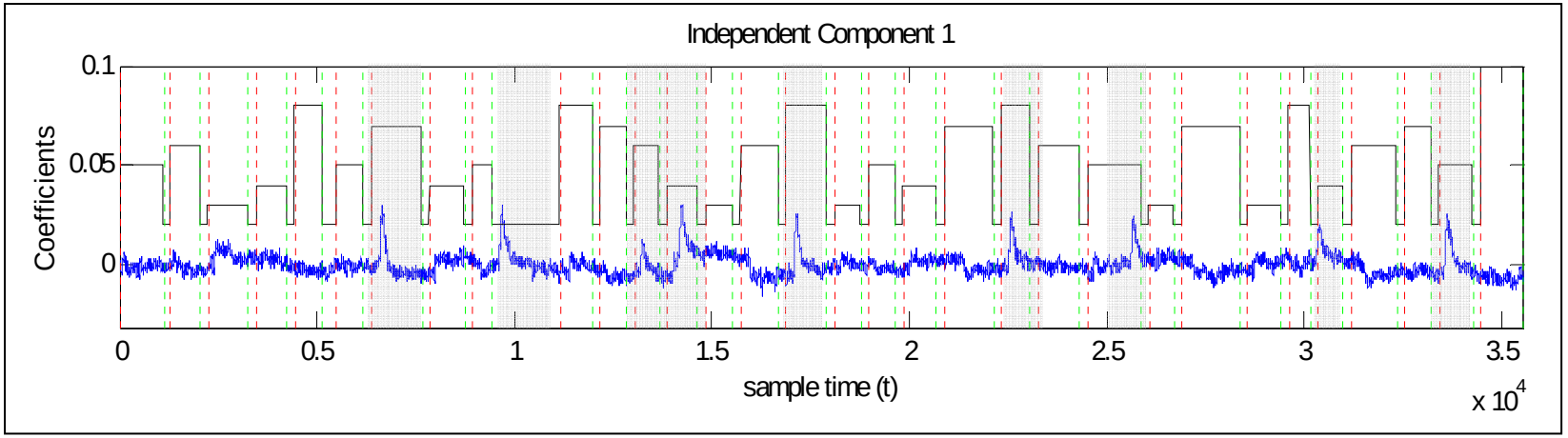

FIG 5.9: Eye-blink artefacts manifested in ICA component. Illustration of the first independent component (from ICA) manifesting the distinct signal peaks of the eye-blink artefacts for subject #1 in a set (#8) of movements. Movement segments contaminated by eye-blink artefacts, highlighted in grey, were omitted in the subsequent analyses. There were 9 out of 30 target-to-target movements being contaminated in this illustration; one of which (the second highlighted blink) occurred during the disappearance of a target and before the onset of the next target. Red and green dotted lines indicate the on- and offsets of target presentations and the target-associated triggers are shown as the black line-bars.

Analysis of the relation between MEG signals and movement tau or movement speed

— Linear Regression with an Autoregressive Error Component (AREG)

The association between the neural signals ($N_{(t,\ i=1to248)}$), and the corresponding movement *tau* ($\tau_{mv(t)}$) and /or speed ($s_{(t)}$) for all movement segments were assessed separately for each sensor. For that purpose a regression analysis was performed in which the time-varying MEG signal was the dependent variable, while the time-varying movement *tau* (EQ 5.8) or the instantaneous speed (EQ 5.9) was the independent variable. In these regression analyses we asked: To what extent are the neural signals related to each of the movement variables of interest? In addition, another regression analysis was performed in which the time-varying MEG signal was the dependent variable, with both movement *tau* and speed (EQ 5.10) as the independent variables. To this end, we asked: To what extent is each of the movement variables represented by the recorded neural signals when both variables are considered. Eye movement components detected via ICA (E_{ica1} and E_{ica2}) were also included as covariates in the regression analyses.

As all of these variables are time series, the regression errors are likely to be correlated (FIG 5.10), which could lead to spurious estimation of the significance of the regression coefficients. Therefore, an autoregressive component ($\mu_{(t)}$) was included in the regression model to improve the estimation. For each sensor, all movements and corresponding neural segments were considered but they were separated by an insertion of a 'NotANumber' (NaN) between segments to generate the full time series. The regression coefficients and their statistical significance were estimated using the Exact Maximum-Likelihood method of the AREG procedure and included a Kalman

Filter to address the 'missing' data due to the incorporation of NaNs (SPSS statistical package for Windows, SPSS Inc., Chicago, IL). The regression models used were:

$$N_{(t,i=1\rightarrow 248)} = b_0 + b_1\tau_{mv(t)} + b_2E_{ica1} + b_3E_{ica2} + \mu_{(t)} \quad \text{EQ 5.8}$$

$$N_{(t,i=1\rightarrow 248)} = b_0 + b_1s_{(t)} + b_2E_{ica1} + b_3E_{ica2} + \mu_{(t)} \quad \text{EQ 5.9}$$

$$N_{(t,i=1\rightarrow 248)} = b_0 + b_1s_{(t)} + b_2\tau_{mv(t)} + b_3E_{ica1} + b_4E_{ica2} + \mu_{(t)} \quad \text{EQ 5.10}$$

$$\mu_{(t)} = \rho * \mu_{(t)-1} + \xi_{(t)} \quad \text{EQ 5.11}$$

where $b_{0,1,2}$ were the regression coefficients to be estimated, i was the sensor number, t the sample time point, μ was the residual error, ρ was the 1st-order autoregressive coefficient, and $\xi_{(t)}$ was a normally distributed, uncorrelated random error with variance σ^2 and mean = 0. The relations of the MEG signals of individual sensors to speed or movement *tau* were assessed for each subject (FIG 5.11). Sensor 182 was omitted from the analyses for all subjects because it was faulty during the acquisition for subject 12. The number of significant ($p < 0.05$) relations to movement *tau* or speed was calculated for each sensor location across subjects and interpolated over the sensors to generate the '*percentage of significant relation*' (PSR) maps in 3D *sensor-space*. The xyz coordinates of the sensor locations were used to render these PSR maps, which illustrated the general distribution of *tau*- or speed related sensors, in three-dimensional (3D) view. In addition, the comparisons of the significantly related sensors and PSR between hemispheres, within the anterior-posterior and parietal sensor-space, for movement *tau* and speed were assessed using paired *t-test* statistics (SPSS statistical package for Windows, SPSS Inc., Chicago, IL).

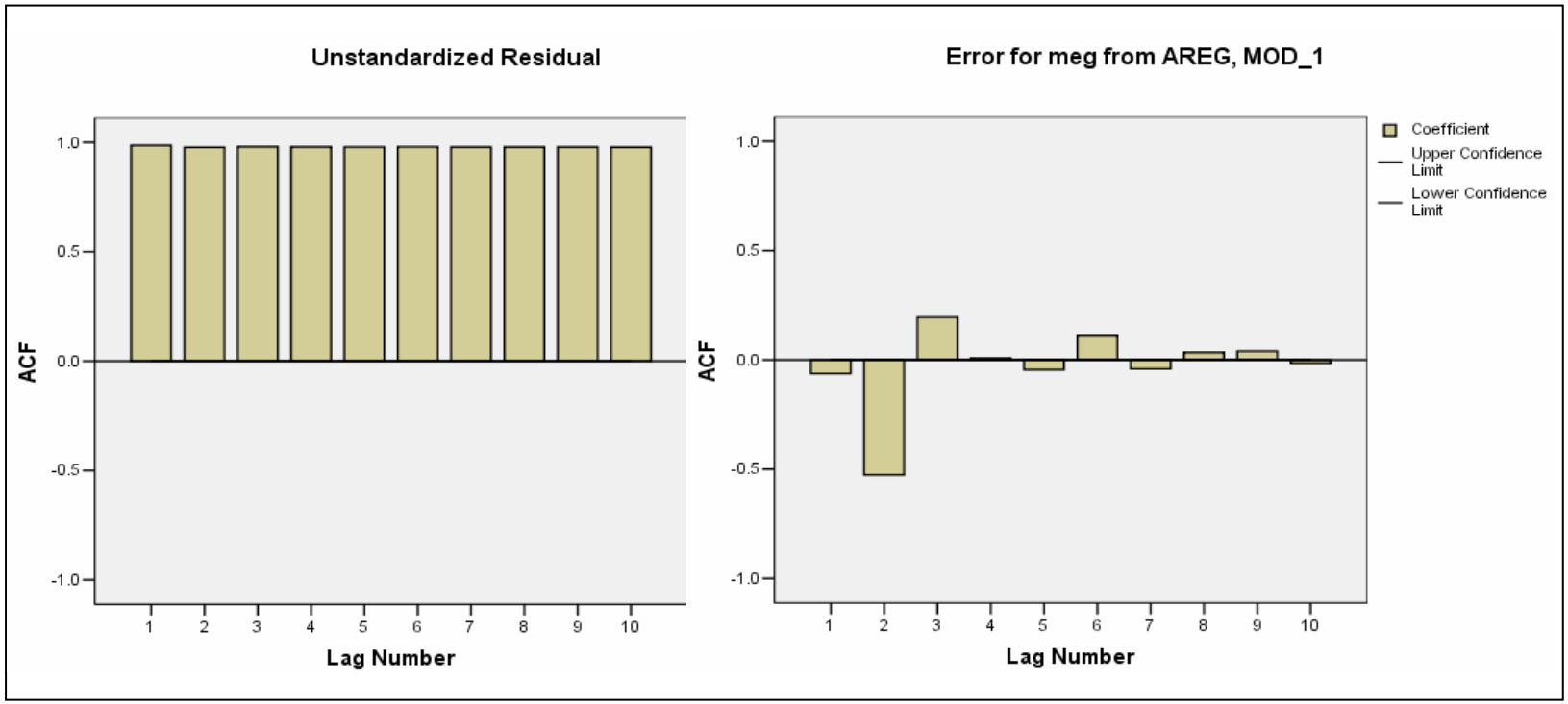

FIG 5.10: Example of auto-correlated errors. Autocorrelation function (AFC) illustrating the high auto-correlation in the residual errors estimated by the Ordinary Linear Regression (OLR) analysis (left) vs. that of the Autoregression (AREG) analysis (right) for a MEG sensor (# 67). Given that the AREG procedure accounts for a lag of 1 in the analysis, the autocorrelated errors for a lag of 1 is minimised in the AREG analysis. This in turn, provided a more accurate estimation of the correlation coefficients and test of significance, relative to the OLR analysis.

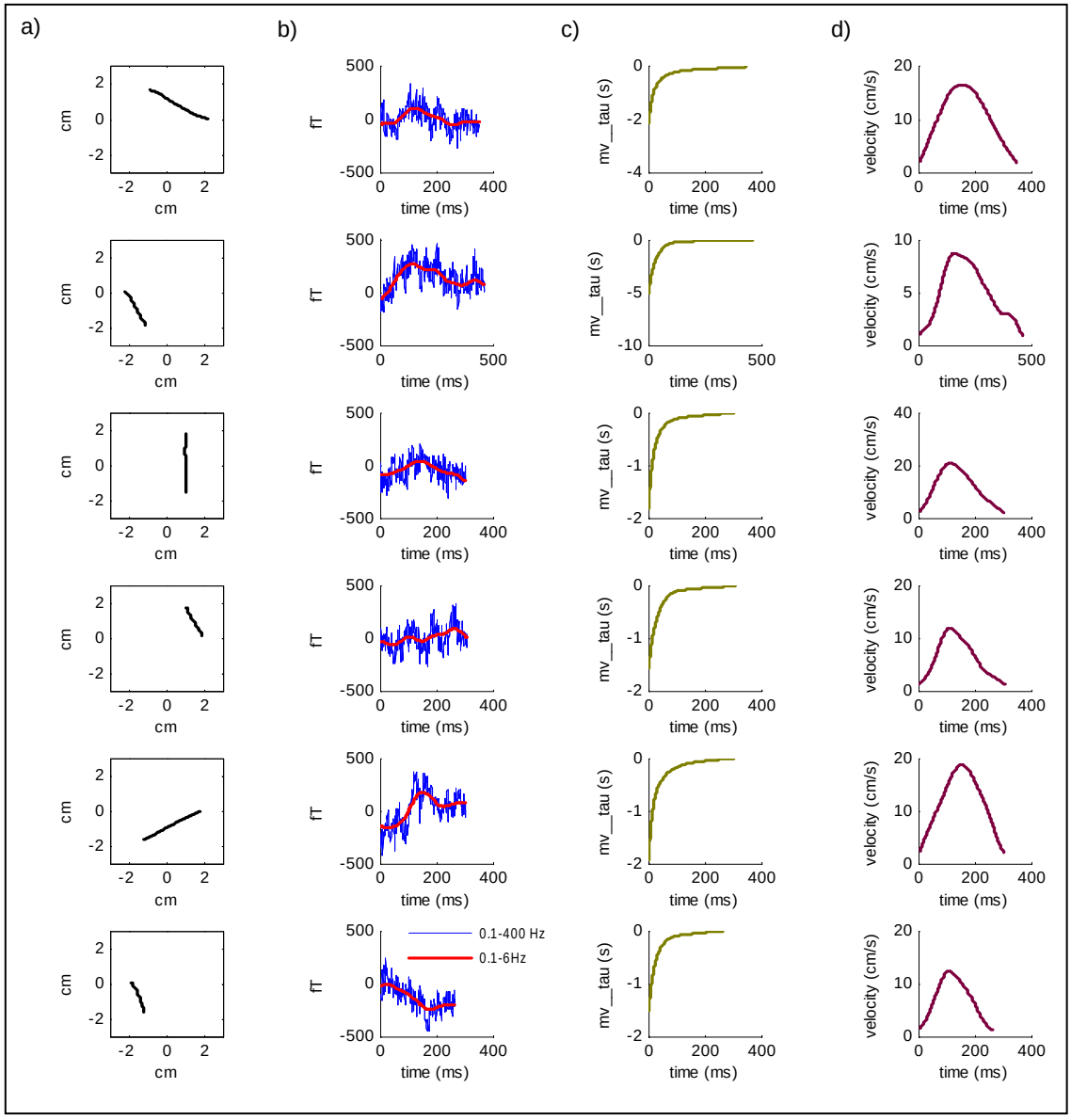

FIG 5.11: Autoregression variables. Examples of the dependent variable are the signals from MEG sensor #98 (b), corresponding movement_*tau* (c), or corresponding movement speed (d) as the independent variable of the regression. Movement speed and *tau* are derived from their respective movement trajectories (a).

— Cluster analysis of the coefficients of the Linear Regressions with an Autoregressive Error Component

In addition, the mean coefficients of the auto-regression (AREG) analyses were tabulated for each sensor location across subjects for movement *tau* and speed. The coefficient of the auto-regression can be appreciated as a measure of how much a movement variable (e.g. movement *tau* or speed) is processed by the brain signals from the particular sensor. The larger the coefficient, the more of a movement variable is processed (or weighted), and vice versa.

For this analysis subject 12 was excluded because of the faulty MEG sensor 182 during the recording session. All other subjects' (N=19) regression coefficients were included and the mean of coefficients were calculated for each sensor across subjects. The distance measure (D) between the mean coefficients ($\bar{\beta}$) of each pair of sensors (i, j) was calculated as follows:

$$D_{ij} = abs\left(\bar{\beta}_i - \bar{\beta}_j\right) \qquad \text{EQ5.12}$$

These distance measures were used in the hierarchical cluster analysis. The rationale for this is that sensors whose auto-regression coefficients (that of either movement *tau* or speed) that are of similar values may be 'coupled' in their processing of the movement variable, and thus 'cluster' as a sub-network. The following functions from the Statistical Toolbox of Matlab® (v.7.3, The MathWorks, Inc., USA): *linkage.m* with unweighted averages (UPGMA; unweighted pair-group method using average distance; Johnson, Wichern 1982), and *cluster.m* with a threshold of 0.990 used to define clusters, were used in the cluster analysis. The hierarchical cluster analysis outputs an ultrametric tree in which all objects (i.e. '*leaves*' or sensors) are of a uniform distance from the root and satisfies the following inequality (Corter 1996):

$$\hat{d}(x, y) \leq \hat{d}(x, z) = \hat{d}(y, z) \qquad \text{EQ5.13}$$

where x, y, and z are three leaves in the tree. The relationship between every three leaves (sensors) in the tree is a classification that maintains the distance between x to z and y to z in equivalence, while distance between x to y is less than the aforementioned distance. Sensors that are connected in the tree by a distance from the root greater than the threshold are classified as belonging to a cluster, with sensor-members whose summed distances to the root being equal, and are assigned a specific colour for their membership. The results are displayed in dendrograms (in which summed vertical branches to the common node between two leaves describe their degree of dissimilarity) and in sensor-space with each cluster, its associations, and members coded in a specific colour.

— Cross-correlation analysis of MEG sensor signals during rest and movement task performance

An Auto-Regressive Integrated Moving Average (ARIMA) method of the Time Series analysis (Box, Jenkins 1970) was used to remove any auto-correlation, and /or seasonal trends in the raw data such that 'true' relations can be assessed between neural time-series recorded from all sensors. The parameters incorporated into the model of ARIMA were based on previous modelling work by Leuthold, Langheim et al. (2005), which aptly removed sufficient non-stationarities that would otherwise affect the subsequent cross-correlation analyses and the related interpretations. The ARIMA parameters used were: Auto-Regressive order (AR) = 25, Differencing order (I) = 1, Moving Average order (MA) = 1. The Box-Jenkins ARIMA analysis was performed on the signals of each of the 248 sensors for each subject using the MATLAB® (v.7.3, The MathWorks, Inc., USA) System Identification Toolbox function *armax.m*.

Next, a cross-correlation (CC) analysis and subsequent partial cross-correlation (PCC) were performed between all combination-pairs (*i and j*, N = 30628) of sensors' de-trended signals at zero-lag. The CC and PCC coefficients were calculated using MATLAB® with the *in-house* function *MEG_coef_pcoef.m*, which closely approximated the results from the IMSL statistical routines DCCF and DPCORR (Compaq Visual FORTRAN Professional edition, v.6.6B). To normalize the distribution of the coefficients before averaging across subjects, the Fisher's z-transformation (Snedecor, Cochran 1989) was applied to all sensor-pair's PCC coefficients (PCC_{ij}^{0}):

$$z_{ij}^{0} = \tfrac{1}{2}[\ln(1+PCC_{ij}^{0}) - \ln(1-PCC_{ij}^{0})] \qquad \text{EQ5.14}$$

Subsequently, a dissimilarity matrix was computed from the averaged normalized PCC coefficients ($\overline{z_{ij}^{0}}$) of all subjects for all sensor pair-combinations. Dissimilarity (D_{ij}^{0}) was calculated as:

$$D_{ij}^{0} = 1 - \overline{z_{ij}^{0}} \qquad \text{EQ5.15}$$

The dissimilarity matrix was used in a hierarchical cluster analysis, which investigated which sensors' recorded activities were most similar (i.e. least dissimilar), and whether they might be clustered together in sensor-space. As before, the Matlab® functions: *linkage.m* with UPGMA, and *cluster.m* with a cutoff of 0.990 used to define clusters, were employed in the cluster analysis. Similarly, the results of the ultrametric trees were displayed in dendrograms and in sensor-space with each cluster, its associations and members coded in a specific colour. The hierarchical clustering analyses performed and described were based on previous work by Merkle, Leuthold et al. (2006).

These procedures were performed for 1) the combined movement task sections and 2) the combined rests sections, from the same block of 6 movement sets performed by each subject. This is illustrated in FIG 5.12.

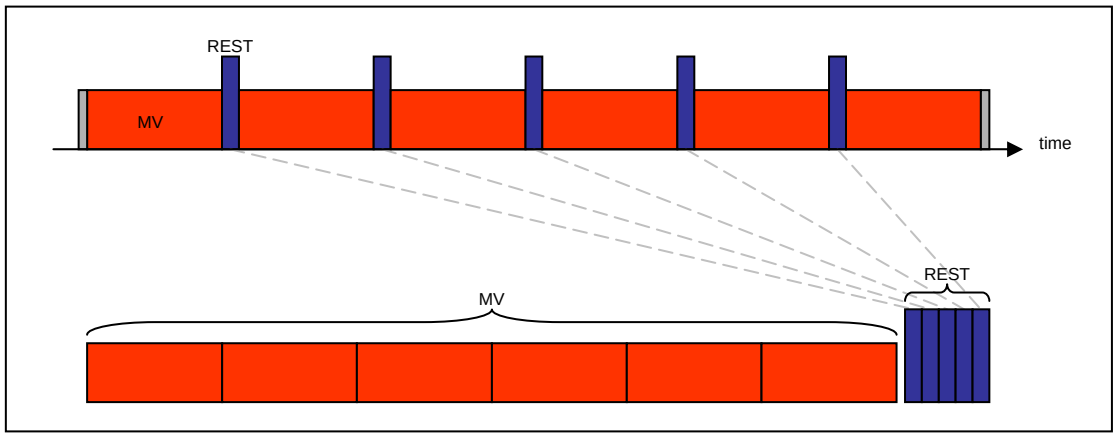

FIG 5.12: Data sections used in the ARIMA, the CC and PCC analyses. Movement sections (MV) are denoted in red and each consisted of 32 target-to-target movements (2 target-to-centre-target and 30 target-to-target movements) which the participants were required to make. In general, a movement section lasted approximately ~26s (assuming that on average subjects took 400ms to make a movement, with 200ms pause at the target, and 200ms reaction time). The rest sections (REST) of 5s each occurred between movement sections.

For this time-series analysis, the cardiac-corrected MEG sensor data (0.1 - 400Hz; without any reference-channel noise reduction) of all subjects except subject 12 (because of the faulty MEG sensor 182 during the recording session) from the appropriate task sections were used. We chose to exclude the subject so that the relations between all sensors could be made, rather than to exclude relations between sensors.

ATKESON, C. and HOLLERBACH, J., 1985. Kinematic features of unrestrained vertical arm movements. *Journal of Neuroscience,* **5**(9), pp. 2318-2330.

BLASCHKE, T. and WISKOTT, L., 2002. An Improved Cumulant Based Method for Independent Component Analysis. J.R. DORRONSORO, ed. In: *Proceedings of the international Conference on Artificial Neural Networks (August 28 - 30, 2002).* August 28 - 30 2002, Springer-Verlag pp1087-1093.

BOX, G.E.P. and JENKINS, G.M., 1970. Time series analysis - forecasting and control. San Francisco, California, USA.: Holden-Day, Inc.

CORTER, J.E., 1996. Tree models of similarity and association. Thousand Oaks, California, USA.: Sage Publications.

FLANAGAN, J.R. and WING, A.M., 1997. The role of internal models in motion planning and control: evidence from grip force adjustments during movements of hand-held loads. *Journal of Neuroscience,* **17**(4), pp. 1519-1528.

JOHNSON, R.A. and WICHERN, D.W., 1982. Applied multivariate statistical analysis. Englewood Cliffs, N.J.: Prentice-Hall.

LEE, D.N., 1998. Guiding Movement by Coupling Taus. *Ecological Psychology,* **10**(3&4), pp. 221-250.

LEE, D.N., CRAIG, C.M. and GREALY, M.A., 1999. Sensory and intrinsic coordination of movement. *Proceedings of the Royal Society B: Biological Sciences,* **266**(1432), pp. 2029-2035.

LEUTHOLD, A.C., 2003. Subtraction of heart artifact from MEG data: The matched filter revisited. *Society for Neuroscience Abstracts,* 2003, pp863.15.

LEUTHOLD, A.C., LANGHEIM, F.J., LEWIS, S.M. and GEORGOPOULOS, A.P., 2005. Time series analysis of magnetoencephalographic data during copying. *Experimental Brain Research,* **164**(4), pp. 411-422.

MERKLE, A.N., LEUTHOLD, A.C., LANGHEIM, F.J.P. and GEORGOPOULOS, A.P., 2006. Hierarchical clustering of magnetoencephalographic (MEG) data. *Society for Neuroscience Abstracts,* 2006, 747.19.

OLDFIELD, R.C., 1971. The assessment and analysis of handedness: the Edinburgh inventory. *Neuropsychologia,* **9**(1), pp. 97-113.

SNEDECOR, G., and COCHRAN, W., 1989. Statistical methods. 8th edn. Ames: Iowa State University Press.

CHAPTER 6:

A MEG Study of Movement Performance:

Neural Correlates of Movement *Tau*

Introduction

Neurophysiological studies have shown that movement kinematics (e.g. position, speed) are correlated with the neural activities of a number of different brain areas, e.g. primary motor, premotor, parietal cortices and the cerebellum (Ashe, Georgopoulos 1994, Averbeck, Chafee et al. 2005, Coltz, Johnson et al. 1999, Moran, Schwartz 1999). That different brain areas act in concert in relation to movement parameters like speed is supported by electrophysiological recordings in multiple brain areas of the behaving non-human primate (Carmena, Lebedev et al. 2003, Wessberg, Stambaugh et al. 2000). However, there have been few studies associating neural activities and movement parameters in humans. Apart from those that were primarily concerned with the predictive value of MEG signals in applied non-invasive neuro-prostheses (e.g. Georgopoulos, Langheim et al. 2005, Wolpaw, Birbaumer et al. 2002, Wolpaw, McFarland 2004), two studies that also explored the relation of MEG signals and movement speed are of particular relevance to the current research.

Kelso, Fuchs et al. (1998) employed a correlation analysis on the recorded neuromagnetic signals and velocity profiles of repetitive finger extension and flexion movements of 5 participants and found highest correlations between averaged velocity profiles and neural signals recorded from sensors located over the contralateral M1. However, the rhythmic finger movements made to a metronome may itself be a source of confusion. To avoid having repetitive task movements to obtain a measure by averaging data, Jerbi, Lachaux et al. (2007) used a continuous movement task that involved the random manipulation required to keep a visual object in place. They employed an exhaustive analysis of coherence between non-averaged time-varying movement speed and cortical source activities (at ~12,000 brain locations) estimated by minimum-norm algorithms and arrived at a similar conclusion as Kelso et al. (1998) in source-space. In addition, Jerbi, Lachaux et al. (2007) also observed a network of brain regions (e.g. contralateral dorsal premotor, supplementary motor, primary somatosensory, inferior and superior parietal lobes, prefrontal, ipsilateral anterior cerebellum and subcortical areas) oscillating in phase with the contralateral M1 activation that yielded the highest coherence with movement speed at 2 - 5 Hz.

Even though oscillatory activities in the motor areas may be related in phase with repeating hand muscle actions or movement kinematics, the strength and significance of these coherences have not been functionally assessed (Salenius, Hari 2003); it is not known, for example, if such oscillations are part of intrinsic physiological homeostasis or involved in cognitive processing of experiences. Moreover, the observed high inter-session variability in cortico-muscular coherence strength (Pohja, Salenius et al. 2005) is also likely to manifest in the measurement of cortico-speed coherence strength across different sessions, and begs the question of what the variation(s) might be associated with. In addition, while it is encouraging that areas with high coherence found from the source-imaging technique have been implicated in motor control, the confidence of minimum-norm-derived source localization is limited to the strongest source with large

bleed-over effects, and the contributions of deeper sources are in general unlikely (Hillebrand, Barnes 2002). Theoretically, there can only be as many sources as there are sensors (n = 151 in Jerbi et al.'s study), and with activity estimation to be generated by up to approximately 12,000 brain locations, the real related brain activity may have actually stemmed from fewer detectable sources. Another important oversight in these previous studies concerns the assumption of stationarity, which was not accounted for in their coherence analyses. Coherence analysis is applicable only to stationary time-series; i.e. time-series with zero mean and variance (Lachaux, Rodriguez et al. 1999). When stationarity is not adequately accounted for, particularly in time-series data, any correlation found might have been an over-estimation due to the inherent likelihood of spurious correlations.

There is little doubt that the signal recorded in each MEG sensor is derived from the brain. Although an appealing pictorial rendition can be made of estimated sources contributing to the measured fields in brain-space, the non-trivial nature of the inverse problem warrants caution in the interpretation of this source-space analysis. We therefore opted for a more conservative sensor-space analysis at the expense of localizing where sources contributing to the representation of the movement parameters of interest might be found in the brain. We were interested in the time-varying aspects of neural activity at different locations and sought to investigate whether the neural correlates of movement speed and *tau* demonstrated in previous neurophysiological and imaging studies (Ashe, Georgopoulos 1994, Averbeck, Chafee et al. 2005, Field, Wann 2005, Merchant, Battaglia-Mayer et al. 2004, Moran, Schwartz 1999), as well as those observed in our neurophysiological analysis discussed in Chapter 3, would also be evident in neural signals recorded by MEG sensors in humans. A time-series analysis, similar to the one applied in our analysis of neurophysiological data was performed. Given that frontal-parietal activities are reported to be involved in

visuomotor tasks, we hypothesized that neural activity in these areas are most likely to be tapped by the axial-gradiometer sensors.

Results

— Behaviour

The movements executed by subjects were generally characterized by trajectories that were generally straight with a main peak speed or tangential velocity hump, which was not necessarily bell-shaped (e.g. FIG 5.6 & 5.11 in Chapter 5). These behavioural performance characteristics are described by the mean movement parameters tabulated in Tables 6.1 to 6.4. On average, 338 target-to-target movements segments (grand mean ± std. = 338.85 ± 24.88) were considered for each of the 20 subjects. The straightness of these movements as measured by the mean Index of Linearity indicated that subjects made very linear movements (grand mean ± std. = 0.09 ± 0.02) and the mean Instantaneous Curvature of these movements ranged between 0.02 and 0.15 cm^{-1} (grand mean ± std. = 0.06 ± 0.05 cm^{-1}). Another means of quantifying how straight the movement performance was came from measurement of the directional difference between the new target (relative to the current position) and movement directions. Measured in degrees, the mean of this directional difference was fairly consistent across subjects, ranging between 1.6° and 2.2° (grand mean ± std. = 1.96 ± 0.13°), which was a rather small deviation from the actual direction of the new target.

With regard to the temporal aspects of performance, the subjects' mean reaction time ranged from 121 to 353 ms (grand mean ± std. = 174.25 ± 52.98) and reflected the fact that although subjects were not required to respond as fast as possible when a new

target appeared, some appeared to have done so, while others took their time to initiate their movements. The mean target-to-target movement time ranged between 290 to 667 ms (grand mean ± std. = 406.19 ± 93.72 ms) and did not appear to follow the reaction times manifested; some subjects with longer mean reaction times had shorter mean movement times, and some with shorter mean reaction times had much longer mean movement times.

The mean maximum movement speed of all subjects ranged between 8 to 19.4 cm/s (grand mean ± std. = 14.04 ± 2.76 cm/s) and the mean time to maximum speed fluctuated around 150.17 ms ± 27.29 ms (range = 112 to 231 ms). In general, the maximum movement speed occurred before half the movement had been made as indicated by the mean proportion of movement time to maximum speed, which varied about 0.39 ± 0.03. This also matched the mean τ_g-coupling slopes, which varied little about 0.32 ± 0.03, indicating that the maximum speed for which the portion of movement that was coupled to the theoretical *tau-guide* (τ_g), occurred early during the movement prior to the middle of the movement time quite consistently, followed by the deceleration. These movement performances with early peak speeds rendered mean percentage τ_g-couplings that ranged between 78% and 96% (grand mean ± std. = 91.88 ± 4.48), indicating a high linear association between the movement *taus* and the theoretical *tau-guide*.

The associations between movement parameters revealed some interesting trends (Table 6.5). Subjects' mean directional differences tended to be larger when mean movement time was shorter (r = -0.140, p = 0.030) and when mean maximum speed was lower (r = -0.192, p = 0.003). Interestingly, mean movement time was inversely related to mean reaction time (r = -0.345, p = 0.000); longer movements tended to be associated with shorter reaction times, and vice versa, as if it were a subconscious goal of the

subjects to maintain a nearly regular total trial duration. Longer mean movement time and shorter mean reaction time were both related to higher mean time to maximum speed (r = 0.821; r = -0.331, p = 0.000 respectively). However, longer mean movement time was associated with shorter mean proportion of movement time to maximum speed (r = -0.513, p = 0.000). While it took longer to reach maximum speeds in movements with longer movement durations and shorter reaction times, the maximum speed tended to occur within the earlier half of each of the whole movement. Moreover, mean movement time was also inversely related to the mean maximum speed (r = -0.762, p = 0.000), which did not appear to increase with movement duration. Mean maximum speed was positively related to mean reaction time (r = 0.383, p = 0.000) and mean proportion of movement time to maximum speed (r = 0.252, p = 0.000) but inversely related to mean time to maximum speed (r = -0.729, p = 0.000). It took less time for subjects to reach peak movement speed when their movement speed was high, yet at the same time, the peak speed occurred relatively later in their movements.

We observed that both mean instantaneous curvature and mean Index of Linearity were similarly positively related to mean directional differences (r = 0.309; r = 0.531, p = 0.000, respectively), while both were negatively associated with mean reaction time (r = -0.163, p = 0.012; r = -0.292, p = 0.000), and mean maximum speed (r = -0.593; r = -0.259, p = 0.000, respectively). In addition, both mean instantaneous curvature and mean Index of Linearity were inversely related to mean % τ_g-coupling (r = -0.566, p = 0.000; r = -0.213, p = 0.001) but positively associated with mean τ_g-coupling slope (r = 0.268; r = 0.316, p = 0.000, respectively). In general, while relatively straight movement trajectories were characterised by small directional deviations from the movement direction specified by the target and higher mean maximum speeds, they were also generally executed after longer deliberations. Nonetheless, straighter movements tended to manifest higher % τ_g-coupling, and the speed of τ_g-coupled movement sections peaked

within the earlier half of the performance (i.e. τ_g-coupling slope ≤ 0.5). Furthermore, mean instantaneous curvature was positively associated with mean movement time (r = 0.566, p = 0.000) and mean time to maximum speed (r = 0.446, p = 0.000), but it was inversely related to mean percentage of movement time to maximum speed (r = -0.286, p = 0.000). While movements that spanned longer durations were generally less straight they also took less time to reach peak speed, which was manifested earlier with respect to the whole movement.

With regards to the parameters derived from the τ_g-analyses, mean % τ_g-coupling was positively associated with mean reaction time (r = 0.261, p = 0.000), mean maximum speed (r = 0.472, p = 0.000), and mean proportion of movement time to maximum speed (r = 0.287, p = 0.000), but negatively associated with mean movement time (r = -0.607, p = 0.000), mean time to maximum speed (r = -0.480, p = 0.000), mean instantaneous curvature (r = -0.566, p = 0.000), mean Index of Linearity (r = -0.213, p = 0.001), as well as mean τ_g-coupling slope (r = -0.655, p = 0.000). Movements that were executed after longer deliberation, spanned shorter durations, performed with higher maximum speeds that occurred toward the later half of the whole movement duration, were generally straighter and more strongly τ_g-coupled. Interestingly too, was that the speed of the τ_g-coupled movement section peaked within the earlier half of the performance. Furthermore, mean τ_g-coupling slope was positively related to mean directional differences (r = 0.188, p = 0.000), mean time to maximum speed (r = 0.228, p = 0.000), mean proportion of movement time to maximum speed (r = 0.368, p = 0.000), mean instantaneous curvature (r = 0.268, p = 0.000), and mean Index of Linearity (r = 0.316, p = 0.000). Thus, when the speed of the τ_g-coupled movement section peaked within the later half of the performance, the movement trajectories were generally less straight, and it took longer for participants to reach peak movement speeds such that these peak speeds tended to occur later in their overall movements.

Subj #	N	Target - Mv Directional Diff. (°)	Index of Linearity	Instantaneous Curvature (cm^{-1})
1	261	2.12 ± 1.95	0.08 ± 0.03	0.03 ± 0.10
2	354	2.04 ± 1.75	0.08 ± 0.02	0.02 ± 0.16
3	329	1.84 ± 1.60	0.07 ± 0.04	0.09 ± 0.30
4	359	1.89 ± 1.72	0.10 ± 0.09	0.05 ± 0.17
5	353	2.09 ± 1.87	0.08 ± 0.05	0.02 ± 0.13
6	356	1.90 ± 1.59	0.08 ± 0.05	0.03 ± 0.13
7	340	1.99 ± 1.61	0.10 ± 0.07	0.06 ± 0.19
8	360	2.02 ± 1.65	0.08 ± 0.05	0.19 ± 0.54
9	336	2.07 ± 1.65	0.10 ± 0.06	0.02 ± 0.08
10	351	2.02 ± 1.75	0.07 ± 0.04	0.10 ± 0.35
11	358	1.67 ± 1.53	0.07 ± 0.04	0.12 ± 0.42
12	355	2.10 ± 1.70	0.10 ± 0.08	0.15 ± 0.39
13	327	2.01 ± 1.72	0.10 ± 0.07	0.03 ± 0.09
14	348	1.90 ± 1.62	0.11 ± 0.08	0.04 ± 0.07
15	295	1.99 ± 1.57	0.09 ± 0.06	0.02 ± 0.07
16	329	2.15 ± 1.76	0.12 ± 0.05	0.02 ± 0.09
17	316	1.73 ± 1.40	0.12 ± 0.09	0.05 ± 0.22
18	344	1.98 ± 1.64	0.10 ± 0.07	0.02 ± 0.08
19	348	1.89 ± 1.69	0.13 ± 0.10	0.04 ± 0.10
20	358	1.85 ± 1.51	0.13 ± 0.11	0.04 ± 0.11
Grand Mean	338.85	1.96	0.09	0.06
Std. Dev.	24.88	0.13	0.02	0.05

TABLE 6.1: Characteristics of movement trajectories. Mean and standard deviations of subjects' movement parameters: angle difference between target and movement directions (Target-Mv Directional Difference), Index of Linearity, and Instantaneous Curvature.

Subj #	N	Rxn Time (ms)	Mv Time (ms)
1	261	352.62 ± 96.65	359.47 ± 91.08
2	354	238.12 ± 40.36	290.81 ± 66.83
3	329	183.89 ± 38.86	397.45 ± 95.28
4	359	136.13 ± 37.30	407.66 ± 76.37
5	353	245.03 ± 73.31	306.53 ± 75.83
6	356	170.00 ± 33.01	311.14 ± 66.76
7	340	147.95 ± 42.88	360.65 ± 96.46
8	360	146.56 ± 34.47	666.52 ± 155.94
9	336	159.12 ± 36.38	383.11 ± 86.34
10	351	185.88 ± 52.63	463.04 ± 85.66
11	358	158.71 ± 41.99	541.49 ± 103.86
12	355	157.93 ± 54.78	540.06 ± 135.73
13	327	138.11 ± 32.40	330.00 ± 77.56
14	348	121.47 ± 59.21	438.13 ± 93.84
15	295	155.01 ± 38.92	356.75 ± 75.82
16	329	202.58 ± 58.10	312.57 ± 83.35
17	316	141.02 ± 49.70	447.10 ± 95.86
18	344	152.38 ± 42.04	368.27 ± 70.96
19	348	138.48 ± 64.98	442.71 ± 114.07
20	358	153.96 ± 70.34	400.27 ± 97.29
Grand Mean	338.85	174.25	406.19
Std. Dev.	24.88	52.98	93.72

TABLE 6.2: Temporal aspects of movement task performance. Mean and standard deviations of subjects' movement parameters: Reaction Time (Rxn Time), and Movement Time (Mv Time).

Subj #	N	Time-to-Max. Speed (ms)	Proportion of Mv Time to Max. Speed	Max. Speed (cm/s)
1	261	136.43 ± 26.02	0.39 ± 0.07	14.53 ± 3.65
2	354	124.83 ± 22.50	0.44 ± 0.08	19.38 ± 5.47
3	329	146.73 ± 44.50	0.38 ± 0.15	13.51 ± 3.79
4	359	146.69 ± 32.05	0.37 ± 0.08	13.81 ± 3.00
5	353	120.98 ± 24.77	0.41 ± 0.10	19.01 ± 5.03
6	356	126.98 ± 32.08	0.42 ± 0.10	16.31 ± 3.89
7	340	125.49 ± 38.15	0.36 ± 0.10	15.43 ± 4.08
8	360	230.76 ± 76.86	0.36 ± 0.12	8.10 ± 1.92
9	336	145.99 ± 39.28	0.39 ± 0.10	13.72 ± 3.49
10	351	171.72 ± 36.36	0.38 ± 0.08	11.96 ± 3.26
11	358	190.54 ± 50.04	0.36 ± 0.10	10.32 ± 2.34
12	355	169.85 ± 58.13	0.33 ± 0.12	10.83 ± 2.79
13	327	134.77 ± 28.11	0.42 ± 0.09	16.44 ± 4.07
14	348	172.97 ± 49.07	0.40 ± 0.11	12.13 ± 2.74
15	295	141.06 ± 32.13	0.40 ± 0.09	15.03 ± 3.84
16	329	112.71 ± 24.29	0.38 ± 0.10	16.29 ± 3.56
17	316	153.22 ± 40.55	0.35 ± 0.09	12.53 ± 2.72
18	344	147.66 ± 39.60	0.41 ± 0.10	14.28 ± 3.35
19	348	156.47 ± 48.01	0.37 ± 0.12	12.66 ± 3.09
20	358	147.63 ± 43.14	0.38 ± 0.11	14.50 ± 3.17
Grand Mean	338.85	150.17	0.39	14.04
Std. Dev.	24.88	27.29	0.03	2.76

TABLE 6.3: Speed-related parameters of target-to-target movements. Mean and standard deviations of subjects' movement parameters: Time-to-Maximum Speed, Proportion of Movement Time to Maximum Speed, and Maximum Speed.

Subj #	N	R^2	% τ_g-coupling	Slope (*k*)
1	261	0.96 ± 0.00	96.30 ± 9.71	0.28 ± 0.13
2	354	0.96 ± 0.00	96.21 ± 7.46	0.36 ± 0.14
3	329	0.96 ± 0.00	90.41 ± 21.08	0.31 ± 0.24
4	359	0.96 ± 0.00	93.33 ± 15.46	0.29 ± 0.18
5	353	0.96 ± 0.00	92.80 ± 16.07	0.35 ± 0.21
6	356	0.96 ± 0.00	96.00 ± 10.43	0.30 ± 0.13
7	340	0.96 ± 0.00	90.27 ± 20.66	0.33 ± 0.26
8	360	0.95 ± 0.00	78.63 ± 28.92	0.38 ± 0.28
9	336	0.96 ± 0.00	91.45 ± 18.36	0.31 ± 0.19
10	351	0.95 ± 0.00	92.68 ± 15.73	0.30 ± 0.16
11	358	0.95 ± 0.00	93.34 ± 15.42	0.25 ± 0.19
12	355	0.95 ± 0.00	82.29 ± 26.97	0.35 ± 0.29
13	327	0.96 ± 0.00	94.56 ± 12.93	0.34 ± 0.24
14	348	0.95 ± 0.00	90.94 ± 18.06	0.33 ± 0.22
15	295	0.96 ± 0.00	95.75 ± 10.64	0.30 ± 0.15
16	329	0.96 ± 0.00	92.77 ± 16.56	0.30 ± 0.19
17	316	0.96 ± 0.00	93.49 ± 15.59	0.28 ± 0.19
18	344	0.96 ± 0.00	95.70 ± 11.46	0.31 ± 0.29
19	348	0.96 ± 0.00	89.38 ± 21.19	0.34 ± 0.24
20	358	0.96 ± 0.00	91.34 ± 17.61	0.34 ± 0.21
Grand Mean	338.85	0.96	91.88	0.32
Std. Dev.	24.88	0.00	4.48	0.03

TABLE 6.4: Results of *tau*-analysis on target-to-target movements. Mean and standard deviations of subjects' parameters: Recursive Regression R^2 cutoff, % *tau*-coupling and *tau*-coupling slope.

Correlations

		Direction Diff. (°)	Rxn Time (ms)	Mv Time (ms)	Time-to-Max. Speed (ms)	Proportion of Mv time to Max. Speed	Max Speed (cm/s)	Inst. Curv. (cm^{-1})	Idx. Linearity	% τ_g-coupling	Slope (*k*)
Direction Diff. (°)	Pearson Correlation	1	.088	-.140(*)	-.123	.052	-.192(**)	.309(**)	.531(**)	-.097	.188(**)
	Sig. (2-tailed)	.	.175	.030	.057	.419	.003	.000	.000	.136	.003
Rxn Time (ms)	Pearson Correlation	.088	1	-.345(**)	-.331(**)	.126	.383(**)	-.163(*)	-.292(**)	.261(**)	-.120
	Sig. (2-tailed)	.175	.	.000	.000	.051	.000	.012	.000	.000	.065
Mv Time (ms)	Pearson Correlation	-.140(*)	-.345(**)	1	.821(**)	-.513(**)	-.762(**)	.566(**)	-.093	-.607(**)	.040
	Sig. (2-tailed)	.030	.000	.	.000	.000	.000	.000	.152	.000	.536
Time-to-Max. Speed (ms)	Pearson Correlation	-.123	-.331(**)	.821(**)	1	.042	-.729(**)	.446(**)	-.123	-.480(**)	.228(**)
	Sig. (2-tailed)	.057	.000	.000	.	.520	.000	.000	.058	.000	.000
Proportion of Mv time to Max. Speed	Pearson Correlation	.052	.126	-.513(**)	.042	1	.252(**)	-.286(**)	-.039	.287(**)	.368(**)
	Sig. (2-tailed)	.419	.051	.000	.520	.	.000	.000	.543	.000	.000
Max Speed (cm/s)	Pearson Correlation	-.192(**)	.383(**)	-.762(**)	-.729(**)	.252(**)	1	-.593(**)	-.259(**)	.472(**)	-.116
	Sig. (2-tailed)	.003	.000	.000	.000	.000	.	.000	.000	.000	.072
Inst. Curv. (cm^{-1})	Pearson Correlation	.309(**)	-.163(*)	.566(**)	.446(**)	-.286(**)	-.593(**)	1	.173(**)	-.566(**)	.268(**)
	Sig. (2-tailed)	.000	.012	.000	.000	.000	.000	.	.007	.000	.000
Idx. Linearity	Pearson Correlation	.531(**)	-.292(**)	-.093	-.123	-.039	-.259(**)	.173(**)	1	-.213(**)	.316(**)
	Sig. (2-tailed)	.000	.000	.152	.058	.543	.000	.007	.	.001	.000
% τ_g-coupling	Pearson Correlation	-.097	.261(**)	-.607(**)	-.480(**)	.287(**)	.472(**)	-.566(**)	-.213(**)	1	-.655(**)
	Sig. (2-tailed)	.136	.000	.000	.000	.000	.000	.000	.001	.	.000
Slope (*k*)	Pearson Correlation	.188(**)	-.120	.040	.228(**)	.368(**)	-.116	.268(**)	.316(**)	-.655(**)	1
	Sig. (2-tailed)	.003	.065	.536	.000	.000	.072	.000	.000	.000	.

TABLE 6.5: Correlation between mean movement parameters for all target-to-target movements. *: Correlation is significant at the 0.05 level (2-tailed). **: Correlation is significant at the 0.01 level (2-tailed).

— Relations between MEG sensors' signals and movement tau or speed.

We applied the same AREG analyses as we did in the Monkey study to our MEG data to investigate if there would also be a neural correlate for movement *tau* in humans performing a target-to-target movement task. The significance test of the relation between individual sensor's signals and movement *tau* or speed for all movements performed provides an indication of the probability of this relation against the null-hypothesis. The results (in Table 6.6) show the percentages of MEG sensors whose signals are significantly ($p < 0.05$) linearly related to movement *tau* or to speed, as obtained from the AREG analyses with either one or both of these movement parameters as independent variables, for all 20 subjects.

Across all subjects, the mean percentage (± SEM) of sensors for which the AREG analysis yielded significance for speed (80.51 ± 2.89 %) was significantly higher than that for movement *tau* (21.68 ± 5.60%); $t_{(19)} = -9.758$, $p = 0.000$. When taking into account that the neural signals may be related to both movement parameters, the mean percentage (± SEM) of sensors for which the AREG analysis yielded significance for speed, with or without significant effects for movement *tau* (80.61 ± 2.86 %), was also significantly higher than that for movement *tau* (with or without significant association to speed; 21.98 ± 6.08 %), $t_{(19)} = -9.137$, $p = 0.000$. We noted that in this AREG, which included both speed and *tau* as independent variables, the majority of the *tau*-related sensor-signals over all subjects (1086/4940) were also related to speed (909/1086, 83.70%), and about 15.80% (781/4940) of the sensors' signals were neither related to speed nor movement *tau*. In addition, the percentages for *tau*- or speed related sensors derived from both AREG analyses were not significantly different; percentage of *tau*-related and speed-related sensors: $t_{(19)} = -0.37$, $p = 0.716$; $t_{(19)} = -0.52$, $p = 0.609$, respectively.

We also investigated if there would be any hemispheric or anterior-posterior sensor-space differences in the number of sensors whose signals were significantly related to either movement *tau* or speed. Table 6.7 lists the mean number of *tau*- and speed-related sensors across subjects with respect to the hemisphere and anterior-posterior sensor-space as partitioned according to FIG 6.1. There were generally more *tau*-related sensors in the left hemisphere but the only significant difference was found for the numbers derived from the AREG which included both parameters as independent variables ($t_{(19)} = 2.10$, $p < 0.05$). On the other hand, speed-related sensors tended to manifest with similar numbers in both hemispheres. With respect to the anterior-posterior sensor-space, there were consistently higher numbers of mean *tau*- and speed-related sensors in the posterior compared to the anterior sensor-space. However, the anterior-posterior difference was only significant in the left hemisphere for *tau*-related sensors ($t_{(19)} = 3.42$, $p < 0.005$; $t_{(19)} = 4.19$, $p < 0.001$; AREG analyses with one or two independent variables respectively), while the difference was significant in both hemispheres for speed-related sensors (left hemisphere: $t_{(19)} = 5.40$; $t_{(19)} = 5.66$; right hemisphere: $t_{(19)} = 6.82$; $t_{(19)} = 7.20$, $p < 0.001$; AREG analyses with one or two independent variables respectively). Thus in general, there were more posterior processes involved in the representation of movement *tau* and speed.

AREG Independent Variable(s)	Speed & Mv *tau*			Speed OR Mv *tau*	
Significant Relations b/w Sensor Signal & Parameter	**Mv *tau***	**Speed**		**Mv *tau***	**Speed**
Subj #	**%**	**%**		**%**	**%**
1	65.99	79.76		61.94	79.35
2	57.89	79.35		59.92	76.52
3	78.14	76.52		71.26	75.30
4	8.10	89.07		7.69	89.07
5	22.67	85.83		24.70	85.43
6	6.07	85.02		9.31	85.02
7	2.83	85.43		3.64	85.43
8	8.50	82.59		8.10	82.59
9	1.62	82.59		1.62	82.59
10	13.36	85.83		12.96	85.83
11	8.10	90.28		8.10	90.28
12	5.26	78.95		4.86	78.95
13	8.50	88.26		13.36	88.26
14	4.45	86.64		4.86	86.64
15	0.81	31.58		0.81	31.58
16	76.52	90.69		64.78	91.50
17	5.67	77.33		5.26	77.33
18	53.44	81.78		56.68	83.81
19	6.88	67.61		7.69	67.61
20	4.86	87.04		6.07	87.04
MEAN	21.98	80.61		21.68	80.51
STD.	27.17	12.80		25.06	12.90
SEM.	6.08	2.86		5.60	2.89

TABLE 6.6: Neuromagnetic correlates of movement *tau* or speed. Percentages of movement *tau*- or speed- related sensors determined from AREG with one or both movement parameters as independent variables (where level of significance relation was $p < 0.05$) for individual subjects, as well as mean, standard deviation (STD.) and standard error of mean (SEM) across subjects.

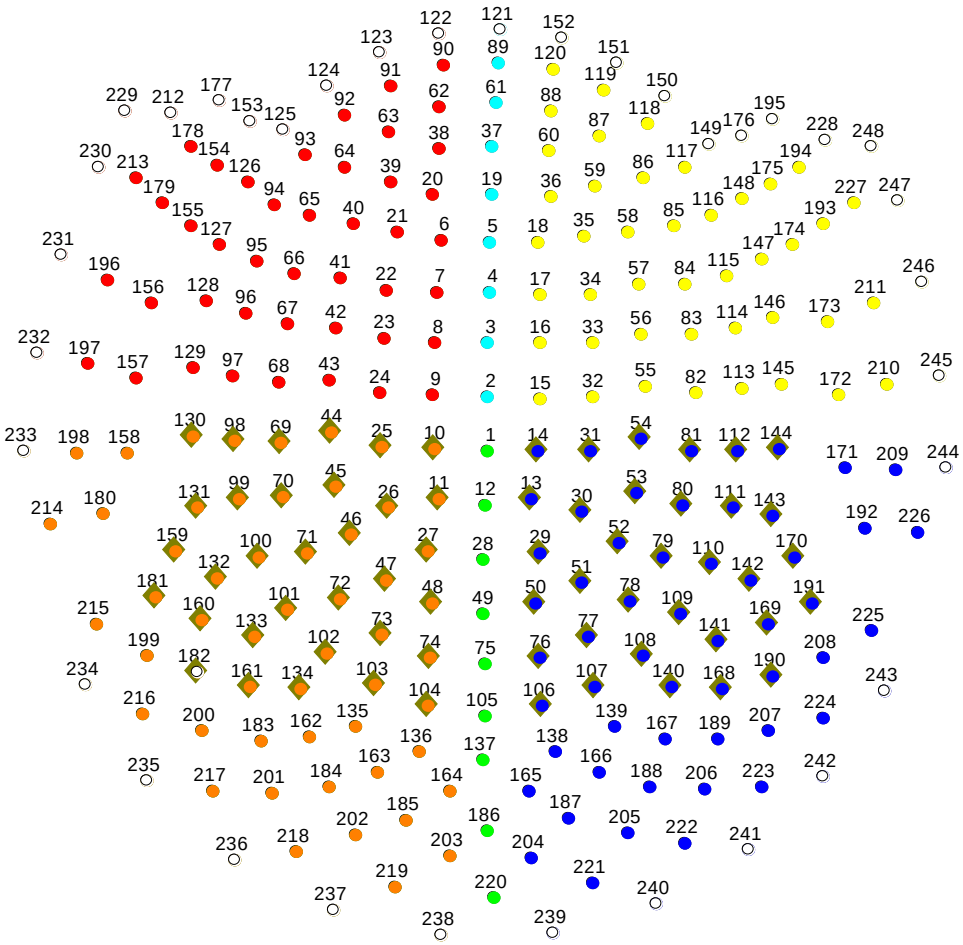

FIG 6.1: Sensors partitioned into the respective hemispheres and anterior-posterior sensor-space: Left anterior (red), Left posterior (orange), Right anterior (yellow), Right posterior (blue), Midline anterior (cyan), Midline posterior (green), edge sensors and sensor #182 not included (white). Sensors (except #182) depicted with an additional diamond background were considered as left and right hemisphere parietal sensors for subsequent analyses (refer to text for further details).

AREG Independent Variable(s)			Speed & Mv tau			Speed OR Mv tau		
	Sensor-space	HEMs	Mean #	SEM		Mean #	SEM	
Mv *tau*-related sensors	Anterior	L	9.00	2.76	ns	8.20	2.27	ns
		R	8.90	2.45		8.15	2.15	
	Posterior	L	13.65	3.63	*	13.85	3.37	ns
		R	11.75	3.41		12.20	3.55	
Speed-related sensors	Anterior	L	35.25	1.54	ns	35.35	1.54	ns
		R	33.90	1.45		33.65	1.49	
	Posterior	L	45.55	2.12	ns	45.50	2.18	ns
		R	45.55	1.76		45.60	1.79	

TABLE 6.7: Hemispheric and anterior-posterior sensor-space distribution of neuromagnetic correlates of movement *tau* or speed. Mean number (and SEM) of movement *tau*- or speed-related sensors (from AREG with one or both movement parameters as independent variables) within the different sensor hemispheres (L, or R) and sensor-space (anterior or posterior), across subjects (N=20). Asterisk indicates the paired t-test significance ($p < 0.05$) of the difference between the mean number of *tau*-related sensors in the L and R parietal sensor-space.

AREG Independent Variable(s)				Speed & Mv tau			Speed OR Mv tau		
	Sensor-space	HEMs	N sensors	Mean %	SEM		Mean %	SEM	
Mv *tau*-PSR	Anterior	L	54	20.83	0.71	ns	19.63	0.91	ns
		R		19.81	1.12		19.07	0.91	
	Posterior	L	61	25.50	0.73	**	25.58	0.95	**
		R		21.42	0.91		22.33	0.86	
	Parietal	L	32	24.69	1.12	**	24.69	1.44	**
		R		20.78	1.15		19.38	1.12	
Speed-PSR	Anterior	L	54	79.63	1.53	ns	79.63	1.54	*
		R		76.94	1.42		76.20	1.37	
	Posterior	L	61	83.67	1.13	ns	83.75	1.07	ns
		R		81.42	1.21		81.58	1.17	
	Parietal	L	32	88.75	1.23	**	88.13	1.28	**
		R		83.13	1.43		83.13	1.40	

TABLE 6.8: Mean '*percentage of significant relation*' (PSR) for movement *tau* or speed, relative to sensor-space. Mean (and SEM) PSR for movement *tau* or speed (from AREG with one or both movement parameters as independent variables) with respect to the different hemispheres (L, or R), and anterior, posterior, or parietal sensor-space. Asterisk indicates the paired t-test significance (*: $p < 0.05$; **: $p < 0.001$) of the difference between the mean *tau*- or speed-PSR of the L and R hemisphere sensors.

— Relations between behavioural performance and percentages of MEG sensors significantly related to movement tau or speed.

We observed that for both AREG analyses, subjects' mean reaction times were positively associated with the percentage of *tau*-related sensors (r = 0.628, p = 0.003; r = 0.622, p= 0.003; AREG with one and two independent variables respectively), while in the AREG with *tau* as the independent variable, percentage of *tau*-related sensors and subjects' mean instantaneous curvature just reached significance for a negative association (r = -0.450, p = 0.047). There was no significant correlation found for percentage of speed-related sensors and all other movement variables considered. It seemed that subjects who took their time to initiate their target-to-target movements had relatively more sensors whose signals were associated with movement *tau*.

— Distribution of percentage of significant relation for movement tau or speed in sensor-space.

As some subjects (e.g. subject # 15, 9, and 7) had far fewer *tau*-related sensors, the concern was that these sensors might be randomly located in the sensor space. We pooled all the *tau*-related sensors across subjects to generate '*percentage of significant relation*' (PSR) maps in *sensor-space.* Using percentages derived from both AREG analyses, which included movement *tau* and/or speed as independent variables, we plotted the sensors with highest range of PSR for movement *tau* (30-40%) including all subjects' *tau*-related sensors, and subsequently removed the contributions from subjects 15, 9, and 7, to see how the distribution of these tau-related sensors might change. FIG 6.2 (a, b) illustrates that while these subjects have far fewer *tau*-related sensors, the sensors were nonetheless distributed close to the other *tau*-related sensors contributed

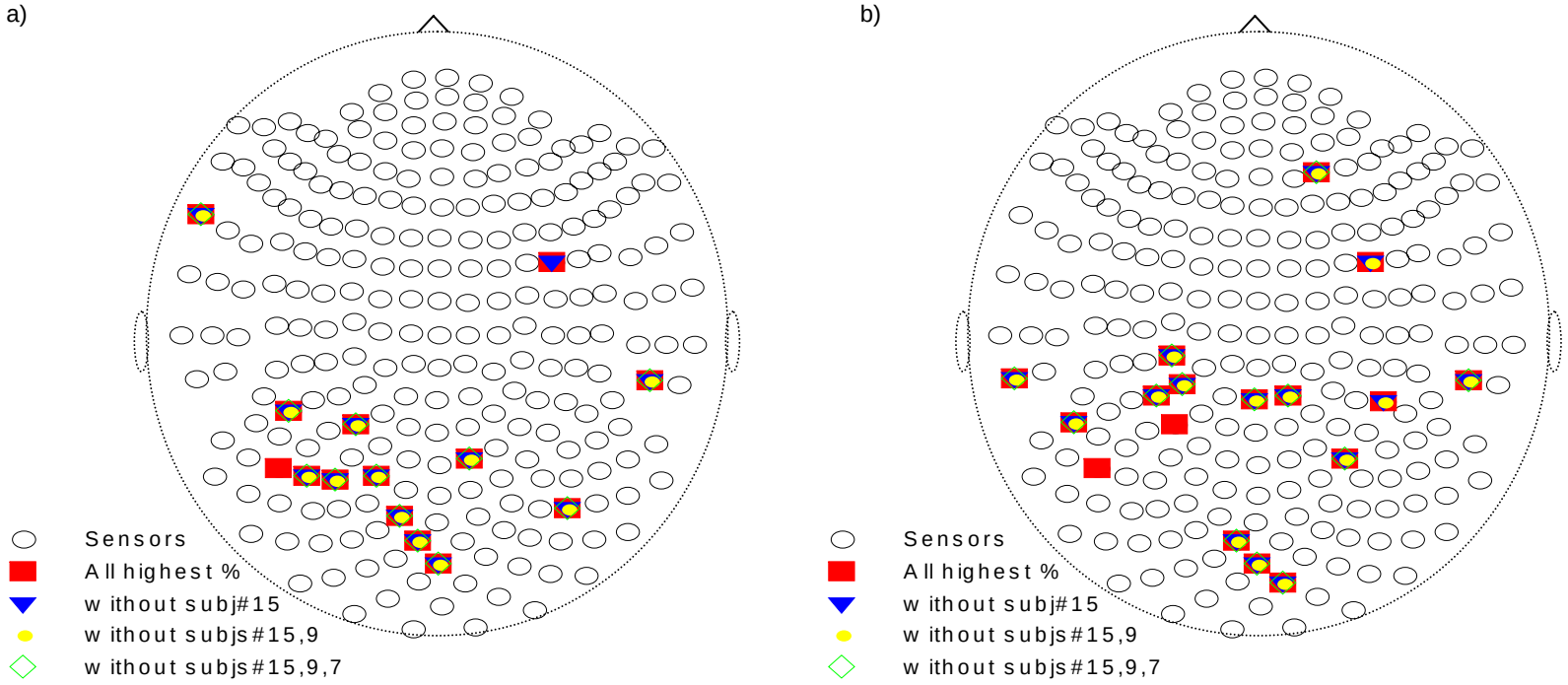

FIG 6.2: Spatial distribution of '*percentage of significant relation*' (PSR) for movement *tau*. Two-dimensional array of MEG sensors displaying the PSR for movement *tau* pooled across all subjects (N=20). The distribution of sensors with 30-40% PSR with and without subjects with low percentage of *tau*-related sensors is shown for AREG analysis with movement *tau* as the independent variable in (a), and for AREG analysis with both movement *tau* and speed as independent variables in (b).

by the rest of the subjects. Consequently, we took the more conservative approach and included all subjects' *tau*- or speed-related sensors in generating the PSR maps for an overview of where these parameter-related sensors were distributed in 3D MEG sensor-space (FIGs 6.3 & 6.4).

Given that the mean percentage of *tau*-related sensors was not very high there was less of an overlap in the *tau*-related sensors across subjects, hence, the PSR manifested by the 248 sensors was low; highest sensor PSR = 40%. Nonetheless, there was some clustering of these *tau*-related sensors in sensor-space. Although the mean percentages of *tau*-related sensors obtained from the two different AREG analyses did not differ, the spatial distribution of the PSR for movement *tau* was slightly different. When the AREG analysis included only movement *tau* as the independent variable, *tau*-related sensors were distributed primarily in bilateral (dorso-lateral) frontal sensorimotor, and left parietal-temporo-occipital sensor-space. When the AREG analysis involved both movement *tau* and speed as the independent variables, the *tau*-related sensors (with or without the presence of significant speed effect) were distributed more dorsally; predominantly in the left temporo-parietal, right frontal sensorimotor, right medial parietal, and right temporo-occipital sensor-space. In contrast, with consistently higher mean percentage of speed-related sensors, and a larger overlap of speed-related sensors across subjects, high PSR (50-100%) was manifested over the 248 sensors. Moreover, the speed-related sensors determined from either AREG analyses showed very similar PSR distributions; with high PSR found primarily over the left frontal sensorimotor, left temporo-parietal, bilateral mid-dorsal, and right dorso-lateral frontal sensor-space.

We quantified and compared the PSR between hemispheres, within the anterior-posterior and parietal sensor-space (refer to FIG 6.1), for movement *tau* and speed. TABLE 6.8 shows the mean PSR for the sensors within the hemispheres or regional sensor-space. There were generally higher mean PSRs in the left relative to the right

hemisphere; however this difference was not significant for the anterior sensors for movement *tau* although it reached significance ($p < 0.05$) for speed when the AREG included the parameter as the only independent variable. The difference in mean PSR between hemispheres was significant ($p < 0.001$) in the posterior sensors for movement *tau* but not for speed (for both AREG analyses). When restricting the sensors to the putative parietal sensor-space, mean PSR differences between hemispheres were significant for both movement parameters.

Thus, for both movement *tau* and speed PSR maps, there was the recruitment of clusters of signals tapped by the anterior and posterior sensors. The left posterior process appeared to dominate in the representation of movement *tau* and speed, and in particular, the left parietal processes for movement *tau*.

— Distribution & Clusters of AREG Coefficients for movement tau or speed in sensor-space.

While significance tests of the AREG coefficients indicate that the neural signals tapped by the individual MEG sensors are linearly related to the movement variables of interest, they do not provide a measure of how this relation might be manifested. To appreciate the association between the neural and behavioural variables, the direction and magnitude of the AREG coefficients provide one with an idea of how much of one variable is related to the other in time. That is, in terms of how much of movement *tau* or speed is represented in the recorded neural signals per unit time. Thus, a larger coefficient would suggest a larger processing of movement *tau* or speed by each unit of recorded neural signals in time, and vice versa. The sign of the coefficients, which is related to the dipolar nature of the magnetic field induced by the underlying current sources, shows the direction of the relation; a positive being the same direction of processing change while a negative being an inverse relation.

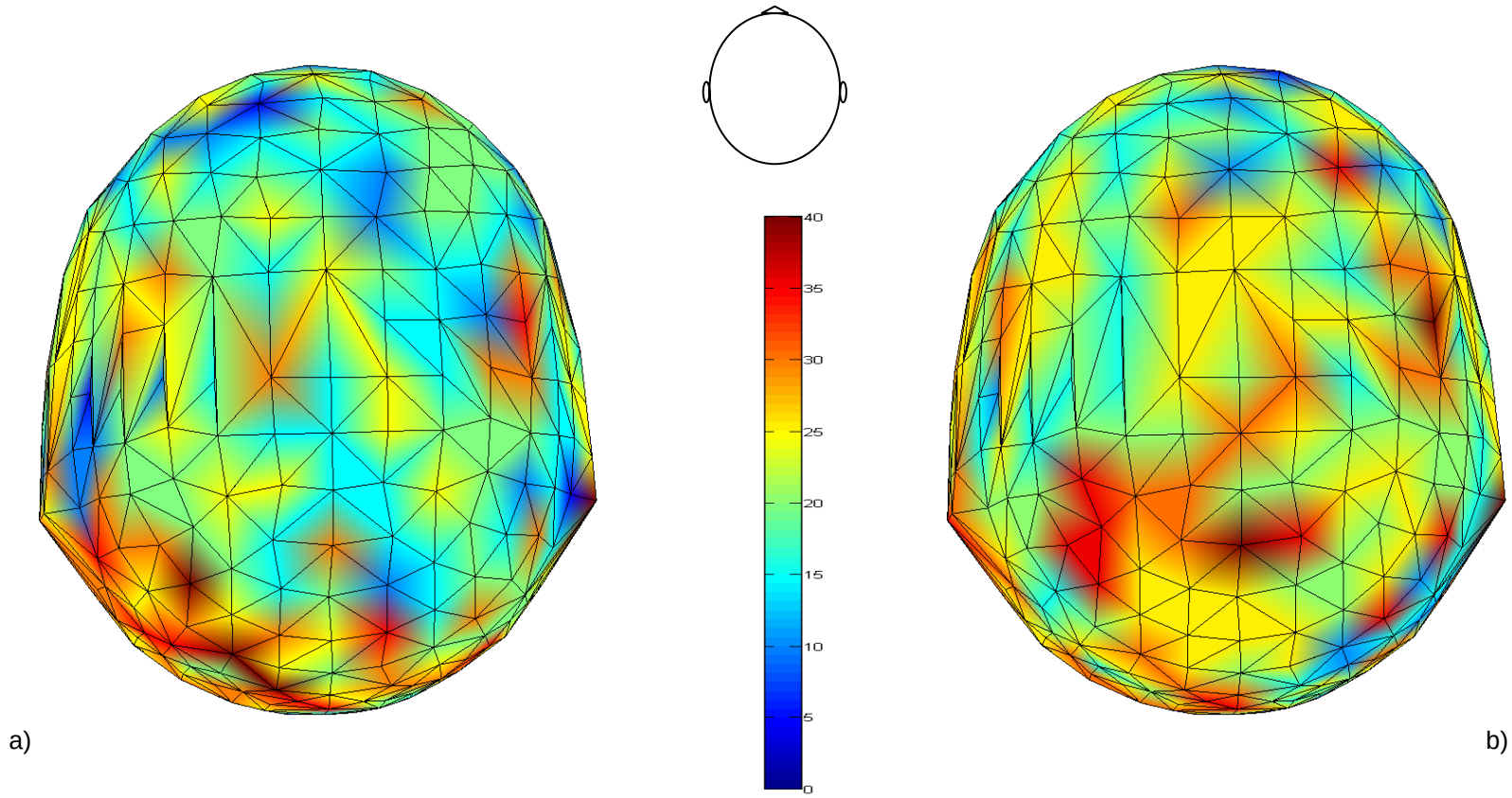

FIG 6.3: '*Percentage of significant relation*' (PSR) for movement *tau*. Three-dimensional array of MEG sensors displaying the PSR for movement *tau* pooled across all subjects (N=20). In (a) the distribution of *tau*-related sensors based on the AREG analysis with movement *tau* as the only independent variable, and in (b) the distribution of *tau*-related sensors based on the AREG analysis with both movement *tau* and speed as the independent variables.

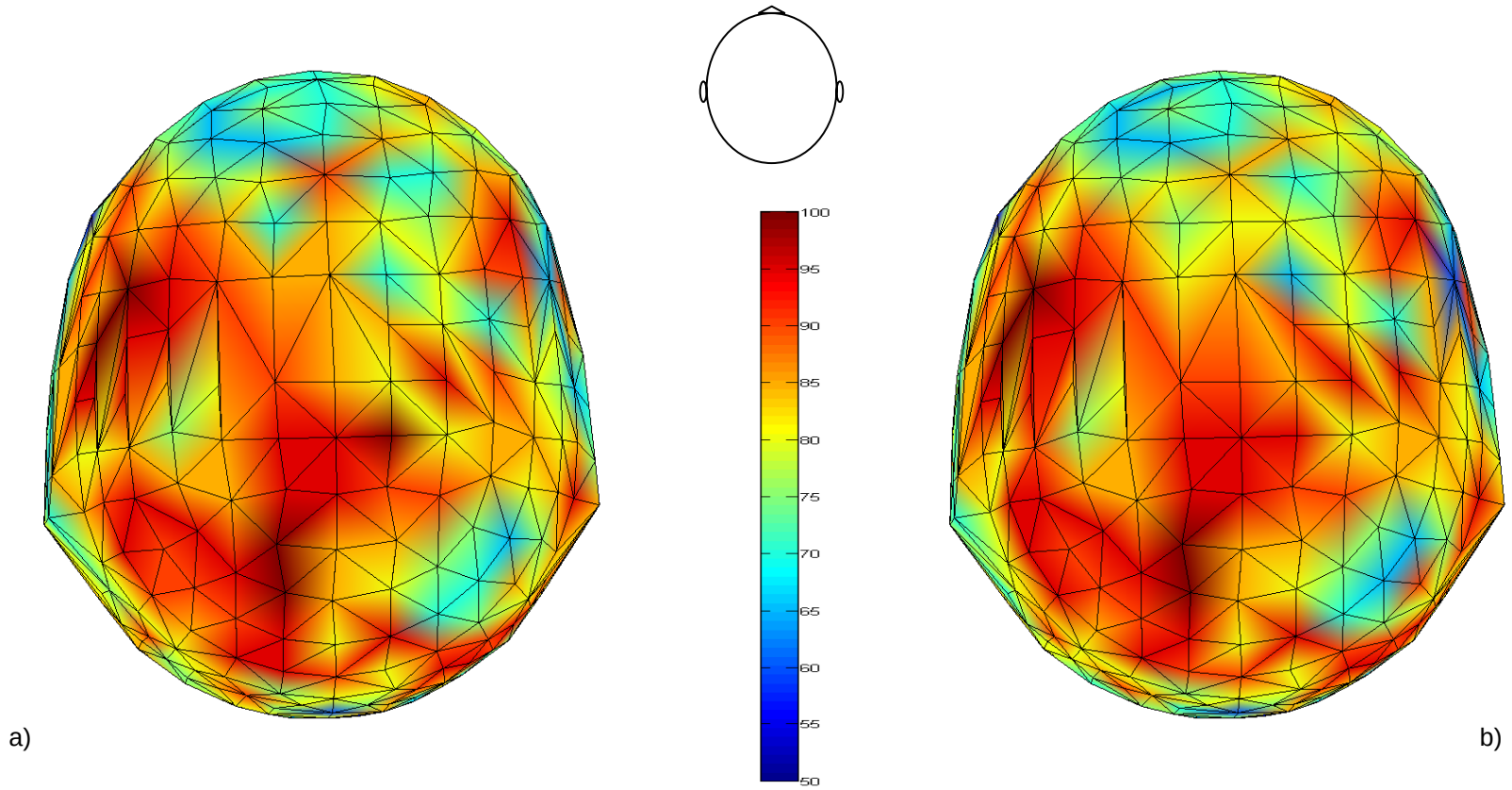

FIG 6.4: '*Percentage of significant relation*' (PSR) for speed. Three-dimensional array of MEG sensors displaying the '*percentage of significant relation*' (PSR) for speed pooled across all subjects (N=20). In (a) the distribution of speed-related sensors based on the AREG analysis with speed as the only independent variable, and in (b) the distribution of speed-related sensors based on the AREG analysis with both movement *tau* and speed as the independent variables.

The mean coefficients of both AREG analyses[i] for which the independent variable of interest was either movement tau or tangential velocity were derived across subjects for each sensor. The mean coefficients were normalized (scaled) relative to the maximum absolute mean value (for each movement variable) and plotted with respect to their signs in FIG 6.5 and FIG 6.6. We observed that the mean coefficients of similar absolute values (magnitude varied positively with colour brightness) and sign (positive: red; negative: blue) tended to be spatially close to each other. With respect to movement *tau*, negative coefficients were mostly distributed in the right hemisphere and left dorso-parietal sensor-space, while positive coefficients were distributed bilaterally in the frontal sensor-space, and left, in the temporo-occipital sensor-space. A different spatial distribution emerged for speed-related sensors; positive coefficients congregated in a diagonal along the right frontal, middle-dorsal, to left parietal-temporo-occipital sensor space, while negative coefficients were distributed in the left frontal and right parietal-temporo-occipital sensor space.

The cluster-analysis of the mean AREG coefficients further revealed subsets of sensors' signals exhibiting similar magnitude. Higher mean coefficient magnitudes were correlated with higher PSR for speed ($r = 0.298$, $p = 0.000$; $r = 0.326$, $p = 0.000$; AREG with one or two independent variables respectively) as well as for movement *tau* ($r = 0.246$, $p = 0.000$; $r = 0.211$, $p = 0.001$). Thus, the sensor distribution of these clusters closely paralleled those of the PSR distributions for movement *tau* and speed (FIG 6.3 and FIG 6.4). An interesting observation was that smaller but more clusters were classified for movement *tau* coefficients derived from the AREG with both movement parameters as independent variables (cf. AREG with movement *tau* as the single independent variable, FIG 6.5). These additional clusters were delineated among the negative AREG coefficients distributed in the right hemisphere (frontal, parieto-temporo-occipital) and encompassing also the left dorso-parietal sensor-space.

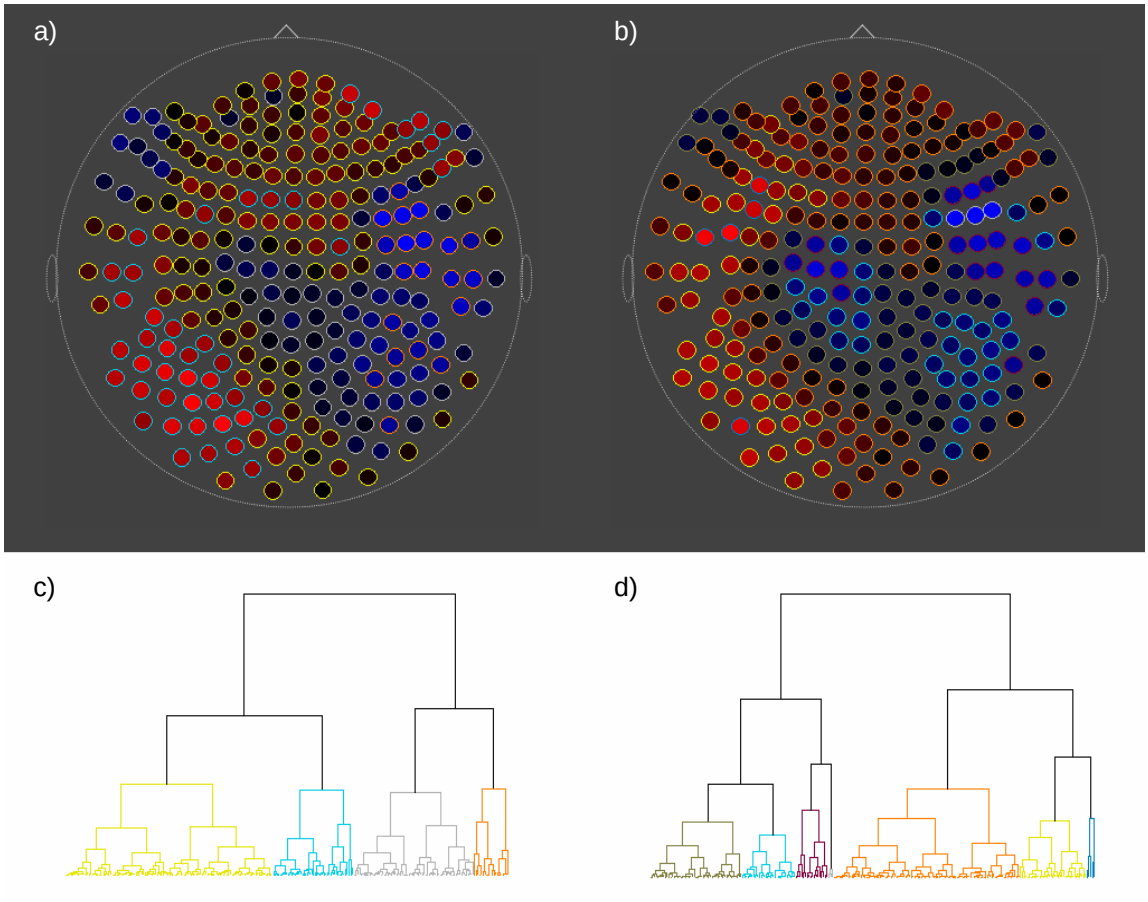

FIG 6.5: Sensor-space distribution and clusters of mean AREG coefficients for movement *tau*. Distribution of sensors (circles) in 2D sensor space depicting mean AREG coefficients for movement *tau* for each sensor across subjects: a) AREG with movement *tau* as the independent variable, and b) AREG with movement *tau* and speed as the independent variables. Filled colour intensity is normalised by the largest mean coefficient value for all sensors considered for the movement variable: the larger the value of the coefficient, the brighter the colour, vice versa. Red indicates positive slopes, blue indicates negative slopes. Tree-diagrams depicting the clusters of sensors with similar magnitude of coefficients are shown in c) and d) below the respective AREG analyses. The same cluster-colours were used in colouring the circumferences of the sensors in a) and b). Subject 12 was removed from this analysis because of faulty sensor 182, N=19.

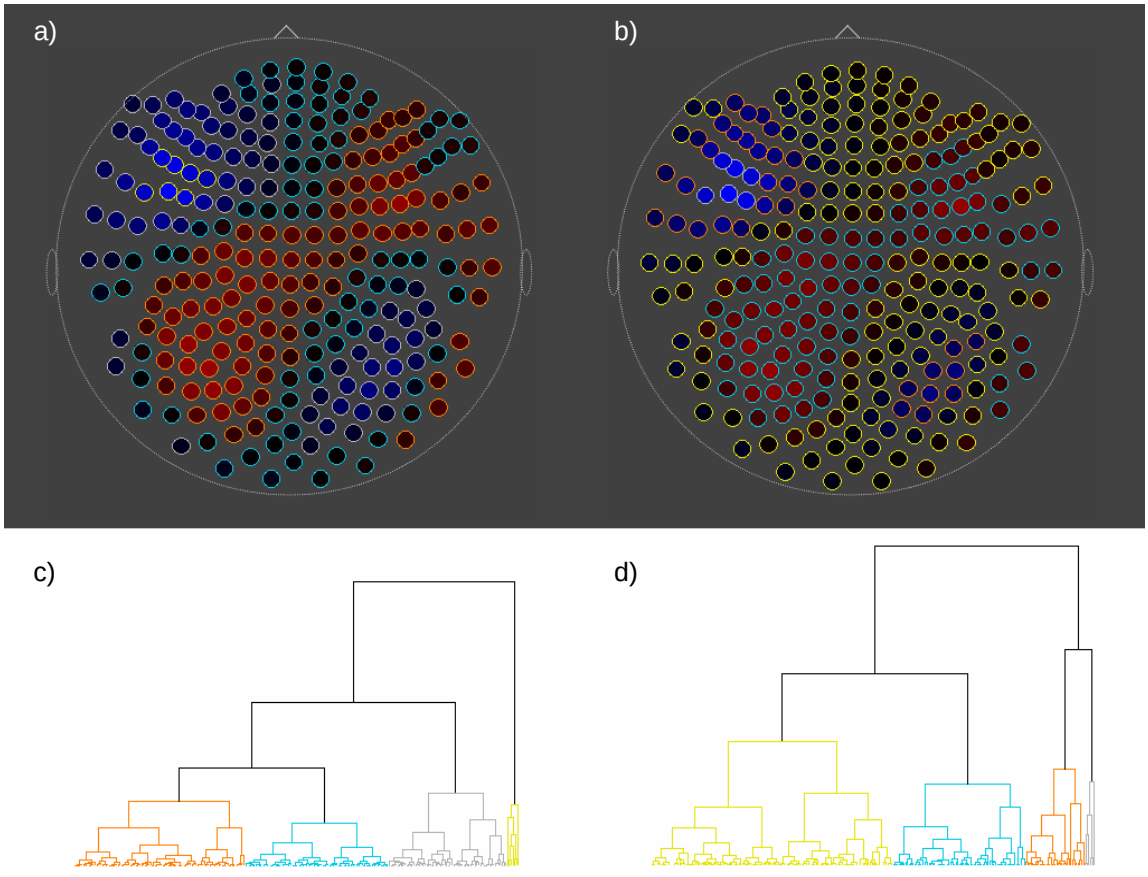

FIG 6.6: Sensor-space distribution and clusters of mean AREG coefficients for speed. Distribution of sensors (circles) in 2D sensor space depicting mean AREG coefficients for movement speed for each sensor across subjects; a) AREG with speed as the independent variable, and b) AREG with movement *tau* and speed as the independent variables. Colour intensity is normalised by the largest mean coefficient value for all sensors considered for the movement variable: the larger the value of the coefficient, the brighter the colour, vice versa. Red indicates positive slopes, blue indicates negative slopes. Tree-diagrams depicting the clusters of sensors with similar magnitude of coefficients are shown in c) and d) below the respective AREG analyses. The same cluster-colours were used in colouring the circumferences of the sensors in a) and b). Subject 12 was removed from this analysis because of faulty sensor 182, N=19.

An additional subset of sensors associated with positive AREG coefficients was clustered in the left frontal sensor-space (FIG 6.5b). An inference from this is that the signals tapped by the subsets of sensors, which are clustered by their similar magnitude of mean AREG coefficients, might be processing the movement parameters in a related manner. From this perspective, sub-networks of frontal and parietal neural activities may be involved in representing movement *tau* and /or speed in analogous ways, giving both continuous perpetual information for action and definition of goal-directed movement.

Discussion

The aim of this MEG imaging study was to investigate the neural representation of movement *tau* and speed in a self-paced movement task in healthy humans. The analyses typically performed in MEG/EEG studies are those of source-localization, which attempt to determine the localization of the brain source(s) generating the event-related neural signals evoked relative to task performance using either equivalent current dipole or minimum-norm spatial-filter (or similar) estimations of current distribution. The analyses carried out in this study were performed on the raw signals relative to sensor-space. This is a different way of exploring what neural signals tapped from any sensor-location might represent in time, at the expense of more precise source localization, such as that offered by fMRI, or source analyses of MEG signals, which are more concerned with locating the neural areas that might be involved in the event-related behaviour. The question asked here concerns the temporal regulation. Specifically, we were interested in whether the neural activities underlying movement performance were in any way related to the time-varying movement *tau* or speed. Using raw neural signals, one can directly investigate the neural correlates of the

movement variables of interest, i.e. movement *tau* and speed, which, like the neural signals, are also rhythmic events in a time-series.

The present AREG analyses indicated that speed was represented by neural signals tapped by all sensors in a consistent manner (as shown by the high PSR) across subjects. The main distribution loci of the speed-related sensors were the bilateral dorso-lateral frontal, dorso-parietal, and the left parieto-temporo-occipital sensor-space. Movement *tau*, on the other hand, was represented by significantly fewer neural signals which were nonetheless distributed predominately in the left parietal-temporo-occipital and bilateral dorso-lateral frontal sensor-space. We also observed that the left parieto-temporo-occipital processes dominated in the representation of movement speed and *tau*.

As it is possible for 1st-order axial gradiometer coils in MEG systems, as used for the research, when placed over a maximum field generated by a surface source to see a much stronger signal than neighbouring sensors, the patterns of significance may be tight, and might even be limited to a single isolated detection coil. Therefore the sparser distribution of movement *tau* was likely to have been from specific surface source(s). Multiple or deeper sources would be likely to spread this pattern, such that a broader clusters of sensors would be involved; this was likely to be the case for signals significantly related to movement speed.

While all movements were highly τ_g-coupled, it was interesting to note that reaction time was inversely related to the percentage of *tau*-related sensors. Subjects who took their time to initiate the target-to-target movements might be more engaged in processing the sensory information for prospective movements prior to moving. In addition, the speed (tangential velocity) profiles of the movements were not symmetrically bell-shaped, which demonstrated that the execution of even simple

movements was not ballistic or merely centrally implemented (Desmurget, Turner et al. 2005).

The apparent dominance of left parieto-temporo-occipital processes is an interesting finding from two perspectives: 1) the left inferior parietal cortex has been implicated in linking perception with the preparation of actions (Rizzolatti, Luppino 2001), and 2) from the point of view of clinical studies of apraxic patients with lesions to their posterior parietal cortex, who manifest impairments in visuomotor coordination, e.g. visually guiding their intended movements. Such coordination is particularly affected when online correction of trajectories to intended goal is involved (Battaglia-Mayer, Caminiti 2002, Grea, Pisella et al. 2002, Grefkes, Ritzl et al. 2004, Pisella, Grea et al. 2000, Rushworth, Taylor 2006). Specifically, unilateral left (c.f. right) lesion of the posterior parietal cortex (PPC; including the intraparietal sulcus) induces a profound effect on the ability of these patients to adjust their hand movements or update their sensorimotor representations in response to a sudden change in target location (Rushworth, Johansen-Berg et al. 2003). In addition, similar disruptive effects have also been observed in either left or right hand movements when transient TMS is applied to the left PPC of healthy subjects (Desmurget, Epstein et al. 1999, Rushworth, Krams et al. 2001). Additionally, the fMRI study by (Assmus, Marshall et al. 2003) also reported the involvement of the left inferior parietal cortex (the supramarginal gyrus) in integrating spatial and temporal information during time-to-collision judgements. Therefore the implication of the PPC (inclusive of its mosaic of sub-areas) in online integration of sensorimotor information for the monitoring and control of movements in extrinsic-space makes it aptly suited in processing a variable like movement *tau*, which affords prospective information in gearing actions in time to a goal.

As highlighted earlier (in Chapter 3), the PPC is not an isolated functional region in the brain. Other neural areas that participate in the gradient of processes forming the

parieto-frontal network are also intricately involved. Recent fMRI study by Wenderoth, Toni et al. (2006) demonstrated that the dorsal pre-central cortex, a part of the parietal-frontal network (Hoshi 2006, Marconi, Genovesio et al. 2001) also contributed to the online guidance processing, and was likely to code spatial information of sensory stimuli relevant for behaviour.

Interestingly, a recent cortical current density EEG study using a visual cue that either signaled specific target or 'go'-signal for non-target movements, investigated the neural areas involved in the visuomotor transformation during precise target-reaching movements, and found co-activation of parietal and frontal (prefrontal and premotor) regions during two critical phases (140 to 260 ms) before movement onset (Naranjo, Brovelli et al. 2007). The authors suggested that these temporal phases might correspond to target selection and movement selection during the visuomotor integration processes. Naranjo et al.'s findings also supported the view of a parallel and dynamic parieto-frontal network processing during visually guided movements (Battaglia-Mayer, Archambault et al. 2006, Battaglia-Mayer, Caminiti et al. 2003), as opposed to the view that parieto-frontal areas are activated sequentially during visuomotor coordination (Buneo, Andersen 2006). Our observation that parieto-frontal sensor-space processes were involved and significantly related to *tau* and /or speed during the actual target-to-target movements may be interpreted as extending Naranjo et al.'s (2007) finding of the involvement of simultaneously active parieto-frontal neural processes prior to movement onset to the evolution and unfolding of the movement itself in the present study.

Although the current AREG analyses did not allow for precise anatomical localization, the signals tapped by the left parieto-temporo-occipital and bilateral frontal sensors were significantly related to both movement *tau* and /or speed. Moreover, the AREG coefficients of similar magnitude tended to cluster together, suggesting similar

processing in sub-networks within the frontal and parietal sensor-space. We speculate that the roughly defined frontal-parietal sensor-space processes related to movement *tau* are likely to reflect 1) similar brain activations involved in the judgement of time-to-contact in humans (Field, Wann 2005), 2) the previously reported associations between neuronal activity and movement *tau* in the PPC (Merchant, Battaglia-Mayer et al. 2004), and 3) the complementary findings from the AREG analyses performed on the prefrontal and parietal cortical neurons detailed earlier, in Chapter 3.

Likewise, our findings of frontal-parietal sensor-space processes related to movement speed may also be interpreted as reflecting similar neural representation of speed in the motor cortex (M1) and area 5 of the PPC (Ashe, Georgopoulos 1994, Averbeck, Chafee et al. 2005, Moran, Schwartz 1999). MEG signals from sensors around the sensorimotor sensor-space have been shown to correlate highly with rhythmic finger movement speed (Kelso, Fuchs et al. 1998). In addition, the recent study by Jerbi, Lachaux et al. (2007) who applied coherence analysis between (unaveraged time-series) MEG source-level current amplitude signals and track-ball motion speed also demonstrated the significant involvement of M1, and (with non-threshold criteria) a network of related areas including the contralateral dorsal premotor, primary somatosensory, inferior and superior parietal, and dorsolateral prefrontal cortical areas. While the authors also reported the involvement of sub-cortical areas (e.g. the thalamus) and ipsilateral anterior cerebellum, it is generally assumed that deeper sources are weakly tapped by MEG sensors (Hillebrand, Barnes 2002), and therefore warrants caution in interpretation. Moreover, the functional significance of oscillatory interactions still awaits clarification. Nonetheless, although the current investigation suffers limited spatial resolution, similar cortical regions are expected to contribute to the processing of movement speed and the manifested PSR.

This study shows, for the first time, a neural correlate of the *tau*-variable in humans performing a simple self-paced target-to-target movement task. Both AREG analyses (in which either or both of the movement parameters, *tau* or speed, were independent variables) have been performed, however, it is expected that multi-parametric processing is likely to occur simultaneously within any one neural region. While, the neural correlate of movement *tau* is not as strongly manifested as movement speed, it is nonetheless apparent over the posterior-temporo-occipital and frontal sensor-space. In general, our observations are in agreement with previous neurophysiological and imaging studies that parieto-frontal processes are dynamically involved in visuomotor performance, and support the idea that the representation of variable *tau* plays an important role in movement guidance.

ASHE, J. and GEORGOPOULOS, A.P., 1994. Movement parameters and neural activity in motor cortex and area 5. *Cerebral Cortex,* **4**(6), pp. 590-600.

ASSMUS, A., MARSHALL, J.C., RITZL, A., NOTH, J., ZILLES, K. and FINK, G.R., 2003. Left inferior parietal cortex integrates time and space during collision judgments. *NeuroImage,* **20 Suppl 1**, pp. S82-8.

AVERBECK, B.B., CHAFEE, M.V., CROWE, D.A. and GEORGOPOULOS, A.P., 2005. Parietal representation of hand velocity in a copy task. *Journal of Neurophysiology,* **93**(1), pp. 508-518.

BATTAGLIA-MAYER, A., ARCHAMBAULT, P.S. and CAMINITI, R., 2006. The cortical network for eye-hand coordination and its relevance to understanding motor disorders of parietal patients. *Neuropsychologia,* **44**(13), pp. 2607-2620.

BATTAGLIA-MAYER, A. and CAMINITI, R., 2002. Optic ataxia as a result of the breakdown of the global tuning fields of parietal neurones. *Brain,* **125**(Pt 2), pp. 225-237.

BATTAGLIA-MAYER, A., CAMINITI, R., LACQUANITI, F. and ZAGO, M., 2003. Multiple Levels of Representation of Reaching in the Parieto-frontal Network. *Cerebral Cortex,* **13**(10), pp. 1009-1022.

BUNEO, C.A. and ANDERSEN, R.A., 2006. The posterior parietal cortex: Sensorimotor interface for the planning and online control of visually guided movements. *Neuropsychologia,* **44**(13), pp. 2594-2606.

CARMENA, J.M., LEBEDEV, M.A., CRIST, R.E., O'DOHERTY, J.E., SANTUCCI, D.M., DIMITROV, D.F., PATIL, P.G., HENRIQUEZ, C.S. and NICOLELIS, M.A., 2003. Learning to control a brain-machine interface for reaching and grasping by primates. *PLoS biology,* **1**(2), pp. E42.

COLTZ, J.D., JOHNSON, M.T. and EBNER, T.J., 1999. Cerebellar Purkinje cell simple spike discharge encodes movement velocity in primates during visuomotor arm tracking. *Journal of Neuroscience,* **19**(5), pp. 1782-1803.

DESMURGET, M., EPSTEIN, C.M., TURNER, R.S., PRABLANC, C., ALEXANDER, G.E. and GRAFTON, S.T., 1999. Role of the posterior parietal cortex in updating reaching movements to a visual target. *Nature Neuroscience,* **2**(6), pp. 563-567.

DESMURGET, M., TURNER, R.S., PRABLANC, C., RUSSO, G.S., ALEXANDER, G.E. and GRAFTON, S.T., 2005. Updating target location at the end of an orienting saccade affects the characteristics of simple point-to-point movements. *Journal of experimental psychology.Human perception and performance,* **31**(6), pp. 1510-1536.

FIELD, D.T. and WANN, J.P., 2005. Perceiving time to collision activates the sensorimotor cortex. *Current Biology,* **15**(5), pp. 453-458.

GEORGOPOULOS, A.P., LANGHEIM, F.J., LEUTHOLD, A.C. and MERKLE, A.N., 2005. Magnetoencephalographic signals predict movement trajectory in space. *Experimental Brain Research,* **167**(1), pp. 132-135.

GREA, H., PISELLA, L., ROSSETTI, Y., DESMURGET, M., TILIKETE, C., GRAFTON, S., PRABLANC, C. and VIGHETTO, A., 2002. A lesion of the posterior parietal cortex disrupts on-line adjustments during aiming movements. *Neuropsychologia,* **40**(13), pp. 2471-2480.

GREFKES, C., RITZL, A., ZILLES, K. and FINK, G.R., 2004. Human medial intraparietal cortex subserves visuomotor coordinate transformation. *NeuroImage,* **23**(4), pp. 1494-1506.

HILLEBRAND, A. and BARNES, G.R., 2002. A quantitative assessment of the sensitivity of whole-head MEG to activity in the adult human cortex. *NeuroImage,* **16**(3 Pt 1), pp. 638-650.

HOSHI, E., 2006. Functional specialization within the dorsolateral prefrontal cortex: A review of anatomical and physiological studies of non-human primates. *Neuroscience Research,* **54**(2), pp. 73-84.

JERBI, K., LACHAUX, J.P., N'DIAYE, K., PANTAZIS, D., LEAHY, R.M., GARNERO, L. and BAILLET, S., 2007. Coherent neural representation of hand speed in humans revealed by MEG imaging. *Proceedings of the National Academy of Sciences of the United States of America,* **104**(18), pp. 7676-7681.

KELSO, J.A., FUCHS, A., LANCASTER, R., HOLROYD, T., CHEYNE, D. and WEINBERG, H., 1998. Dynamic cortical activity in the human brain reveals motor equivalence. *Nature,* **392**(6678), pp. 814-818.

LACHAUX, J.P., RODRIGUEZ, E., MARTINERIE, J. and VARELA, F.J., 1999. Measuring phase synchrony in brain signals. *Human Brain Mapping,* **8**(4), pp. 194-208.

MARCONI, B., GENOVESIO, A., BATTAGLIA-MAYER, A., FERRAINA, S., SQUATRITO, S., MOLINARI, M., LACQUANITI, F. and CAMINITI, R., 2001. Eye-

Hand Coordination during Reaching. I. Anatomical Relationships between Parietal and Frontal Cortex. *Cerebral Cortex,* **11**(6), pp. 513-527.

MERCHANT, H., BATTAGLIA-MAYER, A. and GEORGOPOULOS, A.P., 2004. Neural responses during interception of real and apparent circularly moving stimuli in motor cortex and area 7a. *Cerebral Cortex,* **14**(3), pp. 314-331.

MORAN, D.W. and SCHWARTZ, A.B., 1999. Motor cortical representation of speed and direction during reaching. *Journal of Neurophysiology,* **82**(5), pp. 2676-2692.

NARANJO, J.R., BROVELLI, A., LONGO, R., BUDAI, R., KRISTEVA, R. and BATTAGLINI, P.P., 2007. EEG dynamics of the frontoparietal network during reaching preparation in humans. *NeuroImage,* **34**(4), pp. 1673-1682.

PISELLA, L., GREA, H., TILIKETE, C., VIGHETTO, A., DESMURGET, M., RODE, G., BOISSON, D. and ROSSETTI, Y., 2000. An 'automatic pilot' for the hand in human posterior parietal cortex: toward reinterpreting optic ataxia. *Nature Neuroscience,* **3**(7), pp. 729-736.

POHJA, M., SALENIUS, S. and HARI, R., 2005. Reproducibility of cortex-muscle coherence. *NeuroImage,* **26**(3), pp. 764-770.

RIZZOLATTI, G. and LUPPINO, G., 2001. The cortical motor system. *Neuron,* **31**(6), pp. 889-901.

RUSHWORTH, M.F., JOHANSEN-BERG, H., GOBEL, S.M. and DEVLIN, J.T., 2003. The left parietal and premotor cortices: motor attention and selection. *NeuroImage,* **20 Suppl 1**, pp. S89-100.

RUSHWORTH, M.F., KRAMS, M. and PASSINGHAM, R.E., 2001. The attentional role of the left parietal cortex: the distinct lateralization and localization of motor attention in the human brain. *Journal of Cognitive Neuroscience,* **13**(5), pp. 698-710.

RUSHWORTH, M.F. and TAYLOR, P.C., 2006. TMS in the parietal cortex: updating representations for attention and action. *Neuropsychologia,* **44**(13), pp. 2700-2716.

SALENIUS, S. and HARI, R., 2003. Synchronous cortical oscillatory activity during motor action. *Current Opinion in Neurobiology,* **13**(6), pp. 678-684.

WENDEROTH, N., TONI, I., BEDELEEM, S., DEBAERE, F. and SWINNEN, S.P., 2006. Information processing in human parieto-frontal circuits during goal-directed bimanual movements. *NeuroImage,* **31**(1), pp. 264-278.

WESSBERG, J., STAMBAUGH, C.R., KRALIK, J.D., BECK, P.D., LAUBACH, M., CHAPIN, J.K., KIM, J., BIGGS, S.J., SRINIVASAN, M.A. and NICOLELIS, M.A., 2000. Real-time prediction of hand trajectory by ensembles of cortical neurons in primates. *Nature,* **408**(6810), pp. 361-365.

WOLPAW, J.R., BIRBAUMER, N., MCFARLAND, D.J., PFURTSCHELLER, G. and VAUGHAN, T.M., 2002. Brain-computer interfaces for communication and control. *Clinical Neurophysiology,* **113**(6), pp. 767-791.

WOLPAW, J.R. and MCFARLAND, D.J., 2004. Control of a two-dimensional movement signal by a noninvasive brain-computer interface in humans. *Proceedings of the National Academy of Sciences of the United States of America,* **101**(51), pp. 17849-17854.

Note: _____

[I] NOTE: There is no appropriate equivalent for standardizing coefficients in Auto-Regression (AR), compared to Ordinary Linear Regression. In any case, there is no difference between standardized or unstandardized coefficients (*betas*) in AR. This is because the standard deviations (*sd*) of the dependent (*y*) and independent (*x*) variables from the AR analysis are supposed to be equal:

$$sd_x = sd_y \tag{6.i}$$

And therefore, from the formula for deriving betas:

$$\beta = b_x(\frac{sd_x}{sd_y}) = b_x \tag{6.ii}$$

(Bingham 2007; Prof. Christopher Bingham at the Statistics Department of The University of Minnesota, *personal communication*)

CHAPTER 7:

A MEG Study of Movement Performance: Synchronous Neural Interactions during Movement & Rest

Introduction

The very essence of brain function is characterized by the flexible, dynamic integration of the myriad of sensorimotor information, and the processing of such signals in the relevant neural substrates in the service of multiple purposeful actions. Understanding the mechanisms of how the brain performs this seemingly effortless '*binding*' of information that leads to the evolved behaviour is non-trivial as such integrative processes are also under the influences of contextual and attentional expectancies that extend beyond the lived present (Engel, Fries et al. 2001, Fries, Reynolds et al. 2001, Uhlhaas, Singer 2006). A plausible mechanism for coherence in experience, put forward by Singer (1999), proposes that widely distributed neural ensembles are dynamically integrated into functionally meaningful networks that are representative of the cognitive processes and /or neural engrams of behavioural intention by brief synchronization of neural activity. This view was initially substantiated by neurophysiological studies in perceptual feature binding by means of synchrony within

the visual system (Engel, Kreiter et al. 1991, Gray, Singer 1989), across hemispheres (Engel, Konig et al. 1991), and between different sensorimotor cortical areas (Bressler, Coppola et al. 1993, Roelfsema, Engel et al. 1997), as well as by studies showing attention- and task-dependent modulation of neural synchrony (Bressler, Coppola et al. 1993, Fries, Reynolds et al. 2001, Roelfsema, Engel et al. 1997). Subsequent non-invasive studies in humans exploring cortico-cortical and cortico-muscular synchronies (Gross, Kujala et al. 2001, Gross, Timmermann et al. 2002, Pollok, Gross et al. 2006, Schnitzler, Gross 2005), synchronies in visual perception (Rodriguez, George et al. 1999, Womelsdorf, Fries et al. 2006), and in verbal-visual working memory tasks (Sarnthein, Petsche et al. 1998) further highlighted the function of synchronized neural activity distributed across widely spaced brain regions.

It should be emphasised that well-coordinated synaptic events – the primary source of measured signals – are required for signal detection by any of the recording methods used, including local field potentials recorded by microelectrodes, and brain activity detected by EEG/MEG techniques. Activity that is haphazardly coordinated would unwittingly lead to the cancellation of incoherent synaptic events (Mitzdorf, Singer 1979). Although recorded synchronous activities span a wide range of rhythmic frequencies (e.g. Bressler, Coppola et al. 1993), in most aforementioned studies, oscillations in *beta* (15 - 30 Hz) and *gamma* (30 - 80 Hz) ranges have been consistently associated with the observed neural synchrony. There is a reported general trend between frequency of oscillation and the distance between which synchronous neural activity is observed; long-range synchrony tends to engage lower frequency ranges, e.g. *beta*, 8 – 12 Hz *alpha*, or 4 - 8 Hz *theta*, while short-range synchrony is commonly associated with oscillations at higher frequency e.g. *gamma* (Schnitzler, Gross 2005, von Stein, Sarnthein 2000). Cortico-cortical connections are likely to be involved in *beta* and *gamma* activity as evidenced from the effects of sectioning of the corpus callosum (Engel, Konig et al. 1991), while the maintenance of a delicate balance of fast and slow

synchronizations in various states of vigilance and active behaviour have implicated the role of subcortico-cortical associations (Llinas, Steriade 2006).

Analyses employed in studying the putative significance of neuronal synchrony have typically measured correlations between signals at selected frequencies. In coherence analysis, the linear covariance of the amplitude of oscillations at a particular frequency is assessed. While it is true that the amplitude of recorded signals is to some extent related to the measured coherence, the role of amplitude and phase covariance in the derived coherence is not well-understood (Lachaux, Rodriguez et al. 1999). It should also be noted that the calculation of coherence (i.e. the squared modulus of cross-spectra at specified frequency, normalized by the respective auto-spectra of the signals) can only be applied to stationary processes (Lachaux, Rodriguez et al. 1999); in other words, time-series with zero mean and variances, normally attained by 'pre-whitening' the time-series to remove possible trends, seasonal changes, and /or oscillatory behaviour that would otherwise lead to the likelihood of spurious correlations. This is problematic if one considers that the required input spectrum variable in the coherence measure is commonly derived from the recorded signals by first subdividing the whole data set into segments, either by a sliding window through time, or by taking trials as segments, then computing estimated segment spectra, and finally averaging across all segments.

The quality of the estimated coherence for a particular frequency is not only dependent on the size and quantity of each segment, it also requires that every segment constitutes the same process and spectral features. Unfortunately, this theoretical requirement of 'stationarity' is rarely satisfied or accounted for in practice. Moreover, the comparison of each pair of neural signals to independent white noise (H_0, which is unlike neural signals) in the coherence statistics test (Carter 1987) may lead to inappropriate rejection of the null-hypothesis, leading to spurious estimations of significance. To circumvent

the requirements of stationarity, others (Lachaux, Rodriguez et al. 1999, Tass, Fieseler et al. 2003) have developed methods to assess synchrony independently of amplitude, by comparing the phase relations between signals recorded by sensors from different locations. However, such phase-synchrony assessment is limited to working with narrow frequency bands, and requires evoked responses. The inconsistent inter-trial phase-difference in self-induced temporal integration of neural responses, which seems typical of natural perceptual construction (Rodriguez, George et al. 1999, Tallon-Baudry, Bertrand 1999), would not be detected by standard forms of phase-synchrony / time-frequency analysis (Lachaux, Rodriguez et al. 1999).

Available findings on neural synchronization that manifests in various frequency bands concurrently with different cognitive tasks provide correlations between oscillations of electrical activity in the brain and tentative conclusions about their functional roles in integrating sensory information during while such tasks as perceptual discrimination or working memory are being performed (Fries, Reynolds et al. 2001, von Stein, Sarnthein 2000). To date, the only direct experimental tests of the functional relevance of neural synchronization comes from the study by Stopfer, Bhagavan et al. (1997) who demonstrated that discrimination of molecularly similar odorants (e.g. 1-hexanol vs. 1-octanol) but not dissimilar odours was significantly impaired in honey bees when the oscillatory synchronization of projection neuron assemblies in the olfactory system was abolished by picrotoxin (an antagonist of the *Gamma*-aminobutyric acid, $GABA_A$, receptor). The study indicates that temporal encoding through such synchronous neural activity can afford an extra precision with which overlapping features (e.g. molecular carbon chain length of alcohol groups, or spatial features, or sensorimotor signals etc.) in one dimension may be effectively discriminated.

While the normal functional role and sources of such oscillatory synchronizations are still to be explored, an increasing body of work has demonstrated abnormal neural

synchronization in pathological patient groups compared to healthy subjects (see review by Uhlhaas, Singer 2006). For example, the Alzheimer brain manifests simultaneous increased *theta* with decreased *beta* and *alpha* activities, and the severity of the disease and cognitive impairments appear to correlate with the reduction of *alpha* synchrony (Jeong 2004). Schizophrenic patients have been documented to manifest reduced *beta* and *gamma* activities particularly in long-range synchronies (Uhlhaas, Singer 2006), which may explain their cognitive dysfunctions. Similar observations on reduced *gamma* activity have also been reported in studies of Autism (Wilson, Rojas et al. 2007).

On the other hand, the increased *beta* activity documented in Parkinson's disease (PD) within the basal ganglia and multiple cortical regions (Boroud, Brown et al. 2006, Schnitzler, Gross 2005) has been associated with PD akinesia. This conclusion is based on the observed *beta* synchrony prior to movement and during visuomotor tasks (Murthy, Fetz 1996, Roelfsema, Engel et al. 1997), an effect that is suppressed with burst of *gamma* activity in the sub-thalamic nuclei during movement initiation in healthy controls (Boroud, Brown et al. 2006); shorter duration of *beta* suppression being correlated with faster movement initiation. In epilepsy, increased synchronization in *gamma* and *beta* activities, as well as decreased *beta* synchrony prior to seizures have been reported (Le Van Quyen, Navarro et al. 2003, Rampp, Stefan 2006). Depending on the nature and focus of epilepsy, memory and speech disruptions are among the behavioural phenomenon commonly associated with seizures (Motamedi, Meador 2003). As distributed neural ensembles can be coupled by synchronization (Bruno, Sakmann 2006, Fries 2005), low synchrony could potentially lead to functional isolation of important ensembles, which may develop over-excited states locally that spread to other areas, thereby leading to epileptic seizures (Uhlhaas, Singer 2006).

The delicate relation between altered neural synchrony in these patient groups and their documented cognitive and behavioural dysfunctions implies a subtle interplay of neural excitation and synchronization for the normal functioning of the brain and active conscious being. These studies also point to the potential of using such changes in neural synchrony as a means of early clinical diagnosis, particularly in diseases like Alzheimer's for which diagnosis is often achieved too late after onset for potentially effective intervention, and confirmed through post-mortem histological evidence of what are called 'tau neurofibrillary tangles' and 'senile plaques'. A recent study which addressed the diagnostic issue of discriminating between patient groups, employed a different analysis of synchronization from studies mentioned above and yielded promising classifications (Georgopoulos, Karageorgiou et al. 2007). The method employed single-trial partial cross-correlation analysis of pre-whitened (quasi-stationary) signals recorded by 248 sensors in a whole-head MEG system during a simple fixation task. The normalized sensor-pair partial correlation coefficients, which provide estimates of the strength and covariation direction of synchronous coupling at every millisecond, were used as variables in a cross-validated discriminant analysis to reliably classify subjects from six patient groups, including Alzheimer's disease, multiple sclerosis, schizophrenia, as well as healthy controls.

The success of this classification was based on a previous study by Langheim, Leuthold et al. (2006) using partial cross-correlations analysis on the same eyes-open fixation task in healthy subjects. Their finding of a consistent pattern of synchronous neural interactions between sensor signals documented across subjects suggested a putative stability in the brain's resting synchronous activity. Given that altered neural synchronization has been consistently reported in patient groups during rest as well as when they engage in cognitive processing, it is plausible that the consistent neural synchronization observed during rest might also be manifested in some distinctive pattern when healthy controls are performing a task such as the shape copying or

target-to-target movement task we asked our subjects to perform. Therefore, we extended this method of analysis to study the synchronous interactions between neural ensembles both during rest periods and while our subjects were responding to the visuomotor conditions of the target-to-target movement task.

Results

— General

Cross-correlations can be viewed as snap-shots of interaction between two time-series. In the current analysis, we employed cross-correlation to describe the relation between the pre-whitened signals measured by pairs of MEG sensors. Partial cross-correlation (PCC_{ij}^{0}) assesses the relation between signals from any sensor-pair, taking into consideration the interactions of these sensors with all other possible sensors in the network. The resultant cross-correlations are unlikely to be conflated with collinearities (i.e. multiple correlations between one sensor's signals with all other signals such that the correlation between any sensor pair is confounded). If the neural ensembles sampled by each of the 248 sensors could be envisioned as nodes in a densely interconnected neural network, the PCC_{ij}^{0} between a pair of sensors is thus a measure of synchronous association between the activities of neural ensembles underlying the signals measured at the two sensors. The absolute value and sign of PCC_{ij}^{0} indicate the strength and direction of the association. We note here too, that the sign of cross-correlation relates to the covariation (relative to the mean) of the two time-series, and does not give information on the underlying excitatory or inhibitory synaptic activities.

A positive correlation merely reflects a covariation in the same direction (increase-increase; decrease-decrease) while a negative correlation describes a covariation in opposite directions (increase-decrease; decrease-increase).

A total of ([248! /2!246!]) 30,628 PCC_{ij}^{0} per subject and a total combination of (30,628 * 19 subjects) 581932 PCC_{ij}^{0} were derived from 248 MEG sensors. Of these partial correlations, 39% were statistically significant ($p < 0.05$) for the rest condition, while 65% were significant for the movement condition. Among those significant correlations in the rest condition, 42% were negative while 58% were positive. In the movement condition, 46% of the significant correlations were negative while 54% were positive. The increase in significant correlations from rest to movement condition was characterized by a slightly larger increase in negative correlations (16% to 30%; +14% of the total 581932 PCC_{ij}^{0}) compared to the increase in positive correlations (23% to 35%; +12%).

We further assessed the characteristics of those significant partial correlations in both conditions. Within the rest condition, the mean (± SEM) positive $+z_{ij\,rest}^{0}$ was 0.026 ± 0.000052 (maximum $+z_{ij\,rest}^{0}$ = 0.684; $+PCC_{ij\,rest}^{0}$ = 0.594), while the mean negative $-z_{ij\,rest}^{0}$ was 0.019 ± 0.000027 (minimum $-z_{ij\,rest}^{0}$ = -0.172; $-PCC_{ij\,rest}^{0}$ = -0.170). The absolute values of these mean correlations differed significantly ($t_{(18)}$ = 22.000, $p < 1.85\text{x}10^{-14}$), with the average $\left|+z_{ij\,rest}^{0}\right|$ being 28.74% higher than the average $\left|-z_{ij\,rest}^{0}\right|$. In the movement condition, the mean (± SEM) positive $+z_{ij\,mv}^{0}$ was 0.017 ± 0.000033 (maximum $+z_{ij\,mv}^{0}$ = 0.405; $+PCC_{ij\,mv}^{0}$ = 0.385), while the mean negative $-z_{ij\,mv}^{0}$ was -0.0011 ± 0.000018 (minimum $-z_{ij\,mv}^{0}$ = -0.175; $-PCC_{ij\,mv}^{0}$ = -0.174). The absolute values of these mean correlations also differed significantly ($t_{(18)}$ = 35.86, $p < 3.39\text{x}10^{-18}$) and the average $\left|+z_{ij\,mv}^{0}\right|$

was 34.09% higher than the average $\left|-z^0_{ij\,mv}\right|$. Between conditions, both the average $\left|+z^0_{ij\,mv}\right|$ and $\left|-z^0_{ij\,mv}\right|$ were significantly lower than the average $\left|+z^0_{ij\,rest}\right|$ and $\left|-z^0_{ij\,rest}\right|$; $t_{(18)} = -23.54$, $p < 5.69\text{x}10^{-15}$, and $t_{(18)} = -24.518$, $p < 2.79\text{x}10^{-15}$, respectively. FIG 7.1 and FIG 7.2 show the plots of inter-sensor $PCC^0_{ij\,rest}$ and $PCC^0_{ij\,mv}$ for 2 different subjects (3 and 11), with green inter-sensor lines denoting positive and red inter-sensor lines denoting negative associations. Qualitatively very similar interconnected networks were observed across all subjects; the increase in significant partial cross-correlations was apparent in the additional inter-sensor lines in the movement condition.

— Partial cross-correlation coefficients $PCC^0_{ij}(z^0_{ij})$ across subjects

To assess and quantify the overall similarity of the derived z^0_{ij} (between sensors *i* and *j*) across all subjects, the Pearson correlation was performed across all z^0_{ij} for all subject-pairs. For both rest and movement conditions the correlation coefficients were very high and significant. The coefficients for the rest condition ranged from 0.593 to 0.822, with a median of 0.729 ($p < 10^{-20}$). Likewise, the median of the coefficients for the movement condition was 0.803, and the coefficients ranged from 0.694 to 0.878 ($p < 10^{-20}$). These findings suggested a high consistency across subjects in the associations between signals tapped by the 248 MEG sensors.

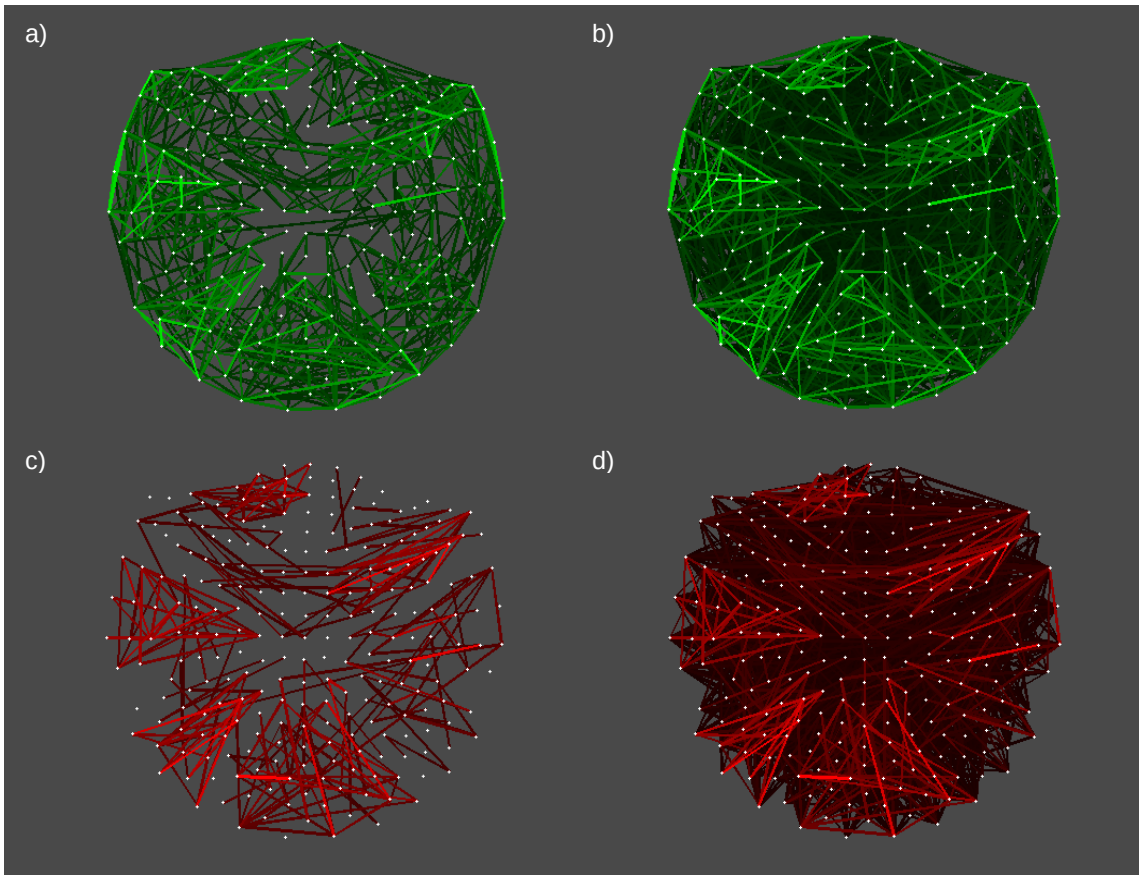

FIG 7.1: Synchronous sensor-signals during rest and movement task performance: inter-sensor PCC_{ij}^{0} for subject #3. Green inter-sensor lines denote positive PCC_{ij}^{0} for a) rest and b) movement conditions, while red inter-sensor lines denote negative PCC_{ij}^{0} for c) rest and d) movement conditions. The plotted lines fulfilled the Bonferroni inequality which accounted for multiple comparisons, such that the significance threshold was actually $p < 0.0001/30{,}628$ (i.e. $p < 0.000000003$).

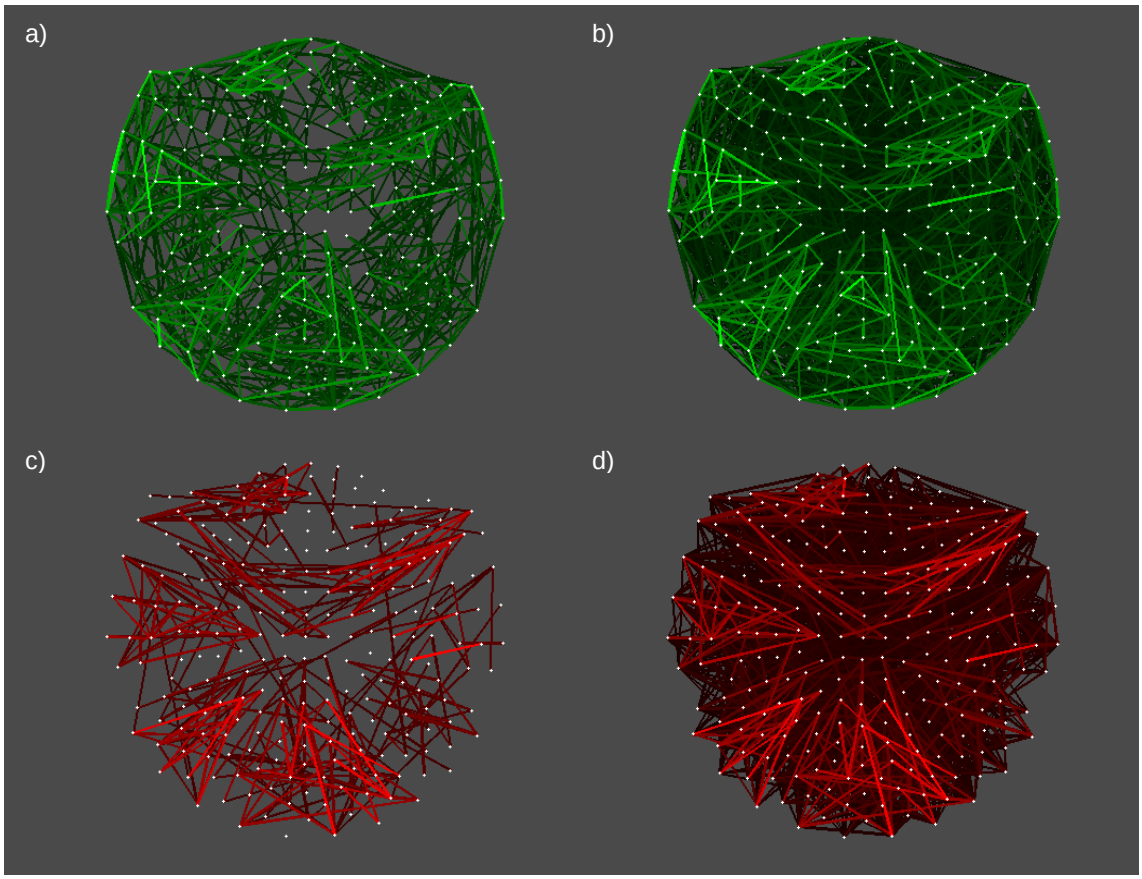

FIG 7.2: Synchronous sensor-signals during rest and movement task performance: inter-sensor PCC_{ij}^{0} for subject #11. Green inter-sensor lines denote positive PCC_{ij}^{0} for a) rest and b) movement conditions, while red inter-sensor lines denote negative PCC_{ij}^{0} for c) rest and d) movement conditions. The plotted lines fulfilled the Bonferroni inequality which accounted for multiple comparisons, such that the significance threshold was actually $p < 0.0001/30{,}628$ (i.e. $p < 0.000000003$).

— *Relation between* PCC_{ij}^{0} *and inter-sensor distance.*

Given the regularity of the sensor-pair z_{ij}^{0} across subjects, we took the mean z_{ij}^{0} of each sensor-pair across subjects ($\overline{z_{ij}^{0}}$) and assessed if there was any relation between sensor-pair $\overline{z_{ij}^{0}}$ and the Euclidean distance between each corresponding pair (*i* and *j*) of the 248 MEG sensors (d_{ij}). For both rest and movement conditions, sensor-pair $\overline{z_{ij}^{0}}$ tended to be positive when they were closer in distance, while it was more likely to be negative when the distance between pairs of sensors was larger. The mean inter-sensor distance (d_{ij}) for $-\overline{z_{ij\ rest}^{0}}$ was 22.46% longer than that for $+\overline{z_{ij\ rest}^{0}}$; average $d_{ij}(-\overline{z_{ij\ rest}^{0}})$ = 204.50 ± 73.46 mm, while average $d_{ij}(+\overline{z_{ij\ rest}^{0}})$ = 158.56 ± 89.30 mm. Similarly, the mean d_{ij} for $-\overline{z_{ij\ mv}^{0}}$ was 25.04% longer than that for $+\overline{z_{ij\ mv}^{0}}$; average $d_{ij}(-\overline{z_{ij\ mv}^{0}})$ = 206.73 ± 72.39 mm, and average $d_{ij}(+\overline{z_{ij\ mv}^{0}})$ = 154.96 ± 88.98 mm. In addition, significant negative association between the signed $\overline{z_{ij}^{0}}$ and the log-transformed d_{ij}, $\ln(d_{ij})$, was observed for both rest and movement conditions; r = -0.473, r = -0.466, respectively ($p < 10^{-20}$). Taken together, the findings indicated that the strength of the synchronous association between sensor-pairs decreased with inter-sensor distance.

— *Clusters of* PCC_{ij}^{0}

Using the signed $\overline{z_{ij}^{0}}$, we computed the dissimilarity (D_{ij}^{0}) between sensor-pairs and performed a hierarchical clustering analysis using these 'distances' to assess the underlying subgroups of sensor networks in both conditions. The tree-diagrams in FIG 7.3a and 7.3b depict the clusters of sensors which were classified in the rest and movement conditions respectively. In the rest condition, 20 clusters were determined,

while 19 clusters of sensors were categorized in the movement condition. Twelve of these clusters of sensors remained the same, in terms of members of sensors and spatial distribution, in both conditions. These are depicted as the unlabelled clusters in FIG 7.4a and 7.4b with similar colours for rest and movement conditions respectively. For 8 of the clusters in the rest condition (labelled 1 to 8 in FIG7.4a) the sensor members and spatial distribution were altered in the movement condition, and the 'reconfiguration' resulted in the 7 clusters being classified. Most notably, clusters 6, 7, and 8 in the rest condition resulted in the new configuration as clusters 6 and 7 in the movement condition. Clusters 2 and 5 were enlarged by an additional sensor membership, while clusters 3 and 4 lost 4 sensors, and cluster 1 lost 1 sensor from rest to movement conditions. Most of the 'reconfiguration' occurred in the left hemisphere; in the frontal and parieto-temporo-occipital sensor-space. In addition, sensor members for other clusters remained unchanged although their associations within the tree structure showed differences between the conditions (FIG 7.3).

— *Associations between* PCC_{ij}^{0} *clusters*

We also computed the mean partial correlation between each cluster ($\overline{\overline{z_{ij}^{0}}}$), which was the mean of the partial cross-correlations ($\overline{z_{ij}^{0}}$) between those pairs of sensors that make up the different clusters. In addition, we also derived the mean sensor-space location of each cluster, the *centroids*, and plotted the interactions between the cluster $\overline{\overline{z_{ij}^{0}}}$s with green or red lines linking the centroids, denoting positive or negative associations, respectively. This is illustrated in FIG 7.5a and 7.5b for rest and movement conditions. There were 47% (89/190) positive and 53% (101/190) negative cluster associations in the rest condition, while 44% (76/171) of the cluster associations were positive and 56% (95/171) were negative in the movement condition.

The centroids of those clusters of sensors, which underwent reconfiguration from rest (clusters 1 to 8) to movement (clusters 1 to 7) conditions, also showed differences in their spatial locations between the two conditions. Similar to the relation between PCC_{ij}^{0} and inter-sensor distance, cluster-pairs $\overline{\overline{z_{ij}^{0}}}$ tended to be positive when they were closer in distance, while they were more likely to be negative when the distance between clusters was larger. The mean inter-centroid distance (dc_{ij}) for $-\overline{\overline{z_{ij}^{0}}}_{rest}$ was 41.30% longer than that for $+\overline{\overline{z_{ij}^{0}}}_{rest}$; average dc_{ij} ($-\overline{\overline{z_{ij}^{0}}}_{rest}$) = 215.87 ± 58.87 mm, while average dc_{ij} ($+\overline{\overline{z_{ij}^{0}}}_{rest}$) = 126.71 ± 59.33 mm. Similarly, the mean dc_{ij} for $-\overline{\overline{z_{ij}^{0}}}_{mv}$ was 39.82% longer than that for $+\overline{\overline{z_{ij}^{0}}}_{mv}$; average dc_{ij} ($-\overline{\overline{z_{ij}^{0}}}_{mv}$) = 213.05 ± 63.67 mm, and average dc_{ij} ($+\overline{\overline{z_{ij}^{0}}}_{mv}$) = 128.22 ± 64.69 mm. In addition, significant negative association between the signed $\overline{\overline{z_{ij}^{0}}}$ and the log-transformed dc_{ij}, $\ln(dc_{ij})$, was observed for both rest and movement conditions; r = -0.406, r = -0.277, respectively ($p < 10^{-9}$ and $p < 10^{-4}$). Therefore, the strength of the synchronous association between clusters also decreased with inter-centroid distance.

a)

b)

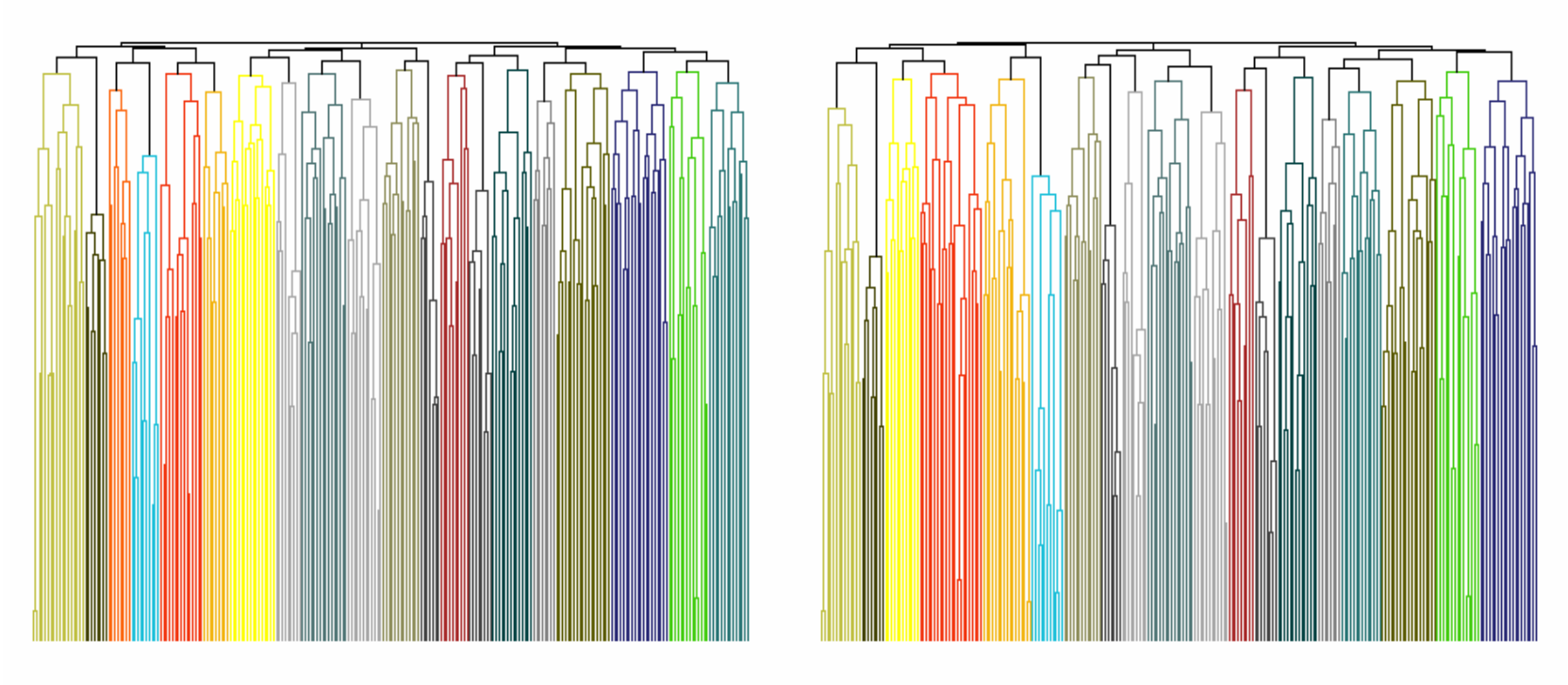

FIG 7.3: Clusters of synchronous sensor signals. Tree diagrams of the results from the hierarchical cluster analyses based on the dissimilarity of mean partial cross-correlations of MEG sensor-signals (N=30628) during a) rest and b) movement sections of the target-to-target movement task across all 19 subjects.

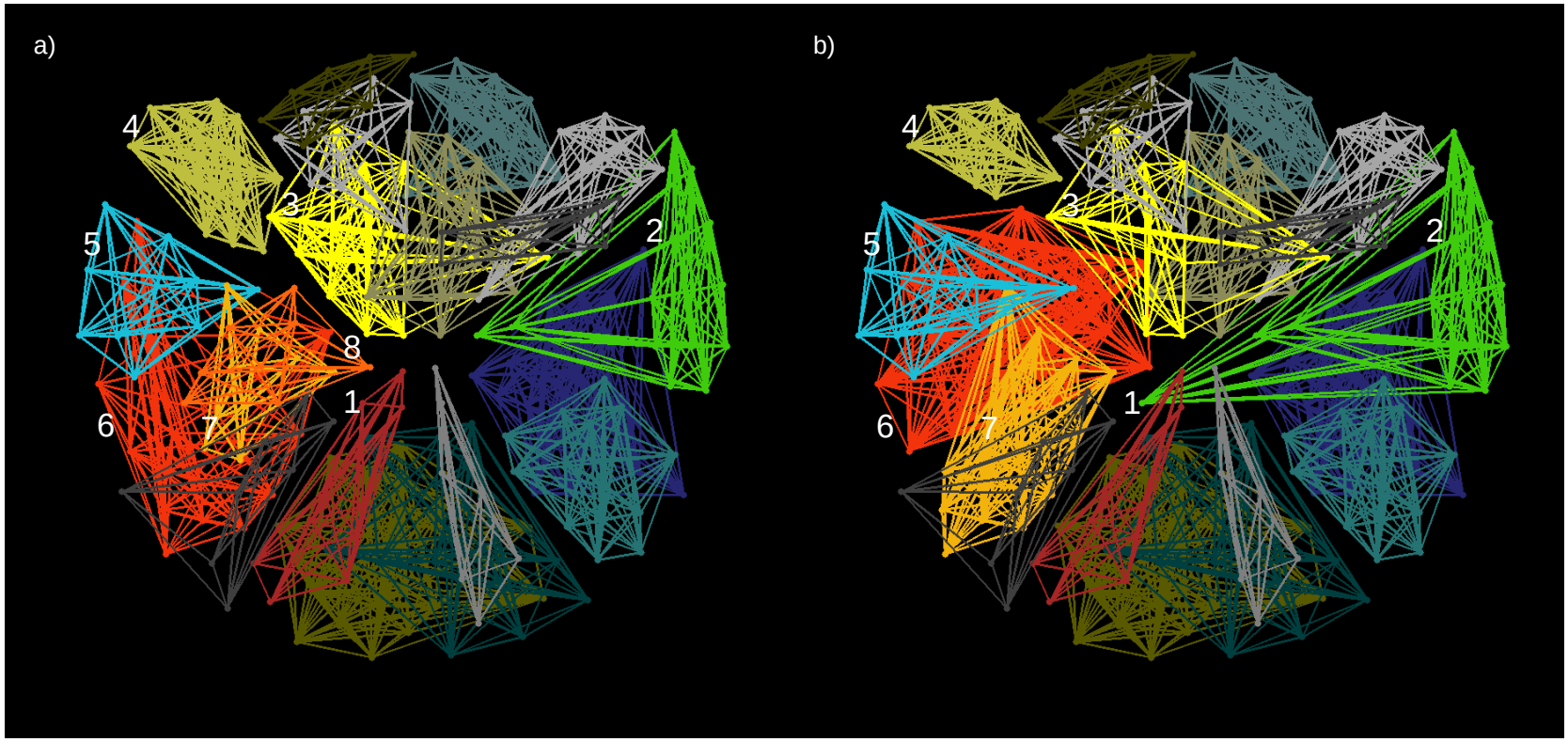

FIG 7.4: Clusters of synchronous sensor signals in sensor-space. Plot of clusters of synchronous sensor signals in sensor-space during a) rest and b) movement sections of the target-to-target movement task. Numerically labelled clusters showed differences in number and location of included sensors across the 2 conditions, while unlabelled clusters remained the same with respect to the sensors (and their respective locations) included within them in both conditions.

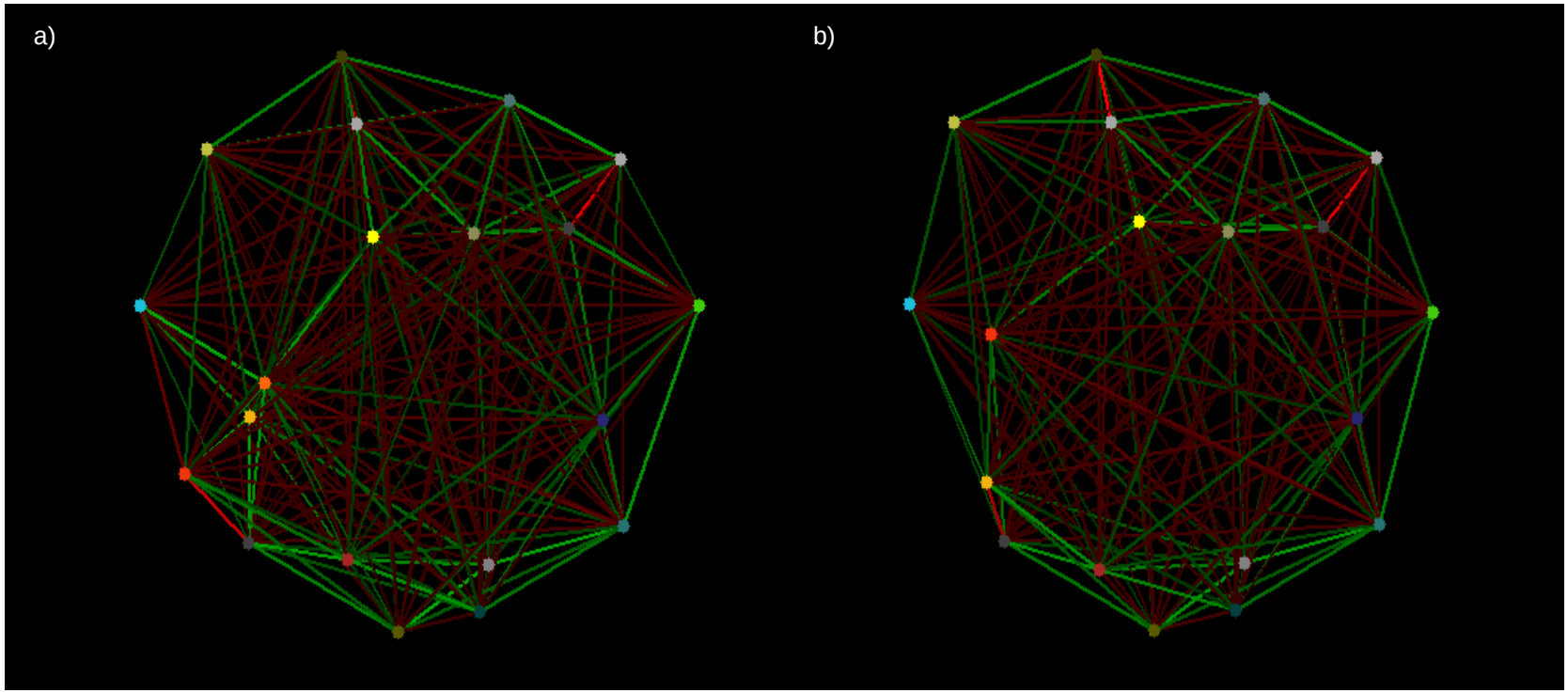

FIG 7.5: Cross-correlations between synchronous clusters of sensor signals. Plots of mean cross-correlations between clusters ($\overline{\overline{z_{ij}^0}}$) for a) rest and b) movement sections of the task. Green lines denote positive $\overline{\overline{z_{ij}^0}}$ and red lines denote negative $\overline{\overline{z_{ij}^0}}$ between the cluster-centroids. The brightness of connecting lines was scaled to the maximum of the overall $\overline{\overline{z_{ij}^0}}$ for all cluster-centroids; brighter lines indicated higher mean $\overline{\overline{z_{ij}^0}}$ between cluster-centroids. The colours of the mean cluster-nodes followed the same coding as the clusters in FIG 7.4.

Discussion

The network of sensor-pair partial cross-correlations made evident by our analysis was consistent across all 19 subjects for both rest and movement-task conditions. There were more significant correlations during the movement-task compared to rest, but the absolute magnitude of the correlation was higher during rest. The ratio of percentage of negative to positive coefficients between sensor-pairs was higher during movement-task performance (46% : 54%; ~0.85) compared to rest (42% : 58%; ~0.71). Furthermore, proximally located sensor-pairs were more likely to be positively and more strongly correlated. The stability of these observations across subjects parallel those reported by Langheim, Leuthold et al. (2006). A similar pattern of negative to positive relations was also observed between the clusters of sensor-pairs, from which population-averaged z-transformed coefficients were hierarchically classified: the higher ratio of percentage of negative to positive coefficients during movement-task performance (rest: 53% / 47% = 1.12; movement: 56% / 44% = 1.27) and the mean cluster-pair distances to coefficient relations (sign and strength) were also maintained. The spatial topography of the clusters at rest was also very similar to that obtained in previous work by Merkle, Leuthold et al. (2006).

Within their respective cluster membership, the spatial overlap in interactions between signals tapped by sensors suggests that multiple functionally related sources are linked in their synchronous activities. In addition, the observed stronger correlations between neighbouring locations are similar to the effects demonstrated by Roelfsema, Engel et al. (1997) who found that functionally related cortical areas in cats, which were also located in closer proximity (e.g. association and visual areas of the parietal cortex; parietal and motor areas), were more strongly correlated in their synchrony during visuomotor performance. Similar distance-to-correlation-strength relations have also been reported by Cardoso de Oliveira, Gribova et al. (2001) who found that cross-

hemispheric pairs of local field potentials (LFP) recorded in bilateral motor cortical arm area in monkeys were weakly correlated compared to intra-hemispheric LFP pairs which were strongly correlated in both uni-manual and bi-manual movement tasks. There have also been observations in cats and monkeys of spatial clustering of neurons into functional groups through the positively related proximal neurons with simultaneously negative associations between distal groups of neurons that may function to accentuate the segregation among neural ensembles (Gray, Konig et al. 1989, Gray, Singer 1989, Vaadia, Haalman et al. 1995). Thus, neurons within a cluster or in neighbouring clusters may be similar in how their neural activities are related to or represent different types of information. This idea could be extended to observations we have made of signals tapped by sensors that were significantly linearly related to movement *tau* or speed (in Chapter 6). The clusters of such sensors were spatially distributed in the fronto-parietal sensor-space across subjects (FIG 6.3 and 6.4). Communicating between and /or integrating information from functional neural clusters in different brain areas may be effected through temporal correlation of their activities.

Two sets of observations were particularly interesting in relation to the differences in neural synchrony between the two conditions. First, the strength of sensor-pair correlation was stronger during rest, but a larger number of significantly correlated sensor-pairs were observed during the movement-task. In addition, more negatively correlated sensor-pairs were found during movement-task performance, which could in part be due to the induced field signal of the sources. Second, subsets of sensor clusters were reorganized during movement-task performance while the remaining clusters maintained their spatial organisation and interactions between members. The sensors that participated in the reorganization were primarily located in the frontal, middle, and parietal sensor-space contralateral to the performing hand. The most prominent reorganization of cluster membership involved sensors located in the middle-dorsal

and lateral-frontal sensor-space of the left hemisphere, suggestive of the involvement of areas concerned with motor control. These observations are comparable to studies which have reported changes in coherence and phase-synchrony within and between tasks (Cardoso de Oliveira, Gribova et al. 2001, Lutz, Lachaux et al. 2002, Rodriguez, George et al. 1999).

Of particular relevance is the visual perception study involving Mooney faces by Rodriguez, George et al. (1999). The authors documented phase synchrony at the *gamma* band between sensors located in the frontal, parietal and occipital EEG sensor-space during a face recognition task, but not when the high-contrast Mooney faces were inverted during presentation, which made them harder to recognise. A new distribution of synchrony was manifested when their subjects made a movement response to denote their perception. In addition, between the periods when these two patterns of synchronization emerged, the probability of phase-synchrony between many sensor-pairs fell below the base level in the face-perception condition, a phenomenon which the authors described as *phase-scattering*. Although we did not further segregate the movement-task events into 'perception' and 'action' phases, similar transitions between coupling (*phase-synchrony*), decoupling (*phase-scattering*), and re-coupling between underlying neural ensembles were also observed between rest and performance conditions, as manifested by the reorganisation of clusters. Furthermore, the zero-lag synchronicities found in our study are in line with previous studies that have reported intra- and inter-hemispheric correlations at zero-lag (Bressler, Coppola et al. 1993, Cardoso de Oliveira, Gribova et al. 2001, Roelfsema, Engel et al. 1997).

The analysis employed in this investigation has certain advantages over existing more popular measures of neural synchrony. In both temporal and frequency domains, the relation between time-series can only be properly assessed if the time-series satisfy

stationary (or quasi-stationary) requirements; correlation estimates based on non-stationary variables are prone to false associations. In pre-whitening our data to obtain quasi-stationary time-series for the analysis, we improve the estimates of synchronicity between sensor-pairs. In addition, through partial cross-correlation analyses, we accounted for the effects of other possible contributing interactions between these sensors with all other sensors in the network. This approach accepts the possibility that signals measured from neighbouring sensors might come from a single underlying source. The spatial overlap in the clusters' sensor-membership attests to view that signals from immediate sensor neighbours do not necessarily co-vary. Furthermore, instead of cross-correlating averaged, evoked-response trials or estimating coherence from multiple coherence measures made from fragments of data or single trials, we used non-averaged trials in the time-series analysis, which are more likely to reflect the induced responses associated with self-paced temporally-coordinated neural activities (Uhlhaas, Singer 2006), which are more intuitive and reflect the self-paced movement task conditions more closely. While computationally costly, the snap-shots we identified of instantaneous synchronicities are thus more objectively derived. Furthermore, the hierarchical clustering offers a meaningful description of these neural synchronizations and their reorganization between conditions.

The main disadvantage of any analysis of neural signals in sensor-space is that the underlying source(s) and their interactions are not easily identified. It is proposed that the current methods used here should be extended in future investigations in appropriate source-space analyses for a holistic appreciation of neural synchronization. The consistency of the observed pattern of neural synchrony across subjects and the distinct spatial organization of sensor-clusters between task conditions suggests potential for further research and /or clinical applications. An extension of these analyses could involve performing the partial cross-correlations of the time-series (after appropriate ARIMA modelling) in segments of approximately 40-50ms, followed by the

hierarchical clustering procedure during the task performance, to study if there might be systematic changes in members of sensors forming the clusters. In the event that the cluster-membership is relatively stable, it would be interesting to explore whether 1) the location of clusters' centroids, 2) the strength and sign of the partial cross-correlations between sensor-clusters, and /or 3) if the clusters of sensors' signals would vary as a function of movement variables like *tau*, speed, position, or simply vary during the whole evolving period of task performance.

On the clinical side, application of the method might be found in the context of monitoring the recovery of motor function in stroke patients. Cortical reorganisation is common after stroke as a compensatory mechanism. In the case of unilateral brain damage, the increased activity in the intact hemisphere has often been demonstrated in patients who have recovered the use of their affected limb (Gerloff, Braun et al. 2006, Johansen-Berg, Rushworth et al. 2002, Seitz, Hoflich et al. 1998, Takeda, Gomi et al. 2007). Transient disruption to the motor areas of the intact hemisphere has also been shown to disrupt this recovered ability (Johansen-Berg, Rushworth et al. 2002, Lotze, Markert et al. 2006), suggesting the functional relevance of the apparent reorganization. Thus, it appears that the typical contralateral motor activity and related synchronous connectivity that is abolished following stroke or damage can be replaced by an ipsilateral re-organization of neural synchronization that becomes progressively more stable with recovery of function. Interestingly, in addition to strong contralateral motor activity, concurrent activity in the ipsilateral cortex has also been associated with the initial phase of skill acquisition (e.g. Lotze, Scheler et al. 2003) and could potentially be used as an indicator of changes in motor learning and plasticity. It seems that extension of the current analysis further into the source-space would allow investigation of ideas concerning dynamical functional connectivity between multiple brain areas implicated in cognitive and sensorimotor processes and their associated synchronicities to benefit

both research and clinical applications. This is but the beginning of an interesting and valuable project.

BOROUD, T., BROWN, P., GOLDBERG, J.A., GRAYBIEL, A.M. and MAGILL, P.J., 2006. Oscillations in the Basal Ganglia: The good, the bad, and the unexpected. In: J.P. BOLAM, C.A. INGHAM and P.J. MAGILL, eds, *The basal ganglia VIII. Advances in behavioral biology, v. 56.* New York: Springer, pp. 3-24.

BRESSLER, S.L., COPPOLA, R. and NAKAMURA, R., 1993. Episodic multiregional cortical coherence at multiple frequencies during visual task performance. *Nature,* **366**(6451), pp. 153-156.

BRUNO, R.M. and SAKMANN, B., 2006. Cortex is driven by weak but synchronously active thalamocortical synapses. *Science,* **312**(5780), pp. 1622-1627.

CARDOSO DE OLIVEIRA, S., GRIBOVA, A., DONCHIN, O., BERGMAN, H. and VAADIA, E., 2001. Neural interactions between motor cortical hemispheres during bimanual and unimanual arm movements. *European Journal of Neuroscience,* **14**(11), pp. 1881-1896.

CARTER, G.C., 1987. Coherence and time delay estimation, *Proceedings of the IEEE*, 1987, pp236-255.

ENGEL, A.K., FRIES, P. and SINGER, W., 2001. Dynamic predictions: oscillations and synchrony in top-down processing. *Nature reviews.Neuroscience,* **2**(10), pp. 704-716.

ENGEL, A.K., KONIG, P., KREITER, A.K. and SINGER, W., 1991. Interhemispheric synchronization of oscillatory neuronal responses in cat visual cortex. *Science,* **252**(5010), pp. 1177-1179.

ENGEL, A.K., KREITER, A.K., KONIG, P. and SINGER, W., 1991. Synchronization of oscillatory neuronal responses between striate and extrastriate visual cortical areas of the cat. *Proceedings of the National Academy of Sciences of the United States of America,* **88**(14), pp. 6048-6052.

FRIES, P., 2005. A mechanism for cognitive dynamics: neuronal communication through neuronal coherence. *Trends in Cognitive Sciences,* **9**(10), pp. 474-480.

FRIES, P., REYNOLDS, J.H., RORIE, A.E. and DESIMONE, R., 2001. Modulation of oscillatory neuronal synchronization by selective visual attention. *Science,* **291**(5508), pp. 1560-1563.

GEORGOPOULOS, A.P., KARAGEORGIOU, E., LEUTHOLD, A.C., LEWIS, S.M., LYNCH, J.K., ALONSO, A.A., ASLAM, Z., CARPENTER, A.F., GEORGOPOULOS, A., HEMMY, L.S., KOUTLAS, I.G., LANGHEIM, F.J.P., MCCARTEN, J.R., MCPHERSON, S.E., PARDO, J.V., PARDO, P.J., PARRY, G.J., ROTTUNDA, S.J., SEGAL, B.M., SPONHEIM, S.R., STANWYCK, J.J., STEPHANE, M. and WESTERMEYER, J.J., 2007. Synchronous neural interactions assessed by magnetoencephalography: a functional biomarker for brain disorders. *Journal of Neural Engineering,* **4**, pp. 349-355.

GERLOFF, C., BRAUN, C., STAUDT, M., HEGNER, Y.L., DICHGANS, J. and KRAGELOH-MANN, I., 2006. Coherent corticomuscular oscillations originate from primary motor cortex: evidence from patients with early brain lesions. *Human Brain Mapping,* **27**(10), pp. 789-798.

GRAY, C.M., KONIG, P., ENGEL, A.K. and SINGER, W., 1989. Oscillatory responses in cat visual cortex exhibit inter-columnar synchronization which reflects global stimulus properties. *Nature,* **338**(6213), pp. 334-337.

GRAY, C.M. and SINGER, W., 1989. Stimulus-specific neuronal oscillations in orientation columns of cat visual cortex. *Proceedings of the National Academy of Sciences of the United States of America,* **86**(5), pp. 1698-1702.

GROSS, J., KUJALA, J., HAMALAINEN, M., TIMMERMANN, L., SCHNITZLER, A. and SALMELIN, R., 2001. Dynamic imaging of coherent sources: Studying neural interactions in the human brain. *Proceedings of the National Academy of Sciences of the United States of America,* **98**(2), pp. 694-699.

GROSS, J., TIMMERMANN, L., KUJALA, J., DIRKS, M., SCHMITZ, F., SALMELIN, R. and SCHNITZLER, A., 2002. The neural basis of intermittent motor control in humans. *Proceedings of the National Academy of Sciences of the United States of America,* **99**(4), pp. 2299-2302.

JEONG, J., 2004. EEG dynamics in patients with Alzheimer's disease. *Clinical Neurophysiology,* **115**(7), pp. 1490-1505.

JOHANSEN-BERG, H., RUSHWORTH, M.F., BOGDANOVIC, M.D., KISCHKA, U., WIMALARATNA, S. and MATTHEWS, P.M., 2002. The role of ipsilateral premotor cortex in hand movement after stroke. *Proceedings of the National Academy of Sciences of the United States of America,* **99**(22), pp. 14518-14523.

LACHAUX, J.P., RODRIGUEZ, E., MARTINERIE, J. and VARELA, F.J., 1999. Measuring phase synchrony in brain signals. *Human Brain Mapping,* **8**(4), pp. 194-208.

LANGHEIM, F.J., LEUTHOLD, A.C. and GEORGOPOULOS, A.P., 2006. Synchronous dynamic brain networks revealed by magnetoencephalography. *Proceedings of the National Academy of Sciences of the United States of America,* **103**(2), pp. 455-459.

LE VAN QUYEN, M., NAVARRO, V., MARTINERIE, J., BAULAC, M. and VARELA, F.J., 2003. Toward a neurodynamical understanding of ictogenesis. *Epilepsia,* **44 Suppl 12**, pp. 30-43.

LLINAS, R.R. and STERIADE, M., 2006. Bursting of thalamic neurons and states of vigilance. *Journal of Neurophysiology,* **95**(6), pp. 3297-3308.

LOTZE, M., MARKERT, J., SAUSENG, P., HOPPE, J., PLEWNIA, C. and GERLOFF, C., 2006. The role of multiple contralesional motor areas for complex hand movements after internal capsular lesion. *Journal of Neuroscience,* **26**(22), pp. 6096-6102.

LOTZE, M., SCHELER, G., TAN, H.R.M., BRAUN, C. and BIRBAUMER, N., 2003. The musician's brain: functional imaging of amateurs and professionals during performance and imagery. *NeuroImage,* **20**(3), pp. 1817-1829.

LUTZ, A., LACHAUX, J., MARTINERIE, J. and VARELA, F., 2002. Guiding the study of brain dynamics by using first-person data: Synchrony patterns correlate with ongoing conscious states during a simple visual task. *Proceedings of the National Academy of Sciences,* **99**(3), pp. 1586-1591.

MERKLE, A.N., LEUTHOLD, A.C., LANGHEIM, F.J.P. and GEORGOPOULOS, A.P., 2006. Hierarchical clustering of magnetoencephalographic (MEG) data. *Society for Neuroscience Abstracts,* 2006, 747.19.

MITZDORF, U. and SINGER, W., 1979. Excitatory synaptic ensemble properties in the visual cortex of the macaque monkey: a current source density analysis of electrically evoked potentials. *Journal of Comparative Neurology,* **187**(1), pp. 71-83.

MOTAMEDI, G. and MEADOR, K., 2003. Epilepsy and cognition. *Epilepsy & Behavior,* **4 Suppl 2**, pp. S25-38.

MURTHY, V.N. and FETZ, E.E., 1996. Oscillatory activity in sensorimotor cortex of awake monkeys: synchronization of local field potentials and relation to behavior. *Journal of Neurophysiology,* **76**(6), pp. 3949-3967.

POLLOK, B., GROSS, J. and SCHNITZLER, A., 2006. How the brain controls repetitive finger movements. *Journal of Physiology, Paris,* **99**(1), pp. 8-13.

RAMPP, S. and STEFAN, H., 2006. Fast activity as a surrogate marker of epileptic network function? *Clinical Neurophysiology,* **117**(10), pp. 2111-2117.

RODRIGUEZ, E., GEORGE, N., LACHAUX, J.P., MARTINERIE, J., RENAULT, B. and VARELA, F.J., 1999. Perception's shadow: long-distance synchronization of human brain activity. *Nature,* **397**(6718), pp. 430-433.

ROELFSEMA, P.R., ENGEL, A.K., KONIG, P. and SINGER, W., 1997. Visuomotor integration is associated with zero time-lag synchronization among cortical areas. *Nature,* **385**(6612), pp. 157-161.

SARNTHEIN, J., PETSCHE, H., RAPPELSBERGER, P., SHAW, G.L. and VON STEIN, A., 1998. Synchronization between prefrontal and posterior association cortex during human working memory. *Proceedings of the National Academy of Sciences of the United States of America,* **95**(12), pp. 7092-7096.

SCHNITZLER, A. and GROSS, J., 2005. Normal and pathological oscillatory communication in the brain. *Nature Reviews Neuroscience,* **6**(4), pp. 285-296.

SEITZ, R.J., HOFLICH, P., BINKOFSKI, F., TELLMANN, L., HERZOG, H. and FREUND, H.J., 1998. Role of the premotor cortex in recovery from middle cerebral artery infarction. *Archives of Neurology,* **55**(8), pp. 1081-1088.

STOPFER, M., BHAGAVAN, S., SMITH, B.H. and LAURENT, G., 1997. Impaired odour discrimination on desynchronization of odour-encoding neural assemblies. *Nature,* **390**(6655), pp. 70-74.

TAKEDA, K., GOMI, Y., IMAI, I., SHIMODA, N., HIWATARI, M. and KATO, H., 2007. Shift of motor activation areas during recovery from hemiparesis after cerebral infarction: A longitudinal study with near-infrared spectroscopy. *Neuroscience Research,* **59**(2), pp. 136-144.

TALLON-BAUDRY, C. and BERTRAND, O., 1999. Oscillatory gamma activity in humans and its role in object representation. *Trends in Cognitive Sciences,* **3**(4), pp. 151-162.

TASS, P.A., FIESELER, T., DAMMERS, J., DOLAN, K., MOROSAN, P., MAJTANIK, M., BOERS, F., MUREN, A., ZILLES, K. and FINK, G.R., 2003. Synchronization tomography: a method for three-dimensional localization of phase synchronized neuronal populations in the human brain using magnetoencephalography. *Physical Review Letters,* **90**(8), pp. 088101.

UHLHAAS, P.J. and SINGER, W., 2006. Neural synchrony in brain disorders: relevance for cognitive dysfunctions and pathophysiology. *Neuron,* **52**(1), pp. 155-168.

VAADIA, E., HAALMAN, I., ABELES, M., BERGMAN, H., PRUT, Y., SLOVIN, H. and AERTSEN, A., 1995. Dynamics of neuronal interactions in monkey cortex in relation to behavioural events. *Nature,* **373**(6514), pp. 515-518.

VON STEIN, A. and SARNTHEIN, J., 2000. Different frequencies for different scales of cortical integration: from local gamma to long range alpha/theta synchronization. *International Journal of Psychophysiology,* **38**(3), pp. 301-313.

WILSON, T.W., ROJAS, D.C., REITE, M.L., TEALE, P.D. and ROGERS, S.J., 2007. Children and adolescents with autism exhibit reduced MEG steady-state gamma responses. *Biological Psychiatry,* **62**(3), pp. 192-197.

WOMELSDORF, T., FRIES, P., MITRA, P.P. and DESIMONE, R., 2006. Gamma-band synchronization in visual cortex predicts speed of change detection. *Nature,* **439**(7077), pp. 733-736.

CHAPTER 8:

General Discussion

A Summary of Findings and Potential Applications

If prospective information like that defined by movement *tau* is useful in gearing movements for intercepting moving targets, such information may also be useful in guiding movements that are not constrained by the time of external events to intended goals. Two parallel investigations of the neural representation of movement *tau* during self-paced movements were performed in this research. One involved the multiple single-cell neurophysiological data recorded from multiple sites in the prefrontal and parietal cortices of a behaving non-human primate performing a shape-copying task. In the other, time-varying neuromagnetic signals simultaneously recorded from 248 MEG sensors during 20 human participants' simple target-to-target movement performance were analysed. The tasks for subjects in both investigations can be regarded as similar in nature: both involved the closure of motion gaps – between targets in the MEG Study and between the corners of each shape in the Shape Copying Study.

Within the prefrontal and parietal cortices of the monkey, the activity (i.e. spike density function) of a small subset of neurons was significantly linearly related to the time-

varying movement *tau*. Compared to the prefrontal cortex, a larger proportion of neuronal activities in area 5 of the parietal cortex were observed to be involved in representing movement *tau*. This was true with (PFC: 8%; Area 5: 17%) or without (PFC: 13%; Area 5: 24%) accounting for the association of neural spike density functions to movement speed. On the other hand, a large majority of the neural activities in both prefrontal and parietal areas were significantly linearly related to movement speed, with a larger significant proportion found in the prefrontal cortex. This, again, was true with (PFC: 77%; Area 5: 61%) or without (PFC: 78%; Area 5: 65%) accounting for the concurrent relation of neural activities to movement tau.

Although the neuromagnetic activities of a large part of the cortex was sampled with the sensor array of the MEG system (unlike the single neurons at selected locations during neurophysiological recordings in the monkey), a similar finding of significant frontal-parietal involvement in the representation of movement *tau*, with respect to sensor-space, was observed bilaterally in human subjects. The neuromagnetic signals that were significantly linearly related to movement *tau* involved more dorsal sensors in the parietal sensor-space when the association of these signals to movement speed was taken into account. In contrast, when movement speed was disregarded, activity related to movement *tau* was concentrated among sensors in the parieto-temporo-occipital areas. The signals significantly linearly related to movement speed were tapped by a larger number of MEG sensors, yielding a more consistent spatial distribution across subjects. Neuromagnetic signals from the contralateral frontal and parietal posterior sensors were consistently involved in representing movement speed. For both movement speed and *tau*, significantly higher PSR (percentage of significant relation across all subjects), to either variable separately, were found in the left parietal sensor-region. This observation is in line with previous findings implicating the left parietal cortex in online update of movement representations particularly where sudden target displacements are introduced, and in which lesions impair the smooth

corrections of movement trajectories when such target-location perturbations occur (Battaglia-Mayer, Archambault et al. 2006, Desmurget, Epstein et al. 1999, Desmurget, Grea et al. 2001, Grea, Pisella et al. 2002, Rushworth, Taylor 2006).

In addition, our findings in both studies are likely to relate to similar activations found in the posterior parietal area during gap-closure-judgements (Field, Wann 2005), the neural processing of the variable *tau* during interceptive movements made by a monkey (Merchant, Battaglia-Mayer et al. 2004), as well as the representation of movement speed in the monkey parietal cortex (Averbeck, Chafee et al. 2005). The overall parieto-frontal involvement with regards to both neural recordings in prefrontal cortex and parietal area 5 as well as signals relative to MEG sensor-space is consistent with the view that a network of neural activities within these regions is intricately involved in visuomotor control in primates. The finding of a neural representation of movement *tau* in humans demonstrated in our MEG study suggests a neural process linked to the reported tight coupling between the theoretical *tau*-guide and movement *tau* in behavioural studies that demonstrated self-regulated movements in humans (Craig, Delay et al. 2000, Craig, Lee 1999, Lee, Craig et al. 1999) comparable to the movements performed in the current studies.

We acknowledge that goals for movements do not always remain stationary, nor do moving targets necessarily maintain a steady course. Moreover, obstacles can also come in the movement path unexpectedly. This uncertainty of goals becomes apparent when we reflect on what is involved in swatting flies or mosquitoes in the summer, or watching cops chase a suspect on the run in movies, and in many similar real life persuit tasks. In these cases, educated guesses (about environmental and physical attributes of the target or context), estimates of gap distances to goal, the instantaneous speed, and the *tau*-coupling constant (k) are likely to occupy a larger confidence interval at any given time (Georgopoulos 2007). Controlled variations on the estimation of

movement *tau* are likely to account for the success of timely gap closures and the question of how this uncertainty is regulated would benefit from further research.

For the present, the finding that the time-varying movement *tau* is represented in a subset of the neural signals obtained in MEG as well as in single cell neurophysiology recordings during movements that were not temporally constrained, as movements are to intercept moving targets, is encouraging. It may have applications to improve the design of neuro-prostheses. In current approaches using neural signals in controlling prostheses, by both invasive (e.g. Taylor, Tillery et al. 2002, Taylor, Tillery et al. 2003) and non-invasive (e.g. Wolpaw, McFarland 2004) brain-computer-interface (BCI) techniques, the predictions of movements to end-points are restricted within a 3D space or within the 2D space of a computer screen (for a review see e.g. Birbaumer, Cohen 2007, Schwartz, Cui et al. 2006). For example, amplitude of cortical signals of different frequencies (*mu*: 8 – 12 Hz and *beta*: 18 – 24 Hz) recorded by EEG drive a computer cursor left or right, and up or down via an adaptive algorithm that weighs the amplitude of the vertical and horizontal component of the cursor movement (Wolpaw, McFarland 2004).

Most extraction algorithms for movement BCIs are based on the concept of directional population vectors. The population vector idea presumes that the firing rates of each cell in a population of cells (e.g. in the motor cortex) contribute in specifying the direction of an intended movement. Each cell can be conceptualized as having a preferred direction to which it fires most intensely when the animal moves in that direction. This directional preference can be described in terms of direction cosines in 3D space and the cell's firing rate modulates the direction cosines by giving them a weight relative to their preferences. Although there are cells within the motor cortex of the brain tuned to different preferred directions, the sum of their weighted direction cosines recorded when a movement is made has been shown to be within ±10° of the

actual movement direction (Georgopoulos, Schwartz et al. 1986). Moreover, both the accuracy and directional tuning of these cells improve with practice on the movement task (Taylor, Tillery et al. 2002). Thus, the population vector provides a rather close approximation to a subject's intended movement direction.

Within a given 3D environment, the instantaneous velocity derived through the population vector algorithm (i.e. the length of the population vector) can be integrated with respect to time to obtain the movement trajectory required to reach the intended target in a particular direction at a particular time (Schwartz, Cui et al. 2006). This information can then be used to calculate the inverse kinematics required to move a robotic arm with the appropriate joint-angles in time to bring the arm-gripper to the destination and target. Given that information about speed or tangential velocity (Averbeck, Chafee et al. 2005, Moran, Schwartz 1999, and this research), XY position (Ashe, Georgopoulos 1994, Georgopoulos, Langheim et al. 2005), and movement *tau* (Merchant, Battaglia-Mayer et al. 2004, and this research) can be recovered from neural signals, it is conceivable that these parameters could be incorporated into the BCI-algorithm to fine-tune the control and movement of the robotic-arm as it approaches the intended goal by providing additional 'forward' information. In particular, the *tau* information, either from intrinsic visuomotor performance parameters or by exproprioceptive information from optical flow etc. is likely to enable more dynamical interactions between BCI-generated movements and the environment. Investigations into the predictive role of movement *tau* together with speed and positional information are currently being explored and will be carried out more thoroughly in further studies.

An additional part of this research investigated how synchronous interactions between neural ensembles might differ between rest and performance in the target-to-target movement task. The consistency in the differing partial cross-correlation networks

across subjects in both rest and movement performance relate to previous observations of stability in neuronal synchrony (Langheim, Leuthold et al. 2006). We also observed reorganization of clusters of MEG sensors whose time-varying neuromagnetic signals were correlated in the different conditions. Just as single neurons have been documented to engage in different interactions with other neurons without altering their firing rates (Vaadia, Haalman et al. 1995), it seems likely that ensembles of synchronously active neurons could also dynamically engage in different interactions within and across different brain regions. In general, the positive correlations between neighbouring (or 'proximal') sensor-pairs and sensor-clusters relative to the negative correlations between more spatially distant (or 'distal') sensor-pairs and clusters of sensors also parallel neurophysiological data bringing evidence of the spatial clustering of neurons into functional groups. Activities of neighbouring neurons which are positively related and simultaneous negative neuronal associations between groups of neurons separated by a larger distance may be a way to highlight the segregation among subsets of functional neural networks (Gray, Konig et al. 1989, Vaadia, Haalman et al. 1995). Synchronous interactions between neurons and neural ensembles may offer a means of integrating relevant information, such as *tau*, tangential velocity, etc., between different but functionally related brain areas for guiding behaviour.

This body of work encompassed different techniques and different levels of analyses -- multiple single-cell neurophysiology, and the MEG recording of magnetic fields generated by synchronously active neural ensembles over large cortical regions – but the consistent theme and underlying essence is that of time, as in the temporal evolution and regulation of movement. Movements do not occur by concatenation of static states and the processes that lead to their evolution require an active sensorimotor dialogue. The variable *tau* affords instantaneous temporal information for the guidance of movement to an intended goal and has been previously shown to be represented in the primary motor cortex and the inferior parietal lobe (area 7a) during interceptive

actions. We extend the understanding of the neural correlate of this variable to area 5 of the superior parietal lobe and the prefrontal cortex in non-interceptive behaviour in monkeys, and we show similar fronto-parietal involvement in the representation of movement *tau* in the cortex of humans. The observed reorganisation of clusters of synchronous neural interactions from rest to movement performance suggests a dynamic integration of relevant information, including movement *tau* and tangential velocity, for the motivation of intended behaviour. In sum, these findings pave the way for further analyses to relate current MEG data in source-space, for applications of predictive *tau* information in fine-tuning neuro-prosthesis, as well as for furthering the understanding of synchronous neural networks during cognitive processing and the representation of movement in imagination and memory.

Bibliography for this section

ASHE, J. and GEORGOPOULOS, A.P., 1994. Movement parameters and neural activity in motor cortex and area 5. *Cerebral Cortex,* **4**(6), pp. 590-600.

AVERBECK, B.B., CHAFEE, M.V., CROWE, D.A. and GEORGOPOULOS, A.P., 2005. Parietal representation of hand velocity in a copy task. *Journal of Neurophysiology,* **93**(1), pp. 508-518.

BATTAGLIA-MAYER, A., ARCHAMBAULT, P.S. and CAMINITI, R., 2006. The cortical network for eye-hand coordination and its relevance to understanding motor disorders of parietal patients. *Neuropsychologia,* **44**(13), pp. 2607-2620.

BIRBAUMER, N. and COHEN, L.G., 2007. Brain-computer interfaces: communication and restoration of movement in paralysis. *The Journal of Physiology,* **579**(Pt 3), pp. 621-636.

CRAIG, C.M., DELAY, D., GREALY, M.A. and LEE, D.N., 2000. Guiding the swing in golf putting. *Nature,* **405**(6784), pp. 295-296.

CRAIG, C.M. and LEE, D.N., 1999. Neonatal control of nutritive sucking pressure: evidence for an intrinsic tau-guide. *Experimental Brain Research,* **124**(3), pp. 371-382.

DESMURGET, M., EPSTEIN, C.M., TURNER, R.S., PRABLANC, C., ALEXANDER, G.E. and GRAFTON, S.T., 1999. Role of the posterior parietal cortex in updating reaching movements to a visual target. *Nature Neuroscience,* **2**(6), pp. 563-567.

DESMURGET, M., GREA, H., GRETHE, J.S., PRABLANC, C., ALEXANDER, G.E. and GRAFTON, S.T., 2001. Functional anatomy of nonvisual feedback loops during reaching: a positron emission tomography study. *Journal of Neuroscience,* **21**(8), pp. 2919-2928.

FIELD, D.T. and WANN, J.P., 2005. Perceiving time to collision activates the sensorimotor cortex. *Current Biology,* **15**(5), pp. 453-458.

GEORGOPOULOS, A.P., 2007. A tribute to tau. In: G.-. PEPPING and M.A. GREALY, eds, *Closing the Gap The Scientific Writings of David N. Lee.* Lawrence Erlbaum Assoc Inc., pp. 157-161.

GEORGOPOULOS, A.P., LANGHEIM, F.J., LEUTHOLD, A.C. and MERKLE, A.N., 2005. Magnetoencephalographic signals predict movement trajectory in space. *Experimental Brain Research,* **167**(1), pp. 132-135.

GEORGOPOULOS, A.P., SCHWARTZ, A.B. and KETTNER, R.E., 1986. Neuronal population coding of movement direction. *Science,* **233**(4771), pp. 1416-1419.

GRAY, C.M., KONIG, P., ENGEL, A.K. and SINGER, W., 1989. Oscillatory responses in cat visual cortex exhibit inter-columnar synchronization which reflects global stimulus properties. *Nature,* **338**(6213), pp. 334-337.

GREA, H., PISELLA, L., ROSSETTI, Y., DESMURGET, M., TILIKETE, C., GRAFTON, S., PRABLANC, C. and VIGHETTO, A., 2002. A lesion of the posterior parietal cortex disrupts on-line adjustments during aiming movements. *Neuropsychologia,* **40**(13), pp. 2471-2480.

LANGHEIM, F.J., LEUTHOLD, A.C. and GEORGOPOULOS, A.P., 2006. Synchronous dynamic brain networks revealed by magnetoencephalography. *Proceedings of the National Academy of Sciences of the United States of America,* **103**(2), pp. 455-459.

LEE, D.N., CRAIG, C.M. and GREALY, M.A., 1999. Sensory and intrinsic coordination of movement. *Proceedings of the Royal Society B: Biological Sciences,* **266**(1432), pp. 2029-2035.

MERCHANT, H., BATTAGLIA-MAYER, A. and GEORGOPOULOS, A.P., 2004. Neural responses during interception of real and apparent circularly moving stimuli in motor cortex and area 7a. *Cerebral Cortex,* **14**(3), pp. 314-331.

MORAN, D.W. and SCHWARTZ, A.B., 1999. Motor cortical representation of speed and direction during reaching. *Journal of Neurophysiology,* **82**(5), pp. 2676-2692.

RUSHWORTH, M.F. and TAYLOR, P.C., 2006. TMS in the parietal cortex: updating representations for attention and action. *Neuropsychologia,* **44**(13), pp. 2700-2716.

SCHWARTZ, A.B., CUI, X.T., WEBER, D.J. and MORAN, D.W., 2006. Brain-controlled interfaces: movement restoration with neural prosthetics. *Neuron,* **52**(1), pp. 205-220.

TAYLOR, D.M., TILLERY, S.I. and SCHWARTZ, A.B., 2003. Information conveyed through brain-control: cursor versus robot. *IEEE Transactions on Neural Systems and Rehabilitation Engineering,* **11**(2), pp. 195-199.

TAYLOR, D.M., TILLERY, S.I. and SCHWARTZ, A.B., 2002. Direct cortical control of 3D neuroprosthetic devices. *Science,* **296**(5574), pp. 1829-1832.

VAADIA, E., HAALMAN, I., ABELES, M., BERGMAN, H., PRUT, Y., SLOVIN, H. and AERTSEN, A., 1995. Dynamics of neuronal interactions in monkey cortex in relation to behavioural events. *Nature,* **373**(6514), pp. 515-518.

WOLPAW, J.R. and MCFARLAND, D.J., 2004. Control of a two-dimensional movement signal by a noninvasive brain-computer interface in humans. *Proceedings of the National Academy of Sciences of the United States of America,* **101**(51), pp. 17849-17854.